Parallel manipulators with two end-effectors

Getting a grip on Jacobian-based stiffness analysis

Hoevenaars, Teun

DOI

Publication date
2016

Document Version
Final published version

Citation (APA)

Important note

To cite this publication, please use the final published version (if applicable).
Please check the document version above.

PARALLEL MANIPULATORS WITH TWO END-EFFECTORS

GETTING A GRIP ON JACOBIAN-BASED STIFFNESS ANALYSIS

PARALLEL MANIPULATORS WITH TWO END-EFFECTORS

GETTING A GRIP ON JACOBIAN-BASED STIFFNESS ANALYSIS

Proefschrift

ter verkrijging van de graad van doctor
aan de Technische Universiteit Delft,
op gezag van de Rector Magnificus prof. ir. K.C.A.M. Luyben,
voorzitter van het College voor Promoties,
in het openbaar te verdedigen op donderdag 7 juli 2016 om 15:00 uur

door

Antonius Gerardus Leonardus (Teun) HOEVENAARS

Master of Science in Aerospace Engineering,
Technische Universiteit Delft, Nederland,
geboren te 's-Hertogenbosch, Nederland.

To my family.

CONTENTS

SUMMARY

Robots that are developed for applications which require a high stiffness-over-inertia ratio, such as pick-and-place robots, machining robots, or haptic devices, are often based on parallel manipulators. Parallel manipulators connect an end-effector to an inertial base using multiple serial kinematic chains. This architecture enables the design of robots with all actuators located at the base, which greatly reduces the effective inertia with no detrimental effect on the stiffness, thus improving the stiffness-over-inertia ratio.

One of the limitations of current parallel manipulators is that gripping requires an additional, dedicated subsystem, which either degrades performance or can only handle objects with a flat surface. A promising alternative solution for future gripping robots are parallel manipulators with two end-effectors (PM2Es). These PM2Es facilitate mechanical gripping using an internal closed-loop chain, which enables gripping robots that have all their actuators located at the base. As such, PM2Es combine mechanical gripping with a favorable stiffness-over-inertia ratio. Because of the potential benefits in both cost and hygiene, the integration of compliant joints is identified as a second promising development for future gripping robots. The benefits of PM2Es and those of compliant joints can be enjoyed simultaneously if compliant PM2Es are designed.

However, it is currently not possible to effectively design compliant PM2Es, because existing stiffness analyses methods do not directly apply to PM2Es. To overcome this limitation, in this thesis a stiffness analysis method is developed that is also valid for compliant PM2Es.

In Chapter 2 insights from screw theory are used to develop a novel Jacobian-based stiffness analysis method for parallel manipulators, which is more general than existing methods. The stiffness analysis method takes the influence of actuators, compliant joints, as well as structural elements into account, and also considers the effect of loading. Stiffness in the constrained directions of individual serial chains is represented using virtual joints, which allows structural compliance to be considered for any parallel manipulator with non-redundant legs. This includes lower mobility parallel manipulators, which have less than six degrees of freedom. Loading is taken into account using a term that depends on the derivative of a Jacobian matrix.

The developed stiffness analysis method is experimentally validated in Chapter 3. It is shown that the accuracy of a stiffness analysis improves if the effect of loading is considered and also if structural compliance is included in the analysis. The example stiffness matrices in Chapter 3 are all symmetric, which is in line with the definition of a stiffness matrix.

In contrast, Griffis and Duffy (1993) found asymmetric stiffness matrices when they analyzed two mechanisms under loading. Loading cannot be part of a stiffness analysis if it can lead to asymmetric matrices, which explains the extensive discussions surrounding their work. Chapter 4 demonstrates that the asymmetry in the work by Griffis

and Duffy can be explained as a modeling inconsistency. It is also shown that consistent modeling results in symmetric matrices, which supports the notion that loading is an integral part of a stiffness analysis of parallel manipulators.

Chapter 5 presents a systematic approach for the Jacobian analysis of PM2Es in order to extend the Jacobian-based stiffness analysis method of Chapter 2 to PM2Es. Previously, Jacobian analyses of PM2Es have only been performed for specific examples, but this thesis introduces structure to the Jacobian analysis of PM2Es by considering each end-effector as a rigid body with its own six-dimensional motion vector, and by representing a PM2E as an organization of serial chains. In Chapter 5 it is also shown that the structural compliance of internal serial chains must be considered in order to deal with relative degrees of freedom that are constrained between the two end-effectors.

In Chapter 6 the stiffness analysis method of Chapter 2 and the Jacobian analysis of Chapter 5 are integrated and the very first stiffness matrices of PM2Es are presented. An experimental verification of these stiffness matrices demonstrates that the developed stiffness analysis method also applies to compliant parallel manipulators with two end-effectors. Therefore, the method introduced in this thesis is ready to be used for the effective design of novel gripping robots.

SAMENVATTING

Robots die ontwikkeld worden voor toepassingen waarbij een hoge stijfheid-over-inertie ratio vereist is, zoals pak-en-plaats robots, verspaningsmachines, of haptische apparaten, zijn vaak gebaseerd op parallelle manipulatoren. Parallelle manipulatoren verbinden een eindeffector, i.e. het lichaam dat bestuurd wordt, met een inerte basis door middel van meerdere seriële kinematische ketens. Deze architectuur maakt het mogelijk om robots te ontwerpen waarbij alle actuatoren direct zijn bevestigd aan de inerte basis. Een parallelle architectuur vermindert daarmee de effectieve inertie zonder negatieve bijeffecten voor de stijfheid, zodat een hogere stijfheid-over-inertie ratio behaald kan worden.

Eén van de beperkingen van bestaande parallelle manipulatoren is dat voor grijptaken een extra, toegewijd subsysteem nodig is, wat de algehele prestatie vermindert dan wel alleen werkbaar is in combinatie met objecten met een vlak oppervlak. Een veelbelovende alternatieve oplossing voor toekomstige grijprobots zijn parallelle manipulatoren met twee eindeffectoren (PM2Es). Deze PM2Es kunnen mechanische grijpacties uitvoeren door middel van een interne gesloten kinematische keten, wat grijprobots mogelijk maakt waarin alle actuatoren bevestigd zijn aan de inerte basis. Op deze wijze combineren PM2Es mechanisch grijpen met een gunstige stijfheid-over-inertie ratio. Vanwege de potentiële voordelen in termen van kosten en hygiëne is de integratie van compliante mechanische gewrichten een tweede veelbelovende ontwikkeling voor toekomstige grijprobots. De voordelen van PM2Es en compliante gewrichten kunnen gecombineerd worden met het ontwerp van compliante PM2Es.

Echter is het momenteel niet mogelijk om compliante PM2Es effectief te ontwerpen, omdat bestaande stijfheidsanalysemethoden niet direct toegepast kunnen worden op PM2Es. Om deze beperking te overwinnen wordt er in dit proefschrift een stijfheidsanalysemethode ontwikkeld die ook geldig is voor compliante PM2Es.

In Hoofdstuk 2 worden inzichten uit *screw theory* gebruikt om een nieuwe stijfheidsanalysemethode te ontwikkelen voor parallelle manipulatoren die gebruik maakt van Jacobiaanmatrices, en welke breder inzetbaar is dan bestaande methoden. Deze stijfheidsanalysemethode houdt rekening met de invloed van actuatoren, compliante mechanische gewrichten, en de compliantie in structurele elementen, waarbij ook het effect van belasting meegenomen wordt. Stijfheid in de onderdrukte vrijheidsgraden van individuele seriële ketens wordt gepresenteerd door middel van virtuele mechanische gewrichten. Dit concept staat het toe om de structurele compliantie te modelleren van elke parallelle manipulator die is opgebouwd uit niet-redundante benen. Dit omvat parallelle manipulatoren waarin de eindeffector minder dan zes graden van vrijheid heeft. Belasting wordt in de ontwikkelde methode meegenomen door middel van een term die een functie is van de afgeleide van een Jacobiaanmatrix.

De ontwikkelde stijfheidsanalysemethode wordt experimenteel gevalideerd in Hoofdstuk 3. Daar wordt gevalideerd dat de nauwkeurigheid van een stijfheidsanalyse verbe-

tert als het effect van belasting in ogenschouw wordt genomen en ook als structurele compliantie onderdeel wordt gemaakt van de analyse. De voorbeelden van stijfheids-matrices in Hoofdstuk 3 zijn allemaal symmetrisch, wat in lijn is met de definitie van stijfheidsmatrices.

Daartegenover vonden Griffis en Duffy (1993) asymmetrische stijfheidsmatrices toen zij twee mechanismen onder belasting analyseerden. Belasting kan geen integraal on-derdeel van een stijfheidsanalyse zijn als het tot asymmetrische matrices kan leiden, wat verklaart waarom die bevindingen ter discussie staan. Hoofdstuk 4 demonstreert dat de asymmetrie in het werk van Griffis en Duffy verklaard kan worden door middel van inconsistente modellering. In hetzelfde hoofdstuk wordt ook aangetoond dat consistent modelleren resulteert in symmetrische matrices, wat de notie ondersteunt dat belasting een integraal onderdeel is van de stijfheidsanalyse van parallelle manipulatoren.

Hoofdstuk 5 presenteert een systematische aanpak voor de Jacobiaananalyse van PM2Es om de stijfheidsanalysemethode uit Hoofdstuk 2 toe te kunnen passen op PM2Es. Tot heden is de Jacobiaananalyse van PM2Es alleen uitgevoerd voor specifieke gevallen, maar dit proefschrift brengt structuur aan in de Jacobiaananalyse van PM2Es door elke eindeffector te beschouwen als een rigide lichaam met zijn eigen zes-dimensionale be-wegingsvector, en door een PM2E te beschouwen als een organisatie van seriële ketens. In Hoofdstuk 5 wordt het ook aangetoond dat de structurele compliantie van interne seriële ketens meegenomen moet worden in de analyse om te kunnen omgaan met on-derdrukte, relatieve graden van vrijheid tussen de twee eindeffectoren.

In Hoofdstuk 6 wordt de stijfheidsanalysemethode uit Hoofdstuk 2 gecombineerd met de Jacobiaananalyse uit Hoofdstuk 5, waarna de eerste stijfheidsmatrices van PM2Es worden gepresenteerd. Een experimentele verificatie van deze stijfheidsmatrices de-monstreert dat de resulterende stijfheidsanalysemethode ook geldig is voor compliante parallelle manipulatoren met twee eindeffectoren. De methode die geïntroduceerd is in dit proefschrift is daarom klaar om gebruikt te worden voor het effectief ontwerpen van nieuwe grijprobots.

PREFACE

Defying Newton's gravitational law, I am not attracted to those bodies with the greatest mass, but to those with complex motion. However, motion is relative and depends on one's reference frame, so before I could make a move Descartes had to make his point. From that origin of geometry I made my way to Euler, where I turned around my three axes to get his perspective on things. By now I was lost in both translation and rotation. Confused by all this relativity I climbed up Lagrange's hill, because I felt this had some potential and was worth the kinetic energy. Indeed, from there I spotted Jacobi, who I knew would not be indifferential to my pleas for an explanation. Although his explanation was only partial, he introduced me to Ball who brought the whole story to a close. He taught me how to Plück the day and screw the rest. Thus, although life looks like a set of complex motions, it is nothing but a mindset.

If you're not completely puzzled at this point, then you just might be my target audience. In this thesis I namely assume that you, the reader, have a firm understanding of screw theory. I realize that this disqualifies this thesis as a coffee table book, but enough coffee has already been spilled during its making.

Although my research was part of a project on the design of haptic devices, the methods that I developed and validated during my research are more generally applicable. In fact, over time I came to believe that my contributions are more valuable for future pick-and-place robots, which I therefore introduce as the most relevant application for the methods developed in this dissertation. Nonetheless, you are welcome to project these methods on any other potential application. Whatever your application, thank you for reading.

Teun Hoevenaars
The Hague, May 2016

1

INTRODUCTION

What you don't know
You can feel it somehow

Paul David Hewson
U2 - Beautiful Day

This chapter introduces the objective of this thesis within the context of current robotic developments. Robots that are developed for applications which require high stiffness-over-inertia, such as pick-and-place robots, machining robots, or haptic devices, are often based on parallel manipulators. One of the limitations of current parallel manipulators is that gripping requires an additional dedicated system, which either degrades performance or reduces the range of objects that can be handled. This thesis identifies parallel manipulators with two end-effectors as an opportunity for the high-speed handling of a wider range of objects. In addition, the integration of compliant joints is considered, because this has potential benefits in both cost and hygiene. Because stiffness is a key aspect in the analysis and design of robotic manipulators, this thesis aims to develop a stiffness analysis method that is also valid for compliant parallel manipulators with two end-effectors.

1
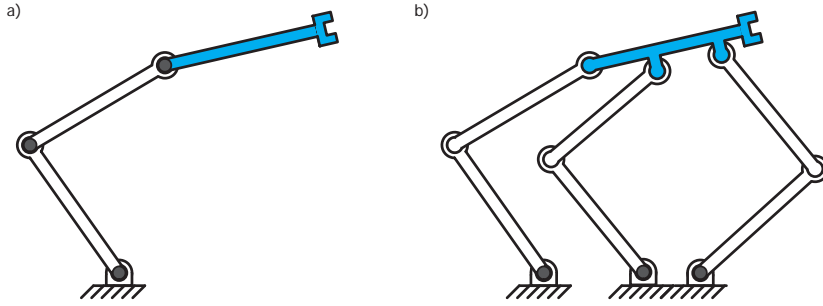
Figure 1.1: a) traditional serial manipulators connect an end-effector (the blue body) to the inertial base using a single serial chain, where all joints are actuated, while b) parallel manipulators connect an end-effector to the base using multiple serial chains, which allows all actuators (the dark gray dots) to be located at the base.

We live in a robotic age. Haptic devices and exoskeletons are breaking down the boundaries between humans and robots, while behind factory doors a rising army of robots continues to produce an increasing variety of our goods. Compared to humans, robots can be simultaneously faster, more powerful, and more precise, which makes them popular among manufacturers of products ranging from cars to foods and electronics [1]. In 2014, worldwide an estimated 220,000 new industrial robots were deployed, bringing their total number to around 1.5 million [2]. According to the McKinsey Global Institute, by 2025 this number could increase by another "15 million to 25 million robots, requiring investments totaling about $900 billion to $1.2 trillion." [3] Clearly, industrial robots represent a significant growth market. In order to address these growth markets, Europe has drafted a roadmap [4] in which key focus areas for technological development were identified. In this roadmap, flexible gripping was identified as an enabler to extend the reach of current industrial robots. This thesis contributes to that development introducing novel analysis methods for a recently proposed type of gripping robots.

1.1. STIFFNESS IS KEY FOR PARALLEL MANIPULATORS

T HIS thesis is about parallel manipulators (PMs) for applications where high dynamic performance and high accuracy are required of a robotic manipulator, such as stabilization platforms, flight simulators, machining robots, haptic devices, and pick-and-place robots. Examples of such robotic manipulators are shown in Fig. 1.2. Parallel manipulators are characterized by an end-effector that is connected to an inertial base via multiple serial chains, as opposed to serial manipulators, where the end-effector is connected to the base using a single serial chain. Figure 1.1 schematically shows this difference for the example of a planar manipulator. The individual serial chains that make up a PM are often referred to as legs. The end-effector of a PM can only access points which can be reached by all legs, so that its workspace is generally low compared to that of a serial manipulator. On the other hand, the dynamic performance, e.g. achievable position and force bandwidths, and accuracy of a PM are typically superior.

Figure 1.2: Parallel manipulators are applied in a wide range of applications, such as a) stabilization platforms [5], b) flight simulators [6], c) machining [7], d) haptic devices [8], and e) pick-and-place robots [9]
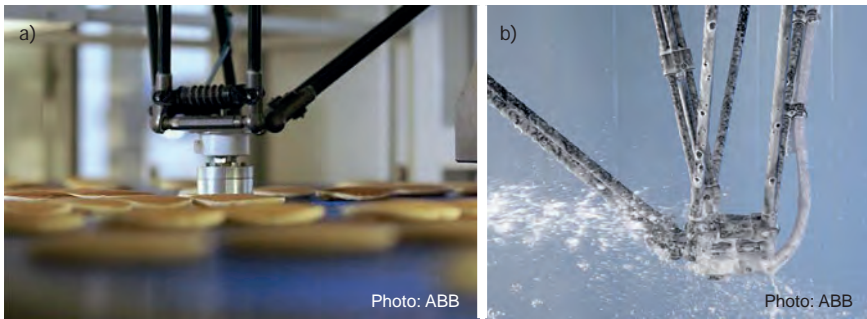
Figure 1.3: a) Hygiene is an important characteristic for pick-and-place in the many industries, such as the food industry [19]. b) Because in a PM the sensitive components are located at the base, the end-effector can be easily cleaned [20].

Dynamic performance of PMs is superior to that of traditional serial manipulators because in a PM the contribution of the actuators to the effective inertia is minimized. In a PM the actuators can be located at the base, so that the stators of the actuators do not contribute to the effective inertia, thereby minimizing their contribution. Serial manipulators can also be designed with all motors located at the base, but this requires power transmission using e.g. tendons or belts. Such transmission systems introduce flexibility, friction, and hysteresis [10], while the necessary guiding of the transmission lines around joints complicates the design [11]. In PMs the power transmission is achieved by the legs, which avoids these problems.

A reduced effective inertia has two main advantages. Firstly, a lower inertia results in a lower gravitational force acting on the end-effector. Therefore, a PM requires less power to carry its own weight and thereby can use the available power more effectively. Secondly, reduced inertia means that higher stiffness-over-inertia ratios can be achieved. Together, more available power and a higher stiffness-over-inertia ratio result in a higher dynamic performance. This is an important argument behind the use of parallel manipulators in the applications introduced in Fig. 1.2. The beneficial stiffness-over-inertia ratio is therefore key to the success of PMs in highly dynamic applications.

The accuracy of a PM is superior to that of a serial manipulator because in a PM measurement errors are averaged instead of added [12]. Accuracy in this case means accuracy of the end-effector pose, which is a combination of position and orientation. In a PM the pose is typically measured indirectly using sensors collocated with the actuators. Given the measured actuator positions, the pose of the end-effector is then obtained as an intersection of all remaining pose possibilities of the individual legs [13]. Because the resulting pose error also corresponds to an intersection of individual errors, measurement errors are averaged out. The pose can thus be determined with greater accuracy. This gives haptic devices a smoother feel and it allows more accurate closed loop control, which is another reason why PMs are popular as machining robots, but also explains their use as precision manipulators [14–16]. If a PM is under loading, the accuracy also depends on the stiffness that can be achieved [17, 18].

Figure 1.4: The Force Dimension Omega.7 is a 7-DoF haptic device with a dedicated motor at the end-effector to facilitate gripping [21] (courtesy of Force Dimension, Switzerland).

1.2. Opportunities for Future Gripping Robots

Hygiene is another important reason why PMs are preferred over alternative options. Because in a PM the sensitive components are located at the base, the end-effector can be easily cleaned, for example with high pressure water [20]. This makes PMs ideal for pick-and-place applications that have strict requirements on cleanliness or hygiene, such as handling solar cells or pancakes (see Fig. 1.3). But gripping cannot be achieved with a rigid end-effector, so that current PMs require an additional subsystem to perform the gripping action. Existing PMs typically use a suction subsystem connected to their end-effector to perform the gripping, such as the example shown in Fig. 1.3a.

Unfortunately, a suction gripper is only useful for flat and smooth surfaces, such as solar cells or pancakes. These robots are therefore ill-suited for more advanced pick-and-place tasks that require the high-speed handling of delicate and/or irregular objects. One solution would be to attach an electromechanical gripper to the end-effector, as is shown for the example of a haptic device in Fig. 1.4. However, this solution puts sensitive components at the end-effector, which complicates cleaning, while particles released through wear of these components may conflict with hygiene requirements.

A second solution to enable grasping, also applied in the field of haptics, is to use two individual PMs simultaneously [22]. The downsides of the latter solution are the introduction of unnecessary degrees of freedom (DoFs), significant additional control complexity, and a doubling of the inertia. Therefore, neither a dedicated actuator at the end-effector, nor the use of two PMs, is considered a viable solution to extend pick-and-place robots beyond their current reach.

1.2.1. Parallel Manipulators with Two End-Effectors

A promising alternative solution for opening up new markets for pick-and-place robots is formed by a relatively novel class of PMs, which enable gripping through the introduction of internal DoFs that are realized using an internal closed-loop chain [24–27]. The first example of such a mechanism was described in 2002 by Yi et al., who showed that gripping robots can be designed with all motors located at the base, including those required for gripping [24].

Figure 1.5: A parallel manipulator with two end-effectors enables gripping through the introduction of an internal closed-loop chain, here shown for a 7-DoF haptic device [23].

Figure 1.6: a) Traditional joints require significant design effort to prevent play, friction, and backlash, while they also suffer from wear. b) Compliant joints do not suffer from these effects and therefore pose an interesting alternative (image adapted from Trease et al. [30]).

Gripping robots where all actuators are located at the base have two main advantages. Firstly, placement of the actuators at the base reduces the effective inertia, which is beneficial for the dynamic performance. Secondly, the fact that no actuators have to be integrated at the end-effector is beneficial for both cleaning and hygiene. In the literature, these manipulators have been referred to as parallel manipulators with configurable platforms (PMCPs) [27, 28] and non-series parallel mechanisms [29]. Since there is no established name for these robotic grippers, in this thesis these manipulators will be referred to as parallel manipulators with multiple end-effectors (PMxEs) to emphasize the multipoint contact involved in gripping. Because gripping is usually done using a two-point contact, this thesis focuses especially on Parallel Manipulators with Two End-Effectors (PM2Es), of which Fig. 1.5 shows a recent example.

1.2.2. Integration of Compliant Joints
One disadvantage of PMs is that they typically contain many passive joints. Passive joints are often realized using ball-bearings, which can introduce non-linear effects such as play, friction, and backlash. These non-linear effects are detrimental for both the accuracy and the dynamic performance of the PM. If hygiene is important, the lubrication

and wear of ball-bearings is also an issue, because released particles can contaminate the object being manipulated.

To avoid the issues associated with ball-bearings, the integration of compliant joints is a promising development. An example of a compliant joint is shown in Fig. 1.6b. Compliant joints facilitate motion through the deformation of material and can therefore be monolithic, which has several advantages [31]. Firstly, a monolithic joint does not require lubrication and has no wear so that no particles are produced, which is beneficial for hygiene. Secondly, because compliant joints do not require complex assembly, assembly costs can be greatly reduced. These properties make compliant joints interesting for use in pick-and-place robots as well as in other applications.

However, the integration of compliant joints also introduces new design challenges. One challenge is that they must be operated in their elastic range to ensure linear behavior. Because the elastic range is limited, this poses a challenge in the design of an adequate workspace. A second challenge is that the integration of compliant joints requires a careful consideration of the elastic forces and moments that they introduce. This thesis develops methods that enable the consideration of these forces and moments.

1.3. PROBLEM OF EXISTING STIFFNESS ANALYSIS METHODS

As was discussed in Section 1.1, stiffness is one of the key parameters in parallel manipulator design. Stiffness is determined by the combination of kinematic design, mechanical design and controlled actuator stiffness. The kinematic design describes how the individual bodies in a manipulator move with respect to each other. Many existing stiffness analyses rely on the classical matrix structural analysis (MSA) [15, 32] or its finer meshed brother of the computer age, the finite element method (FEM) [33]. These methods have been primarily developed for the analysis of mechanical structures and rely on computationally intensive numerical schemes to take kinematic relations into account. This makes these methods unsuitable for closed-loop control, where computing time is critical, as well as optimization, where symbolical methods are preferred because they provide "much more insight into the nature of the optimum design" compared to numeric models [34].

A symbolic stiffness analysis can be achieved by including the kinematic relations directly using Jacobian matrices. A Jacobian matrix describes how physical vectors, such as velocities, differential displacements, force and moments, can be transformed from a Cartesian space to a set of generalized coordinates and vice versa [35]. A set of generalized coordinates that consists only of joint coordinates is referred to as a joint space [36]. Jacobian matrices are symbolically expressed so that they can be evaluated at any valid pose of the manipulator. This makes them extremely useful for manipulator design and control, because the state of a robotic manipulator is often sensed in a joint space, while a manipulator is generally controlled in a Cartesian space [37]. Jacobian matrices are also at the basis of the standard symbolic expression of a PM's stiffness matrix [38].

Unfortunately, standard Jacobian analysis methods for parallel manipulators have not been extended to PM2Es, which thus prevents their effective design and control. A second problem is that existing Jacobian-based stiffness analysis methods for traditional PMs do not take the effect of loading into account, which is relevant if compliant joints are considered, while they also struggle to take the structural stiffness of PMs fully into

account. Both a complete stiffness analysis method and a Jacobian analysis are required to optimize PM2Es or to enable an effective integration of compliant joints in PM2Es. The absence of these analysis methods is thus blocking the road towards the optimal design of novel robotic grippers based on PM2Es.

1.4. THESIS OBJECTIVE AND OUTLINE

BECAUSE the opportunities posed by PM2Es as well as the integration of compliant joints can only be fully seized if an appropriate stiffness analysis is available, the objective of this thesis is

to develop a Jacobian-based stiffness analysis method for parallel manipulators that is also valid for compliant parallel manipulators with two end-effectors.

The outline of this thesis is visually represented in Fig. 1.7. First, Chapter 2 develops a novel Jacobian-based stiffness analysis method for parallel manipulators that is more general than existing Jacobian-based stiffness analysis methods. This generalization is required to extend Jacobian-based stiffness analysis to more complex mechanisms such as PM2Es and to take all aspects of compliant joint integration into account. To confirm that the mathematics in Chapter 2 are correct, the method is experimentally validated in Chapter 3. Additionally, in this chapter examples of the obtained stiffness matrices are presented, all of which are symmetric. This observation raises the question: why did previous research find asymmetric stiffness matrices? Chapter 4 answers that question by identifying and correcting the modeling error in a much-cited work from 1993 by Griffis and Duffy [39], which first reported such an asymmetric stiffness matrix.

The stiffness analysis that is proposed in Chapter 2 relies on Jacobian matrices. However, existing Jacobian analysis methods generally do not apply to PM2Es. Chapter 5 therefore develops a structured approach for the Jacobian analysis of PM2Es. Combination of this Jacobian analysis methods with the stiffness analysis method of Chapter 2 leads to a stiffness analysis method for PM2Es. In Chapter 6 it is verified for two partially compliant PM2Es that the resulting stiffness analyses have an accuracy that is similar to that of traditional PMs.

REFERENCES

[1] T. M. Anandan, *Robotics in 2014: Market diversity, cobots and global investment,* http://www.robotics.org/content-detail.cfm/Industrial-Robotics-Industry-Insights/Robotics-in-2014-Market-Diversity-Cobots-and-Global-Investment/content_id/4614 (2014), accessed: Dec, 2015.

[2] International Federation of Robotics, *Industrial robot statistics,* http://www.ifr.org/industrial-robots/statistics/ (2015), accessed: Dec, 2015.

[3] J. Manyika, M. Chui, J. Bughin, R. Dobbs, P. Bisson, and A. Marrs, *Disruptive technologies: Advances that will transform life, business, and the global economy*, Tech. Rep. (McKinsey Global Institute, 2013, p. 75).
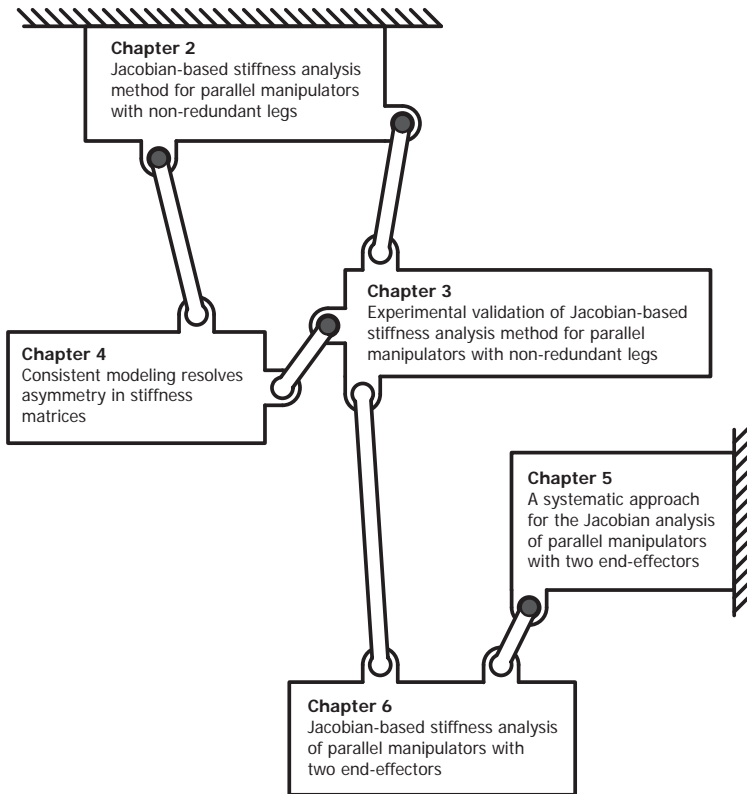
Figure 1.7: An overview of the chapters in this thesis and their cohesion. The dark gray dots indicate that the considered chapter is a driving force for the connected chapter.

[4] *Robotics 2020 Multi-Annual Roadmap*, Tech. Rep. (SPARC, 2015).

[5] *Ampelmann Operations,* http://www.yesdelft.nl/DetailsCompany/CompanyID/6, accessed: Dec, 2015.

[6] *The SIMONA Research Simulator,* http://www.simona.tudelft.nl/, accessed: Dec, 2015.

[7] Y. Jin, Z. M. Bi, H. T. Liu, C. Higgins, M. Price, W. H. Chen, and T. Huang, *Kinematic Analysis and Dimensional Synthesis of Exechon Parallel Kinematic Machine for Large Volume Machining,* Journal of Mechanisms and Robotics **7**, 041004 (2015).

[8] *Simodont dental trainer,* http://www.moog.com/literature/ICD/Moog-Haptics-SimodontDentalTrainer-Datasheet-en.pdf (2014), accessed: Dec, 2015.

[9] ABB, *Efficient robot-based automation for solar cell and module production,* https:

1

//library.e.abb.com/public/59fc86166d477f41c125766b004d05d5/
Solarbroschuere_engl_Internet.pdf (2009), accessed: Dec, 2015.

[10] L.-W. Tsai, *Design of Tendon-Driven Manipulators,* Journal of Vibration and Acoustics **117**, 80 (1995).

[11] M. Hiller, S. Fang, S. Mielczarek, R. Verhoeven, and D. Franitza, *Design, analysis and realization of tendon-based parallel manipulators,* Mechanism and Machine Theory **40**, 429 (2005).

[12] S. Briot and I. A. Bonev, *Are Parallel Robots More Accurate than Serial Robots?* Transactions of the Canadian Society for Mechanical Engineering **31**, 445 (2007).

[13] J.-P. Merlet, *Parallel Robots*, 2nd ed., edited by G. Gladwell, Solid Mechanics and its Application, Vol. 128 (Springer, Dordrecht, 2006).

[14] J. Hesselbach, J. Wrege, A. Raatz, and O. Becker, *Aspects on design of high precision parallel robots,* Assembly Automation **24**, 49 (2004).

[15] W. Dong, L. Sun, and Z. Du, *Stiffness research on a high-precision, large-workspace parallel mechanism with compliant joints,* Precision Engineering **32**, 222 (2008).

[16] T. J. Teo, G. Yang, and I.-M. Chen, *A large deflection and high payload flexure-based parallel manipulator for UV nanoimprint lithography: Part I. Modeling and analyses,* Precision Engineering **38**, 861 (2014).

[17] I. Prause, T. Mbarek, and B. Corves, *Increasing the stiffness of a 3-PUU parallel kinematic positioning device for high payloads by modifying the leg configuration,* in *Proceedings of 2014 Workshop on Fundamental Issues and Future Research Directions for Parallel Mechanisms and Manipulators* (2014).

[18] M. Wang, H. Liu, T. Huang, and D. G. Chetwynd, *Compliance analysis of a 3-SPR parallel mechanism with consideration of gravity,* Mechanism and Machine Theory **84**, 99 (2015).

[19] ABB, *IRB 360 FlexPicker™,* http://new.abb.com/products/robotics/industrial-robots/irb-360, accessed: Dec, 2015.

[20] J. Huston, *Healthy production, healthy profit,* Packaging Magazine (2008).

[21] Force Dimension, *omega.7,* http://www.forcedimension.com/products/omega-7/overview, accessed: Dec, 2015.

[22] S. Mulatto, A. Formaglio, M. Malvezzi, and D. Prattichizzo, *Using Postural Synergies to Animate a Low-Dimensional Hand Avatar in Haptic Simulation,* IEEE Transactions on Haptics **6**, 106 (2013).

[23] P. Lambert and J. Herder, *A novel parallel haptic device with 7 degrees of freedom,* in *2015 IEEE World Haptics Conference (WHC)*, Vol. 31 (IEEE, 2015) pp. 183–188.

1

[24] B.-J. Yi, Y. N. Heung, H. L. Jae, Y.-S. Hong, S.-R. Oh, I. H. Suh, and W. K. Kim, *Design of a Parallel-Type Gripper Mechanism,* The International Journal of Robotics Research **21**, 661 (2002).

[25] B.-J. Park, B.-J. Yi, and W.-K. Kim, *Design and analysis of a new parallel grasper having spherical motion,* in *2004 IEEE/RSJ International Conference on Intelligent Robots and Systems (IROS) (IEEE Cat. No.04CH37566),* Vol. 1 (IEEE, 2004) pp. 106–111.

[26] V. Nabat, M. de la O Rodriguez, O. Company, S. Krut, and F. Pierrot, *Par4: very high speed parallel robot for pick-and-place,* in *IEEE/RSJ International Conference on Intelligent Robots and Systems* (IEEE, 2005) pp. 553–558.

[27] P. Lambert, *Parallel Robots with Configurable Platforms,* Phd thesis, Delft University of Technology (2013).

[28] M. G. Mohamed and C. M. Gosselin, *Design and analysis of kinematically redundant parallel manipulators with configurable platforms,* IEEE Transactions on Robotics **21**, 277 (2005).

[29] P. Lambert and J. L. Herder, *Mobility Analysis of Non Series-Parallel Mechanisms,* in *New Trends in Mechanism and Machine Science,* Mechanisms and Machine Science, Vol. 7, edited by F. Viadero and M. Ceccarelli (Springer Netherlands, Dordrecht, 2013) pp. 63–71.

[30] B. P. Trease, Y.-M. Moon, and S. Kota, *Design of Large-Displacement Compliant Joints,* Journal of Mechanical Design **127**, 788 (2005).

[31] L. L. Howell, *Compliant Mechanisms,* in *21st Century Kinematics* (Springer London, London, 2013) pp. 189–216.

[32] G. D. L. Soares Júnior, J. C. M. Carvalho, and R. S. Gonçalves, *Stiffness analysis of multibody systems using matrix structural analysis—MSA,* Robotica , 1 (2015).

[33] S. K. Dwivedy and P. Eberhard, *Dynamic analysis of flexible manipulators, a literature review,* Mechanism and Machine Theory **41**, 749 (2006).

[34] P. Y. Papalambros and J. W. Douglas, *Principles of Optimal Design* (Cambridge University Press, Cambridge, UK, 2000) p. 17.

[35] S. A. Joshi and L.-W. Tsai, *Jacobian Analysis of Limited-DOF Parallel Manipulators,* Journal of Mechanical Design **124**, 254 (2002).

[36] R. M. Murray, Z. Li, and S. S. Sastry, *A Mathematical Introduction to Robotic Manipulation* (CRC Press, 1994).

[37] S. Tadokoro, *Control of parallel mechanisms,* Advanced Robotics **8**, 559 (1993).

[38] C. Gosselin, *Stiffness mapping for parallel manipulators,* IEEE Transactions on Robotics and Automation **6**, 377 (1990).

[39] M. Griffis and J. Duffy, *Global stiffness modeling of a class of simple compliant couplings,* Mechanism and Machine Theory **28**, 207 (1993).

2

JACOBIAN-BASED STIFFNESS ANALYSIS METHOD FOR PARALLEL MANIPULATORS WITH NON-REDUNDANT LEGS

Throw a stone and watch the ripples flow
Moving out across the bay

David Gray
David Gray - Please forgive me

Stiffness is an important element in the model of a parallel manipulator. A complete stiffness analysis includes the contributions of joints as well as structural elements. Parallel manipulators potentially include both actuated joints, passive compliant joints, and zero stiffness joints, while a leg may impose constraints on the end-effector in the case of lower mobility parallel manipulators. Additionally, parallel manipulators are often designed to interact with an environment, which means that an external wrench may be applied to the end-effector. Also, the integration of compliant joints may introduce internal loading. This chapter presents a Jacobian-based stiffness analysis method, based on screw theory, that effectively considers all above aspects and which also applies to parallel manipulators with non-redundant legs. As such, this chapter generalizes much of the existing Jacobian-based stiffness analysis methods.

2.1. Introduction to Stiffness Analysis of Parallel Manipulators

Parallel manipulators consist of multiple serial chains that connect an end-effector to an inertial base. Ever since parallel manipulators first entered the industrial market, they have been praised for their high end-effector position accuracy and fast dynamics compared to traditional serial manipulators. To design and optimize a parallel manipulator for the desired accuracy and dynamic performance, a mathematical model is developed. An important parameter in this model is the Cartesian stiffness matrix, which expresses the stiffness of the end-effector body relative to the inertial base.

The main elements in the stiffness analysis of parallel manipulators are the actuated joints [2]. If the design includes passive compliant joints, where relative motion is due to deformation of slender segments within the joint instead of relative motion between rigid parts, their stiffness is also considered [3–5]. The structural stiffness of links has been analysed for applications with fast and precise dynamics [6–8], as well as in the analysis of compliant manipulators [9–14].

A symbolic expression of the Cartesian stiffness matrix is often valuable, e.g. for optimization purposes in the early design phase. A well-known method to symbolically express the Cartesian stiffness matrix was introduced by Salisbury and Craig [15]. Their method uses the Jacobian to map actuator stiffness from joint space to Cartesian space and applies to serial manipulators in which all actuators are modelled as springs. Gosselin [16] developed an equivalent analysis for parallel manipulators. Chen and Kao [17] extended the analysis that was presented by Salisbury and Craig to account for a change in force transmission as a result of a small, finite deflection from the instantaneous pose. Measurements by Alici and Shirinzadeh [18] confirmed this effect. Quennouelle and Gosselin [19] later integrated these results in their stiffness analysis method for parallel mechanisms, which also considered the presence of compliant joints.

More detailed stiffness analysis methods also consider the finite stiffness of links. Symbolic expressions of structural stiffness matrices are typically developed using a combination of linear beam theory and the rules for addition of elastic elements in series and parallel. The variation lies in the implementation. If compliant parallel manipulators are concerned, the implementation is relatively straightforward, because the Cartesian stiffness matrices of individual legs are invertible [9, 10]. However, if a leg contains zero stiffness joints, the Cartesian stiffness matrix of this leg will be singular. Therefore, often only the stiffness along the actuated load vector is considered [20–22]. In the Virtual Joint Method (VJM) this is achieved through a lumped representation of the elasticity in links by virtual joints (see Fig. 2.1) [23]. The VJM has also been applied to represent the stiffness in constrained directions of lower mobility parallel manipulators (also known as limited-DoF parallel manipulators) with a properly constrained passive leg [24, 25]. Using a comparable approach of stiffness mapping, Li and Xu [26] included the stiffness in constrained directions for a 3-PUU manipulator. A method that uses the VJM to analyse the stiffness of a general lower mobility parallel manipulators was developed by Pashkevich et al. [27].

However, the method by Pashkevich et al. has its shortcomings. The first is that many of the introduced virtual joint coordinates are dependent. As a result, their method re-
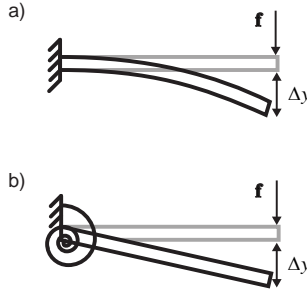
Figure 2.1: a) The finite compliance of a link results in a deformation under loading. b) In the Virtual Joint Method this distributed compliance is lumped and represented by a virtual spring with equivalent stiffness.

quires inversion of relatively large matrices, which is computational expensive. Methods to alleviate the computational burden were proposed by Klimchik et al. [28], but at the expense of an additional implementation effort. Secondly, the effect of an external load applied at the end-effector is not considered in this method.

This chapter aims to develop a stiffness analysis method that is valid for lower mobility manipulators, and which considers the presence of compliant joints, the finite stiffness of links, and also recognises the effect of an applied load. The structure of this chapter is as following. First, a novel Jacobian-based stiffness analysis method will be developed. Next, the developed stiffness analysis method will be applied to a 3-R̲RR mechanism as an example. Finally, the analysis will be simplified for several specific cases, followed by a discussion on the limitations of the presented analysis method.

2.2. NOVEL JACOBIAN-BASED STIFFNESS ANALYSIS METHOD

I̲N this section a stiffness analysis method will be developed, starting from the static equilibrium equation. Insights from Jacobian analysis methods will be used to deal with the possible presence of zero stiffness joints.

A parallel manipulator consists of multiple serial chains (in this thesis referred to as *legs*) that connect the same end-effector to an inertial base. The displacement twist of the end-effector is defined as $\$_d = [d\boldsymbol{\phi}^\top \quad d\mathbf{p}^\top]^\top$, where $d\boldsymbol{\phi}$ and $d\mathbf{p}$ are the differential rotational and linear displacements of the end-effector, considered at the point that coincides with the origin of a defined Cartesian end-effector reference frame.

The wrench whose transpose maps $\$_d$ on the scalar field of work is $\$_w = [\mathbf{m}^\top \quad \mathbf{f}^\top]^\top$, where $\mathbf{m}$ is a moment applied on the end-effector at the point that coincides with the origin of the Cartesian end-effector reference frame and $\mathbf{f}$ is a force applied to the end-effector. In a static equilibrium

$$\$_{w,pm} = -\$_{w,ext} \tag{2.1}$$

where $\$_{w,ext}$ is the net wrench applied on the end-effector by the environment and $\$_{w,pm}$ is the net wrench applied on the end-effector by all legs of the parallel manip-

ulator, so

$$\$_{w,pm} = \sum_{i=1}^{N} \$_{w,i} \tag{2.2}$$

where $\$_{w,i}$ is the wrench applied on the end-effector by leg i, for a parallel manipulator with N legs.

In the remainder of this section, first the basic assumptions are listed. Next, an existing Jacobian analysis method is used to express joint torques as a wrench in the defined Cartesian end-effector reference frame. A derivation of this wrench then leads to an expression for the Cartesian stiffness matrix.

2.2.1. BASIC ASSUMPTIONS
In the analysis presented in this chapter, several assumptions are made. Firstly, it is assumed that the manipulator is in a static equilibrium and that all wrenches exerted by the parallel manipulator on the end-effector are caused by elastic deformations, and therefore are all conservative. As such, actuators are modelled as springs, which means that proportional control is assumed to dominate the actuator torque. All other wrenches acting on the end-effector are combined in a single external wrench.

It is also assumed that the vector τ, which is the vector containing all joint torques in the parallel manipulator, can be determined based on the configuration of the manipulator. This determination is a separate topic and will not be further discussed in this chapter.

In addition it is assumed that the parallel manipulator has $0 < F \leq 6$ Degrees of Freedom (DoFs), with $N \geq F$. It is further assumed that there are no redundant kinematic joints in each leg (see Wang and Gosselin [29] for an example of a parallel manipulator with redundant joints). Then, the number of 1-DoF joints in leg i is equal to its number of kinematic degrees of freedom, which Joshi and Tsai [30] refer to as the leg's connectivity C_i.

Finally, while the finite structural stiffness of the legs will be included in the analysis, it is assumed that the end-effector body and the inertial body are rigid.

2.2.2. FULL INVERSE JACOBIAN ANALYSIS
Typically, the various wrenches $\$_{w,i}$ in Eq. (2.2) are not directly available, but are expressed as a function of a vector τ_i, which is the vector containing all joint torques in leg i of the parallel manipulator. A Jacobian matrix is used to transform τ_i into $\$_{w,i}$. Here we will briefly summarize the Jacobian analysis presented by Huang et al. [31], which is an extension of work by Joshi and Tsai. [30]. The method is based on screw theory and uses the reciprocity of twists and wrenches to define a set of six linearly independent twists and a set of six linearly independent wrenches.[1]

Each of the linearly independent twists, as defined in Ref. [31], maps a single joint velocity onto end-effector Cartesian space. With the assumptions made earlier in this chapter, C_i of these twists can be associated with joints that are physically present in the leg. These twists are referred to as the *twists of permission*. Another $6 - C_i$ twists

---

[1]Earlier, Ling and Huang [32] came to a similar result, but due to its more intuitive interpretation, this chapter will use the method developed by Huang et al. [31].
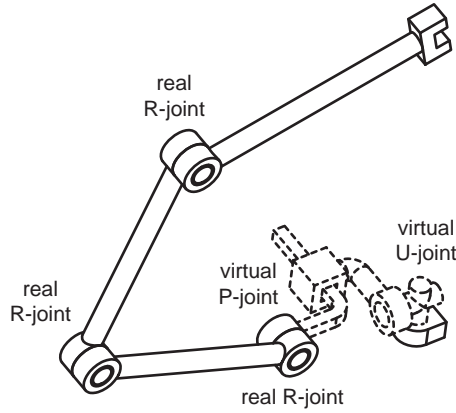
Figure 2.2: The constraints imposed by a leg can be represented by a set of virtual, locked joints, here illustrated for a 3-RRR leg.

are referred to as the *twists of restriction* and are associated with the constrained directions. Because twists describe the instantaneous motion along a screw axis, the twists of restriction allow the constrained directions of a leg to be presented by a set of instantaneous virtual, locked joints. This is illustrated for the example of a 3-RRR leg in Fig. 2.2. Because the end-effector is the terminal link of each individual leg, the end-effector displacement twist can be expressed as

$$\$_d = \sum_{j=1}^{C_i} dq_{a_{i,j}} \hat{\$}_{ta_{i,j}} + \sum_{k=1}^{6-C_i} dq_{c_{i,k}} \hat{\$}_{tc_{i,k}} \tag{2.3}$$

where $\hat{\$}_{ta_{i,j}}$ is the twist of permission that maps a unit differential displacement of the jth real joint of leg i onto $\$_d$, with $dq_{a_{i,j}}$ its intensity. The unit twist of restriction $\hat{\$}_{tc_{i,k}}$ maps the unit differential displacement of the kth virtual joint of leg i onto $\$_d$, with intensity $dq_{c_{i,k}}$.

Together, these unit twists of permission and unit twists of restriction form a set of six linearly independent unit twists. Such set can be defined for any non-redundant leg, including those of lower mobility parallel manipulators. The unit twists of restriction are generally not unique, but Huang et al. [33] describe how unique solutions can be found through the introduction of some simple additional conditions, which hold for most existing parallel manipulators.

Additionally, a set of six linearly independent unit wrenches can be defined, where each unit wrench is associated with a single joint. Each of these wrenches is reciprocal to all twists in Eq. (2.3) except one. Therefore, for each leg C_i unit *wrenches of actuation* can be found, where each unit wrench of actuation is associated to a separate real joint. Another $6 - C_i$ unit wrenches can be found which are each associated with one of the virtual joints, and are termed unit *wrenches of constraint*.

Based on the reciprocity relations between the defined twists and wrenches, left-multiplication of both sides of Eq. (2.3) with the transpose of each of the unit wrenches

of actuation and unit wrenches of constraint leads to the inverse Jacobian matrix of leg i [31]

$$\mathbf{J}_i^{-1}\$_d = d\mathbf{q}_i \tag{2.4}$$

with

$$\dim(\mathbf{q}_i) = 6 \tag{2.5}$$

and

$$\mathbf{J}_i^{-1} = \begin{bmatrix} \hat{\$}_{wa_{i,1}}^\top / (\hat{\$}_{wa_{i,1}}^\top \hat{\$}_{ta_{i,1}}) \\ \hat{\$}_{wa_{i,2}}^\top / (\hat{\$}_{wa_{i,2}}^\top \hat{\$}_{ta_{i,2}}) \\ \vdots \\ \hat{\$}_{wa_{i,C_i}}^\top / (\hat{\$}_{wa_{i,C_i}}^\top \hat{\$}_{ta_{i,C_i}}) \\ \hat{\$}_{wc_{i,1}}^\top / (\hat{\$}_{wc_{i,1}}^\top \hat{\$}_{tc_{i,1}}) \\ \hat{\$}_{wc_{i,2}}^\top / (\hat{\$}_{wc_{i,2}}^\top \hat{\$}_{tc_{i,2}}) \\ \vdots \\ \hat{\$}_{wc_{i,6-C_i}}^\top / (\hat{\$}_{wc_{i,6-C_i}}^\top \hat{\$}_{tc_{i,6-C_i}}) \end{bmatrix} \tag{2.6}$$

where $\hat{\$}_{wa_{i,j}}$ is the unit wrench of actuation associated with the jth real joint, while $\hat{\$}_{wc_{i,k}}$ is the unit wrench of constraint associated with the kth virtual joint of leg i. See Huang et al. [31] for more details.

The inverse Jacobian matrix presented in Eq. (2.6) transforms the end-effector displacement twist into a vector containing the differential displacements of all joints of leg i, both real and virtual. Because each row in $\mathbf{J}_i^{-1}$ maps the end-effector displacement twist onto one differential joint displacement, a given order in which the differential joint displacements appear in $d\mathbf{q}_i$ determines the order of the rows in $\mathbf{J}_i^{-1}$, or vice versa. The inverse Jacobian expressed by Eq. (2.6) is a 6×6 matrix and will be referred to as the *full inverse Jacobian* of leg i. It is a function of the instantaneous configuration of the parallel manipulator.

Equation (2.4) applies to each individual leg, so that for the complete parallel manipulator it holds that

$$\mathbf{J}^{-1}\$_d = d\mathbf{q} \tag{2.7}$$

with

$$\mathbf{J}^{-1} = \begin{bmatrix} \mathbf{J}_1^{-1} \\ \mathbf{J}_2^{-1} \\ \vdots \\ \mathbf{J}_N^{-1} \end{bmatrix} \tag{2.8}$$

$$d\mathbf{q} = \begin{bmatrix} d\mathbf{q}_1^\top & d\mathbf{q}_2^\top & \cdots & d\mathbf{q}_N^\top \end{bmatrix}^\top \tag{2.9}$$

where $\mathbf{J}^{-1}$ is the full inverse Jacobian of the parallel manipulator and $d\mathbf{q}$ is the vector that contains all differential joint displacements. As such, $\mathbf{q}$ is the vector containing all joint coordinates, both real and virtual, with $\dim(\mathbf{q}) = 6N$.

2.2.3. JACOBIAN OF ELASTICITY FOR PARALLEL MANIPULATOR

Because the work delivered by each leg is independent of the coordinate frame in which it is expressed

$$\$_{w,i}^\top \$_d = \boldsymbol{\tau}_i^\top d\mathbf{q}_i \tag{2.10}$$

where $\boldsymbol{\tau}_i$ is thus the vector that maps $d\mathbf{q}_i$ onto work. Combination of Eqs. (2.4) and (2.10) results in

$$\$_{w,i}^\top \$_d = \boldsymbol{\tau}_i^\top \mathbf{J}_i^{-1} \$_d \tag{2.11}$$

and therefore

$$\$_{w,i} = \mathbf{J}_i^{-\top} \boldsymbol{\tau}_i \tag{2.12}$$

where the order of the joints associated to the torques in $\boldsymbol{\tau}_i$ is thus equal to that of $d\mathbf{q}_i$.

In this chapter, all joints of the parallel manipulator are modelled as springs. However, different joints have different properties:

1. **actuated joints** have a stiffness that is controllable. The joint torque transferred by an actuated joint is τ_a, which depends on its position, q_a, with respect to a controllable reference position.

2. **passive, compliant joints** have a finite stiffness that depends on the specific design. This type of joint transfers a joint torque τ_{pc}, related to its position q_{pc} with respect to its unloaded position.

3. **passive, zero stiffness joints** are not capable of transferring a torque, so $\tau_{pz} = 0$ for all positions q_{pz}. An example of a joint that can be modelled as a zero stiffness joint is a ball-bearing joint.

4. **virtual joints** are a representation of the directions in which the leg is constrained. They represent the instantaneous motion directions which are not permitted by the kinematic model, but which are feasible in practice due to the finite structural stiffness of joints and links. Then, the equivalent joint torque τ_c represents the elastic force resulting from a deformation that can be represented by a deflection dq_c of the virtual joint. Because the virtual joints themselves are mere constructs, as was illustrated in Fig. 2.2, they have no physical properties and are represented in the kinematic model as locked joints, i.e. as joints with infinite stiffness, or zero compliance.

Since the order in which joints appear in the joint coordinate vector is arbitrary, we can define

$$\mathbf{q}_i = \begin{bmatrix} \mathbf{q}_{a,i}^\top & \mathbf{q}_{pc,i}^\top & \mathbf{q}_{pz,i}^\top & \mathbf{q}_{c,i}^\top \end{bmatrix}^\top \tag{2.13}$$

Because Eq. (2.10), this also determines

$$\boldsymbol{\tau}_i = \begin{bmatrix} \boldsymbol{\tau}_{a,i}^\top & \boldsymbol{\tau}_{pc,i}^\top & \boldsymbol{\tau}_{pz,i}^\top & \boldsymbol{\tau}_{c,i}^\top \end{bmatrix}^\top \tag{2.14}$$

The torque transferred by the zero stiffness joints is zero at all times, so if a leg contains Z_i zero stiffness joints, then $\boldsymbol{\tau}_{pz,i} = \mathbf{0}_{Z_i \times 1}$. This means that the equivalent wrench in

Cartesian end-effector space does not depend on $\boldsymbol{\tau}_{pz,i}$ and Eq. (2.12) can also be written as

$$\$_{w,i} = \mathbf{J}_{e,i}^{-\top} \boldsymbol{\tau}_{e,i} \tag{2.15}$$

where

$$\boldsymbol{\tau}_{e,i} = \begin{bmatrix} \boldsymbol{\tau}_{a,i}^{\top} & \boldsymbol{\tau}_{pc,i}^{\top} & \boldsymbol{\tau}_{c,i}^{\top} \end{bmatrix}^{\top} \tag{2.16}$$

and $\mathbf{J}_{e,i}^{-1}$ is termed the inverse *Jacobian of elasticity* of leg i. It is obtained from $\mathbf{J}_i^{-1}$, expressed in Eq. (2.6), by removing the rows associated to the zero stiffness joints. With this definition, it holds that

$$\mathbf{J}_{e,i}^{-1} \$_d = d\mathbf{q}_{e,i} \tag{2.17}$$

with

$$d\mathbf{q}_{e,i} = \begin{bmatrix} d\mathbf{q}_{a,i}^{\top} & d\mathbf{q}_{pc,i}^{\top} & d\mathbf{q}_{c,i}^{\top} \end{bmatrix}^{\top} \tag{2.18}$$

where $\mathbf{q}_{e,i}$ is thus the vector containing all joint coordinates of leg i except those of the zero stiffness joints. The components of the vector $\mathbf{q}_{e,i}$ will be referred to as the *elastic joint coordinates* of leg i and its associated unit twists are said to span the *elastic joint space*.

Earlier we concluded that if a leg contains C_i real joints, the number of virtual joints is $6 - C_i$, so that $\dim(\mathbf{q}_{c,i}) = 6 - C_i$. If we now consider a leg with A_i actuated joints and Z_i zero stiffness joints, then $\dim(\mathbf{q}_{a,i}) = A_i$, $\dim(\mathbf{q}_{pz,i}) = Z_i$, and thus $\dim(\mathbf{q}_{pc,i}) = C_i - A_i - Z_i$. As a result,

$$\dim(\mathbf{q}_{e,i}) = \dim(\boldsymbol{\tau}_{e,i}) = 6 - Z_i \tag{2.19}$$

and $\mathbf{J}_{e,i}^{-1}$ is a $(6 - Z_i) \times 6$ matrix.

Because the wrench that is applied by each leg on the end-effector is expressed by Eq. (2.15), Eq. (2.2) can be rewritten in the form

$$\$_{w,pm} = \mathbf{J}_e^{-\top} \boldsymbol{\tau}_e \tag{2.20}$$

where

$$\mathbf{J}_e^{-\top} = \begin{bmatrix} \mathbf{J}_{e,1}^{-\top} & \mathbf{J}_{e,2}^{-\top} & \cdots & \mathbf{J}_{e,N}^{-\top} \end{bmatrix}, \tag{2.21}$$

$$\boldsymbol{\tau}_e = \begin{bmatrix} \boldsymbol{\tau}_{e,1}^{\top} & \boldsymbol{\tau}_{e,2}^{\top} & \cdots & \boldsymbol{\tau}_{e,N}^{\top} \end{bmatrix}^{\top} \tag{2.22}$$

Equation (2.20) thus expresses the net wrench applied by the legs of the parallel manipulator on the end-effector as a function of the instantaneous configuration of the parallel manipulator and the torques of all joints except those with zero stiffness.

2.2.4. STIFFNESS ANALYSIS METHOD
Following the standard definition of positive stiffness, where a displacement results in an opposing force, the Cartesian stiffness matrix of the manipulator is obtained by taking the negative of the derivative of $\$_{w,pm}$ with respect to the six basis vectors of Cartesian space,

$$\mathbf{K} = -\frac{d\$_{w,pm}}{d\mathbf{x}} \tag{2.23}$$

where $\mathbf{K}$ is the Cartesian stiffness matrix of the end-effector body relative to the inertial base, expressed in the end-effector reference frame. This 6×6 tensor can only be defined if the end-effector can indeed be displaced along all six basis vectors of Cartesian space [34]. In this chapter the finite stiffness of the structural elements of a parallel manipulator will be included in the analysis model, which means that the end-effector can be displaced in any direction irrespective of the kinematic DoFs of the manipulator.

Combination of Eq. (2.20) and Eq. (2.23) gives

$$\mathbf{K} = -\frac{d\left(\mathbf{J}_e^{-\top}\boldsymbol{\tau}_e\right)}{d\mathbf{x}} \tag{2.24}$$

Application of the chain rule then leads to

$$\mathbf{K} = \left(-\frac{\partial \mathbf{J}_e^{-\top}}{\partial \mathbf{q}}\boldsymbol{\tau}_e\right)\frac{d\mathbf{q}}{d\mathbf{x}} - \mathbf{J}_e^{-\top}\frac{\partial \boldsymbol{\tau}_e}{\partial \mathbf{q}}\frac{d\mathbf{q}}{d\mathbf{x}} \tag{2.25}$$

Expressions for the required terms in Eq. (2.25) are developed below.

Expression for the term $\frac{\partial \mathbf{J}_e^{-\top}}{\partial \mathbf{q}}\boldsymbol{\tau}_e$.

As is discussed in more detail by e.g. Chen and Kao [17],

$$\frac{\partial \mathbf{J}_e^{-\top}}{\partial \mathbf{q}}\boldsymbol{\tau}_e = \begin{bmatrix} \frac{\partial \mathbf{J}_e^{-\top}}{\partial q_{1,1}}\boldsymbol{\tau}_e & \frac{\partial \mathbf{J}_e^{-\top}}{\partial q_{1,2}}\boldsymbol{\tau}_e & \cdots & \frac{\partial \mathbf{J}_e^{-\top}}{\partial q_{N,6}}\boldsymbol{\tau}_e \end{bmatrix} \tag{2.26}$$

where in this case each term $(\partial \mathbf{J}_e^{-\top})/(\partial q_{i,m})\boldsymbol{\tau}_e$ is a 6×1 column vector, with $i = 1\ldots N$, and where $q_{i,m}$ is the mth element of the vector defined in Eq. (2.13).

Expression for the term $\frac{\partial \boldsymbol{\tau}_e^{\top}}{\partial \mathbf{q}}\frac{d\mathbf{q}}{d\mathbf{x}}$.

Because all joint torques, including those associated to the virtual joints, are assumed to be the result of elastic deformations, we can express $\boldsymbol{\tau}_e$ as

$$\boldsymbol{\tau}_e = -\int_{\mathbf{q}_0}^{\mathbf{q}} \mathbf{K}_q d\mathbf{q} \tag{2.27}$$

where $\mathbf{K}_q$ is the stiffness matrix which maps a differential joint displacement vector $d\mathbf{q}$ onto a differential joint torque vector $d\boldsymbol{\tau}_e$. Using Eq. (2.27) and the Leibniz integral rule

$$\frac{\partial \boldsymbol{\tau}_e}{\partial \mathbf{q}}\frac{d\mathbf{q}}{d\mathbf{x}} = -\mathbf{K}_q\frac{d\mathbf{q}}{d\mathbf{x}} \tag{2.28}$$

In traditional stiffness analyses, in which links are assumed infinitely rigid, $\mathbf{K}_q$ is a diagonal matrix containing the individual joint stiffness values [35]. If the finite stiffness of links is also included, this matrix will not be a diagonal matrix and will need to be obtained using a different approach, as is outlined below.

To include the finite stiffness of links in the stiffness analysis, we make use of the stiffness rules for series and parallel connections,

$$\mathbf{K} = \sum_i \mathbf{K}_i \quad \text{for parallel connections} \tag{2.29}$$

$$\mathbf{K}^{-1} = \sum_i \mathbf{K}_i^{-1} \quad \text{for series connections} \tag{2.30}$$

In a parallel manipulator, the matrix $\mathbf{K}$ is thus the summation of the stiffness matrices of the individual parallel connections between the inertial base and the end-effector. Since the inertial base and the end-effector were assumed rigid, each of these individual parallel connections is formed by one individual leg. If this summation is expressed in joint space it becomes the block-diagonal concatenation of the stiffness matrices of individual legs, because each leg has its own set of joint coordinates. For a parallel manipulator with N legs, Eq. (2.28) can then be written as

$$-\mathbf{K}_q \frac{d\mathbf{q}}{d\mathbf{x}} = -\begin{bmatrix} \mathbf{K}_{q,1} & \mathbf{0} & \cdots & \mathbf{0} \\ \mathbf{0} & \mathbf{K}_{q,2} & \cdots & \mathbf{0} \\ \vdots & \vdots & \ddots & \vdots \\ \mathbf{0} & \mathbf{0} & \cdots & \mathbf{K}_{q,N} \end{bmatrix} \begin{bmatrix} \frac{d\mathbf{q}_1}{d\mathbf{x}} \\ \frac{d\mathbf{q}_2}{d\mathbf{x}} \\ \vdots \\ \frac{d\mathbf{q}_N}{d\mathbf{x}} \end{bmatrix} \tag{2.31}$$

where

$$\mathbf{K}_{q,i} = \frac{\partial \boldsymbol{\tau}_{e,i}}{\partial \mathbf{q}_i} \tag{2.32}$$

is the stiffness matrix of the ith leg, expressed in joint space. It is a tensor that maps a differential joint displacement vector $d\mathbf{q}_i$ onto a differential joint torque vector $d\boldsymbol{\tau}_{e,i}$. Because Eqs. (2.5) and (2.19), each tensor $\mathbf{K}_{q,i}$ is a $(6 - Z_i) \times 6$ matrix. Thus, $\mathbf{K}_{q,i}$ is generally not a square matrix.

The fact that $\mathbf{K}_{q,i}$ generally is not a square matrix is problematic, because in this paper it is obtained by inverting a matrix $\mathbf{K}_{q,i}^{-1}$. The inverse of stiffness is called compliance, so Eq. (2.30) states that the compliance matrix for an individual leg, $\mathbf{K}_{q,i}^{-1}$, can be constructed by adding the compliance matrices of its serially connected parts. Then, to obtain $\mathbf{K}_{q,i}$, this matrix is inverted and should therefore be a non-singular square matrix.

In order to obtain a non-singular square stiffness matrix in joint space, the assumption is made that

$$\frac{\partial \boldsymbol{\tau}_{e,i}}{\partial \mathbf{q}_{pz,i}} \frac{d\mathbf{q}_{pz,i}}{d\mathbf{x}} \approx 0, \tag{2.33}$$

which means that the change in joint torques caused by a displacement of a passive, zero stiffness joint as a function of an end-effector displacement is negligible. With this assumption in place, $\mathbf{K}_{q,i}$ only acts on the vector components of $d\mathbf{q}_i$ associated to joints with a non-zero stiffness. Because in Eq. (2.18) the vector that contains these joints was defined as $\mathbf{q}_{e,i}$, the assumption presented in Eq. (2.33) allows Eq. (2.28) to be written as

$$\frac{\partial \boldsymbol{\tau}_e}{\partial \mathbf{q}} \frac{d\mathbf{q}}{d\mathbf{x}} \approx \frac{\partial \boldsymbol{\tau}_e}{\partial \mathbf{q}_e} \frac{d\mathbf{q}_e}{d\mathbf{x}} = -\mathbf{K}_{q,e} \frac{d\mathbf{q}_e}{d\mathbf{x}} \tag{2.34}$$

with

$$\mathbf{K}_{q,e} = \begin{bmatrix} \mathbf{K}_{q,e,1} & \mathbf{0} & \cdots & \mathbf{0} \\ \mathbf{0} & \mathbf{K}_{q,e,2} & \cdots & \mathbf{0} \\ \vdots & \vdots & \ddots & \vdots \\ \mathbf{0} & \mathbf{0} & \cdots & \mathbf{K}_{q,e,N} \end{bmatrix} \tag{2.35}$$

and where each stiffness matrix $\mathbf{K}_{q,e,i}$ is an invertible $(6 - Z_i) \times (6 - Z_i)$ matrix that acts on $d\mathbf{q}_{e,i}$.

To construct each matrix $\mathbf{K}_{q,e,i}$, Eq. (2.30) is used. In this chapter it is chosen to express this equation as a summation of two parts: one part that only includes the compliance of all joints in their kinematic DoF, the *kinematic compliance matrix*, $\mathbf{K}_{q,e,k,i}^{-1}$, and another part that represents the *structural compliance matrix*, $\mathbf{K}_{q,e,s,i}^{-1}$. Then

$$\mathbf{K}_{q,e,i}^{-1} = \mathbf{K}_{q,e,k,i}^{-1} + \mathbf{K}_{q,e,s,i}^{-1} \tag{2.36}$$

The kinematic compliance matrix, $\mathbf{K}_{q,e,k,i}^{-1}$, is a $(6 - Z_i) \times (6 - Z_i)$ diagonal matrix where each term is the compliance of the respective actuated joint, passive compliant joint or virtual joint. The compliance of actuated and passive compliant joints are real and non-zero, while the compliance of virtual joints is zero, as was earlier discussed. It should be noted that if the zero stiffness joints had not been removed from the analysis, this would have introduced elements of infinite compliance in $\mathbf{K}_{q,e,k,i}^{-1}$. By expressing the compliance matrix in elastic joint space, this problem was effectively avoided.

The structural compliance matrix of leg i can be thought of as the leg's compliance with all kinematic joints locked in place. The matrix $\mathbf{K}_{q,e,s,i}^{-1}$ represents this structural compliance matrix in elastic joint space. This matrix is obtained in two steps. First an expression is obtained of the structural compliance matrix of leg i in end-effector Cartesian space, $\mathbf{K}_{s,i}^{-1}$. Secondly, this matrix is mapped onto elastic joint space.

An established method to obtain $\mathbf{K}_{s,i}^{-1}$ is to use adjoint matrices to express the structural compliance matrix of each individual structural element in the Cartesian end-effector reference frame [9, 10, 36], so that they can be added as in Eq. (2.30). This leads to

$$\mathbf{K}_{s,i}^{-1} = \sum_l \mathbf{Ad}_{\mathbf{H}_{i,l}^{ee}} \mathbf{K}_{s,i,l}^{-1} \mathbf{Ad}_{\mathbf{H}_{i,l}^{ee}}^{\top} \tag{2.37}$$

where $\mathbf{K}_{s,i,l}^{-1}$ is the 6×6 structural compliance matrix of the lth individual structural element of leg i. This matrix is typically expressed in a reference frame connected to the respective structural body, so $\mathbf{Ad}_{\mathbf{H}_{i,l}^{ee}}$ is the 6×6 adjoint matrix which transforms a vector from this reference frame into the Cartesian reference frame connected to the end-effector.

Next, the transformation

$$\mathbf{K}_{q,e,s,i}^{-1} = \mathbf{J}_{e,i}^{-1} \mathbf{K}_{s,i}^{-1} \mathbf{J}_{e,i}^{-\top} \tag{2.38}$$

is used to map $\mathbf{K}_{s,i}^{-1}$ onto the elastic joint space of leg i. This transformation enables the addition introduced in Eq. (2.36).

Equations (2.36)-(2.38) can be combined into a single expression,

$$\mathbf{K}_{q,e,i}^{-1} = \mathbf{K}_{q,e,k,i}^{-1} + \mathbf{J}_{e,i}^{-1} \left(\sum_l \mathbf{Ad}_{\mathbf{H}_{i,l}^{ee}} \mathbf{K}_{s,i,l}^{-1} \mathbf{Ad}_{\mathbf{H}_{i,l}^{ee}}^{\top} \right) \mathbf{J}_{e,i}^{-\top} \tag{2.39}$$

It will generally be computationally intensive to invert this symbolic matrix directly and obtain a symbolic expression for $\mathbf{K}_{q,e,i}$. A more practical strategy will be to invert $\mathbf{K}_{q,e,i}^{-1}$ numerically for a given configuration. From Eq. (2.35) it follows that inversion of N matrices, each of dimension $(6 - Z_i) \times (6 - Z_i)$, is required to obtain an instantaneous numerical expression of matrix $\mathbf{K}_{q,e}$.

2

CARTESIAN STIFFNESS ANALYSIS.

Considering the foregoing derivations and expressions, Eq. (2.25) can be rewritten by inserting Eq. (2.34), which gives

$$\mathbf{K} = \left(-\frac{\partial \mathbf{J}_e^{-\top}}{\partial \mathbf{q}} \boldsymbol{\tau}_e \right) \frac{d\mathbf{q}}{d\mathbf{x}} + \mathbf{J}_e^{-\top} \mathbf{K}_{q,e} \frac{d\mathbf{q}_e}{d\mathbf{x}} \tag{2.40}$$

Then, because [35]

$$\frac{d\mathbf{q}}{d\mathbf{x}} = \mathbf{J}^{-1} \tag{2.41}$$

and

$$\frac{d\mathbf{q}_e}{d\mathbf{x}} = \mathbf{J}_e^{-1} \tag{2.42}$$

it is possible to express Eq. (2.40) in the form

$$\mathbf{K} = \left(-\frac{\partial \mathbf{J}_e^{-\top}}{\partial \mathbf{q}} \boldsymbol{\tau}_e \right) \mathbf{J}^{-1} + \mathbf{J}_e^{-\top} \mathbf{K}_{q,e} \mathbf{J}_e^{-1} \tag{2.43}$$

where $\mathbf{J}^{-1}$ was expressed in (2.8). Equation (2.43) is an expression for the Cartesian stiffness matrix of a parallel manipulator with non-redundant legs under loading, which takes the structural stiffness of the legs into account and which is also valid for lower mobility parallel manipulators.[2]

2.3. EXAMPLE ANALYSIS OF A 1-DoF 3-RRR MANIPULATOR

IN this section the introduced stiffness analysis method is applied to a 3-RRR spatial 1-DoF manipulator with three identical legs, shown in Fig. 2.3. The manipulator only allows linear motion along the Z-axis. Each leg consists of an actuated revolute joint (indicated by R), a passive compliant revolute joint and a zero stiffness revolute joint. The spatial manipulator is overconstrained in linear motion along the Y-axis as well as in rotations around the X-axis and the Z-axis. Due to these characteristics, the manipulator presented in Fig. 2.3 is considered as an example of a general parallel manipulator with non-redundant legs.

To perform the stiffness analysis, for each leg first a set of six linearly independent unit twists is determined, as well as the unit wrenches which each do work on only one of the unit twists. All twists and wrenches are expressed in a right-handed Cartesian reference frame connected to the end-effector at point $\mathcal{O}'$. The basis vectors of this reference frame are parallel to those of the inertial Cartesian reference frame with origin $\mathcal{O}$. Based on observation of the kinematic structure of an individual leg, and the properties

---

[2]Inserting the expression $\boldsymbol{\tau}_e = -\mathbf{J}_e^\top \$_{w,ext}$, which follows from Eqs. (2.1) and (2.20), and the rule $\frac{\partial \mathbf{J}_e^{-\top}}{\partial \mathbf{q}} = -\mathbf{J}_e^{-\top} \frac{\partial \mathbf{J}_e^\top}{\partial \mathbf{q}} \mathbf{J}_e^{-\top}$ in Eq. (2.43) gives $\mathbf{K} = \mathbf{J}_e^{-\top} \mathbf{K}_{q,e} \mathbf{J}_e^{-1} - \mathbf{J}_e^{-\top} \frac{\partial \mathbf{J}_e^\top}{\partial \mathbf{q}} \$_{w,ext} \mathbf{J}^{-1}$. This equation is comparable to expressions derived by Chen and Kao [17] and Quennouelle and Gosselin [37]. However, since a direct symbolic expression for $\mathbf{J}_e^\top$ is typically not available for a parallel manipulator, while such expression is typically available for $\mathbf{J}_e^{-\top}$, Eq. (2.43) is preferred.
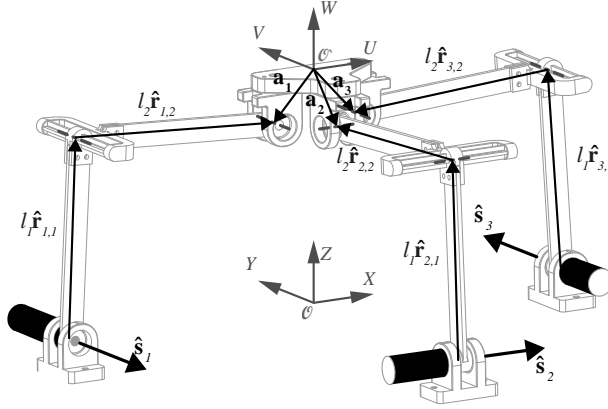
Figure 2.3: A 3-RRR manipulator, where each leg consists of an actuated revolute joint, represented by a filled drum, a passive compliant joint and a zero stiffness revolute joint. The only kinematically allowed DoF of this spatial 1-DoF manipulator is a translation along the Z-axis.

described by Huang et al. [31], the unit twists of permission can be identified as

$$\hat{\$}_{ta_{i,1}} = \begin{bmatrix} \hat{\mathbf{s}}_i \\ -(l_1\hat{\mathbf{r}}_{i,1} + l_2\hat{\mathbf{r}}_{i,2} - \mathbf{a}_i) \times \hat{\mathbf{s}}_i \end{bmatrix} \tag{2.44}$$

$$\hat{\$}_{ta_{i,2}} = \begin{bmatrix} \hat{\mathbf{s}}_i \\ -(l_2\hat{\mathbf{r}}_{i,2} - \mathbf{a}_i) \times \hat{\mathbf{s}}_i \end{bmatrix} \tag{2.45}$$

$$\hat{\$}_{ta_{i,3}} = \begin{bmatrix} \hat{\mathbf{s}}_i \\ \mathbf{a}_i \times \hat{\mathbf{s}}_i \end{bmatrix} \tag{2.46}$$

where $\hat{\$}_{ta_{i,1}}$, $\hat{\$}_{ta_{i,2}}$, and $\hat{\$}_{ta_{i,3}}$ are the unit twists associated to the actuated joint, passive compliant joint, and zero stiffness joint respectively. Furthermore, $\hat{\mathbf{s}}_1 = -\hat{\mathbf{e}}_2$, which is the unit vector aligned with the negative Y-axis, $\hat{\mathbf{s}}_2 = \hat{\mathbf{e}}_1$, which is the unit vector aligned with the X-axis, and $\hat{\mathbf{s}}_3 = \hat{\mathbf{e}}_2$, which is the unit vector aligned with the Y-axis. The other vectors are illustrated in Fig. 2.3, where $\hat{\mathbf{r}}_{i,l}$ is the unit vector pointing along the lth link of leg i and $\mathbf{a}_i$ is the vector pointing from $\mathcal{O}'$ to the center of the third joint of the ith leg.

Next, taking the conditions posed by Ref. [33] into account, a set of wrenches of constraint can also be identified,

$$\hat{\$}_{wc_{i,1}} = \begin{bmatrix} \mathbf{0}_{3\times 1} \\ \hat{\mathbf{s}}_i \end{bmatrix} \tag{2.47}$$

$$\hat{\$}_{wc_{i,2}} = \begin{bmatrix} \hat{\mathbf{e}}_3 \\ \mathbf{0}_{3\times 1} \end{bmatrix} \tag{2.48}$$

$$\hat{\$}_{wc_{i,3}} = \begin{bmatrix} \hat{\mathbf{e}}_3 \times \hat{\mathbf{s}}_i \\ \mathbf{0}_{3\times 1} \end{bmatrix} \tag{2.49}$$

Following the methodology described by Huang et al. [31], these sets of unit twists of permission and unit wrenches of constraint then enable the identification of a set of

unit wrenches of actuation

$$\hat{\$}_{wa_{i,1}} = \begin{bmatrix} \mathbf{a}_i \times \hat{\mathbf{r}}_{i,2} \\ \hat{\mathbf{r}}_{i,2} \end{bmatrix} \tag{2.50}$$

$$\hat{\$}_{wa_{i,2}} = \begin{bmatrix} \mathbf{a}_i \times \hat{\mathbf{f}}_{i,2} \\ \hat{\mathbf{f}}_{i,2} \end{bmatrix} \tag{2.51}$$

$$\hat{\$}_{wa_{i,3}} = \begin{bmatrix} -(l_2\hat{\mathbf{r}}_{i,2} - \mathbf{a}_i) \times \hat{\mathbf{r}}_{i,1} \\ \hat{\mathbf{r}}_{i,1} \end{bmatrix} \tag{2.52}$$

with

$$\hat{\mathbf{f}}_{i,2} = \frac{l_1\hat{\mathbf{r}}_{i,1} + l_2\hat{\mathbf{r}}_{i,2}}{\left| l_1\hat{\mathbf{r}}_{i,1} + l_2\hat{\mathbf{r}}_{i,2} \right|}$$

and finally also a set of unit twists of restriction can be identified,

$$\hat{\$}_{tc_{i,1}} = \begin{bmatrix} \mathbf{0}_{3\times 1} \\ \hat{\mathbf{s}}_i \end{bmatrix} \tag{2.53}$$

$$\hat{\$}_{tc_{i,2}} = \begin{bmatrix} \hat{\mathbf{e}}_3 \\ \mathbf{0}_{3\times 1} \end{bmatrix} \tag{2.54}$$

$$\hat{\$}_{tc_{i,3}} = \begin{bmatrix} \hat{\mathbf{e}}_3 \times \hat{\mathbf{s}}_i \\ \mathbf{0}_{3\times 1} \end{bmatrix} \tag{2.55}$$

From Eqs. (2.53)-(2.55) we can conclude that for each leg the constrained directions can be visualised as a locked prismatic joint, positioned at $\mathcal{O}'$ and aligned with the vector $\hat{\mathbf{s}}_i$, and two locked revolute joints, both also positioned at $\mathcal{O}'$ and aligned with the W-axis and either the U- or V-axis, depending on the leg.

Equations (2.44)-(2.55) are then used to obtain the full inverse Jacobian for each leg as in Eq. (2.6),

$$\mathbf{J}_i^{-1} = \begin{bmatrix} \hat{\$}_{wa_{i,1}}^{\top}/(\hat{\$}_{wa_{i,1}}^{\top}\hat{\$}_{ta_{i,1}}) \\ \hat{\$}_{wa_{i,2}}^{\top}/(\hat{\$}_{wa_{i,2}}^{\top}\hat{\$}_{ta_{i,2}}) \\ \hat{\$}_{wa_{i,3}}^{\top}/(\hat{\$}_{wa_{i,3}}^{\top}\hat{\$}_{ta_{i,3}}) \\ \hat{\$}_{wc_{i,1}}^{\top}/(\hat{\$}_{wc_{i,1}}^{\top}\hat{\$}_{tc_{i,1}}) \\ \hat{\$}_{wc_{i,2}}^{\top}/(\hat{\$}_{wc_{i,2}}^{\top}\hat{\$}_{tc_{i,2}}) \\ \hat{\$}_{wc_{i,3}}^{\top}/(\hat{\$}_{wc_{i,3}}^{\top}\hat{\$}_{tc_{i,3}}) \end{bmatrix} \tag{2.56}$$

Because the third joint in each leg is a zero stiffness joint and the torque transferred by it will be zero at all times, we can remove the associated row from $\mathbf{J}_i^{-1}$ to form the inverse Jacobian of elasticity, whose transpose,

$$\mathbf{J}_{e,i}^{-\top} = \begin{bmatrix} \hat{\$}_{wa_{i,1}}^{\top}/(\hat{\$}_{wa_{i,1}}^{\top}\hat{\$}_{ta_{i,1}}) \\ \hat{\$}_{wa_{i,2}}^{\top}/(\hat{\$}_{wa_{i,2}}^{\top}\hat{\$}_{ta_{i,2}}) \\ \hat{\$}_{wc_{i,1}}^{\top}/(\hat{\$}_{wc_{i,1}}^{\top}\hat{\$}_{tc_{i,1}}) \\ \hat{\$}_{wc_{i,2}}^{\top}/(\hat{\$}_{wc_{i,2}}^{\top}\hat{\$}_{tc_{i,2}}) \\ \hat{\$}_{wc_{i,3}}^{\top}/(\hat{\$}_{wc_{i,3}}^{\top}\hat{\$}_{tc_{i,3}}) \end{bmatrix}^{\top} \tag{2.57}$$

maps all non-zero torques transferred by leg i from joint space onto end-effector Cartesian space as in Eq. (2.15). Since each of the three legs includes one zero stiffness joint, $Z_i = 1$ for $i = 1 \ldots 3$.

Because $Z_i \neq 0$, the stiffness matrix of leg i, expressed as $\mathbf{K}_{q,i}$ in Eq. (2.32) is not a square matrix. We will therefore make use of the assumption expressed in Eq. (2.33). The resulting stiffness matrix $\mathbf{K}_{q,e,i}$ for each individual leg is invertible and can be developed using Eqs. (2.36)-(2.38).

Equation (2.39) expresses $\mathbf{K}_{q,e,i}^{-1}$ as a function of the matrices $\mathbf{K}_{q,e,k,i}^{-1}$ and the compliance matrices of individual structural elements $\mathbf{K}_{s,i,l}^{-1}$. Using Eq. (2.16), and because virtual joints are modelled with zero compliance

$$\mathbf{K}_{q,e,k,i}^{-1} = \begin{bmatrix} k_{a,i}^{-1} & \mathbf{0} & \mathbf{0}_{1\times3} \\ \mathbf{0} & k_{pc,i}^{-1} & \mathbf{0}_{1\times3} \\ \mathbf{0}_{3\times1} & \mathbf{0}_{3\times1} & \mathbf{0}_{3\times3} \end{bmatrix} \tag{2.58}$$

where, $k_{a,i}$ is the actuator stiffness and $k_{pc,i}$ is the stiffness of the compliant joint of leg i. The symbolic matrices $\mathbf{K}_{s,i,l}^{-1}$ can be developed using linear beam theory [9, 10].

With above expressions, the Cartesian stiffness matrix can be obtained from Eq. (2.43), which is repeated here for convenience

$$\mathbf{K} = \left(-\frac{\partial \mathbf{J}_e^{-\top}}{\partial \mathbf{q}} \boldsymbol{\tau}_e \right) \mathbf{J}^{-1} + \mathbf{J}_e^{-\top} \mathbf{K}_{q,e} \mathbf{J}_e^{-1}$$

where for this example

$$\mathbf{J}^{-1} = \begin{bmatrix} \mathbf{J}_1^{-1} \\ \mathbf{J}_2^{-1} \\ \mathbf{J}_3^{-1} \end{bmatrix} \qquad \mathbf{J}_e^{-\top} = \begin{bmatrix} \mathbf{J}_{e,1}^{-\top} & \mathbf{J}_{e,2}^{-\top} & \mathbf{J}_{e,3}^{-\top} \end{bmatrix}$$

$$\boldsymbol{\tau}_e = \begin{bmatrix} \boldsymbol{\tau}_{e,1}^{\top} & \boldsymbol{\tau}_{e,2}^{\top} & \boldsymbol{\tau}_{e,3}^{\top} \end{bmatrix}^{\top}$$

with $\mathbf{J}_i^{-1}$ defined by Eq. (2.56), $\mathbf{J}_{e,i}^{-\top}$ by Eq. (2.57), and

$$\boldsymbol{\tau}_{e,i} = \begin{bmatrix} \tau_{a,i} & \tau_{pc,i} & \tau_{c,i,1} & \tau_{c,i,2} & \tau_{c,i,3} \end{bmatrix}^{\top}$$

For the presented example, $\tau_{a,i}$ is controlled, $\tau_{pc,i}$ can be determined from the manipulator configuration and the properties of the implemented compliant joint, while $\tau_{c,i,j} = 0$ if the individual legs are not loaded in their respective constrained directions. Finally, the matrix $\mathbf{K}_{q,e}$ is obtained using Eq. (2.35) as

$$\mathbf{K}_{q,e} = \begin{bmatrix} \mathbf{K}_{q,e,1} & \mathbf{0}_{5\times5} & \mathbf{0}_{5\times5} \\ \mathbf{0}_{5\times5} & \mathbf{K}_{q,e,2} & \mathbf{0}_{5\times5} \\ \mathbf{0}_{5\times5} & \mathbf{0}_{5\times5} & \mathbf{K}_{q,e,3} \end{bmatrix}$$

where each matrix $\mathbf{K}_{q,e,i}$ can thus be obtained by (numerically) inverting the symbolically expressed matrix $\mathbf{K}_{q,e,i}^{-1}$, which was expressed in Eq. (2.39).

Thus, all partial matrices necessary to determine $\mathbf{K}$ are directly available in symbolic form, except $\mathbf{K}_{q,e}$, which would in this example require the numerical inversion of three 5×5 matrices.

2.4. DISCUSSION, SIMPLIFICATIONS AND LIMITATIONS

T HE presented Jacobian-based stiffness analysis method applies to a general paral-
lel manipulator with non-redundant legs in a loaded condition and takes both joint
compliance and structural compliance into account. Comparable existing analysis meth-
ods were either developed for more specific manipulators or did not consider loading,
which makes the presented analysis method more complete.

Besides its completeness, the presented method has two implementation advan-
tages over comparable existing methods. The first advantage is that the matrices that
need to be inverted are relatively small. To obtain the stiffness matrix of individual legs
requires an inversion of the corresponding compliance matrix. In the method by Pashke-
vich et al. [27] each of these matrices is of size $(6 + Z_i) \times (6 + Z_i)$, while in the presented
method they are $(6 - Z_i) \times (6 - Z_i)$ matrices. This size reduction is likely to result in a
computational advantage.

The second advantage of the presented analysis is that despite its completeness, its
structure allows for easy simplifications if desired. This makes the presented analysis
very flexible. To demonstrate this, three possible simplifications are discussed here.

2.4.1. NO LOADING
In case of no loading, $\boldsymbol{\tau}_e = 0$. Then, the first term after the equal sign in Eq. (2.43) is zero
and the stiffness analysis reduces to

$$\mathbf{K} = \mathbf{J}_e^{-T} \mathbf{K}_{q,e} \mathbf{J}_e^{-1} \tag{2.59}$$

which is the transformation of the stiffness matrix from elastic joint space to Cartesian
space.

It should be noted that $\boldsymbol{\tau}_e = \mathbf{0}$ is not the same as $\$_{w,pm} = 0$. From Eq. (2.2) it can
be concluded that the latter only means that the net wrench is zero, which allows for
situations where the wrenches applied by individual legs are finite, but cancel each other
out. In that case internal loading occurs and $\boldsymbol{\tau}_e \neq \mathbf{0}$. Thus, a parallel manipulator can be
in a loaded condition, even if no external wrench is applied to the end-effector.

2.4.2. INFINITE STRUCTURAL STIFFNESS
If the structural stiffness is assumed infinite, the Cartesian stiffness matrix can only be
defined if none of the individual legs of a parallel manipulator are structurally constrained,
so for a 6-DoF parallel manipulator. This is because $\mathbf{K}$ is only well-defined if the end-
effector can be displaced along all six basis vectors of Cartesian space. This is not the
case for lower mobility manipulators with a structural stiffness that is assumed infinite,
because in that case the modeled stiffness in the constrained directions is infinite.

However, if none of the individual legs of a parallel manipulator are structurally con-
strained (e.g. a Stewart platform), the vector $\mathbf{q}_{c,i}$ is the zero vector and the configuration
of each leg is defined by the vector which contains all real, kinematic joint coordinates

$$\mathbf{q}_i = \begin{bmatrix} \mathbf{q}_{a,i}^\top & \mathbf{q}_{pc,i}^\top & \mathbf{q}_{pz,i}^\top \end{bmatrix}^\top \tag{2.60}$$

Also for this class of manipulators Eq. (2.43) expresses the Cartesian stiffness matrix,

$$\mathbf{K} = \left(-\frac{\partial \mathbf{J}_e^{-T}}{\partial \mathbf{q}} \boldsymbol{\tau}_e\right) \mathbf{J}^{-1} + \mathbf{J}_e^{-T} \mathbf{K}_{q,e} \mathbf{J}_e^{-1},$$

where the stiffness matrix $\mathbf{K}_{q,e}$ is expressed by Eq. (2.34). However, without elasticity in the structural elements, $\mathbf{K}_{q,e,s,i}^{-1} = \mathbf{0}$ for each leg and thus $\mathbf{K}_{q,e}$ is simply the diagonal matrix containing the stiffness values of all actuated joints and passive, compliant joints of the manipulator.

2.4.3. Compliant Parallel Manipulator

Compliant parallel manipulators are parallel manipulators which do not contain any passive, zero stiffness joints. Instead, all passive joints are compliant joints. In these compliant parallel manipulators, the vector $\mathbf{q}_{pz,i}$ is the zero vector for all legs and therefore

$$\mathbf{q}_i = \begin{bmatrix} \mathbf{q}_{a,i}^\top & \mathbf{q}_{pc,i}^\top & \mathbf{q}_{c,i}^\top \end{bmatrix}^\top \tag{2.61}$$

so that

$$\mathbf{J}_{e,i}^{-T} = \mathbf{J}_i^{-T} \tag{2.62}$$

In this case, Eq. (2.43) simplifies to

$$\mathbf{K} = \left(-\frac{\partial \mathbf{J}^{-T}}{\partial \mathbf{q}} \boldsymbol{\tau}_e + \mathbf{J}^{-T} \mathbf{K}_{q,e}\right) \mathbf{J}^{-1} \tag{2.63}$$

2.4.4. Complications and Limitations

Although the presented analysis method is valid for a general parallel manipulator with non-redundant legs, there are several factors which may complicate this analysis or limit its use. Firstly, it is assumed that all joint torques are known, including those associated to the virtual joints. Especially if a parallel manipulator is overconstrained, there may be additional difficulties in determining the constraint torques.

Second, because both the Jacobian and the structural stiffness matrices are linear approximation, appropriate care should be taken if the presented stiffness analysis method is used to quantitatively assess displacements as a result of external loads. Especially if the parallel manipulator is close to a singularity or if displacements under loading become relatively large, the predicted displacements will likely be less accurate. Another limitation comes from the fact that we assumed the end-effector itself to be rigid. Thus, users of this analysis method should verify that the compliance of the end-effector body is indeed negligible.

Finally, if a parallel manipulator contains zero stiffness joints and the finite stiffness of structural elements is included in the stiffness analysis, the assumption presented in Eq. (2.33) was made. Although we consider it very unlikely that a deflection of a passive, zero stiffness joint as a function of an end-effector deflection causes a significant change in elastic joint torques, users of the presented analysis should keep this assumption in mind.

2.5. CONCLUSIONS ON THE DEVELOPED STIFFNESS ANALYSIS METHOD

THIS chapter has presented a novel[3] Jacobian-based stiffness analysis method for parallel manipulators with non-redundant legs, based on the static equilibrium equation. Because parallel manipulators often interact with an environment, an external wrench acting on the end-effector was included in this equilibrium equation. The method is valid for both 6-DoF and lower mobility manipulators, and it considers the presence of compliant joints and the finite stiffness of links.

The presented analysis uses an existing method based on screw theory to define for each leg a set of six linearly dependent, instantaneous joint axes. Each axis is associated to either an actuated joint, a passive compliant joint, a zero stiffness joint or a virtual joint. Virtual joints represent the motion restricted by the kinematic joints of the leg in question. The four different types of joints have different stiffness properties, and therefore affect the resulting end-effector stiffness in different ways. The joint coordinates associated to actuated, passive flexure, and virtual joints are together referred to as elastic joint coordinates.

The method presented in this chapter integrates a symbolic structural stiffness analysis method based on adjoint matrices with a stiffness analysis method that relies on the transformation between a joint space and a Cartesian space. The resulting method is also valid for parallel manipulators with zero stiffness joints, because this method uses a mapping of the 6×6 structural stiffness matrix of a leg into the space spanned by its elastic joint coordinates. The resulting matrix of reduced dimension can be inverted.

To demonstrate the presented stiffness analysis method, it has been aplied to a spatial 1-DoF parallel manipulator. Additionally, to illustrate the generality of the method, three specific cases were discussed. One case assumed the absence of loading, another infinite structural stiffness, and a third considered the stiffness analysis of a compliant parallel manipulator. The presented Cartesian stiffness analysis method therefore generalises much of the existing Jacobian-based stiffness analysis methods for parallel manipulators with non-redundant legs.

REFERENCES

[1] A. G. L. Hoevenaars, P. Lambert, and J. L. Herder, *Jacobian-based stiffness analysis method for parallel manipulators with non-redundant legs*, Proceedings of the Institution of Mechanical Engineers, Part C: Journal of Mechanical Engineering Science **230**, 341 (2016).

[2] J.-P. Merlet, *Parallel Robots*, 2nd ed., edited by G. Gladwell, Solid Mechanics and its Application, Vol. 128 (Springer, Dordrecht, 2006).

[3] W. Wei and N. Simaan, *Design of Planar Parallel Robots With Preloaded Flexures for*

---

[3]Sung Kim and Lipkin [38] have published a stiffness analysis method which also uses constraint relations to include structural compliance. However, their method does not take the effect of loading into account. In addition, their paper was not yet published when this chapter was first submitted for review. As such, the word 'novel' is justified.

2

Guaranteed Backlash Prevention, Journal of Mechanisms and Robotics **2**, 011012 (2010).

[4] J. Borras and A. M. Dollar, *Static analysis of parallel robots with compliant joints for in-hand manipulation,* in *2012 IEEE/RSJ International Conference on Intelligent Robots and Systems* (IEEE, 2012) pp. 3086–3092.

[5] D. Kang and D. Gweon, *Analysis of large range rotational flexure in precision 6-DOF tripod robot,* in *Control, Automation and Systems (ICCAS), 2012 12th International Conference on* (IEEE, New York, 2012) pp. 2117–2120.

[6] C. M. Clinton, G. Zhang, and A. J. Wavering, *Stiffness Modeling of a Stewart Platform Based Milling Machine,* Tech. Rep. (ISR, 1997).

[7] O. Company, S. Krut, and F. Pierrot, *Modelling and preliminary design issues of a four-axis parallel machine for heavy parts handling,* Proceedings of the Institution of Mechanical Engineers, Part K: Journal of Multi-body Dynamics **216**, 1 (2002).

[8] Y. Li, E. Zhang, Y. Song, and Z. Feng, *Stiffness modeling and analysis of a novel 4-DOF PKM for manufacturing large components,* Chinese Journal of Aeronautics (2013), 10.1016/j.cja.2013.07.040.

[9] H.-H. Pham and I.-M. Chen, *Stiffness modeling of flexure parallel mechanism,* Precision Engineering **29**, 467 (2005).

[10] J. S. Dai and X. Ding, *Compliance Analysis of a Three-Legged Rigidly-Connected Platform Device,* Journal of Mechanical Design **128**, 755 (2006).

[11] A. Raatz, J. Wrege, A. Burisch, and J. Hesselbach, *Compliant Parallel Robots,* in *Precision Assembly Technologies for Mini and Micro Products,* edited by S. Ratchev (Kluwer Academic Publishers, Boston, 2006) pp. 83–92, arXiv:15715736 .

[12] W. Dong, L. Sun, and Z. Du, *Stiffness research on a high-precision, large-workspace parallel mechanism with compliant joints,* Precision Engineering **32**, 222 (2008).

[13] Y. Yue, F. Gao, X. Zhao, and Q. J. Ge, *Relationship Among Input-Force, Payload, Stiffness, and Displacement of a 6-DOF Perpendicular Parallel Micromanipulator,* Journal of Mechanisms and Robotics **2**, 011007 (2010).

[14] Z. Gao and D. Zhang, *Simulation driven performance characterization of a spatial compliant parallel mechanism,* International Journal of Mechanics and Materials in Design (2014), 10.1007/s10999-014-9243-4.

[15] J. K. Salisbury and J. J. Craig, *Articulated Hands: Force Control and Kinematic Issues,* The International Journal of Robotics Research **1**, 4 (1982).

[16] C. Gosselin, *Stiffness mapping for parallel manipulators,* IEEE Transactions on Robotics and Automation **6**, 377 (1990).

[17] S.-F. Chen and I. Kao, *Conservative Congruence Transformation for Joint and Carte-sian Stiffness Matrices of Robotic Hands and Fingers,* The International Journal of Robotics Research **19**, 835 (2000).

[18] G. Alici and B. Shirinzadeh, *Enhanced stiffness modeling, identification and charac-terization for robot manipulators,* IEEE Transactions on Robotics **21**, 554 (2005).

[19] C. Quennouelle and C. Gosselin, *A Quasi-Static Model for Planar Compliant Parallel Mechanisms,* Journal of Mechanisms and Robotics **1**, 021012 (2009).

[20] T. Huang, X. Zhao, and D. J. Whitehouse, *Stiffness estimation of a tripod-based parallel kinematic machine,* IEEE Transactions on Robotics and Automation **18**, 50 (2002).

[21] M. Wahle and B. Corves, *Stiffness Analysis of Clavel's DELTA Robot,* in *Intelligent Robotics and Applications,* Lecture Notes in Computer Science, Vol. 7101, edited by S. Jeschke, H. Liu, and D. Schilberg (Springer Berlin Heidelberg, Berlin, Heidelberg, 2011) pp. 240–249.

[22] A. Ahmad, K. Andersson, U. Sellgren, and S. Khan, *A stiffness modeling methodology for simulation-driven design of haptic devices,* Engineering with Computers **30**, 125 (2012).

[23] D. Zhang, *Kinetostatic Analysis and Optimization of Parallel and Hybrid Architec-tures for Machine Tools,* Phd thesis, Laval University (2000).

[24] D. Zhang and S. Y. Lang, *Stiffness modeling for a class of reconfigurable PKMs with three to five degrees of freedom,* Journal of Manufacturing Systems **23**, 316 (2004).

[25] Y. Wang, H. Liu, T. Huang, and D. G. Chetwynd, *Stiffness Modeling of the Tricept Robot Using the Overall Jacobian Matrix,* Journal of Mechanisms and Robotics **1**, 021002 (2009).

[26] Y. Li and Q. Xu, *Stiffness analysis for a 3-PUU parallel kinematic machine,* Mecha-nism and Machine Theory **43**, 186 (2008).

[27] A. Pashkevich, D. Chablat, and P. Wenger, *Stiffness analysis of overconstrained par-allel manipulators,* Mechanism and Machine Theory **44**, 966 (2009).

[28] A. Klimchik, A. Pashkevich, S. Caro, and D. Chablat, *Stiffness Matrix of Manipulators With Passive Joints: Computational Aspects,* IEEE Transactions on Robotics **28**, 955 (2012).

[29] J. Wang and C. M. Gosselin, *Kinematic Analysis and Design of Kinematically Redun-dant Parallel Mechanisms,* Journal of Mechanical Design **126**, 109 (2004).

[30] S. A. Joshi and L.-W. Tsai, *Jacobian Analysis of Limited-DOF Parallel Manipulators,* Journal of Mechanical Design **124**, 254 (2002).

[31] T. Huang, H. T. Liu, and D. G. Chetwynd, *Generalized Jacobian analysis of lower mobility manipulators,* Mechanism and Machine Theory **46**, 831 (2011).

[32] S.-H. Ling and M. Z. Huang, *Kinestatic Analysis of General Parallel Manipulators,* Journal of Mechanical Design **117**, 601 (1995).

[33] T. Huang, S. Yang, M. Wang, T. Sun, and D. G. Chetwynd, *An Approach to Determining the Unknown Twist/Wrench Subspaces of Lower Mobility Serial Kinematic Chains,* Journal of Mechanisms and Robotics **7**, 031003 (2014).

[34] M. Zefran and V. Kumar, *Affine connections for the Cartesian stiffness matrix,* in *Proceedings of International Conference on Robotics and Automation,* Vol. 2 (IEEE, 1997) pp. 1376–1381.

[35] J.-P. Merlet and C. Gosselin, *Parallel Mechanisms and Robots,* in *Springer Handbook of Robotics,* edited by B. Siciliano and O. Khatib (Springer Berlin Heidelberg, Berlin, Heidelberg, 2008) pp. 269–285.

[36] R. M. Murray, Z. Li, and S. S. Sastry, *A Mathematical Introduction to Robotic Manipulation* (CRC Press, 1994).

[37] C. Quennouelle and C. M. Gosselin, *A General Formulation for the Stiffness Matrix of Parallel Mechanisms,* (2012), arXiv:1212.0950 [physics.class-ph] .

[38] H. Sung Kim and H. Lipkin, *Stiffness of Parallel Manipulators With Serially Connected Legs,* Journal of Mechanisms and Robotics **6**, 031001 (2014).

2

3

EXPERIMENTAL VALIDATION OF JACOBIAN-BASED STIFFNESS ANALYSIS METHOD FOR PARALLEL MANIPULATORS WITH NON-REDUNDANT LEGS

Now take a look at what you see
Do a little walking in your sleep

Felix Riebl
The Cat Empire - Go

Chapter 2 introduced a novel Jacobian-based stiffness analysis method for parallel manipulators, in which both the effect of loading and the structural compliance of all elements was considered. This chapter presents the experimental validation of this method. The experimental validation was performed by comparing differential wrench measurements with predictions based on stiffness analyses with increasing levels of detail. For this purpose two passive parallel mechanisms were designed, namely a planar 3-DoF mechanism and a spatial 1-DoF mechanism. For these mechanisms it was shown that a stiffness analysis becomes more accurate both if loading and structural compliance are considered.

3.1. PURPOSE OF EXPERIMENTAL VALIDATION

S TIFFNESS is an important parameter in the modeling of a parallel manipulator. It describes the relation between forces and displacements in the low frequency domain and thereby affects a manipulator's positioning accuracy under loading. Stiffness also has a large influence on the achievable force- and position bandwidth. Of particular interest for parallel manipulators is the Cartesian stiffness matrix which describes the stiffness of the end-effector with respect to the inertial base. For early phase design and optimization, symbolic stiffness analysis methods are preferred [2, 3].

If only actuator stiffness is considered, a compact symbolic expression of a parallel manipulator's Cartesian stiffness matrix can be obtained using Jacobian mappings [4]. This expression can be extended to manipulators (or mechanisms) which include compliant joints [5]. If a manipulator is loaded, a term including the derivative of the Jacobian with respect to the joint coordinate vector can also be part of the analysis [5–8].

Several researchers have recently presented symbolic stiffness analysis methods which also consider the finite structural stiffness of the legs. Some of these methods only consider structural stiffness along the actuated load vectors [9, 10]. This approach is valid for 3-DoF planar parallel manipulators and 6-DoF spatial parallel manipulators in which all passive joints are zero stiffness joints, because in that case no passive wrenches or constraint wrenches are transferred by the legs. Constraint wrenches can be transferred by the legs of lower mobility parallel manipulators [11, 12], but if constrained directions are ignored in the stiffness analysis a similar approach has also be applied for the stiffness analysis of these lower mobility parallel manipulators [13, 14].

However, in general a lower mobility parallel manipulator can be loaded along its constrained directions, which means that the stiffness along these constrained DoFs is relevant. Stiffness analysis methods that consider constrained directions have been developed for specific types of lower mobility parallel manipulators, such as lower mobility compliant manipulators [15], parallel manipulators with a properly constrained leg [16–18], or a 3-PUU parallel manipulator [18]. Pashkevich et al. [19] presented a method that applies to more general lower mobility parallel manipulators. Their method involves the inversion of a $(6 + Z_i) \times (6 + Z_i)$ matrix for each leg, where Z_i is the number of zero stiffness joints in leg i.

Chapter 2 as well as Sung Kim and Lipkin [20] have presented stiffness analysis methods that apply to more general lower mobility parallel manipulators, and which makes use of the constraint relations in a Jacobian analysis. This has enabled them to reduce the size of the matrix that needs to be inverted for each leg to $(6 - Z_i) \times (6 - Z_i)$. Like the method by Pashkevich et al. [19], the method presented by Sung Kim and Lipkin [20] does not consider the effect of loading, while this effect is included in the analysis method in Chapter 2.

Both Pashkevich et al. [19] and Sung Kim and Lipkin [20] validated the inclusion of structural compliance in their analysis method by comparison with models obtained using the finite element method (FEM). At the basis of FEM models lay inevitable approximations and assumptions, which may affect the results. Experimental validation activities can improve the confidence in results obtained from FEM models.

Experimental validation activities have been performed for the stiffness analysis of specific parallel manipulators, such as a compliant parallel manipulator [15], or a 6-DoF

parallel manipulators [9]. Neither of these analyses considered the effect of loading. Both Yi et al. [21] and Alici and Shirinzadeh [22] remark that the effect of loading on accuracy can be significant, but they did not conclude whether this effect is positive or negative.

The purpose of this research is to experimentally validate the stiffness analysis method for parallel manipulators with non-redundant legs proposed in Chapter 2, which considers both the effect of loading and structural compliance. Two main contributions are foreseen. Firstly, it will be experimentally validated whether the accuracy of a stiffness analysis improves if the effect of loading is considered, which has not been demonstrated before. Secondly, experiments will be performed to determine whether the inclusion of structural compliance based on the constraint relations in the Jacobian analysis leads to valid results, which will support earlier conclusions based on comparison with FEM models.

This chapter is structured as follows. First, in the Method section two passive mechanisms are introduced, for which stiffness models with different levels of detail are described. The Method section also describes the measurement system and the data post-processing, which enables a comparison of the accuracy of different stiffness models in order to determine whether additional detail indeed increases accuracy. In the Results section the processed measurements are presented together with examples of resulting stiffness matrices for both mechanisms. Finally, the implications of these results are discussed.

3.2. EXPERIMENTAL VALIDATION METHOD

T HE central idea in this chapter is to develop dedicated mechanisms in tandem with a dedicated measurement system to validate the stiffness analysis method as presented in Chapter 2. The formulation of that method consists of two independent terms, and therefore two independent sets of data were collected so that the two terms could be analyzed independently. To facilitate independent data sets, two passive mechanisms were designed, each with a compliance that is tuned to the measurement accuracy.

In the remainder of this section first the general formulation of the stiffness analysis as presented in Chapter 2 is summarized. Next, the two developed passive mechanisms are introduced. Finally, the measurement system is presented, which consists of an inertial measurement frame that was used to control the end-effector pose, and a reaction wrench sensor.

3.2.1. GENERAL FORMULATION OF STIFFNESS ANALYSIS

A Cartesian stiffness matrix $\mathbf{K}$ is a 6×6 matrix that maps a displacement twist $\$_d$ onto a differential wrench $d\$_w$, where

$$\$_d = \begin{bmatrix} d\boldsymbol{\phi} \\ d\mathbf{p} \end{bmatrix}, \quad d\$_w = \begin{bmatrix} d\mathbf{m} \\ d\mathbf{f} \end{bmatrix}$$

in which $d\boldsymbol{\phi}$ and $d\mathbf{p}$ are the differential angular and linear displacements of the end-effector, and $d\mathbf{m}$ and $d\mathbf{f}$ the resulting change in moment- and force vector applied by the parallel manipulator to the end-effector.
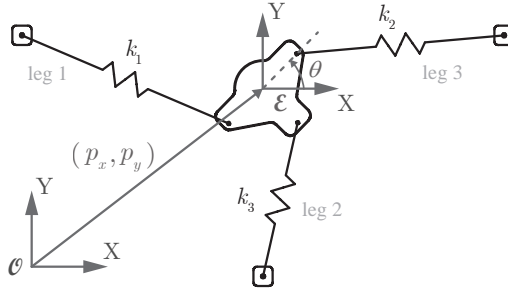
Figure 3.1: Mechanism I is a passive planar 3-RPR mechanism, where the interaction wrenches are the result of elongation/contraction of the linear springs, depending on the pose of the end-effector. Here mechanism I is shown in pose I-d as introduced in Table 3.1, where the pose is determined by a position of reference frame $\mathscr{E}$ with respect to $\mathscr{O}$ and a rotation θ.

The general formulation of the stiffness analysis that is validated in this chapter was presented in Chapter 2, and is repeated here for convenience,

$$\mathbf{K} = \left(-\frac{\partial \mathbf{J}_e^{-\top}}{\partial \mathbf{q}} \boldsymbol{\tau}_e \right) \mathbf{J}^{-1} + \mathbf{J}_e^{-\top} \mathbf{K}_{q,e} \mathbf{J}_e^{-1} \tag{3.1}$$

where for a parallel manipulator with N legs, $\mathbf{q}$ is the $6N \times 1$ vector that contains all real and virtual joint coordinates (where the virtual joint coordinates represent the constrained directions in joint space), $\boldsymbol{\tau}_e$ is the joint torque vector where all zero entries associated to zero stiffness joints were removed, $\mathbf{J}^{-1}$ is the $6N \times 6$ full inverse Jacobian. The matrix $\mathbf{J}_e^{-1}$ is the inverse Jacobian of elasticity, which corresponds to the matrix $\mathbf{J}^{-1}$ with all rows associated to zero stiffness joints removed. As such, $\mathbf{J}_e^{-1}$ maps an end-effector displacement twist on the elastic joint deformation vector $d\mathbf{q}_e$. Finally, matrix $\mathbf{K}_{q,e}$ is the stiffness matrix of the parallel manipulator expressed in the space spanned by the elastic joint coordinates, which includes the effect of actuated joints, compliant joints, as well as structural compliance.

Equation (3.1) shows that in the method presented in Chapter 2 the Cartesian stiffness matrix is a summation of two terms. The effect of loading is covered by the first term, which includes the derivative of $\mathbf{J}_e^{-\top}$ with respect to $\mathbf{q}$. The second term represents the mapping of the stiffness matrix from the elastic joint space to the Cartesian space.

3.2.2. MECHANISM I: PASSIVE PLANAR 3-DOF
To validate whether the accuracy of a stiffness model increases when loading is taken into account by means of a Jacobian-derivative term, a passive planar 3-DoF mechanism was designed. This mechanism will be referred to as *mechanism I* and was kept as simple as possible to avoid that uncertainties in the mechanical design affect the results.

MECHANICAL DESIGN OF MECHANISM I
The designed planar mechanism is a 3-RPR mechanism with zero stiffness revolute joints and passive compliant prismatic joints constructed from linear springs. A schematic

representation of mechanism I is shown in Fig. 3.1. Out-of-plane stiffness was not considered. The inverse kinematics of the mechanism are given in Appendix A. The stiffness k_i [N/m] and the zero length $q_{i,2_0}$ [m] of the linear spring in each leg were identified as

$$k_i = 114.2, \qquad q_{i,2_0} = 0.092 \qquad \text{for } i = 1,2,3 \tag{3.2}$$

JACOBIAN ANALYSES OF MECHANISM I

To perform the planar stiffness analysis as in Eq. (3.1), two Jacobian matrices are required, namely the full inverse Jacobian and the inverse Jacobian of elasticity, see Section 2.2.3. To obtain these matrices, the Jacobian analysis method as presented by Huang et al.[12] was used. For that, three unit twists of permission, and three unit wrenches of actuation were identified for each leg. They are formulated in Appendix A, so that the planar full inverse Jacobian for each leg of mechanism I can be obtained as

$$\mathbf{J}_{I,i}^{-1} = \begin{bmatrix} \hat{\$}_{wa_{i,1}}^{\top} / (\hat{\$}_{wa_{i,1}}^{\top} \hat{\$}_{ta_{i,1}}) \\ \hat{\$}_{wa_{i,2}}^{\top} / (\hat{\$}_{wa_{i,2}}^{\top} \hat{\$}_{ta_{i,2}}) \\ \hat{\$}_{wa_{i,3}}^{\top} / (\hat{\$}_{wa_{i,3}}^{\top} \hat{\$}_{ta_{i,3}}) \end{bmatrix} \tag{3.3}$$

The full inverse Jacobian of mechanism I can then be assembled as

$$\mathbf{J}_I^{-1} = \begin{bmatrix} \mathbf{J}_{I,1}^{-1} \\ \mathbf{J}_{I,2}^{-1} \\ \mathbf{J}_{I,3}^{-1} \end{bmatrix} \tag{3.4}$$

where each matrix $\mathbf{J}_{I,i}^{-1}$ is expressed by Eq. (3.3).

The inverse Jacobian of elasticity of mechanism I, $\mathbf{J}_{I,e}^{-1}$, is obtained by removing the rows from Eq. (3.4) which are associated to zero stiffness joints. Because the first and third joint of each leg are zero stiffness joints, the inverse Jacobian of elasticity for mechanism I is obtained as

$$\mathbf{J}_{I,e}^{-1} = \begin{bmatrix} \hat{\$}_{wa_{1,2}}^{\top} / (\hat{\$}_{wa_{1,2}}^{\top} \hat{\$}_{ta_{1,2}}) \\ \hat{\$}_{wa_{2,2}}^{\top} / (\hat{\$}_{wa_{2,2}}^{\top} \hat{\$}_{ta_{2,2}}) \\ \hat{\$}_{wa_{3,2}}^{\top} / (\hat{\$}_{wa_{3,2}}^{\top} \hat{\$}_{ta_{3,2}}) \end{bmatrix} \tag{3.5}$$

COMPETING STIFFNESS MODELS FOR MECHANISM I

For this mechanism the only compliance is in the linear springs, which are described by Eq. (3.2). Then, the stiffness matrix in joint space is

$$\mathbf{K}_{I,q,e} = \text{diag}\left([k_1 \quad k_2 \quad k_3]\right) \tag{3.6}$$

Inserting Eqs. (3.4)-(3.6) in Eq. (3.1) then gives

$$\mathbf{K}_{I,ld} = \left(-\frac{\partial \mathbf{J}_{I,e}^{-\top}}{\partial \mathbf{q}_I} \boldsymbol{\tau}_{I,e} \right) \mathbf{J}_I^{-1} + \mathbf{J}_{I,e}^{-\top} \mathbf{K}_{I,q,e} \mathbf{J}_{I,e}^{-1} \tag{3.7}$$

where $\mathbf{K}_{I,ld}$ is the resulting stiffness matrix in which loading is considered. The vector $\boldsymbol{\tau}_{I,e}$ is obtained as

$$\boldsymbol{\tau}_{I,e} = \begin{bmatrix} k_1 \left(q_{1,2} - q_{1,2_0} \right) \\ k_2 \left(q_{2,2} - q_{2,2_0} \right) \\ k_3 \left(q_{3,2} - q_{3,2_0} \right) \end{bmatrix} \tag{3.8}$$
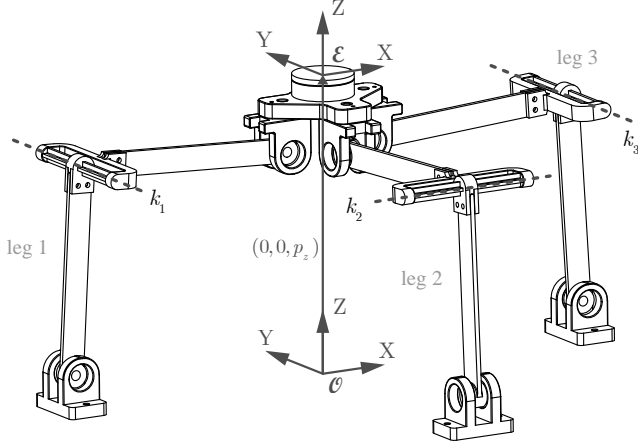
Figure 3.2: Mechanism II is a 1-DoF passive spatial 3-RRR mechanism, where the interaction wrenches are the result of elastic deformation of the compliant joints that make up the second revolute joint of each leg. The pose is determined by a position of reference frame $\mathscr{E}$ with respect to $\mathscr{O}$.

where k_i and $q_{i,2_0}$ were defined in Eq. (3.2).

Since $\mathbf{K}_{I,q,e}$ is the diagonal matrix introduced in Eq. (3.6), the last term of Eq. (3.7) corresponds to the conventional stiffness mapping from joint space to Cartesian space [4], which serves as the benchmark model,

$$\mathbf{K}_{I,bm} = \mathbf{J}_{I,e}^{-\top}\mathbf{K}_{I,q,e}\mathbf{J}_{I,e}^{-1} \tag{3.9}$$

3.2.3. Mechanism II: Passive Spatial 1-DoF

A second mechanism was designed to validate whether inclusion of structural compliance increases stiffness modeling accuracy. This mechanism will be referred to as *mechanism II*. Mechanism II was deliberately designed with significant structural compliance, so that displacements could also be imposed in constrained directions and the reaction wrenches resulting from these displacements were within the measurement range of the wrench sensor.

Mechanical Design of Mechanism II

The designed spatial mechanism is a passive 3-RRR mechanism, in which each second revolute joint is a compliant joint. By positioning one of three legs perpendicularly to the other two, mechanism II has become a 1-DoF mechanism that allows linear motion along the Z-axis. A schematic representation of mechanism II is presented in Fig. 3.2. The inverse kinematic equations are given in Appendix B. Stiffness in the second revolute joints was realized by implementing cross-type compliant revolute joints, whose stiffness in the kinematic DoF, k_i (Nm/rad), was modeled by Trease et al. [23] as

$$k_i = \left(\frac{w}{t} - 0.373\right)\frac{4Gt^4}{3L_j}, \qquad \text{for } i = 1,2,3 \tag{3.10}$$
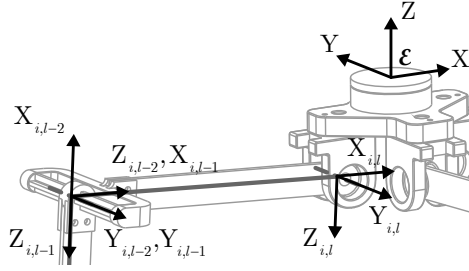
Figure 3.3: Reference frames used to express the structural compliance matrices of the spatial mechanism

3

where the designed cross-type compliant joint has width $w = 9$ mm, thickness $t = 2$ mm, length $L_j = 40$ mm. The compliant joints were manufactured using a Stratasys Dimension BST 1200es 3D printer with Stratasys ABS*plus* material, the shear modulus of which was calculated as $G = 740 \cdot 10^6$ N/m^2 from

$$G = E / (2 + 2\nu)$$

for which the Young's modulus $E = 1.95 \cdot 10^9$ N/m^2 and the Poisson's ratio $\nu = 0.32$ were determined as the average values of two tensile tests. Individual values for E had a 4% difference from this value. The zero angle $q_{i,2_0}$ (rad) of each compliant joint was designed as

$$q_{i,2_0} = \frac{3\pi}{2} \qquad \text{for } i = 1, 2, 3 \tag{3.11}$$

Structural compliance was deliberately introduced in the links so that relatively large displacements could be imposed in constrained directions while the reaction wrenches remained within the measurement range of the wrench sensor. Solid rectangular beams were designed and linear beam theory was used to express the compliance of the point coinciding with the origin of frame $XYZ_{i,l}$ with respect to the point coinciding with the origin of frame $XYZ_{i,l-1}$, as shown in Fig. 3.3. With twists and wrenches expressed in frame $XYZ_{i,l}$, link compliance can be expressed as

$$\mathbf{K}_{link}^{-1} = \begin{bmatrix} \frac{L_{i,j}}{GI_x} & 0 & 0 & 0 & 0 & 0 \\ 0 & \frac{L_{i,j}}{EI_y} & 0 & 0 & 0 & \frac{-L_{i,j}^2}{2EI_y} \\ 0 & 0 & \frac{L_{i,j}}{EI_z} & 0 & \frac{L_{i,j}^2}{2EI_z} & 0 \\ 0 & 0 & 0 & \frac{L_{i,j}}{AE} & 0 & 0 \\ 0 & 0 & \frac{L_{i,j}^2}{2EI_z} & 0 & \frac{L_{i,j}^3}{3EI_z} & 0 \\ 0 & -\frac{L_{i,j}^2}{2EI_y} & 0 & 0 & 0 & \frac{L_{i,j}^3}{3EI_y} \end{bmatrix} \tag{3.12}$$

where $L_{i,1} = 0.135$ m is the length of the first link in each leg and $L_{i,2} = 0.150$ m is the length of the second link in each leg (see Appendix B). The area and the area moments

of inertia, respectively, are

$$A = bh$$
$$I_x = 1/12bh(h^2 + b^2)$$
$$I_y = 1/12bh^3$$
$$I_z = 1/12b^3 h$$

with $b = 3$ mm and $h = 16$ mm. The links were manufactured using the same 3D-printer and material as the compliant joints.

Because structural compliance in the constrained directions of a compliant joint may not be negligible, this compliance was also considered. It is the unintended compliance of the point connected to the origin of frame $XYZ_{i,l-1}$ with respect to frame $XYZ_{i,l-2}$ as in Fig. 3.3. The structural compliance of the joint, so excluding kinematic compliance, and with both displacement twist and reaction wrench expressed in frame $XYZ_{i,l-1}$, can be expressed as[23]

$$\mathbf{K}_{joint}^{-1} = \text{diag}\left(\left[\begin{array}{cccccc} \frac{8EI}{L_j} & 0 & \frac{8EI}{L_j} & \frac{24EI}{L_j^3} & \frac{2AE}{L_j} & \frac{24EI}{L_j^3} \end{array}\right]\right) \tag{3.13}$$

where in this case the area moment of inertia I and area A are

$$I = 1/12 \left(wt^3 + tw^3 - t^4\right)$$
$$A = 2wt - t^2$$

Measurements were done within the elastic range of both joints and links.

Jacobian Analyses of Mechanism II
Each leg of mechanism II has three kinematic joints and three constrained directions. The mechanism has the same kinematic structure as the example mechanism presented in Chapter 2, in which the various unit twists and unit wrenches were described, as well as the full inverse Jacobian. The full inverse Jacobian of mechanism II will be referred to as $\mathbf{J}_{II}^{-1}$.

The joint types of mechanism II are however slightly different from the mechanism presented in Chapter 2. In the mechanism developed in this section there are no actu-ated joints, but similar to the mechanism in Section 2.3, the second kinematic joint is a compliant joint and stiffness in constrained directions is also considered. Therefore, the Jacobian of elasticity for each leg becomes

$$\mathbf{J}_{II,e,i}^{-1} = \begin{bmatrix} \hat{\$}_{wa_{i,2}}^{\top} / (\hat{\$}_{wa_{i,2}}^{\top} \hat{\$}_{ta_{i,2}}) \\ \hat{\$}_{wc_{i,1}}^{\top} / (\hat{\$}_{wc_{i,1}}^{\top} \hat{\$}_{tc_{i,1}}) \\ \hat{\$}_{wc_{i,2}}^{\top} / (\hat{\$}_{wc_{i,2}}^{\top} \hat{\$}_{tc_{i,2}}) \\ \hat{\$}_{wc_{i,3}}^{\top} / (\hat{\$}_{wc_{i,3}}^{\top} \hat{\$}_{tc_{i,3}}) \end{bmatrix} \tag{3.14}$$

The full inverse Jacobian of elasticity for mechanism II is then constructed as

$$\mathbf{J}_{II,e}^{-1} = \begin{bmatrix} \mathbf{J}_{II,e,1}^{-1} \\ \mathbf{J}_{II,e,2}^{-1} \\ \mathbf{J}_{II,e,3}^{-1} \end{bmatrix} \tag{3.15}$$

where each matrix $\mathbf{J}_{II,e,i}^{-1}$ was expressed in (3.14).
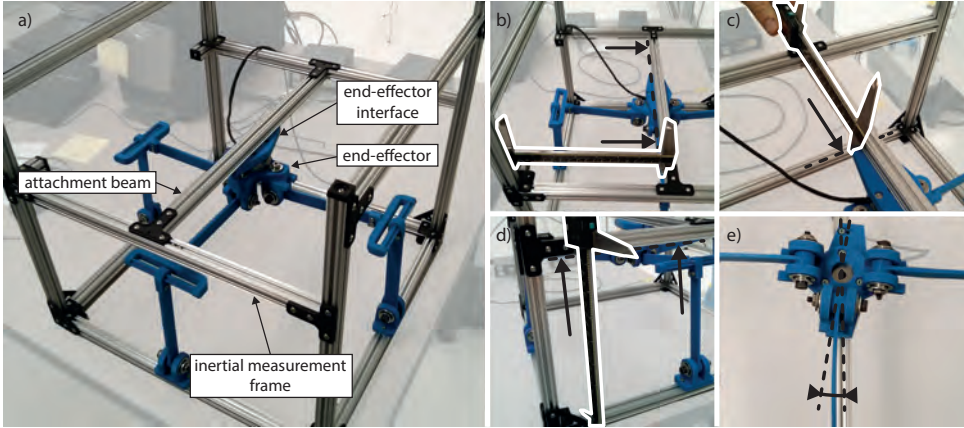
Figure 3.4: a) The end-effector was connected via the end-effector interface to the attachment beam, which is part of the inertial measurement frame. A caliper was used to control the position of the end-effector interface along b) the X-axis, c) the Y-axis, and d) the Z-axis, while e) screw holes in the end-effector interface allowed for a discrete rotation of $1/8$ radians about the Z-axis. This figure illustrates this concept for mechanism II, where the caliper is outlined in white. The same concept holds for mechanism I, but because mechanism I is a planar mechanism it was not displaced along the Z-axis.

COMPETING STIFFNESS MODELS FOR MECHANISM II

The 1-DoF 3-RRR mechanism was developed to experimentally validate a stiffness model in which both loading and structural compliance are included as in Eq. (3.1). The reference model for this validation is the stiffness model in which only loading is considered. Replacing $\mathbf{J}^{-1}$, $\mathbf{J}_e^{-1}$ and $\mathbf{K}_{q,e}$ in Eq. (3.1) with the inverse Jacobian from Section 2.3, Eq. (3.15), and a matrix $\mathbf{K}_{II,q,e}$ gives the expression

$$\mathbf{K}_{II} = \left(-\frac{\partial \mathbf{J}_{II,e}^{-\top}}{\partial \mathbf{q}_{II}} \boldsymbol{\tau}_{II,e} \right) \mathbf{J}_{II}^{-1} + \mathbf{J}_{II,e}^{-\top} \mathbf{K}_{II,q,e} \mathbf{J}_{II,e}^{-1} \tag{3.16}$$

where $\boldsymbol{\tau}_{II,e}$ can be obtained similar to Eq. (3.8), but with k_i and $q_{i,2_0}$ now expressed by Eqs. (3.10) and (3.11). The matrix $\mathbf{K}_{II,q,e}$ in (3.16) is expressed as

$$\mathbf{K}_{II,q,e} = \mathrm{diag}\begin{pmatrix} \mathbf{K}_{II,q,e,1} & \mathbf{K}_{II,q,e,2} & \mathbf{K}_{II,q,e,3} \end{pmatrix} \tag{3.17}$$

with $\mathbf{K}_{II,q,e,i}$ being the stiffness matrix of leg i in elastic joint space.

The two competing stiffness models differ in the description of matrices $\mathbf{K}_{II,q,e,i}$. For the stiffness model in which only loading is considered and not structural compliance, $\mathbf{K}_{II,q,e,i}$ is a function of only the joint stiffness in the kinematic DoFs, which is written as

$$\mathbf{K}_{II,q,e,ld,i} = \mathrm{diag}\left(\begin{bmatrix} k_i & 0 & 0 & 0 \end{bmatrix} \right) \tag{3.18}$$

where k_i was described by Eq. (3.10). In the competing stiffness analysis both loading and structural compliance are considered. Because the individual elements of a leg are connected in series, the compliance matrices of individual elements can be added. This

summation of partial compliance matrices was expressed in Section 2.2.4 as

$$\mathbf{K}_{II,q,e,ld+sc,i}^{-1} = \mathbf{K}_{II,q,e,k,i}^{-1} + \mathbf{J}_{II,e,i}^{-1}\left(\sum_l \mathbf{Ad}_{H_{i,l}^{\mathscr{E}}} \mathbf{K}_{s,i,l}^{-1} \mathbf{Ad}_{H_{i,l}^{\mathscr{E}}}^{\top}\right)\mathbf{J}_{II,e,i}^{-\top} \qquad (3.19)$$

where

$$\mathbf{K}_{II,q,e,k,i}^{-1} = \mathrm{diag}([1/k_i \quad 0 \quad 0 \quad 0])$$

is the kinematic compliance matrix. The matrix $\mathbf{K}_{s,i,l}^{-1}$ is the invertible 6×6 structural compliance matrix of the lth individual structural element of leg i, which was expressed in Eq. (3.12) for links and in Eq. (3.13) for compliant joints. Matrix $\mathbf{Ad}_{H_{i,l}^{\mathscr{E}}}$ is the 6×6 adjoint matrix which maps a vector from the reference frame in which $\mathbf{K}_{s,i,l}^{-1}$ was expressed onto reference frame $\mathscr{E}$, which is connected to the end-effector. See [24] for details on adjoint transformation. The compliance matrix obtained using (3.19) can be (numerically) inverted to obtain $\mathbf{K}_{II,q,e,ld+sc,i}$ so that it can be used to replace each matrix $\mathbf{K}_{II,q,e,i}$ in (3.17).

3.2.4. MEASUREMENT SYSTEM
Because there exists no such thing as a stiffness sensor, a Cartesian stiffness matrix can only be validated by correlating a displacement twist with a differential reaction wrench. Therefore, either the displacement twist or the differential reaction wrench needs to be controlled, while the other is measured. In this research it was chosen to impose a displacement twist and measure the change in reaction wrench using a wrench sensor. Linear displacements were imposed in all three directions, while angular displacements were only imposed about the Z-axis. The measurement system that was developed consists of an adjustable inertial measurement frame and a wrench sensor, which are discussed below in more detail.

ADJUSTABLE INERTIAL MEASUREMENT FRAME
An inertial measurement frame was constructed using commercial OpenBeam components and designed such that its compliance is negligible compared to the compliance of the designed passive mechanisms. One at a time, mechanism I and mechanism II were connected to this inertial measurement frame through their legs as well as their end-effector, as shown in Fig. 3.4 for mechanism II. An attachment beam and an end-effector interface, both considered part of the inertial reference frame, were used to control the pose of the end-effector.

The considered stiffness analyses were validated by comparing the measured differential reaction wrench, i.e., the change in measured wrench before and after a discrete displacement, with the differential reaction wrench as predicted by the considered stiffness analyses. The reference position of the end-effector within the measurement frame as well as the subsequently imposed linear displacements were manually controlled using a caliper, as also visualized in Fig. 3.4. The position of the end-effector along the Y-axis was controlled by moving the end-effector interface along the attachment beam, while the attachment beam itself was moveable in the X- and Z-directions. A digital leveler was used to confirm that all beams in the inertial frame remained parallel to the
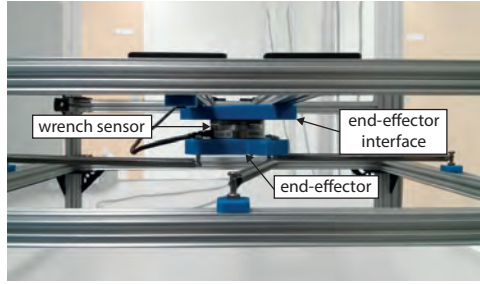
Figure 3.5: To measure the interaction wrench, a wrench sensor is integrated between the end-effector body and the end-effector interface, which is rigidly connected to the inertial frame, here shown for mechanism I.

3

inertial reference frame axes within a margin of 0.2 degrees. Furthermore, a discrete rotation of 1/8 radians about the Z-axis was facilitated by the end-effector interface, as shown in Fig. 3.4e.

Measurements were performed for a range of poses spread over the workspace of each mechanism. This avoided the possibility that pose-specific stiffness behavior affected the results. The poses were randomly selected, except for the pose in which the net wrench on the end-effector is approximately zero. Each displacement was only imposed once, so no repetitive measurements were taken.

To determine whether additional detail in the stiffness analysis improved accuracy, measurement errors had to be smaller than the difference between the predicted values from competing stiffness models. This depended among others on the accuracy with which displacement twist were imposed. It was estimated that the angular positioning resolution $\epsilon_{\Delta\phi}$ [rad] and the linear positioning resolution $\epsilon_{\Delta p}$ [m] were

$$\epsilon_{\Delta\phi} = 1/80, \qquad \epsilon_{\Delta p} = 1/2000 \tag{3.20}$$

REACTION WRENCH SENSOR

Reaction wrenches were measured using an ATI Mini40 sensor with SI-40-2 calibration, whose compliance is negligible compared to the compliance in the mechanism. The wrench sensor was connected in series between the end-effector and the end-effector interface, as is shown in Fig. 3.5. The end-effector interface in turn was rigidly connected to the attachment beam of the inertial measurement frame. As such, the wrench sensor was displaced together with the end-effector body. Before the start of every measurement series, the wrench sensor was initialized at the pose where the net elastic wrench on the end-effector is approximately zero. The specified maximum moment resolution ϵ_m [Nm] and force resolution ϵ_f [N] of the wrench sensor are

$$\epsilon_m = 1/4000, \qquad \epsilon_f = 1/100 \tag{3.21}$$

Because this chapter aims to validate a stiffness analysis, only elastic wrenches are of interest. The influence of gravity on the differential reaction wrench was ignored. Since it is the difference in accuracy of competing stiffness models that is of interest, and because neither model accounts for gravity, this was not expected to affect the results.
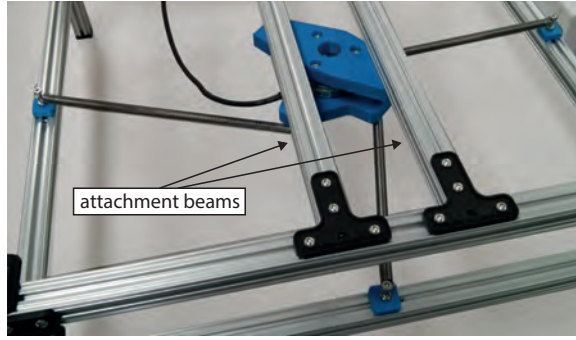
Figure 3.6: Two attachment beams were required to put mechanism I at a reference pose where $\theta \neq 0$.

Table 3.1: Poses at which displacements were imposed on mechanism I to measure the resulting change in reaction wrench

Pose	θ [rad]	p_x [m]	p_y [m]
I-a	0.00	0.180	0.147
I-b	0.00	0.180	0.180
I-c	0.00	0.150	0.150
I-d	$\pi/4$	0.180	0.140
I-e	$-\pi/2$	0.200	0.160
I-f	0.00	0.210	0.170
I-g	$-\pi/4$	0.140	0.140
I-h	0.00	0.170	0.190

MEASUREMENT PLAN FOR MECHANISM I

For the planar 3-RPR mechanism three displacements were imposed at eight different poses. The displacements are:

1. a 5 millimeter displacement along the X-axis, Δx,

2. a 5 millimeter displacement along the Y-axis, Δy, and

3. a rotation of 1/8 radians around the Z-axis, $\Delta \theta$.

The poses at which these displacements were imposed are listed in Table 3.1. Due to the design of the measurement set-up two attachment beams were required to put the mechanism at a pose where $\theta \neq 0$, as shown in Fig. 3.6. Because it was expected that the positioning accuracy would be significantly lower for these poses, only three such poses were included. Also, since Mechanism I is a planar mechanism, only the components m_z, f_x, and f_y of the reaction wrenches were recorded.

Table 3.2: Poses at which displacements were imposed on mechanism II to measure the resulting change in reaction wrench

	II-a	II-b	II-c	II-d	II-e	II-f
p_z [m]	0.197	0.170	0.180	0.190	0.210	0.220
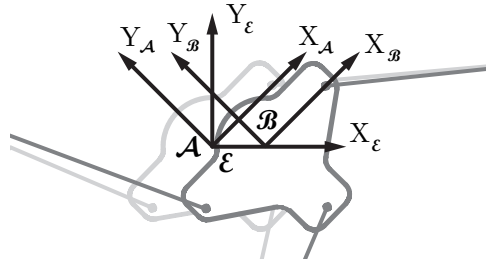
Figure 3.7: The end-effector reference frame $\mathcal{E}$, the rotated measurement frame before imposing the displacement, $\mathcal{A}$, and the rotated measurement frame after imposing a displacement in the X-direction, $\mathcal{B}$, for mechanism I in pose I-d

MEASUREMENT PLAN FOR THE MECHANISM II

For the 1-DoF 3-RRR mechanism four displacements were imposed at six different poses. The displacements are:

1. a 5 millimeter displacement along the X-axis, Δx,

2. a 5 millimeter displacement along the Y-axis, Δy,

3. a 5 millimeter displacement along the Z-axis, Δz, and

4. a rotation of 1/8 radians around the Z-axis, $\Delta\theta$.

These displacements span the allowed DoF (displacement 3), a simply constrained direction (displacement 1), and two overconstrained directions (displacements 2 and 4). The poses at which these displacements were imposed are listed in Table 3.2. Since the only kinematic DoF of mechanism II is a linear displacement along the Z-coordinate, this is the only variable that was changed between poses.

3.2.5. POST-PROCESSING OF MEASUREMENT DATA

To draw conclusions on the difference in accuracy between competing models raw measurements were first post-processed. In the remainder of this section the various post-processing steps are described, namely the transformation of measured wrenches, filtering, and normalization.

TRANSFORMATION OF MEASURED WRENCHES

The change between the reaction wrench before and after a displacement is $\Delta\$_w$. Displacements are assumed sufficiently small so that $\Delta\$_w \approx d\$_w$. At each pose and for each displacement, this differential wrench can be obtained both from the measurements and from the developed stiffness analyses. To compare measured and predicted differential wrenches, all wrenches were expressed in the end-effector reference frame, $\mathscr{E}$, at the respective reference pose. In order to prevent errors as described in Ref. [25], this required some transformations for the case of the measured reaction wrenches, namely

$$\Delta\$_{w,meas} = \mathbf{Ad}_{H_{\mathscr{E}}^{\mathscr{B}}}{}^{\top}\$_{w,meas,\mathscr{B}} - \mathbf{Ad}_{H_{\mathscr{E}}^{\mathscr{A}}}{}^{\top}\$_{w,meas,\mathscr{A}} \tag{3.22}$$

where $\$_{w,meas,\mathscr{A}}$ and $\$_{w,meas,\mathscr{B}}$ are the wrench measurements in the measurement frame respectively before and after imposing the displacement (see Fig. 3.7), and $\mathbf{Ad}_{H_{\mathscr{E}}^{\mathscr{A}}}$ and $\mathbf{Ad}_{H_{\mathscr{E}}^{\mathscr{B}}}$ are the 6×6 adjoint matrices that map vectors expressed in reference frame $\mathscr{E}$ into reference frames $\mathscr{A}$ and $\mathscr{B}$ respectively. The homogenous matrices associated to these adjoint matrices are expressed as

$$H_{\mathscr{E}}^{\mathscr{A}} = \begin{bmatrix} \cos\theta & \sin\theta & 0 & 0 \\ -\sin\theta & \cos\theta & 0 & 0 \\ 0 & 0 & 1 & 0 \\ 0 & 0 & 0 & 1 \end{bmatrix}$$

$$H_{\mathscr{E}}^{\mathscr{A}} = \begin{bmatrix} \cos(\theta+\Delta\theta) & \sin(\theta+\Delta\theta) & 0 & -\cos(\theta+\Delta\theta)\Delta x - \sin(\theta+\Delta\theta)\Delta y \\ -\sin(\theta+\Delta\theta) & \cos(\theta+\Delta\theta) & 0 & \sin(\theta+\Delta\theta)\Delta x - \cos(\theta+\Delta\theta)\Delta y \\ 0 & 0 & 1 & -\Delta z \\ 0 & 0 & 0 & 1 \end{bmatrix}$$

The differential wrench $\Delta\$_w$ can also be predicted using the Cartesian stiffness matrix, evaluated at the pose in question, as

$$\Delta\$_{w,pred} = -\mathbf{K}\Delta\$_d \tag{3.23}$$

where the resulting $\Delta\$_{w,pred}$ is expressed in frame $\mathscr{E}$, and $\Delta\$_d$ is the imposed displacement twist.

FILTERING OF WRENCH ELEMENTS

The next step in the post-processing is to remove all elements below the measurement threshold in each vector $\Delta\$_{w,meas}$. The resulting moment- and force thresholds were determined as

$$\Delta m_{thres} = k_{\phi,min}\epsilon_{\Delta\phi} + 2\epsilon_m \tag{3.24}$$

$$\Delta f_{thres} = k_{p,min}\epsilon_{\Delta p} + 2\epsilon_f \tag{3.25}$$

where $k_{\phi,min}$ and $k_{p,min}$ are the minimum angular and linear values found on the diagonals of the stiffness matrices evaluated at all poses introduced in Table 3.1 or Table 3.2 respectively. The values for the angular and linear positioning resolution, $\epsilon_{\Delta\phi}$ and $\epsilon_{\Delta p}$, were introduced in (3.20). The moment and force measurement resolution values, ϵ_m

and ϵ_f, were introduced in Eq. (3.21) and are multiplied by two because $\Delta\$_{w,meas}$ is the difference between two wrench measurements. The vector $\Delta\$_{w,meas}$ in which all elements below the respective thresholds have been removed is labeled $\Delta\$^*_{w,meas}$. The same elements can also be removed from $\Delta\$_{w,pred}$ to obtain $\Delta\$^*_{w,pred}$, such that

$$\dim(\Delta\$^*_{w,pred}) = \dim(\Delta\$^*_{w,meas}) \leq 6$$

Normalization of Filtered Wrench Elements

The difference between $\Delta\$^*_{w,meas}$ and $\Delta\$^*_{w,pred}$ gives the filtered differential wrench error. This vector contains force error values and moment error values. Because reaction wrench magnitudes are highly mechanism-dependent, normalization was performed to produce more general results. Normalization also allowed all data to be combined. Normalization was performed with respect to $\Delta\$^*_{w,meas}$, namely

$$\boldsymbol{\epsilon}_{\Delta\$^*_w} = \left(\Delta\$^*_{w,pred} - \Delta\$^*_{w,meas}\right)^\top \left[\text{diag}\left(\Delta\$^*_{w,meas}\right)\right]^{-1} \tag{3.26}$$

where $\boldsymbol{\epsilon}_{\Delta\$^*_w}$ is a non-dimensional vector. It should be noted that if an element in $\Delta\$^*_{w,pred}$ is zero, then the corresponding element in $\boldsymbol{\epsilon}_{\Delta\$^*_w}$ is minus unity.

3.3. Processed Measurement Results

Because two independent validation activities have been executed using two separate mechanisms, their results are also presented separately in this section. For both mechanisms a box plot summarizes the normalized errors for the competing stiffness models. In each box plot the central mark indicates the median and the size of the notch shows the confidence interval around the median. If the notches of two box plots do not overlap, this is a strong indication that their medians are significantly different. The outer edges of each box indicate the 25th and 75th percentiles. Besides box plots, this section also presents example matrices.

3.3.1. Results on Effect of Loading

For mechanism I in the poses presented in Table 3.1 it was found that $k_{\phi,min} = 0.180$ and $k_{p,min} = 1.9 \cdot 10^2$. Then, Eqs. (3.24) and (3.25) result in

$$\Delta m_{thres} = 0.0027$$
$$\Delta f_{thres} = 0.117$$

As a result of filtering with the above thresholds, 21 of initial 72 vector elements were removed from further analysis. The raw data can be obtained from Ref. [26].

For all filtered differential wrenches, the corresponding normalized error vector $\boldsymbol{\epsilon}_{\Delta\$^*_w}$ can be determined using Eq. (3.26) for the two competing stiffness models introduced in Eqs. (3.7) and (3.9). The individual values in all resulting normalized error vectors for both the benchmark model introduced in Eq. (3.9) and the model including the effect of loading, expressed in Eq. (3.7), have been combined in box plots, which are shown in Fig. 3.8. The figure shows that the median of the normalized errors is closer to zero for
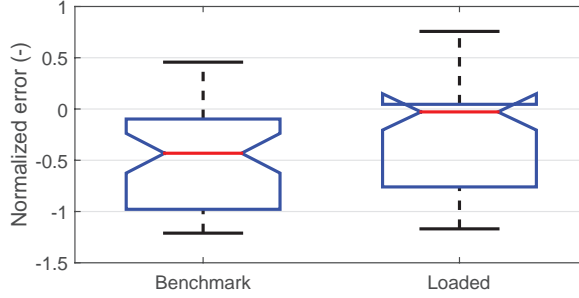
Figure 3.8: Box plots of the normalized error values for the stiffness models without (benchmark model) and with consideration of the effect of loading, as obtained from measurements on mechanism I.

the stiffness model which considers loading. A Wilcoxon rank-sum test demonstrates that the null hypothesis that the two sets have equal medians can be rejected at the 5% significance level. This means that the increase in accuracy caused by the inclusion of the effect of loading in the stiffness analysis is significant.

To further illustrate the impact of loading on the stiffness behavior of a parallel mechanism, the stiffness matrix is evaluated at pose I-a, as introduced in Table 3.1, for both stiffness models. The benchmark stiffness matrix, which only involves Jacobian transformations, at this pose is

$$\mathbf{K}_{I,bm}\big|_a = \begin{bmatrix} 0.02 & 1.83 & 0 \\ 1.83 & 218 & 0 \\ 0 & 0 & 125 \end{bmatrix} \tag{3.27}$$

In pose I-a the net wrench applied by the three linear springs on the end-effector is approximately zero. However, the internal loading is not zero, and as a result also the Jacobian-derivative term is not zero. The stiffness matrix which includes this term is evaluated as

$$\mathbf{K}_{I,ld}\big|_a = \begin{bmatrix} 0.18 & 2.01 & 0 \\ 2.01 & 246 & 0 \\ 0 & 0 & 212 \end{bmatrix} \tag{3.28}$$

The difference between Eqs. (3.27) and (3.28) is due to loading, captured by the Jacobian-derivative term in Eq. (3.1).

3.3.2. Results on Inclusion of Structural Compliance

For mechanism II in the poses presented in Table 3.2 it was found that $k_{\phi,min} = 0.95$ and $k_{p,min} = 76$. Then, Eqs. (3.24) and (3.25) result in

$$\Delta m_{thres} = 0.0124$$
$$\Delta f_{thres} = 0.058$$

As a result of filtering with the above thresholds, 53 of initial 144 vector elements were removed from further analysis. The raw data can be obtained from Ref. [26].
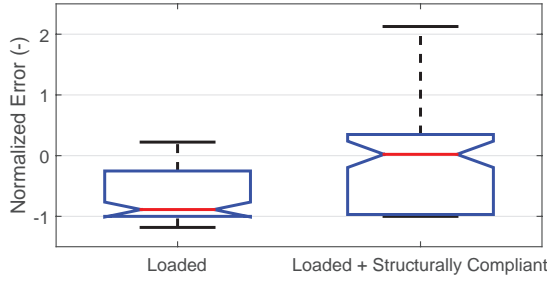
Figure 3.9: Box plots of the normalized error values for the stiffness model which only considers loading and for the stiffness model which also considers structural compliance, as obtained from measurements on mechanism II.

The values of all elements in the resulting normalized error vectors for the two competing stiffness models expressed by Eqs. (3.16)-(3.19) are combined in box plots, which can be found in Fig. 3.9. The median of the errors is closer to zero for the model which also considers structural compliance. A Wilcoxon rank-sum test proves that this difference is significant; the null hypothesis that the two sets have equal medians can be rejected at the 5% significance level (in fact, it can be rejected at the 0.000001% significance level).

To further illustrate the impact of the inclusion of structural stiffness, for both stiffness models the stiffness matrix is evaluated at pose II-a, as introduced in Table 3.2. The stiffness matrix which only includes the stiffness of the compliant joints in their kinematic DoF at this pose is

$$
\mathbf{K}_{II,ld}\big|_a =
\begin{bmatrix}
0.01 & 0 & 0 & 0 & 0.88 & 0.71 \\
0 & 0.02 & 0 & -1.77 & 0 & 0 \\
0 & 0 & 0 & 0 & 0 & 0 \\
0 & -1.77 & 0 & 197 & 0 & 0 \\
0.88 & 0 & 0 & 0 & 98.5 & 78.9 \\
0.71 & 0 & 0 & 0 & 78.9 & 189
\end{bmatrix}
\tag{3.29}
$$

The stiffness matrix based on the model which also considers structural compliance is evaluated at pose II-a as

$$
\mathbf{K}_{II,ld+sc}\big|_a =
\begin{bmatrix}
2.74 & 0 & 0 & 0 & 21.1 & 0.66 \\
0 & 1.38 & -1.16 & -11.8 & 0 & 0 \\
0 & -1.16 & 5.77 & 13.0 & 0 & 0 \\
0 & -11.8 & 13.0 & 296 & 0 & 0 \\
21.1 & 0 & 0 & 0 & 319 & 73.0 \\
0.66 & 0 & 0 & 0 & 73.0 & 175
\end{bmatrix}
\tag{3.30}
$$

The difference between Eqs. (3.29) and (3.30) is due to the modeled structural stiffness of the links and joints.

3.4. SIGNIFICANCE OF THE RESULTS

FIGURES 3.8 and 3.9 have presented the main results of this chapter. Figure 3.8 demonstrates for the passive planar mechanism shown in Fig. 3.1 that the accuracy of the symbolic stiffness analysis improves significantly when the effect of loading is considered. Similarly, Fig. 3.9 shows that this accuracy also improves significantly when structural compliance is considered for the lower mobility, overconstrained mechanism shown in Fig. 3.2. Additionally, the matrix in Eq. (3.30) is full rank despite the fact that the stiffness matrix of individual legs of mechanism II are singular due to the presence of zero stiffness joints. As such, the considered stiffness analysis method has produced valid results for both a very simple planar mechanism and for a more general spatial mechanism.

The results in this chapter are based on measurements that were normalized in order to make the results more general. One characteristic of normalization is that small absolute error values correspond to large normalized error values if the measured value is small. This has partially been alleviated by the applied filtering, but nonetheless this effect is acknowledged by the authors. In fact, this only strengthens the results of this chapter, because significant effects have been found despite this aggravation of measurement errors through normalization. Also, it was pointed out that if an element in $\Delta\$^*_{w,pred}$ is zero, then the corresponding element in $\boldsymbol{\epsilon}_{\Delta\$^*_w}$ is minus unity. This explains the tendency towards minus unity in the box plots shown in Figs. 3.8 and 3.9.

As was also discussed in Chapter 2, even if the net wrench is zero, the Jacobian-derivative term may still be significant due to internal loads, which are also a form of loading. This effect is particularly relevant for mechanisms with compliant joints, as is demonstrated by the difference between the matrices in Eqs. (3.27) and (3.28), which is only due to the Jacobian-derivative term, while the net wrench is approximately zero in the considered pose.

Both mechanisms that were introduced in this chapter are conservative systems, which means that the stiffness matrices should be symmetric. However, for a mechanism similar to mechanism I, an earlier research found an asymmetric stiffness matrix when the effect of loading was considered [27]. The fact that all stiffness matrices presented in this chapter are symmetric is thus noteworthy.

3.5. CONCLUSIONS ON THE STIFFNESS ANALYSIS VALIDATION

THIS chapter has made two main contributions. First, it has been demonstrated that the inclusion of the effect of loading as presented in Chapter 2 can make a symbolic stiffness analysis significantly more accurate, even for a simple mechanism. Secondly, experimentally obtained results have shown that accuracy can also be significantly improved if the structural compliance of a mechanism is considered as is done both in Ref. [20] and Chapter 2, i.e., based on the constraint relations in the Jacobian analysis.

The above results were obtained as part of a set of activities to validate the Jacobian-based stiffness analysis method presented in Chapter 2. Models with an increasing level of detail were compared for two mechanisms, both specifically designed for this purpose. The benchmark model was the stiffness analysis method based on the Jacobian transformation from joint space to Cartesian space. Because it was shown that the ac-

curacy of the resulting models increased with increasing level of detail, the considered stiffness analysis method is considered valid.

For the first time, in this chapter it has been experimentally confirmed that inclusion of the Jacobian-derivative term in a stiffness analysis has a positive effect on its accuracy. Since the Jacobian-derivative term represents the effect of loading this finding is particularly relevant for the field of compliant parallel manipulator design. Also, in contrast to earlier reports, all stiffness matrices obtained throughout this research in which loading was considered are symmetric. This symmetry is consistent with the fact that the designed mechanisms are conservative systems.

Also the observed increase in accuracy when structural compliance is considered in the Jacobian-based stiffness model is a relevant finding. This was demonstrated for a lower mobility mechanism constructed from legs whose individual stiffness matrices are singular due to the presence of zero stiffness joints. So far, Jacobian-based stiffness analysis methods that can take the structural compliance of lower mobility parallel manipulators with zero stiffness joints into account have only been validated using FEM models. This chapter has therefore presented the first experimental results in support of these earlier validation activities.

REFERENCES

[1] A. G. L. Hoevenaars, C. Gosselin, P. Lambert, and J. Herder, *Experimental Validation of Jacobian-Based Stiffness Analysis Method for Parallel Manipulators with Non-Redundant Legs,* Journal of Mechanisms and Robotics (2015), 10.1115/1.4032204.

[2] F. Majou, C. Gosselin, P. Wenger, and D. Chablat, *Parametric stiffness analysis of the Orthoglide,* Mechanism and Machine Theory **42**, 296 (2007), arXiv:0708.3723 .

[3] C. Pinto, J. Corral, O. Altuzarra, and A. Hernández, *A methodology for static stiffness mapping in lower mobility parallel manipulators with decoupled motions,* Robotica **28**, 719 (2010).

[4] C. Gosselin, *Stiffness mapping for parallel manipulators,* IEEE Transactions on Robotics and Automation **6**, 377 (1990).

[5] C. Quennouelle and C. Gosselin, *Kinematostatic modeling of compliant parallel mechanisms,* Meccanica **46**, 155 (2011).

[6] S.-F. Chen and I. Kao, *Conservative Congruence Transformation for Joint and Cartesian Stiffness Matrices of Robotic Hands and Fingers,* The International Journal of Robotics Research **19**, 835 (2000).

[7] J.-P. Merlet and C. Gosselin, *Parallel Mechanisms and Robots,* in *Springer Handbook of Robotics,* edited by B. Siciliano and O. Khatib (Springer Berlin Heidelberg, Berlin, Heidelberg, 2008) pp. 269–285.

[8] C. Quennouelle and C. Gosselin, *A Quasi-Static Model for Planar Compliant Parallel Mechanisms,* Journal of Mechanisms and Robotics **1**, 021012 (2009).

[9] A. Ahmad, K. Andersson, U. Sellgren, and S. Khan, *A stiffness modeling methodology for simulation-driven design of haptic devices,* Engineering with Computers **30**, 125 (2012).

[10] G. Cheng, P. Xu, D. Yang, and H. Liu, *Stiffness analysis of a 3CPS parallel manipulator for mirror active adjusting platform in segmented telescope,* Robotics and Computer-Integrated Manufacturing **29**, 302 (2013).

[11] S. A. Joshi and L.-W. Tsai, *Jacobian Analysis of Limited-DOF Parallel Manipulators,* Journal of Mechanical Design **124**, 254 (2002).

[12] T. Huang, H. T. Liu, and D. G. Chetwynd, *Generalized Jacobian analysis of lower mobility manipulators,* Mechanism and Machine Theory **46**, 831 (2011).

[13] T. Huang, X. Zhao, and D. J. Whitehouse, *Stiffness estimation of a tripod-based parallel kinematic machine,* IEEE Transactions on Robotics and Automation **18**, 50 (2002).

[14] M. Wahle and B. Corves, *Stiffness Analysis of Clavel's DELTA Robot,* in *Intelligent Robotics and Applications,* Lecture Notes in Computer Science, Vol. 7101, edited by S. Jeschke, H. Liu, and D. Schilberg (Springer Berlin Heidelberg, Berlin, Heidelberg, 2011) pp. 240–249.

[15] H.-H. Pham and I.-M. Chen, *Stiffness modeling of flexure parallel mechanism,* Precision Engineering **29**, 467 (2005).

[16] D. Zhang and S. Y. Lang, *Stiffness modeling for a class of reconfigurable PKMs with three to five degrees of freedom,* Journal of Manufacturing Systems **23**, 316 (2004).

[17] Y. Wang, H. Liu, T. Huang, and D. G. Chetwynd, *Stiffness Modeling of the Tricept Robot Using the Overall Jacobian Matrix,* Journal of Mechanisms and Robotics **1**, 021002 (2009).

[18] Y. Li and Q. Xu, *Stiffness analysis for a 3-PUU parallel kinematic machine,* Mechanism and Machine Theory **43**, 186 (2008).

[19] A. Pashkevich, D. Chablat, and P. Wenger, *Stiffness analysis of overconstrained parallel manipulators,* Mechanism and Machine Theory **44**, 966 (2009).

[20] H. Sung Kim and H. Lipkin, *Stiffness of Parallel Manipulators With Serially Connected Legs,* Journal of Mechanisms and Robotics **6**, 031001 (2014).

[21] B.-j. Yi, G. B. Chung, H. Y. Na, W. K. Kim, and I. H. Suh, *Design and experiment of a 3-dof parallel micromechanism utilizing flexure hinges,* IEEE Transactions on Robotics and Automation **19**, 604 (2003).

[22] G. Alici and B. Shirinzadeh, *Enhanced stiffness modeling, identification and characterization for robot manipulators,* IEEE Transactions on Robotics **21**, 554 (2005).

[23] B. P. Trease, Y.-M. Moon, and S. Kota, *Design of Large-Displacement Compliant Joints,* Journal of Mechanical Design **127**, 788 (2005).

[24] R. M. Murray, Z. Li, and S. S. Sastry, *A Mathematical Introduction to Robotic Manipulation* (CRC Press, 1994).

[25] J. Kövecses and J. Angeles, *The stiffness matrix in elastically articulated rigid-body systems,* Multibody System Dynamics **18**, 169 (2007).

[26] A. G. L. Hoevenaars, *Wrench Measurements on a Planar, Passive, 3-DoF, 3-RPR Parallel Mechanism and a Spatial, Passive, 1-DoF, 3-RRR Parallel Mechanism,* (2015).

[27] M. Griffis and J. Duffy, *Global stiffness modeling of a class of simple compliant couplings,* Mechanism and Machine Theory **28**, 207 (1993).

3

4

CONSISTENT MODELING RESOLVES ASYMMETRY IN STIFFNESS MATRICES

Alles komt weer goed,
Vannacht had ik een droom

Thomas Acda et al.

De Poemas - Bang dat dit het is

The example stiffness analyses performed in Chapter 3 produced symmetric Cartesian stiffness matrices. In these analysis loading was captured by the Jacobian-derivative term that is part of the stiffness analysis method developed in Chapter 2. However, early examples of stiffness analyses of parallel manipulators in which the effect of loading was considered resulted in asymmetric stiffness matrices, which goes against the definition of stiffness. By replicating those first analyses using the method presented in Chapter 2, this chapter finds that the earlier observed asymmetry can be explained as a modeling inconsistency. If that inconsistency is corrected, symmetric matrices are obtained, which supports the notion that the Jacobian-derivative term is an integral part of the stiffness analysis of robotic manipulators and mechanisms.

4.1. Introduction to Load Dependence of Stiffness

Jacobian-based stiffness analysis methods are being used in the design and optimization [1, 2], identification [3, 4] and control [5] of robotic manipulators. The popularity of these methods is explained by their compact, symbolic formulation of the Cartesian stiffness matrix as a function of a manipulator's configuration and joint stiffness values. Jacobian-based stiffness analysis methods have been developed both for serial manipulators [6, 7] and parallel manipulators [8–12]. These stiffness analysis methods have been used for the analysis of a wide range of parallel manipulators, such as machining robots [1, 13, 14], haptic devices [15, 16], and precision manipulators [17, 18].

Several researchers have recognized that loading can have a significant effect on a stiffness analysis [19, 20], which in turn can affect stability [21] and accuracy [22]. For serial manipulators, this dependency on loading was expressed by Chen and Kao [23] in a term that depends on the derivative of the Jacobian, and which represents the change in the transmission of the already applied joint torques as a function of a displacement. The effect of loading on the Cartesian stiffness matrix has also been expressed for parallel manipulators [10, 12].

However, when Griffis and Duffy [24] performed the stiffness analysis of two mechanisms under loading, they obtained asymmetric stiffness matrices. This is in contrast to the definition of a stiffness matrix, which is necessarily symmetric.

Over the past decades, various researchers have analyzed the asymmetric stiffness matrices presented by Griffis and Duffy [24]. Ciblak and Lipkin [25] introduced an explicit formulation for the skew-symmetric part of these asymmetric matrices, although Chen [7] later argued that this formulation is not unique. Explanations for the asymmetry have been sought mainly in the choice of basis twists [26–28]. Zefran et al. [26, 27] concluded that asymmetry is a result of the Christoffel symbols not being symmetric, which they explained by the fact that finite screw displacements in general do not commute. Kövecses and Angeles [28] considered this to be the result of an inconsistent definition of twists and wrenches. They observed that if displacement twists are described in the initial configuration, while differential wrenches are defined at the displaced manipulator configuration, an asymmetric mapping occurs similar to those found in Ref. [27]. They argued that the considered mapping therefore does not properly represent a manipulator's stiffness, which is a well-defined physical property at a specific configuration, and which must be symmetric.

Several researchers have replicated the analyses in Ref. [24] using different methods. The stiffness matrices found by Sanger et al. [29] and Metzger et al. [30] confirmed the results of Griffis and Duffy. On the other hand, the numerical method used by Huang and Li [31] resulted in a stiffness matrix in which part of the asymmetry had disappeared. Moreover, in Chapter 2 the Jacobian-derivative term was included in the analyses of two compliant mechanisms, of which one is similar to the planar mechanism analyzed in Ref. [24]. In these analyses only symmetric stiffness matrices were obtained. The fact that different results have been obtained using different modeling methods raises the question whether the observed asymmetry in Ref. [24] is not due to a modeling inconsistency rather than a fundamental problem in the analysis method.

The occurrence of asymmetry is in disagreement with the definition of stiffness, which must be symmetric to comply with the principle of energy conservation. Thus, if the

asymmetric stiffness matrices presented in the literature are correct, then the Jacobian-derivative term cannot be considered as an integral part of the Cartesian stiffness analysis. Understanding the cause of this asymmetry is therefore crucial for the further development and use of the Jacobian-derivative term in stiffness analysis methods.

The goal of this chapter is to show that the asymmetric stiffness matrices in Ref. [24] are the result of inconsistent modeling. For that, first the stiffness analyses in Ref. [24] are replicated using the analysis method introduced in Chapter 2, which results in symmetric stiffness matrices. Next, it is shown that the asymmetry in Ref. [24] is accounted for by an inconsistent expression of the moment arm vectors.

4.2. REPLICATION OF PREVIOUS ANALYSES

I N this section the analysis of the planar three degree of freedom (DoF) compliant mechanism and the spatial 6-DoF mechanism presented in Ref. [24] are replicated using the Jacobian-based stiffness analysis method introduced in Chapter 2. The general formulation of this analysis method is repeated here for convenience, namely

$$\mathbf{K} = \left(-\frac{\partial \mathbf{J}_e^{-\top}}{\partial \mathbf{q}} \boldsymbol{\tau}_e \right) \mathbf{J}^{-1} + \mathbf{J}_e^{-\top} \mathbf{K}_{q,e} \mathbf{J}_e^{-1} \tag{4.1}$$

where $\mathbf{K}$ is the 6×6 Cartesian stiffness matrix, and for a parallel manipulator with N legs $\mathbf{q}$ is the vector of size $6N$, which contains all real and virtual joint coordinates. The vector $\boldsymbol{\tau}_e$ is the joint torque vector where all entries associated to zero stiffness joints were removed (see Section 2.2 for more details), $\mathbf{J}^{-1}$ is the $6N \times 6$ full inverse Jacobian, and $\mathbf{J}_e^{-1}$ is the inverse Jacobian of elasticity that maps an end-effector displacement twist onto $d\mathbf{q}_e$, which is the joint displacement vector in which all entries associated to zero stiffness joints are removed. Finally, matrix $\mathbf{K}_{q,e}$ is the stiffness matrix of the parallel manipulator expressed in the space spanned by the elastic joint coordinates, which is a diagonal matrix whose entries are the spring stiffness values if structural stiffness is not considered. The matrix $\mathbf{K}$ acts on a displacement twist $\$_{\mathbf{d}} = [d\boldsymbol{\phi}^\top \quad d\mathbf{p}^\top]^\top$ and produces a differential wrench $d\$_{\mathbf{w}} = [d\mathbf{m}^\top \quad d\mathbf{f}^\top]^\top$, where $d\boldsymbol{\phi}$ is a differential rotation vector, $d\mathbf{p}$ is a differential displacement vector, $d\mathbf{m}$ is a differential moment vector, and $d\mathbf{f}$ is a differential force vector.

Equation (4.1) consists of two terms, of which the second term covers the traditional mapping of a joint stiffness matrix onto Cartesian space, e.g. as in Ref. [8]. The first term represents the effect of loading, as derived in Section 2.2, and which is the topic of this chapter. How to obtain the derivative of a Jacobian matrix multiplied by a joint torque vector is explained in, for example, the appendix of Ref. [23]. Despite the fact that not all joints necessarily have elastic properties, it is necessary to take the derivative of $\mathbf{J}_e^{-\top}$ with respect to all joint coordinates. This is because the wrench related to a specific joint torque depends on the configuration of the manipulator and can therefore be a function of other joint coordinates.

4.2.1. PLANAR 3DoF MECHANISM

The planar mechanism analyzed in Ref. [24] is a 3-RPR mechanism, shown in Fig. 4.1 in the configuration in which its stiffness matrix was evaluated. Because both revolute
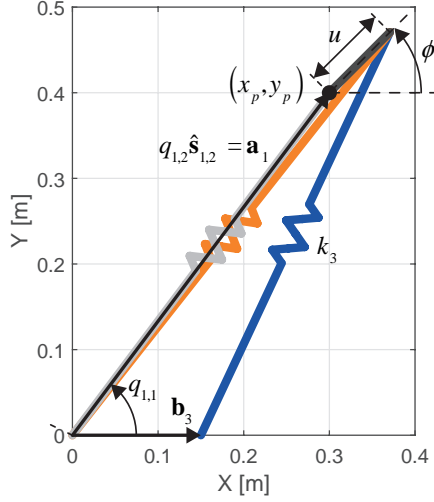
Figure 4.1: The 3-RPR planar mechanism in the configuration in which its stiffness matrix was evaluated in Ref. [24] with some example vectors indicated

joints in each leg are zero stiffness joints and each prismatic joint is modeled as a linear spring, the vector $\boldsymbol{\tau}_{P,e}$ is

$$\boldsymbol{\tau}_{P,e} = \begin{bmatrix} -k_{1,2}\left(q_{1,2} - q_{0_{1,2}}\right) \\ -k_{2,2}\left(q_{2,2} - q_{0_{2,2}}\right) \\ -k_{3,2}\left(q_{3,2} - q_{0_{3,2}}\right) \end{bmatrix} \tag{4.2}$$

where $k_{i,2}$ is the stiffness of the linear spring in leg i and $q_{0_{i,2}}$ its free length. The matrix $\mathbf{K}_{q,e}$ is the 3×3 diagonal matrix whose entries are the three stiffness values.

To develop $\mathbf{J}^{-1}$ and $\mathbf{J}_e^{-\top}$, it was necessary to describe for each leg a complete set of twists of permission and wrenches of actuation, as introduced in Ref. [32]. The mechanism in Fig. 4.1 is similar in structure as mechanism I introduced in Section 3.2.2 and therefore has the same twists of permission, which are for each leg

$$\hat{\$}_{P,ta_{i,1}} = \begin{bmatrix} \hat{\mathbf{s}}_{i,1} \\ -(q_{i,2}\hat{\mathbf{s}}_{i,2} - \mathbf{a}_i) \times \hat{\mathbf{e}}_3 \end{bmatrix} \tag{4.3}$$

$$\hat{\$}_{P,ta_{i,2}} = \begin{bmatrix} \mathbf{0}_{3 \times 1} \\ \hat{\mathbf{s}}_{i,2} \end{bmatrix} \tag{4.4}$$

$$\hat{\$}_{P,ta_{i,3}} = \begin{bmatrix} \hat{\mathbf{s}}_{i,3} \\ \mathbf{a}_i \times \hat{\mathbf{s}}_{i,3} \end{bmatrix} \tag{4.5}$$

where $\hat{\$}_{P,ta_{i,1}}$, $\hat{\$}_{P,ta_{i,2}}$, and $\hat{\$}_{P,ta_{i,3}}$ are the unit twists associated respectively to the lower zero stiffness revolute joint, the passive compliant prismatic joint, and the upper zero stiffness revolute joint of the ith leg of the planar mechanism. The mechanism lies in the XY-plane, so $\hat{\mathbf{s}}_{i,1} = \hat{\mathbf{s}}_{i,3} = \hat{\mathbf{e}}_3$, where $\hat{\mathbf{e}}_3$ is the unit vector aligned with the Z-axis (pointing

out of the page). Furthermore,

$$\hat{\mathbf{s}}_{i,2} = \begin{bmatrix} \cos q_{i,1} \\ \sin q_{i,1} \\ 0 \end{bmatrix} \tag{4.6}$$

is the unit vector along the prismatic joint axis for each leg i, while $\mathbf{a}_i$ is the vector that describes the position of the connection point of the ith leg with respect to the point on the end-effector which coincides with the origin of the inertial reference frame. An example of this vector is included in Fig. 4.1. For each individual leg of the planar mechanism this vector is expressed as

$$\mathbf{a}_1 = \begin{bmatrix} x_p \\ y_p \\ 0 \end{bmatrix}, \qquad \mathbf{a}_2 = \mathbf{a}_3 = \begin{bmatrix} x_p + u\cos\phi \\ y_p + u\sin\phi \\ 0 \end{bmatrix}. \tag{4.7}$$

Because the mechanism is considered in the XY-plane that contains the mechanism, and because Eqs. (4.3)-(4.5) are linearly independent, no constraint wrenches can be identified. Three unit wrenches of actuation can then be identified, which also lie in the XY-plane, namely

$$\hat{\$}_{P,wa_{i,1}} = \begin{bmatrix} \mathbf{a}_i \times (\hat{\mathbf{e}}_3 \times \hat{\mathbf{s}}_{i,2}) \\ (\hat{\mathbf{e}}_3 \times \hat{\mathbf{s}}_{i,2}) \end{bmatrix} \tag{4.8}$$

$$\hat{\$}_{P,wa_{i,2}} = \begin{bmatrix} \mathbf{a}_i \times \hat{\mathbf{s}}_{i,2} \\ \hat{\mathbf{s}}_{i,2} \end{bmatrix} \tag{4.9}$$

$$\hat{\$}_{P,wa_{i,3}} = \begin{bmatrix} -(q_{i,2}\hat{\mathbf{s}}_{i,2} - \mathbf{a}_i) \times (\hat{\mathbf{e}}_3 \times \hat{\mathbf{s}}_{i,2}) \\ (\hat{\mathbf{e}}_3 \times \hat{\mathbf{s}}_{i,2}) \end{bmatrix}. \tag{4.10}$$

Because the twists and wrenches in Eqs. (4.3)-(4.5) and (4.8)-(4.10) are six-dimensional, while the mechanism has been analyzed in the XY-plane, each twist and wrench was transformed into their equivalent two-dimensional twist and wrench. For that, the first, second, and sixth entry of each twist and wrench was removed.

Next, the full inverse Jacobian of the planar mechanism can be assembled as

$$\mathbf{J}_P^{-1} = \begin{bmatrix} \mathbf{J}_{P,1}^{-1} \\ \mathbf{J}_{P,2}^{-1} \\ \mathbf{J}_{P,3}^{-1} \end{bmatrix} \tag{4.11}$$

where each matrix $\mathbf{J}_{P,i}^{-1}$ is expressed as

$$\mathbf{J}_{P,i}^{-1} = \begin{bmatrix} \hat{\$}_{P,wa_{i,1}}^{\top} / (\hat{\$}_{P,wa_{i,1}}^{\top} \hat{\$}_{P,ta_{i,1}}) \\ \hat{\$}_{P,wa_{i,2}}^{\top} / (\hat{\$}_{P,wa_{i,2}}^{\top} \hat{\$}_{P,ta_{i,2}}) \\ \hat{\$}_{P,wa_{i,3}}^{\top} / (\hat{\$}_{P,wa_{i,3}}^{\top} \hat{\$}_{P,ta_{i,3}}) \end{bmatrix} \tag{4.12}$$

with the various twists and wrenches defined in Eqs. (4.3)-(4.5) and (4.8)-(4.10).

Similar to Section 2.3, the inverse Jacobian of elasticity of the planar mechanism, $\mathbf{J}_{P,e}^{-1}$, is obtained by removing the rows from Eq. (4.11) which are associated to zero stiffness

joints. Because the first and third joint of each leg are zero stiffness joints, the inverse Jacobian of elasticity for the planar mechanism is obtained as

$$
\mathbf{J}_{P,e}^{-1} = \begin{bmatrix} \hat{\$}_{P,wa_{1,2}}^{\top} / (\hat{\$}_{P,wa_{1,2}}^{\top} \hat{\$}_{P,ta_{1,2}}) \\ \hat{\$}_{P,wa_{2,2}}^{\top} / (\hat{\$}_{P,wa_{2,2}}^{\top} \hat{\$}_{P,ta_{2,2}}) \\ \hat{\$}_{P,wa_{3,2}}^{\top} / (\hat{\$}_{P,wa_{3,2}}^{\top} \hat{\$}_{P,ta_{3,2}}) \end{bmatrix}.
\tag{4.13}
$$

The derivative of matrix $\mathbf{J}_{P,e}^{-1}$ with respect to complete set of joint coordinates $\mathbf{q}$ multiplied by $\boldsymbol{\tau}_{P,e}$, i.e. the first term in Eq. (4.1), was obtained as in the appendix of Ref. [23] and using MATLAB's *diff* function.

4.2.2. Spatial 6DoF Mechanism

To replicate the analysis of the Stewart-Gough mechanism as in Ref. [24], a 6-UPS mechanism will be considered instead of the 6-SPS mechanism [33]. The reason is that in a 6-SPS mechanism each leg has seven independent joints, which means that there is one redundant DoF in each leg, while the stiffness analysis method presented in Chapter 2 only applies to parallel manipulators with non-redundant legs. Therefore, in order to use the method introduced in Chapter 2, the 6-UPS mechanism must be considered. This will not change the results, because the wrench applied by the elastic prismatic joint is not affected by a rotation around its own axis.

The 6-UPS mechanism in the configuration in which its stiffness matrix was evaluated in Ref. [24] is shown in Fig. 4.2, including examples of vectors that are used in this analysis. Because the universal joint and the spherical joint in each leg are zero stiffness joints, while the third joint of each leg is a prismatic joint that is modeled as a linear spring, the vector $\boldsymbol{\tau}_e$ for the spatial mechanism is

$$
\boldsymbol{\tau}_{S,e} = \begin{bmatrix} -k_{1,3}\left(q_{1,3} - q_{0_{1,3}}\right) \\ -k_{2,3}\left(q_{2,3} - q_{0_{2,3}}\right) \\ \vdots \\ -k_{6,3}\left(q_{6,3} - q_{0_{6,3}}\right) \end{bmatrix}
\tag{4.14}
$$

where $k_{i,3}$ is the stiffness of the linear spring in leg i and $q_{0_{i,3}}$ its free length. The matrix $\mathbf{K}_{q,e}$ is the 6×6 diagonal matrix whose entries are the six stiffness values.

To develop $\mathbf{J}^{-1}$ and $\mathbf{J}_e^{-\top}$ for the considered Stewart-Gough platform it was again necessary to describe for each leg a complete set of twists of permission and wrenches of
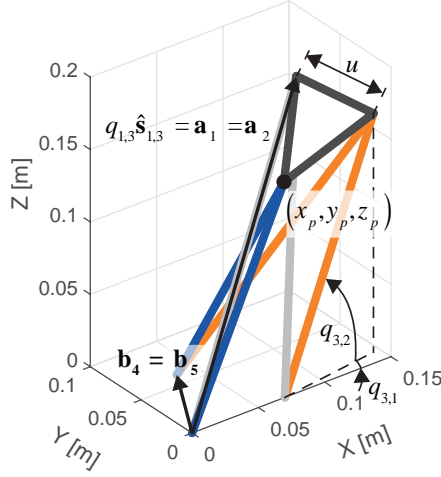
Figure 4.2: The 6-UPS spatial mechanism in the configuration in which the stiffness matrix was evaluated in Ref. [24] with some example vectors indicated

actuation as in Ref. [32]. The twists of permission were identified as

$$\hat{\$}_{S,ta_{i,1}} = \begin{bmatrix} \hat{\mathbf{s}}_{i,1} \\ -(q_{i,3}\hat{\mathbf{s}}_{i,3} - \mathbf{a}_i) \times \hat{\mathbf{s}}_{i,1} \end{bmatrix}, \tag{4.15}$$

$$\hat{\$}_{S,ta_{i,2}} = \begin{bmatrix} \hat{\mathbf{s}}_{i,2} \\ -(q_{i,3}\hat{\mathbf{s}}_{i,3} - \mathbf{a}_i) \times \hat{\mathbf{s}}_{i,2} \end{bmatrix}, \tag{4.16}$$

$$\hat{\$}_{S,ta_{i,3}} = \begin{bmatrix} \mathbf{0}_{3 \times 1} \\ \hat{\mathbf{s}}_{i,3} \end{bmatrix}, \tag{4.17}$$

$$\hat{\$}_{S,ta_{i,4}} = \begin{bmatrix} \hat{\mathbf{s}}_{i,4} \\ \mathbf{a}_i \times \hat{\mathbf{s}}_{i,4} \end{bmatrix}, \tag{4.18}$$

$$\hat{\$}_{S,ta_{i,5}} = \begin{bmatrix} \hat{\mathbf{s}}_{i,5} \\ \mathbf{a}_i \times \hat{\mathbf{s}}_{i,5} \end{bmatrix}, \tag{4.19}$$

$$\hat{\$}_{S,ta_{i,6}} = \begin{bmatrix} \hat{\mathbf{s}}_{i,6} \\ \mathbf{a}_i \times \hat{\mathbf{s}}_{i,6} \end{bmatrix} \tag{4.20}$$

where $\hat{\$}_{S,ta_{i,1}}$ and $\hat{\$}_{S,ta_{i,2}}$ are the two unit twists associated to the zero stiffness universal joint, $\hat{\$}_{S,ta_{i,3}}$ is the unit twists associated to the compliant prismatic joint, and $\hat{\$}_{S,ta_{i,4}}$, $\hat{\$}_{S,ta_{i,5}}$ and $\hat{\$}_{S,ta_{i,6}}$ are the unit twists associated to the zero stiffness spherical joint. Also

for this mechanism $\hat{\mathbf{s}}_{i,1} = \hat{\mathbf{e}}_3$, while

$$\mathbf{s}_{i,2} = \mathbf{R}_z(q_{i,1}) \begin{bmatrix} 0 \\ 1 \\ 0 \end{bmatrix}, \qquad \mathbf{s}_{i,3} = \mathbf{R}_z(q_{i,1})\mathbf{R}_y(q_{i,2}) \begin{bmatrix} 1 \\ 0 \\ 0 \end{bmatrix},$$

$$\mathbf{s}_{i,4} = \mathbf{s}_{i,3}, \qquad \mathbf{s}_{i,5} = \mathbf{R}_z(q_{i,1})\mathbf{R}_y(q_{i,2})\mathbf{R}_x(q_{i,4}) \begin{bmatrix} 0 \\ 1 \\ 0 \end{bmatrix},$$

$$\mathbf{s}_{i,6} = \mathbf{R}_z(q_{i,1})\mathbf{R}_y(q_{i,2})\mathbf{R}_x(q_{i,4})\mathbf{R}_y(q_{i,5}) \begin{bmatrix} 0 \\ 0 \\ 1 \end{bmatrix}$$

where the matrices $\mathbf{R}_x(q_{i,j})$, $\mathbf{R}_y(q_{i,j})$, and $\mathbf{R}_z(q_{i,j})$, are the rotation matrices that rotate a vector by an angle $q_{i,j}$ around respectively the local X-, Y-, or Z-axis.

Finally, because the platform is an equilateral triangle with sides of length u, the various vectors $\mathbf{a}_i$ for the Stewart-Gough platform are

$$\mathbf{a}_1 = \mathbf{a}_2 = \begin{bmatrix} x_p \\ y_p \\ z_p \end{bmatrix} + \mathbf{R}_z(\alpha)\mathbf{R}_x(\beta)\mathbf{R}_z(\gamma) \begin{bmatrix} u \\ 0 \\ 0 \end{bmatrix},$$

$$\mathbf{a}_3 = \mathbf{a}_4 = \begin{bmatrix} x_p \\ y_p \\ z_p \end{bmatrix} + \mathbf{R}_z(\alpha)\mathbf{R}_x(\beta)\mathbf{R}_z(\gamma) \begin{bmatrix} u\cos(\pi/3) \\ u\sin(\pi/3) \\ 0 \end{bmatrix}$$

$$\mathbf{a}_5 = \mathbf{a}_6 = \begin{bmatrix} x_p \\ y_p \\ z_p \end{bmatrix}$$

where α, β and γ are the Euler angles corresponding to a ZXZ rotation convention.

Then, with the twists of permission as defined in Eq. (4.20), the wrenches of actuation can be expressed as

$$\hat{\$}_{S,wa_{i,1}} = \begin{bmatrix} \mathbf{a}_i \times \hat{\mathbf{s}}_{i,2} \\ \hat{\mathbf{s}}_{i,2} \end{bmatrix} \tag{4.21}$$

$$\hat{\$}_{S,wa_{i,2}} = \begin{bmatrix} \mathbf{a}_i \times (\hat{\mathbf{s}}_{i,2} \times \hat{\mathbf{s}}_{i,3}) \\ (\hat{\mathbf{s}}_{i,2} \times \hat{\mathbf{s}}_{i,3}) \end{bmatrix} \tag{4.22}$$

$$\hat{\$}_{S,wa_{i,3}} = \begin{bmatrix} \mathbf{a}_i \times \hat{\mathbf{s}}_{i,3} \\ \hat{\mathbf{s}}_{i,3} \end{bmatrix} \tag{4.23}$$

$$\hat{\$}_{S,wa_{i,4}} = \frac{1}{c_{wa_{i,4}}} \left(\begin{bmatrix} \hat{\mathbf{s}}_{i,3} \\ \mathbf{0}_{3\times1} \end{bmatrix} + \frac{\tan q_{i,2}}{q_{i,3}} \begin{bmatrix} \mathbf{a}_i \times \hat{\mathbf{s}}_{i,2} \\ \hat{\mathbf{s}}_{i,2} \end{bmatrix} + \right.$$
$$\left. \frac{\tan q_{i,5}}{q_{i,3}} \begin{bmatrix} -(q_{i,3}\hat{\mathbf{s}}_{i,3} - \mathbf{a}_i) \times \hat{\mathbf{s}}_{i,5} \\ \hat{\mathbf{s}}_{i,5} \end{bmatrix} \right) \tag{4.24}$$

$$\hat{\$}_{S,wa_{i,5}} = \begin{bmatrix} -(q_{i,3}\hat{\mathbf{s}}_{i,3} - \mathbf{a}_i) \times (\hat{\mathbf{s}}_{i,3} \times \hat{\mathbf{s}}_{i,5}) \\ (\hat{\mathbf{s}}_{i,3} \times \hat{\mathbf{s}}_{i,5}) \end{bmatrix} \tag{4.25}$$

$$\hat{\$}_{S,wa_{i,6}} = \begin{bmatrix} -(q_{i,3}\hat{\mathbf{s}}_{i,3} - \mathbf{a}_i) \times \hat{\mathbf{s}}_{i,5} \\ \hat{\mathbf{s}}_{i,5} \end{bmatrix} \tag{4.26}$$

where

$$c_{wa_{i,4}} = \left| \frac{\tan q_{i,2}}{q_{i,3}} \hat{\mathbf{s}}_{i,2} + \frac{\tan q_{i,5}}{q_{i,3}} \hat{\mathbf{s}}_{i,5} \right|.$$

Next, the full inverse Jacobian of the spatial mechanism can be assembled as

$$\mathbf{J}_S^{-1} = \begin{bmatrix} \mathbf{J}_{S,1}^{-1} \\ \mathbf{J}_{S,2}^{-1} \\ \vdots \\ \mathbf{J}_{S,6}^{-1} \end{bmatrix} \tag{4.27}$$

where each matrix $\mathbf{J}_{S,i}^{-1}$ is expressed as

$$\mathbf{J}_{S,i}^{-1} = \begin{bmatrix} \hat{\$}_{S,wa_{i,1}}^\top / (\hat{\$}_{S,wa_{i,1}}^\top \hat{\$}_{S,ta_{i,1}}) \\ \hat{\$}_{S,wa_{i,2}}^\top / (\hat{\$}_{S,wa_{i,2}}^\top \hat{\$}_{S,ta_{i,2}}) \\ \vdots \\ \hat{\$}_{S,wa_{i,6}}^\top / (\hat{\$}_{S,wa_{i,6}}^\top \hat{\$}_{S,ta_{i,6}}) \end{bmatrix}. \tag{4.28}$$

Finally, since only the prismatic joint of each leg is not a zero stiffness joint, the inverse Jacobian of elasticity for the spatial mechanism is obtained as

$$\mathbf{J}_{S,e}^{-1} = \begin{bmatrix} \hat{\$}_{S,wa_{1,3}}^\top / (\hat{\$}_{S,wa_{1,3}}^\top \hat{\$}_{S,ta_{1,3}}) \\ \hat{\$}_{S,wa_{2,3}}^\top / (\hat{\$}_{S,wa_{2,3}}^\top \hat{\$}_{S,ta_{2,3}}) \\ \vdots \\ \hat{\$}_{S,wa_{6,3}}^\top / (\hat{\$}_{S,wa_{6,3}}^\top \hat{\$}_{S,ta_{6,3}}) \end{bmatrix}. \tag{4.29}$$

Also for the spatial mechanism, the derivative of matrix $\mathbf{J}_{S,e}^{-1}$ with respect to complete set of joint coordinates multiplied by $\boldsymbol{\tau}_{P,e}$ was obtained as in the appendix of Ref. [23] and using MATLAB's *diff* function.

4.2.3. ALTERNATIVE EXPRESSIONS FOR WRENCHES OF ACTUATION

The difference between the analyses presented in this chapter and those presented in Ref. [24] lies in the definition of the moment arm vector that is part of the wrench of actuation applied by each leg on the end-effector. Griffis and Duffy defined this vector using $\mathbf{b}_i$, which describes the (fixed) position of the first joint of leg i with respect to the origin of the inertial reference frame. Examples of this vector are shown in Figs. 4.1 and 4.2. On the other hand, in this chapter the vector $\mathbf{a}_i$ has been used instead, which describes the position of the wrench application point on the end-effector. A Cartesian stiffness analysis considers the change in the wrench acting on the end-effector as a function of a change in end-effector position, and therefore only the expression using $\mathbf{a}_i$ is consistent with that definition.

The moment arm vectors appear in the stiffness analysis via the wrenches of actuation associated to the prismatic joints, which are expressed by Eq. (4.9) in case of the

planar mechanism and by Eq. (4.23) for the spatial mechanism. The expressions that are implicitly used in Ref. [24] are

$$\hat{\$}^*_{P,wa_{i,2}} = \begin{bmatrix} \mathbf{b}_i \times \hat{\mathbf{s}}_{i,2} \\ \hat{\mathbf{s}}_{i,2} \end{bmatrix} \tag{4.30}$$

instead of Eq. (4.9), and

$$\hat{\$}^*_{S,wa_{i,3}} = \begin{bmatrix} \mathbf{b}_i \times \hat{\mathbf{s}}_{i,3} \\ \hat{\mathbf{s}}_{i,3} \end{bmatrix} \tag{4.31}$$

instead of Eq. (4.23).

When Eqs. (4.30) and (4.31) are used instead of Eqs. (4.9) and (4.22), the resulting Jacobians of elasticity as described by Eqs. (4.13) and (4.29) are different. Although both descriptions give equal numerical results when the respective Jacobian matrices are evaluated, the derivatives of these Jacobian matrices with respect to the joint coordinate vector are not equal.

4.3. RESULTS OBTAINED USING ALTERNATIVE EXPRESSIONS

IN this section the stiffness matrices of the 3-RPR and the 6-UPS mechanisms are evaluated in the same configurations as in Ref. [24]. First, each mechanism is evaluated using the formulation of the wrenches developed in Eqs. (4.8)-(4.10) and Eqs. (4.21)-(4.26) respectively. Secondly, each mechanism is evaluated with the wrenches of actuation associated to the linear springs replaced by those in Eqs. (4.30) and (4.31), which are the wrench expressions implicitly used in Ref. [24].

4.3.1. PLANAR MECHANISM

In the configuration in which Griffis and Duffy [24] evaluated the Cartesian stiffness matrix of the planar mechanism, one has

$$k_1 = k_2 = k_3 = 1000 \text{ N/m}, \qquad q_{0_{1,2}} = q_{0_{2,2}} = q_{0_{3,2}} = 0.12 \text{ m},$$

$$u = 0.1 \text{ m}, \qquad x_p = 0.30 \text{ m}, \qquad y_p = 0.40 \text{ m}, \qquad \phi = \pi/4 \text{ rad},$$

$$\begin{bmatrix} q_{1,1} \\ q_{2,1} \\ q_{3,1} \end{bmatrix} = \begin{bmatrix} 0.9273 \\ 0.9037 \\ 1.1323 \end{bmatrix} \text{ rad}, \qquad \begin{bmatrix} q_{1,2} \\ q_{2,2} \\ q_{3,2} \end{bmatrix} = \begin{bmatrix} 0.5000 \\ 0.5992 \\ 0.5199 \end{bmatrix} \text{ m}$$

When these values are inserted into Eq. (2.43), where the required vectors and matrices are expressed by Eqs. (4.2)-(4.13), the matrix

$$\mathbf{K}_P = \begin{bmatrix} 757.5 \text{ Nm} & -1029.2 \text{ N} & 838.0 \text{ N} \\ -1029.2 \text{ N} & 2533.6 \text{ N/m} & 301.3 \text{ N/m} \\ 838.0 \text{ N} & 301.3 \text{ N/m} & 2795.3 \text{ N/m} \end{bmatrix} \tag{4.32}$$

is obtained, which is symmetric. When the wrench of actuation as described in (4.9) is replaced by the wrench of actuation as described in (4.30), with

$$\mathbf{b}_1 = \mathbf{b}_2 = \begin{bmatrix} 0 \\ 0 \\ 0 \end{bmatrix} \text{ m}, \qquad \mathbf{b}_3 = \begin{bmatrix} 0.15 \\ 0 \\ 0 \end{bmatrix} \text{ m}$$

the resulting stiffness matrix becomes asymmetric, namely

$$\mathbf{K}_P = \begin{bmatrix} 47.0\ \text{Nm} & 13.3\ \text{N} & 143.8\ \text{N} \\ -1029.2\ \text{N} & 2533.6\ \text{N/m} & 301.3\ \text{N/m} \\ 838.0\ \text{N} & 301.3\ \text{N/m} & 2795.3\ \text{N/m} \end{bmatrix}. \tag{4.33}$$

4.3.2. Spatial Mechanism

In the configuration in which Griffis and Duffy [24] evaluated the Cartesian stiffness matrix of the spatial mechanism, one has

$$\begin{bmatrix} k_1 \\ k_2 \\ k_3 \\ k_4 \\ k_5 \\ k_6 \end{bmatrix} = \begin{bmatrix} 1000 \\ 2000 \\ 3000 \\ 4000 \\ 5000 \\ 6000 \end{bmatrix} \text{N/m}, \qquad \begin{bmatrix} q_{0_{1,3}} \\ q_{0_{2,3}} \\ q_{0_{3,3}} \\ q_{0_{4,3}} \\ q_{0_{5,3}} \\ q_{0_{6,3}} \end{bmatrix} = \begin{bmatrix} 0.11 \\ 0.12 \\ 0.13 \\ 0.14 \\ 0.15 \\ 0.16 \end{bmatrix} \text{m},$$

$$u = 0.07\ \text{m}, \qquad x_p = 0.10\ \text{m}, \qquad y_p = 0.04\ \text{m}, \qquad z_p = 0.12\ \text{m},$$

$$\alpha = \pi/2\ \text{rad}, \qquad \beta = 3\pi/4\ \text{rad}, \qquad \gamma = 0.9553\ \text{rad},$$

$$\begin{bmatrix} q_{1,1} \\ q_{2,1} \\ q_{3,1} \\ q_{4,1} \\ q_{5,1} \\ q_{6,1} \end{bmatrix} = \begin{bmatrix} 0.5201 \\ 0.8516 \\ 0.1419 \\ 5.8571 \\ 5.9760 \\ 0.3805 \end{bmatrix} \text{rad}, \qquad \begin{bmatrix} q_{1,2} \\ q_{2,2} \\ q_{3,2} \\ q_{4,2} \\ q_{5,2} \\ q_{6,2} \end{bmatrix} = \begin{bmatrix} 5.5021 \\ 5.3001 \\ 5.1427 \\ 5.3443 \\ 5.2291 \\ 5.4438 \end{bmatrix} \text{rad}, \qquad \begin{bmatrix} q_{1,3} \\ q_{2,3} \\ q_{3,3} \\ q_{4,3} \\ q_{5,3} \\ q_{6,3} \end{bmatrix} = \begin{bmatrix} 0.2278 \\ 0.1928 \\ 0.1815 \\ 0.2044 \\ 0.1380 \\ 0.1612 \end{bmatrix} \text{m}.$$

When these values are inserted into Eq. (2.43), where the required vectors are expressed by Eqs. (4.14)-(4.29), then the following symmetric result is obtained

$$\mathbf{K}_S = \begin{bmatrix} 114 & -29 & -90 & 207 & -581 & 467 \\ -29 & 170 & -12 & 304 & 5 & -837 \\ -90 & -12 & 85 & -240 & 517 & -212 \\ 207 & 304 & -240 & 8000 & 521 & 7556 \\ -581 & 5 & 517 & 521 & 3932 & 521 \\ 467 & -837 & -212 & 7556 & 521 & 15061 \end{bmatrix} \tag{4.34}$$

where the upper-left 3 × 3 submatrix has units Nm, the upper-right and lower-left submatrices have units N, and the lower-right submatrix has units N/m. When each wrench of actuation as described in (4.22) is replaced by the wrench of actuation as described in (4.31), with

$$\mathbf{b}_1 = \mathbf{b}_6 = \begin{bmatrix} 0 \\ 0 \\ 0 \end{bmatrix} \text{m}, \qquad \mathbf{b}_2 = \mathbf{b}_3 = \begin{bmatrix} 0.07 \\ 0 \\ 0 \end{bmatrix} \text{m}, \qquad \mathbf{b}_4 = \mathbf{b}_5 = \begin{bmatrix} 0.035 \\ 0.06062 \\ 0 \end{bmatrix} \text{m}$$

the resulting stiffness matrix becomes asymmetric, namely

$$\mathbf{K_S} = \begin{bmatrix} 21 & -21 & -15 & 207 & -75 & 407 \\ -17 & 41 & 6 & -202 & 5 & -532 \\ -39 & -3 & 33 & -180 & 212 & -212 \\ 207 & 304 & -240 & 8000 & 521 & 7556 \\ -581 & 5 & 517 & 521 & 3932 & 521 \\ 467 & -837 & -212 & 7556 & 521 & 15061 \end{bmatrix} \tag{4.35}$$

4.4. Discussion on Resolved Asymmetry

TWO main observations are made from the evaluated stiffness matrices in Section 3.3. The first observation is that the Cartesian stiffness matrices presented in Eqs. (4.32) and (4.34) are symmetric. Because elastic wrenches are conservative and stiffness is the tensor relating elastic wrenches to displacements, a stiffness matrix is symmetric by definition. The matrices in Eqs. (4.32) and (4.34) are thus in agreement with this definition.

The second observation is that the stiffness matrices presented in Eqs. (4.33) and (4.35) are asymmetric and identical to those presented in Ref. [24]. These asymmetric stiffness matrices were reconstructed by implementing expressions for the wrenches of actuation that are inconsistent with the definition of a manipulator's Cartesian stiffness matrix. It is therefore shown that the asymmetry in the stiffness matrices obtained in Ref. [24] can be explained as a modeling inconsistency.

In Chapter 2 it was argued that the Jacobian-derivative term, which represents loading, is an essential part of a Jacobian-based stiffness analysis, and that this term improves the accuracy of the resulting stiffness model as shown in Chapter 3. However, if inclusion of this term could lead to asymmetric stiffness matrices, then it cannot be considered part of a stiffness analysis. By restoring the symmetry in previously obtained asymmetric stiffness matrices, this chapter supports the notion that loading is an integral part of the stiffness analysis of robotic manipulators and mechanisms.

The findings from this chapter can also be used to reinterpret earlier research. In relation to the symmetry of Christoffel symbols [26, 27], it can be said that it is necessary that all vectors are expressed consistently with respect to the end-effector body so that these vectors fully capture the dependency on the end-effector pose. Additionally, it is interesting to note that Kövecses and Angeles considered the option that asymmetry is the result of wrenches being defined with respect to the fixed inertial body as opposed to the rigid end-effector body. They however dismissed that idea because "at any fixed location in space, we also have a point of the rigid body that is instantaneously coincident with the fixed point" [28]. This chapter points out that although these points may coincide, the derivatives of the Jacobian matrices resulting from alternative vector expressions can be different. It is this difference which causes the asymmetry.

4.5. Conclusions on the Role of Loading

THIS chapter demonstrates that the asymmetry in the stiffness matrices obtained by Griffis and Duffy [24] can be resolved by consistent modeling. It is shown that the asymmetry in the stiffness matrices in Ref. [24] can be explained by an inconsistency in the expression of the wrenches of actuation, and more specifically in the expression

of the moment arm vector associated to the linear springs. In Ref. [24] this vector was defined at the inertial base, while it must be defined at the end-effector to be consistent with the definition of stiffness. Additionally, it is shown that if this vector is defined at the end-effector body, symmetric stiffness matrices are obtained.

A stiffness matrix is symmetric by definition, so a stiffness analysis method that can result in asymmetric stiffness matrices is by definition erroneous. The asymmetric stiffness matrices obtained in Ref. [24] have been discussed for decades, but this chapter finally restores symmetry in these matrices. In doing so, this chapter supports the notion that loading is an integral part of the stiffness analysis of robotic manipulators and mechanisms.

REFERENCES

[1] J. Zhang, Y. Zhao, and J. Dai, *Compliance modeling and analysis of a 3-RPS parallel kinematic machine module,* Chinese Journal of Mechanical Engineering **27**, 703 (2014).

[2] I. Prause, T. Mbarek, and B. Corves, *Increasing the stiffness of a 3-PUU parallel kinematic positioning device for high payloads by modifying the leg configuration,* in *Proceedings of 2014 Workshop on Fundamental Issues and Future Research Directions for Parallel Mechanisms and Manipulators* (2014).

[3] C. Dumas, S. Caro, S. Garnier, and B. Furet, *Joint stiffness identification of six-revolute industrial serial robots,* Robotics and Computer-Integrated Manufacturing **27**, 881 (2011).

[4] T. Tsumugiwa, Y. Fukui, and R. Yokogawa, *Compliance measurement for the Mitsubishi PA-10 robot,* Advanced Robotics **28**, 919 (2014).

[5] B.-S. Kim, S. Park, J.-B. Song, and B. Kim, *Equilibrium point control of a robot manipulator using biologically-inspired redundant actuation system,* Advanced Robotics **27**, 567 (2013).

[6] J. Salisbury, *Active stiffness control of a manipulator in cartesian coordinates,* in *19th IEEE Conference on Decision and Control including the Symposium on Adaptive Processes* (IEEE, 1980) pp. 95–100.

[7] S. F. Chen, *The spatial conservative congruence transformation for manipulator stiffness modeling with coordinate and noncoordinate bases,* Journal of Robotic Systems **22**, 31 (2005).

[8] C. Gosselin, *Stiffness mapping for parallel manipulators,* IEEE Transactions on Robotics and Automation **6**, 377 (1990).

[9] A. Pashkevich, D. Chablat, and P. Wenger, *Stiffness analysis of overconstrained parallel manipulators,* Mechanism and Machine Theory **44**, 966 (2009).

[10] C. Quennouelle and C. M. Gosselin, *A General Formulation for the Stiffness Matrix of Parallel Mechanisms,* (2012), arXiv:arXiv:1212.0950 [physics.class-ph] .

4

[11] H. Sung Kim and H. Lipkin, *Stiffness of Parallel Manipulators With Serially Connected Legs,* Journal of Mechanisms and Robotics **6,** 031001 (2014).

[12] A. G. L. Hoevenaars, P. Lambert, and J. L. Herder, *Jacobian-based stiffness analysis method for parallel manipulators with non-redundant legs,* Proceedings of the Institution of Mechanical Engineers, Part C: Journal of Mechanical Engineering Science (2015), 10.1177/0954406215602283.

[13] D. Zhang and S. Y. Lang, *Stiffness modeling for a class of reconfigurable PKMs with three to five degrees of freedom,* Journal of Manufacturing Systems **23,** 316 (2004).

[14] Y. Wang, H. Liu, T. Huang, and D. G. Chetwynd, *Stiffness Modeling of the Tricept Robot Using the Overall Jacobian Matrix,* Journal of Mechanisms and Robotics **1,** 021002 (2009).

[15] M. Uchiyama, Y. Tsumaki, and W.-K. Yoon, *Design of a Compact 6-DOF Haptic Device to Use Parallel Mechanisms,* in *Robotics Research,* Springer Tracts in Advanced Robotics, edited by S. Thrun, R. Brooks, and H. Durrant-Whyte (Springer Berlin Heidelberg, Berlin, Heidelberg, 2007) pp. 145–162.

[16] A. Ahmad, K. Andersson, U. Sellgren, and S. Khan, *A stiffness modeling methodology for simulation-driven design of haptic devices,* Engineering with Computers **30,** 125 (2012).

[17] G. Cheng, P. Xu, D. Yang, and H. Liu, *Stiffness analysis of a 3CPS parallel manipulator for mirror active adjusting platform in segmented telescope,* Robotics and Computer-Integrated Manufacturing **29,** 302 (2013).

[18] T. J. Teo, I.-M. Chen, and G. Yang, *A large deflection and high payload flexure-based parallel manipulator for UV nanoimprint lithography: Part II. Stiffness modeling and performance evaluation,* Precision Engineering **38,** 872 (2014).

[19] B.-j. Yi, G. B. Chung, H. Y. Na, W. K. Kim, and I. H. Suh, *Design and experiment of a 3-dof parallel micromechanism utilizing flexure hinges,* IEEE Transactions on Robotics and Automation **19,** 604 (2003).

[20] G. Alici and B. Shirinzadeh, *Enhanced stiffness modeling, identification and characterization for robot manipulators,* IEEE Transactions on Robotics **21,** 554 (2005).

[21] A. Klimchik, D. Chablat, and A. Pashkevich, *Static stability of manipulator configuration: Influence of the external loading,* European Journal of Mechanics - A/Solids **51,** 193 (2015).

[22] B. Ding, B. S. Cazzolato, R. M. Stanley, S. Grainger, and J. J. Costi, *Stiffness Analysis and Control of a Stewart Platform-Based Manipulator With Decoupled Sensor – Actuator Locations for Ultrahigh Accuracy Positioning Under Large External Loads,* Journal of Dynamic Systems, Measurment, and Control **136,** 1 (2015).

[23] S.-F. Chen and I. Kao, *Conservative Congruence Transformation for Joint and Cartesian Stiffness Matrices of Robotic Hands and Fingers,* The International Journal of Robotics Research **19**, 835 (2000).

[24] M. Griffis and J. Duffy, *Global stiffness modeling of a class of simple compliant couplings,* Mechanism and Machine Theory **28**, 207 (1993).

[25] N. Ciblak and H. Lipkin, *Asymmetric Cartesian Stiffness for the Modelling of Compliant Robotic Systems,* in *Proceedings of the 1994 ASME Design Technical Conferences. Part 1 (of 3)* (ASME,New York, NY, United States, 1994) pp. 197–204.

[26] M. Zefran and V. Kumar, *Affine connections for the Cartesian stiffness matrix,* in *Proceedings of International Conference on Robotics and Automation*, Vol. 2 (IEEE, 1997) pp. 1376–1381.

[27] S. Howard, M. Zefran, and V. Kumar, *On the 6×6 cartesian stiffness matrix for three-dimensional motions,* Mechanism and Machine Theory **33**, 389 (1998).

[28] J. Kövecses and J. Angeles, *The stiffness matrix in elastically articulated rigid-body systems,* Multibody System Dynamics **18**, 169 (2007).

[29] D. J. Sanger, J. Q. Chen, S. J. Zhang, and D. Howard, *A general method for the stiffness analysis of manipulator mechanisms,* Proceedings of the Institution of Mechanical Engineers, Part C: Journal of Mechanical Engineering Science **214**, 673 (2000).

[30] M. F. Metzger, N. A. Faruk Senan, and O. M. O'Reilly, *On Cartesian stiffness matrices in rigid body dynamics: an energetic perspective,* Multibody System Dynamics **24**, 441 (2010).

[31] Z. Huang and Q. Li, *General Methodology for Type Synthesis of Symmetrical Lower-Mobility Parallel Manipulators and Several Novel Manipulators,* The International Journal of Robotics Research **21**, 131 (2002).

[32] S. A. Joshi and L.-W. Tsai, *Jacobian Analysis of Limited-DOF Parallel Manipulators,* Journal of Mechanical Design **124**, 254 (2002).

[33] B. Dasgupta and T. Mruthyunjaya, *The Stewart platform manipulator: a review,* Mechanism and Machine Theory **35**, 15 (2000).

4

5

A SYSTEMATIC APPROACH FOR THE JACOBIAN ANALYSIS OF PARALLEL MANIPULATORS WITH TWO END-EFFECTORS

We only stay in orbit
For a moment of time

Adam F. Duritz

Counting Crows - Recovering the satellites

The stiffness analysis method introduced in Chapter 2 is a function of Jacobian matrices. Therefore, in order to apply this method to parallel manipulators with two end-effectors (PM2Es), a Jacobian analysis of PM2Es is required. A Jacobian analysis is also required for many other standard analyses, such as a velocity analysis and a static force analysis. A complete Jacobian analysis includes constraint relations, but these constraint relations have not been consistently included in previous analyses of PM2Es. However, they are specifically relevant for the static force analysis and stiffness analysis of PM2Es, because wrenches applied by the actuators can be transferred to the end-effectors through internal constraints. This chapter presents a systematic approach to perform the Jacobian analysis of PM2Es, which is based on screw theory, and that takes all constraint relations into account. The approach is applied to a PM2E with three legs and one internal closed-loop chain. An example mechanism was built to experimentally validate the resulting Jacobian analysis using a static force analysis.

5.1. Introduction to the Jacobian Analysis of PM2Es

Gripping is an important aspect of many modern robotic systems, such as pick-and-place robots [2, 3], microassembly robots [4, 5], and haptic devices [6, 7]. An important category of grippers are those which mechanically engage an object in a multi-point contact [8, 9].

For many applications a driving requirement is dynamic performance, which asks for robotic systems with a high stiffness-over-inertia ratio. Despite their advantageous stiffness-over-inertia ratio, only few mechanically gripping robots are based on parallel manipulators (PMs). A PM can have all actuators located at the base, which significantly reduces the effective inertia. However, the standard solution for adding a gripping capability to a PM is to connect an additional, dedicated gripper in series to the end-effector as, for example, in Refs. [4, 7]. Because of its placement at the end-effector, the inertia of a gripper can significantly degrade the dynamic performance of the resulting manipulator.
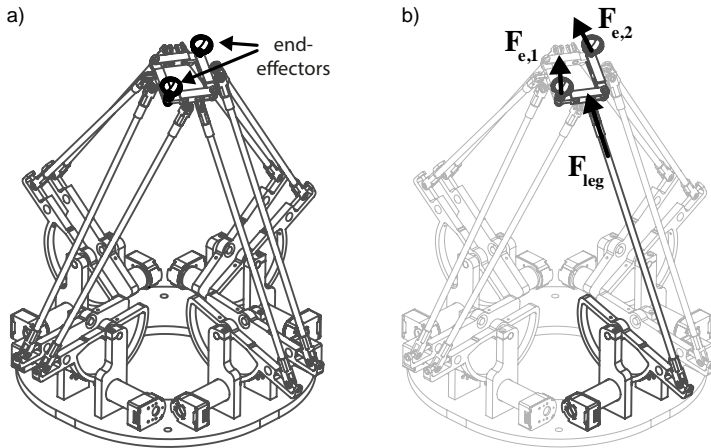
Figure 5.1: a) A parallel manipulator with two end-effectors (PM2E) interacts with the environment via two specific bodies, where b) wrenches applied by the legs can be transferred to the end-effectors through internal constraints, as is illustrated here for one leg of the overactuated 7-DoF haptic master device introduced by Lambert and Herder [10].

Parallel manipulators with two end-effectors (PM2Es) are a relatively novel class of PMs and form a promising alternative solution for gripping robots. PM2Es are an interpretation of parallel manipulators with a configurable platform [10, 12–16], where a closed-loop chain replaces the rigid platform of a traditional PM. This architecture enables the design of gripping robots with all motors located at the base, which is beneficial for the overall dynamic performance. The first example of such gripping robot was introduced by Yi et al. [13], where the whole closed-loop chain acts as the gripper. This thesis focuses on PMCPs where two specific bodies of the closed-loop chain interact with the environment, which is illustrated using an example in Fig. 5.1. Therefore, the term PM2E is preferred.

For the analysis and control of PMs a Jacobian is used [17–20] and therefore various
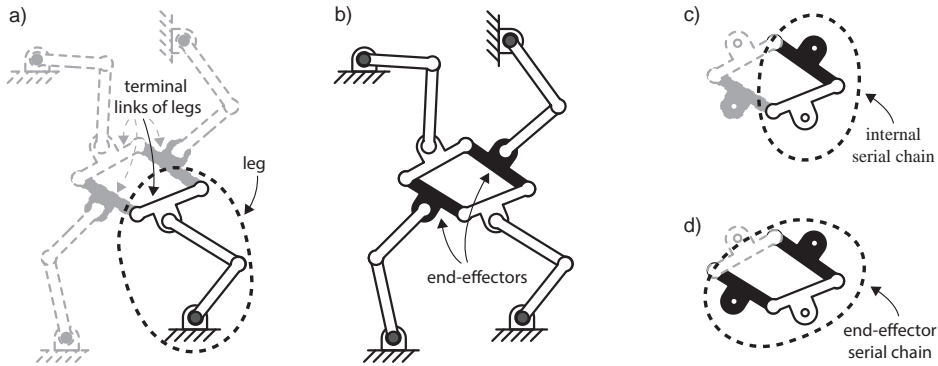
Figure 5.2: An illustration of the definitions introduced in this chapter using a planar manipulator based on Ref. [11], where a) the terminal links of the different legs are also part of an internal closed loop chain. b) The term PM2E is used if two specific bodies in the internal closed loop chain are designated as the end-effectors. c) Each serial chain that connects two adjacent terminal links is referred to as an internal serial chain. Here one of the four internal serial chains is highlighted. d) Additionally, an end-effector serial chain is defined as a serial chain connecting two end-effectors. This chapter focuses on PM2Es with one internal closed loop chain, which can be modeled as two end-effector serial chains in parallel, one of which is highlighted here.

researchers have focused on the Jacobian analysis of PM2Es. Yi et al. [13] differentiated the inverse kinematic relations to obtain an expression for the Jacobian. Mohamed and Gosselin [11] performed a Jacobian analysis based on a set of loop-closure equations that must be solved simultaneously. Lambert et al. [12] applied a stepwise approach in which they first obtained an expression for the motion of the connection point of each *leg*, which is a serial chain that connects the internal closed-loop chain to the base as illustrated in Fig. 5.2a. They then developed a Jacobian based on the relations between allowed end-effector motions, motions of the leg connection points and motions of the actuators. Nabat et al. [15] considered the end-effector velocity state of their manipulator as the combination of a platform twist and an additional velocity term to represent the internal platform motion.

More recently, the author of this thesis made a first attempt to generalize the Jacobian analysis of PM2Es based on screw theory and using a mapping of a set of twists [1]. The resulting Jacobian analysis expresses the velocity state of a spatial PM2E as a combination of two twists with respect to the ground, one for each end-effector. As opposed to other analyses, the analysis in Ref. [1] does include constraint relations, but not those within the internal closed-loop chain.

However, internal constraint relations can be particularly relevant for PM2Es, because wrenches applied by the legs can be transferred to the end-effectors through internal constraints, as illustrated in Fig. 5.1b. As such, an incomplete consideration of constraint relations can make the obtained Jacobian analysis invalid for use in a static force analysis. Because gripping is mainly a force task, a static force analysis is of particular interest in gripping robots. Therefore, the absence of a Jacobian analysis that is also valid for use in a static force analysis represents a significant gap in the existing knowledge of PM2Es.

The aim of this chapter is to develop a systematic approach for the Jacobian analysis of PM2Es. Special attention will be given to the analysis of constraints so that the resulting Jacobian can be used in a static force analysis. Constraint relations in a Jacobian can also be relevant in a stiffness analysis [21, 22].

The structure of this chapter is as follows. First, definitions and assumptions are introduced, which will be used throughout this chapter. Then, a novel structure for the Jacobian analysis of PM2Es with an internal closed-loop chain is developed, which maps the set of all terminal link twists on the joint velocities of all serial chains. Next, for the example of a three-legged PM2E with an internal closed-loop chain the matrix which maps the two end-effector twists on the set of all terminal link twists is developed. An example Jacobian analysis is performed for a three-legged PM2E by combining the novel structure with the mapping of end-effector twists. An experimental static force analysis is performed to validate this Jacobian analysis.

5.2. DEFINITIONS AND ASSUMPTIONS

THIS chapter focuses on PM2Es with a single internal closed-loop chain. This internal closed-loop chain can impose constraints on the relative motion between the two end-effectors, while the legs may impose additional constraints. All twists introduced in this chapter are expressed in a Cartesian reference frame attached to the body in question. Each twist is expressed as $\$_t = [\boldsymbol{\omega}^\top \quad \mathbf{v}^\top]^\top$, where $\boldsymbol{\omega}$ is the angular velocity vector and $\mathbf{v}$ is the velocity vector of the body, expressed in the Cartesian reference frame. The linear operator that maps $\$_t$ on the scalar representing power is the transpose of the wrench defined as $\$_w = [\mathbf{m}^\top \quad \mathbf{f}^\top]^\top$, where $\mathbf{m}$ and $\mathbf{f}$ are the moment and force applied at the point that coincides with the origin of the Cartesian reference frame of the body in question.

A number of additional definitions and related assumptions are used throughout this chapter, namely:

- **Terminal link.** The rigid body of a leg which is also part of the internal closed-loop chain is termed the leg's terminal link, see Fig. 5.2a. The terminal link of the leg i is labeled n_i.

- **Internal serial chain.** Each serial chain connecting two adjacent terminal links will be referred to as an internal serial chain. See Fig. 5.2c for an example.

- **End-effector serial chain.** The closed-loop chain of a PM2E can also be considered as two serial chains connecting the two end-effectors in parallel. Each of these serial chains will be referred to as an end-effector serial chain and contains one or more internal serial chains. It is assumed that there are no redundant joints in each end-effector serial chain. This concept will be important for later derivations. See Fig. 5.2d for an example.

- **Connectivity.** Similar to Joshi and Tsai [23], it is assumed that the number of degrees of freedom of a serial chain, referred to as its connectivity C, corresponds to the number of kinematic joints in that serial chain. It is assumed that this also holds for each end-effector serial chain, so that also within an end-effector serial chain there are no redundant joints.

- **Virtual joint.** If a serial chain has $C < 6$, then $6 - C$ basis twists are constrained. Each basis twist represents the motion of a 1-DoF joint, and since the joints associated to constrained twists are not part of the kinematic chain, they are termed virtual joints. See Section 2.2.2 for more details.

5.3. STRUCTURE FOR NOVEL JACOBIAN ANALYSIS OF PM2ES

IN this section a novel structure for the Jacobian analysis of PM2Es with a single internal closed-loop chain is presented. The main idea is to organize the partial inverse Jacobian matrices of individual serial chains based on the structure in the graph representation. The resulting Jacobian analysis is a function of the twists of the various terminal links.

At the basis of existing Jacobian analysis methods for traditional PMs lies the structured combination of inverse Jacobian matrices of individual legs,

$$
\begin{bmatrix} \dot{\mathbf{q}}_1 \\ \dot{\mathbf{q}}_2 \\ \vdots \\ \dot{\mathbf{q}}_N \end{bmatrix} = \begin{bmatrix} \mathbf{J}_1^{-1} \\ \mathbf{J}_2^{-1} \\ \vdots \\ \mathbf{J}_N^{-1} \end{bmatrix} \mathbf{\$}_{t,e}
\tag{5.1}
$$

where N is the number of legs and $\mathbf{\$}_{t,e}$ is the twist of the end-effector. Also, if the full inverse Jacobian analysis is considered as in [24], for each leg i the matrix $\mathbf{J}_i^{-1}$ is a 6×6 inverse Jacobian matrix and each vector $\dot{\mathbf{q}}_i$ is a six-dimensional vector that contains both kinematic joint velocities and virtual joint velocities of a leg. Any component of $\mathbf{\$}_{t,e}$ that is mapped onto virtual joint velocities therefore implies that there are deformations in the manipulator.

To illustrate the difference between traditional PMs and PM2Es, it is helpful to look at their respective graph representations. Figure 5.3 shows a three-legged PM and a three-legged PM2E with their respective graphs. Firstly, in order to compare the associated Jacobian matrices, the twist of the the terminal link of each leg i of a traditional PM is expressed as $\mathbf{\$}_{t,i}$, so that Eq. (5.1) can be rewritten as

$$
\begin{bmatrix} \dot{\mathbf{q}}_1 \\ \dot{\mathbf{q}}_2 \\ \vdots \\ \dot{\mathbf{q}}_N \end{bmatrix} = \begin{bmatrix} \mathbf{J}_1^{-1} & \mathbf{0}_{6\times6} & \cdots & \mathbf{0}_{6\times6} \\ \mathbf{0}_{6\times6} & \mathbf{J}_2^{-1} & \cdots & \mathbf{0}_{6\times6} \\ \vdots & \vdots & \ddots & \vdots \\ \mathbf{0}_{6\times6} & \mathbf{0}_{6\times6} & \cdots & \mathbf{J}_N^{-1} \end{bmatrix} \begin{bmatrix} \mathbf{\$}_{t,1} \\ \mathbf{\$}_{t,2} \\ \vdots \\ \mathbf{\$}_{t,N} \end{bmatrix}
\tag{5.2}
$$

A PM2E with N legs and a single closed-loop chain, has in addition N internal serial chains. Each internal serial chain connects two terminal links, so that the twist of each internal serial chain can be expressed as

$$
\mathbf{\$}_{t,o_i^{i+1}} = \begin{cases} \mathbf{\$}_{t,i+1} - \mathbf{\$}_{t,i} & \text{for } i = 1, 2, \dots, (N-1) \\ \mathbf{\$}_{t,1} - \mathbf{\$}_{t,N} & \text{for } i = N \end{cases}
\tag{5.3}
$$

where $\mathbf{\$}_{t,o_i^{i+1}}$ is the twist of the internal serial chain connecting the ith terminal link with the $(i+1)$th terminal link. Equation (5.3) states that the Nth terminal link is connected to the first terminal link.
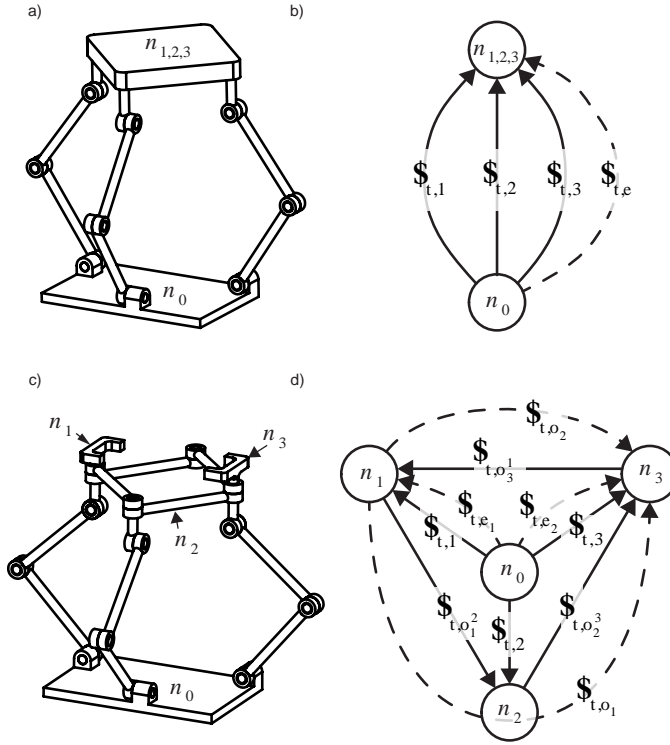
Figure 5.3: a) An example of a traditional PM with three legs and b) its graph theory representation, as well as c) an example of a PM2E with three legs as introduced in Appendix C and d) its graph theory representation. For each twist, the arrow points from the reference body to the body moving relative to it. Overlaid with dotted lines are the known end-effector twists, $\$_{t,e_1}$ and $\$_{t,e_2}$, as well as the twists related to the two end-effector serial chains, $\$_{t,o_1}$ and $\$_{t,o_2}$.

The full Jacobian analysis of a PM2E can therefore be obtained by extending Eq. (5.2) with the relations described by Eq. (5.3),

$$
\begin{bmatrix}
\dot{\mathbf{q}}_1 \\
\dot{\mathbf{q}}_2 \\
\vdots \\
\dot{\mathbf{q}}_N \\
\dot{\mathbf{q}}_{o_1^2} \\
\dot{\mathbf{q}}_{o_2^3} \\
\vdots \\
\dot{\mathbf{q}}_{o_N^1}
\end{bmatrix}
= \mathbf{J}_n^{-1}
\begin{bmatrix}
\$_{t,1} \\
\$_{t,2} \\
\vdots \\
\$_{t,N}
\end{bmatrix}
\tag{5.4}
$$

where $\dot{\mathbf{q}}_{o_i^{i+1}}$ (or $\dot{\mathbf{q}}_{o_N^1}$) is the six-dimensional joint velocity vector of the ith internal serial

chain, and

$$
\mathbf{J}_n^{-1} = \begin{bmatrix}
\mathbf{J}_1^{-1} & \mathbf{0}_{6\times6} & \cdots & \mathbf{0}_{6\times6} \\
\mathbf{0}_{6\times6} & \mathbf{J}_2^{-1} & \cdots & \mathbf{0}_{6\times6} \\
\vdots & \vdots & \ddots & \vdots \\
\mathbf{0}_{6\times6} & \mathbf{0}_{6\times6} & \cdots & \mathbf{J}_N^{-1} \\
-\mathbf{J}_{o_1^2}^{-1} & \mathbf{J}_{o_1^2}^{-1} & \cdots & \mathbf{0}_{6\times6} \\
\mathbf{0}_{6\times6} & -\mathbf{J}_{o_2^3}^{-1} & \cdots & \mathbf{0}_{6\times6} \\
\vdots & \vdots & \ddots & \vdots \\
\mathbf{J}_{o_N^1}^{-1} & \mathbf{0}_{6\times6} & \cdots & -\mathbf{J}_{o_N^1}^{-1}
\end{bmatrix}
\tag{5.5}
$$

As in Eq. (5.1), each of the inverse Jacobian matrices in Eq. (5.5) is a 6×6 matrix and can be obtained using the reciprocity rules of twists and wrenches as described in Ref. [24].

As opposed to a traditional PM, the twist of each terminal link of a PM2E can be different. And because typically only the twists of the two terminal links that are the end-effectors are directly available as inputs, not all twists in Eq. (5.4) are directly defined. This is the topic of the next section.

5.4. MAPPING OF TWISTS FOR THREE-LEGGED PM2E

IN this section the matrix is developed that maps the two end-effector twists onto the complete set of terminal link twists for the example of a PM2E with three legs, whose graph representation was already introduced in Fig. 5.3d. Thus, a matrix $\mathbf{M}_t$ is developed such that

$$
\begin{bmatrix}
\$_{t,1} \\
\$_{t,2} \\
\$_{t,3}
\end{bmatrix} = \mathbf{M}_t \begin{bmatrix}
\$_{t,e_1} \\
\$_{t,e_2}
\end{bmatrix}
\tag{5.6}
$$

In the example considered in this chapter the terminal links of the first and third leg, n_1 and n_3, are the end-effectors, so that

$$
\$_{t,1} = \$_{t,e_1} \qquad \$_{t,3} = \$_{t,e_2}
\tag{5.7}
$$

and the difficulty in developing $\mathbf{M}_t$ lies in the mapping of the two end-effector twists onto $\$_{t,2}$.

To enable a mapping of the two end-effector twists onto $\$_{t,2}$, either $\$_{t,o_1^2}$ or $\$_{t,o_2^3}$ needs to be expressed, because from Fig. 5.3d it can be established that

$$
\$_{t,2} = \$_{t,1} + \$_{t,o_1^2}
\tag{5.8}
$$

and also

$$
\$_{t,2} = \$_{t,3} - \$_{t,o_2^3}
\tag{5.9}
$$

To express $\$_{t,o_1^2}$ or $\$_{t,o_2^3}$, this chapter first develops a set of basis twists to express $\$_{t,o_1}$, which is here defined as the twist of the end-effector serial chain that connects n_1 and n_3 via n_2, see Fig. 5.3d. In the remainder of this research, this end-effector serial chain will be referred to as the *first end-effector serial chain* (and as a logical consequence, the

other end-effector serial chain will be referred to as the *second end-effector serial chain*). It was assumed that the number of kinematic joints in each end-effector serial chain is equal to its connectivity, where the connectivity of the first end-effector serial chain is labeled C_{o_1}. Then it holds that

$$C_{o_1} = C_{o_1^2} + C_{o_2^3} \tag{5.10}$$

where $C_{o_1^2}$ is the connectivity of the internal serial chain connecting n_1 and n_2, and $C_{o_2^3}$ is the connectivity of the internal serial chain connecting n_2 and n_3. The twist $\$_{t,o_1}$ can then be expressed as

$$\$_{t,o_1} = \sum_{j=1}^{C_{o_1^2}} \dot{q}_{a,o_{1,j}} \hat{\$}_{ta_{o_{1,j}}} + \sum_{j=1}^{C_{o_2^3}} \dot{q}_{a,o_{1,j*}} \hat{\$}_{ta_{o_{1,j*}}} + \sum_{j=1}^{6-C_{o_1}} \dot{q}_{c,o_{1,j}} \hat{\$}_{tc_{o_{1,j}}} \tag{5.11}$$

where

$$j^* = j + C_{o_1^2} \tag{5.12}$$

and $\hat{\$}_{ta_{o_{1,j}}}$ is the unit twist of permission associated to the jth joint of the first end-effector serial chain, with $\dot{q}_{a,o_{1,j}}$ its magnitude. The unit twist of restriction $\hat{\$}_{tc_{o_{1,j}}}$ represents the motion of the jth virtual joint of the first end-effector serial chain, with magnitude $\dot{q}_{c,o_{1,j}}$. These six unit twists together span six-dimensional Cartesian space.

Next, the set of unit twists introduced in Eq. (5.11) is also used to express $\$_{t,o_1^2}$ and $\$_{t,o_2^3}$. However, each unit twists of permission in Eq. (5.11) is constrained in one of the internal serial chains. Therefore, this chapter makes a distinction between three types of unit twists, expressed using their magnitudes:

- **Permitted twist magnitudes.** The unit twists associated to joints that represent a kinematic DoF of the considered internal serial chain are given a magnitude $\dot{q}_{a,o_i^{i+1},j}$.

- **Simple constrained internal twist magnitudes.** The unit twists associated to joints that represent a constraint in the considered internal serial chain, but which represent a kinematic DoF in the first end-effector serial chain, are simple constrained internal twists. These twists are given a magnitude $\dot{q}_{c_s,o_i^{i+1},j}$.

- **Multiple constrained internal twist magnitudes.** The unit twists associated to joints that represent a constrained DoF in the first end-effector serial chain necessarily also represent a constrained DoF in both internal serial chains of which it is constructed. These twists are therefore multiple constrained and in the considered internal serial chain are attributed a magnitude $\dot{q}_{c_m,o_i^{i+1},j}$.

With the distinction as above, each internal joint velocity vector is then constructed as

$$\dot{\mathbf{q}}_{o_i^{i+1}} = \begin{bmatrix} \dot{\mathbf{q}}_{a,o_i^{i+1}} \\ \dot{\mathbf{q}}_{c_s,o_i^{i+1}} \\ \dot{\mathbf{q}}_{c_m,o_i^{i+1}} \end{bmatrix} \tag{5.13}$$

Now, $\$_{t,o_1^2}$ and $\$_{t,o_2^3}$ can be expressed respectively as

$$\$_{t,o_1^2} = \sum_{j=1}^{C_{o_1^2}} \dot{q}_{a,o_1^2,j} \hat{\$}ta_{o_1,j} + \sum_{j=1}^{C_{o_2^3}} \dot{q}_{c_s,o_1^2,j} \hat{\$}ta_{o_1,j^*} + \sum_{j=1}^{6-C_{o_1}} \dot{q}_{c_m,o_1^2,j} \hat{\$}tc_{o_1,j} \tag{5.14}$$

and

$$\$_{t,o_2^3} = \sum_{j=1}^{C_{o_2^3}} \dot{q}_{a,o_2^3,j} \hat{\$}ta_{o_1,j^*} + \sum_{j=1}^{C_{o_1^2}} \dot{q}_{c_s,o_2^3,j} \hat{\$}ta_{o_1,j} + \sum_{j=1}^{6-C_{o_1}} \dot{q}_{c_m,o_1^2,j} \hat{\$}tc_{o_1,j} \tag{5.15}$$

where j^* was introduced in Eq. (5.12). The remaining challenge is to obtain expressions for all twist magnitudes in either Eq. (5.14) or Eq. (5.15).

To express the twist magnitudes in Eqs. (5.14) and (5.15) velocity relations are derived from the knowledge that the sum of all twists in a closed loop is zero. Therefore, as can be observed from Fig. 5.3d, for a PM2E with three legs it holds among others that

$$\$_{t,o_1^2} + \$_{t,o_2^3} + \$_{t,o_3^1} = \mathbf{0} \tag{5.16}$$

Additionally, using another loop, $\$_{t,o_3^1}$ can be expressed as

$$\$_{t,o_3^1} = \$_{t,1} - \$_{t,3} \tag{5.17}$$

and because Eq. (5.7), it is possible to combine Eqs. (5.16) and (5.17) into

$$\$_{t,e_2} - \$_{t,e_1} = \$_{t,o_1^2} + \$_{t,o_2^3} \tag{5.18}$$

Furthermore, because the first end-effector serial chain was defined as the combination of the internal serial chain connecting n_1 and n_2, and the internal serial chain connecting n_2 and n_3, it also holds that

$$\$_{t,e_2} - \$_{t,e_1} = \$_{t,o_1} \tag{5.19}$$

5.4.1. Expression for Actuated and Simple Constrained Joint Velocities in the First End-Effector Serial Chain

In this subsection expressions are derived for $\dot{\mathbf{q}}_{a,o_1^2}$, $\dot{\mathbf{q}}_{c_s,o_1^2}$, $\dot{\mathbf{q}}_{a,o_2^3}$, and $\dot{\mathbf{q}}_{c_s,o_2^3}$, as introduced in Eq. (5.13), using the method and notation as introduced in Ref. [24]. These expressions are necessary for later steps in the proposed analysis and are based on the definition of the first end-effector serial chain as the series connection of two internal serial. Thus, each of the kinematic joints in the first end-effector serial chain is part of either the internal serial chain connecting n_1 and n_2, or the internal serial chain connecting n_2 and n_3, and therefore it holds that

$$\dot{q}_{a,o_{1,j}} = \dot{q}_{a,o_1^2,j} \qquad \text{for } j = 1,2,...C_{o_1^2} \tag{5.20}$$

$$\dot{q}_{a,o_{1,j^*}} = \dot{q}_{a,o_2^3,j} \qquad \text{for } j = 1,2,...C_{o_2^3} \tag{5.21}$$

where j^* was expressed in Eq. (5.12). Then, using Eq. (5.11) and Eq. (5.20)-(5.21), Eq. (5.19) can be expressed as

$$\$_{t,e_2} - \$_{t,e_1} = \sum_{j=1}^{C_{o_1^2}} \dot{q}_{a,o_1^2,j} \hat{\$}_{ta_{o_1,j}} + \sum_{j=1}^{C_{o_2^3}} \dot{q}_{a,o_2^3,j} \hat{\$}_{ta_{o_1,j^*}} + \sum_{j=1}^{6-C_{o_1}} \dot{q}_{c,o_1,j} \hat{\$}_{tc_{o_1,j}} \tag{5.22}$$

Alternatively, inserting Eqs. (5.14) and (5.15) into Eq. (5.18) gives

$$\$_{t,e_2} - \$_{t,e_1} = \sum_{j=1}^{C_{o_1^2}} \dot{q}_{a,o_1^2,j} \hat{\$}_{ta_{o_1,j}} + \sum_{j=1}^{C_{o_2^3}} \dot{q}_{c_s,o_1^2,j} \hat{\$}_{ta_{o_1,j^*}} \sum_{j=1}^{6-C_{o_1}} \dot{q}_{c_m,o_1^2,j} \hat{\$}_{tc_{o_1,j}} + \sum_{j=1}^{C_{o_1^2}} \dot{q}_{c_s,o_2^3,j} \hat{\$}_{ta_{o_1,j}} +$$

$$\sum_{j=1}^{C_{o_2^3}} \dot{q}_{a,o_2^3,j} \hat{\$}_{ta_{o_1,j^*}} + \sum_{j=1}^{6-C_{o_1}} \dot{q}_{c_m,o_2^3,j} \hat{\$}_{tc_{o_1,j}} \tag{5.23}$$

Using the methodology presented by Huang et al. [24], for each unit twist of permission a unit wrench of actuation can be defined which only does work on the considered twist of permission, but that is reciprocal to all other unit twists. Left-multiplication of Eq. (5.22) with the transposed unit wrenches of actuation associated to the first $C_{o_1^2}$ unit twists $\hat{\$}_{ta_{o_1,j}}$ leads to

$$\mathbf{J}_{a,o_1^2}^{-1} \left(\$_{t,e_2} - \$_{t,e_1} \right) = \dot{\mathbf{q}}_{a,o_1^2} \tag{5.24}$$

where

$$\mathbf{J}_{a,o_1^2}^{-1} = \begin{bmatrix} \hat{\$}_{wa_{o_1,1}}^{\top} / (\hat{\$}_{wa_{o_1,1}}^{\top} \hat{\$}_{ta_{o_1,1}}) \\ \hat{\$}_{wa_{o_1,2}}^{\top} / (\hat{\$}_{wa_{o_1,2}}^{\top} \hat{\$}_{ta_{o_1,2}}) \\ \vdots \\ \hat{\$}_{wa_{o_1,C_{o_1^2}}}^{\top} / (\hat{\$}_{wa_{o_1,C_{o_1^2}}}^{\top} \hat{\$}_{ta_{o_1,C_{o_1^2}}}) \end{bmatrix} \tag{5.25}$$

while left-multiplication of Eq. (5.23) with the same transposed wrenches results in

$$\mathbf{J}_{a,o_1^2}^{-1} \left(\$_{t,e_2} - \$_{t,e_1} \right) = \dot{\mathbf{q}}_{a,o_1^2} + \dot{\mathbf{q}}_{c_s,o_2^3} \tag{5.26}$$

where $\mathbf{J}_{a,o_1^2}^{-1}$ was defined in Eq. (5.25). Equations (5.24) and (5.26) can be combined into

$$\dot{\mathbf{q}}_{c_s,o_2^3} = \mathbf{0} \tag{5.27}$$

which confirms that a motion that is kinematically allowed by the internal serial chain connecting n_1 and n_2, will have zero magnitude in the internal serial chain connecting n_2 and n_3, in which this motion is constrained.

Similarly, left-multiplication of Eq. (5.22) with the transposed unit wrenches of actuation associated to the last $C_{o_2^3}$ twists of permission of the first end-effector serial chain leads to

$$\mathbf{J}_{a,o_2^3}^{-1} \left(\$_{t,e_2} - \$_{t,e_1} \right) = \dot{\mathbf{q}}_{a,o_2^3} \tag{5.28}$$

where

$$\mathbf{J}_{a,o_2^3}^{-1} = \begin{bmatrix} \hat{\$}_{wa_{o_{1,1+C_{o_1^2}}}}^{\top} / (\hat{\$}_{wa_{o_{1,1+C_{o_1^2}}}}^{\top} \hat{\$}_{ta_{o_{1,1+C_{o_1^2}}}}) \\ \hat{\$}_{wa_{o_{1,2+C_{o_1^2}}}}^{\top} / (\hat{\$}_{wa_{o_{1,2+C_{o_1^2}}}}^{\top} \hat{\$}_{ta_{o_{1,2+C_{o_1^2}}}}) \\ \vdots \\ \hat{\$}_{wa_{o_{1,C_{o_1}}}}^{\top} / (\hat{\$}_{wa_{o_{1,C_{o_1}}}}^{\top} \hat{\$}_{ta_{o_{1,C_{o_1}}}}) \end{bmatrix} \tag{5.29}$$

and left-multiplication of Eq. (5.23) with those same twists gives

$$\mathbf{J}_{a,o_2^3}^{-1} \left(\$_{t,e_2} - \$_{t,e_1} \right) = \dot{\mathbf{q}}_{c_s,o_1^2} + \dot{\mathbf{q}}_{a,o_2^3} \tag{5.30}$$

where $\mathbf{J}_{a,o_2^3}^{-1}$ was defined in Eq. (5.29). Equations (5.28) and (5.30) can then be combined into

$$\dot{\mathbf{q}}_{c_s,o_1^2} = \mathbf{0} \tag{5.31}$$

which confirms that the magnitude of the constrained motion in the internal serial chain connecting n_1 and n_2 is zero for those motions that are kinematically allowed by the internal serial chain connecting n_2 and n_3.

Thus, $\dot{\mathbf{q}}_{c_s,o_1^2} = \mathbf{0}$, $\dot{\mathbf{q}}_{c_s,o_2^3} = \mathbf{0}$, and Eqs. (5.24) and (5.28) respectively express $\dot{\mathbf{q}}_{a,o_1^2}$ and $\dot{\mathbf{q}}_{a,o_2^3}$ as a function of the two end-effector twists and the kinematics captured by partial Jacobian matrices. What remains in order to define $\dot{\mathbf{q}}_{o_1^2}$ and $\dot{\mathbf{q}}_{o_2^3}$ as in Eq. (5.13), is to derive expressions for $\dot{\mathbf{q}}_{c_m,o_1^2}$ and $\dot{\mathbf{q}}_{c_m,o_2^3}$.

5.4.2. EXPRESSION FOR MULTIPLE CONSTRAINED JOINT VELOCITIES IN THE FIRST END-EFFECTOR SERIAL CHAIN

Unfortunately, the multiple constrained joint velocities, $\mathbf{q}_{c_m,o_1^2}$ and $\mathbf{q}_{c_m,o_2^3}$ as part of Eq. (5.13), cannot be expressed directly as a function of unit twists and unit wrenches. This becomes clear when the result of left-multiplying Eq. (5.22) with the $6-C_{o_1}$ unit wrenches of constraint of the first end-effector serial chain is compared with the result of left-multiplying Eq. (5.23) with those same unit wrenches. Left-multiplication of Eq. (5.22) with these unit wrenches of constraint gives

$$\mathbf{J}_{c,o_1}^{-1} \left(\$_{t,e_2} - \$_{t,e_1} \right) = \dot{\mathbf{q}}_{c,o_1} \tag{5.32}$$

where

$$\mathbf{J}_{c,o_1}^{-1} = \begin{bmatrix} \hat{\$}_{wc_{o_{1,1}}}^{\top} / (\hat{\$}_{wc_{o_{1,1}}}^{\top} \hat{\$}_{tc_{o_{1,1}}}) \\ \hat{\$}_{wc_{o_{1,2}}}^{\top} / (\hat{\$}_{wc_{o_{1,2}}}^{\top} \hat{\$}_{tc_{o_{1,2}}}) \\ \vdots \\ \hat{\$}_{wc_{o_{1,6-C_{o_1}}}}^{\top} / (\hat{\$}_{wc_{o_{1,6-C_{o_1}}}}^{\top} \hat{\$}_{tc_{o_{1,6-C_{o_1}}}}) \end{bmatrix} \tag{5.33}$$

On the other hand, left-multiplying Eq. (5.23) with the same unit wrenches of constraint gives

$$\mathbf{J}_{c,o_1}^{-1} \left(\$_{t,e_2} - \$_{t,e_1} \right) = \dot{\mathbf{q}}_{c_m,o_1^2} + \dot{\mathbf{q}}_{c_m,o_2^3} \tag{5.34}$$

Equations (5.32) and (5.34) can be combined into

$$\dot{\mathbf{q}}_{c_m,o_1^2} + \dot{\mathbf{q}}_{c_m,o_2^3} = \dot{\mathbf{q}}_{c,o_1} \tag{5.35}$$

where $\dot{\mathbf{q}}_{c,o_1}$ is defined by Eq. (5.32). Equation (5.35) cannot be solved for $\dot{\mathbf{q}}_{c_m,o_1^2}$ and $\dot{\mathbf{q}}_{c_m,o_2^3}$ directly.

To obtain a closed form expression for $\dot{\mathbf{q}}_{c_m,o_1^2}$ and $\dot{\mathbf{q}}_{c_m,o_2^3}$, Eq. (5.35) is complemented with an additional set of equations, which are based on static force relations. For each node of the PM2E it holds that in a static equilibrium the sum of all wrenches is zero. In a quasi-static equilibrium, also the derivative with respect to time of this sum is zero, and for body n_2 it holds that

$$\frac{d\$_{w,2}}{dt} + \frac{d\$_{w,o_1^2}}{dt} - \frac{d\$_{w,o_2^3}}{dt} = \mathbf{0} \tag{5.36}$$

In order to complement Eq. (5.35), only the motions that are multiple constrained by the internal serial chains are of interest. To simplify the further derivation, it is assumed that the change in wrenches is dominated by stiffness and that along those directions the stiffness of the second leg is significantly less than the stiffness of the internal serial chains. Then, the term $d\$_{w,2}/dt$ in Eq. (5.36) can be neglected for those directions. Next, because the two internal serial chains share the same joint coordinates, Eq. (5.36) can be also expressed in those multiple constrained joint coordinates, so that

$$\mathbf{K}_{q_{c_m,o_1^2}} \dot{\mathbf{q}}_{c_m,o_1^2} - \mathbf{K}_{q_{c_m,o_2^3}} \dot{\mathbf{q}}_{c_m,o_2^3} = \mathbf{0} \tag{5.37}$$

where $\mathbf{K}_{q_{c_m,o_1^2}}$ is the stiffness matrix of the internal chain connecting n_1 to n_2 and $\mathbf{K}_{q_{c_m,o_2^3}}$ is the stiffness matrix of the internal chain connecting n_2 to n_3, both expressed in the multiple constrained joint space of the first end-effector serial chain.

Equations (5.35) and (5.37) can be combined into

$$\begin{bmatrix} \mathbf{I}_{(6-C_{o_1})} & \mathbf{I}_{(6-C_{o_1})} \\ \mathbf{K}_{q_{c_m,o_1^2}} & -\mathbf{K}_{q_{c_m,o_2^3}} \end{bmatrix} \begin{bmatrix} \dot{\mathbf{q}}_{c_m,o_1^2} \\ \dot{\mathbf{q}}_{c_m,o_2^3} \end{bmatrix} = \begin{bmatrix} \mathbf{I}_{(6-C_{o_1})} \\ \mathbf{0}_{(6-C_{o_1})} \end{bmatrix} \dot{\mathbf{q}}_{c,o_1} \tag{5.38}$$

in which the identity matrix $\mathbf{I}_{(6-C_{o_1})}$, and the stiffness matrices $\mathbf{K}_{q_{c_m,o_1^2}}$ and $\mathbf{K}_{q_{c_m,o_2^3}}$ are all of size $(6-C_{o_1}) \times (6-C_{o_1})$. Equation (5.38) can be written as

$$\begin{bmatrix} \dot{\mathbf{q}}_{c_m,o_1^2} \\ \dot{\mathbf{q}}_{c_m,o_2^3} \end{bmatrix} = \begin{bmatrix} \mathbf{I}_{(6-C_{o_1})} & \mathbf{I}_{(6-C_{o_1})} \\ \mathbf{K}_{q_{c_m,o_1^2}} & -\mathbf{K}_{q_{c_m,o_2^3}} \end{bmatrix}^{-1} \begin{bmatrix} \mathbf{I}_{(6-C_{o_1})} \\ \mathbf{0}_{(6-C_{o_1})} \end{bmatrix} \dot{\mathbf{q}}_{c,o_1} \tag{5.39}$$

which can be developed using matrix inversion rules into

$$\begin{bmatrix} \dot{\mathbf{q}}_{c_m,o_1^2} \\ \dot{\mathbf{q}}_{c_m,o_2^3} \end{bmatrix} = \begin{bmatrix} \mathbf{K}_{q_{c_m,o_1^2}}^{-1} \left(\mathbf{K}_{q_{c_m,o_1^2}}^{-1} + \mathbf{K}_{q_{c_m,o_2^3}}^{-1} \right)^{-1} \\ \mathbf{K}_{q_{c_m,o_2^3}}^{-1} \left(\mathbf{K}_{q_{c_m,o_1^2}}^{-1} + \mathbf{K}_{q_{c_m,o_2^3}}^{-1} \right)^{-1} \end{bmatrix} \dot{\mathbf{q}}_{c,o_1} \tag{5.40}$$

where $\dot{\mathbf{q}}_{c,o_1}$ was expressed in Eq. (5.32) as function of the two end-effector twists. As such, Eq. (5.40) expresses $\dot{\mathbf{q}}_{c_m,o_1^2}$ and $\dot{\mathbf{q}}_{c_m,o_2^3}$ as a function of the two end-effector twists and the relative compliance of the two respective internal serial chains.

5.4.3. INTERNAL MAPPING OF TWISTS

Equations (5.24), (5.26), (5.28), (5.31), and (5.40) have expressed all joint velocities of the two internal serial chains that make up the first end-effector serial chain as a function of the two end-effector twists. Then, forward Jacobian mapping can be used to express the twist of n_2 as a function of the two end-effector twists. There are two equivalent options to do so, namely those introduced in Eqs. (5.8) and (5.9). In this chapter the representation in Eq. (5.8) is chosen, but it should be noted that this is an arbitrary choice and does not affect the results.

The twist of the first internal serial chain was expressed as the sum of six unit twists in Eq. (5.14), which can also be expressed in matrix form as

$$\$_{t,o_1^2} = \begin{bmatrix} \mathbf{J}_{a,o_1^2} & \mathbf{J}_{a,o_2^3} & \mathbf{J}_{c,o_1} \end{bmatrix} \begin{bmatrix} \dot{\mathbf{q}}_{a,o_1^2} \\ \dot{\mathbf{q}}_{cs,o_1^2} \\ \dot{\mathbf{q}}_{cm,o_1^2} \end{bmatrix} \tag{5.41}$$

where

$$\mathbf{J}_{a,o_1^2} = \begin{bmatrix} \hat{\$}_{ta_{o_{1,1}}} & \hat{\$}_{ta_{o_{1,2}}} & \cdots & \hat{\$}_{ta_{o_{1,C_{o_1^2}}}} \end{bmatrix} \tag{5.42}$$

$$\mathbf{J}_{a,o_2^3} = \begin{bmatrix} \hat{\$}_{ta_{o_{1,1+C_{o_1^2}}}} & \hat{\$}_{ta_{o_{1,2+C_{o_1^2}}}} & \cdots & \hat{\$}_{ta_{o_{1,C_{o_1}}}} \end{bmatrix} \tag{5.43}$$

$$\mathbf{J}_{c,o_1} = \begin{bmatrix} \hat{\$}_{tc_{o_{1,1}}} & \hat{\$}_{tc_{o_{1,2}}} & \cdots & \hat{\$}_{tc_{o_{1,(6-C_{o_1})}}} \end{bmatrix} \tag{5.44}$$

Then, using the part of Eq. (5.40) that expresses $\dot{\mathbf{q}}_{cm,o_1^2}$, Eq. (5.41) can be rewritten as

$$\$_{t,o_1^2} = \begin{bmatrix} \mathbf{J}_{a,o_1^2} & \mathbf{J}_{a,o_2^3} & \mathbf{J}_{c,o_1} \end{bmatrix} \begin{bmatrix} \dot{\mathbf{q}}_{a,o_1^2} \\ \dot{\mathbf{q}}_{cs,o_1^2} \\ \mathbf{M}_{q_{cm,o_1^2}} \dot{\mathbf{q}}_{c,o_1} \end{bmatrix} \tag{5.45}$$

in which

$$\mathbf{M}_{q_{cm,o_1^2}} = \mathbf{K}_{q_{cm,o_1^2}}^{-1} \left(\mathbf{K}_{q_{cm,o_1^2}}^{-1} + \mathbf{K}_{q_{cm,o_2^3}}^{-1} \right)^{-1} \tag{5.46}$$

Next, the expressions for $\dot{\mathbf{q}}_{a,o_1^2}$ and $\dot{\mathbf{q}}_{c,o_1}$ as introduced in Eqs. (5.24) and (5.32), and the relation $\dot{\mathbf{q}}_{cs,o_1^2} = \mathbf{0}$ as introduced in Eq. (5.31), allows Eq. (5.45) to be written as

$$\$_{t,o_1^2} = \left(\mathbf{M}_{a,o_1^2} + \mathbf{M}_{c,o_1^2} \right) \left(\$_{t_{e_2}} - \$_{t_{e_1}} \right) \tag{5.47}$$

where

$$\mathbf{M}_{a,o_1^2} = \mathbf{J}_{a,o_1^2} \mathbf{J}_{a,o_1^2}^{-1} \tag{5.48}$$

$$\mathbf{M}_{c,o_1^2} = \mathbf{J}_{c,o_1} \mathbf{M}_{q_{cm,o_1^2}} \mathbf{J}_{c,o_1}^{-1} \tag{5.49}$$

Finally, Eqs. (5.47) and (5.7) can be inserted in Eq. (5.8), such that $\mathbf{M}_t$ in Eq. (5.6) is developed as

$$\mathbf{M}_t = \begin{bmatrix} \mathbf{I} & \mathbf{0} \\ \left(\mathbf{I} - \mathbf{M}_{a,o_1^2} - \mathbf{M}_{c,o_1^2} \right) & \left(\mathbf{M}_{a,o_1^2} + \mathbf{M}_{c,o_1^2} \right) \\ \mathbf{0} & \mathbf{I} \end{bmatrix} \tag{5.50}$$

where all matrices are 6×6 matrices. Equation (5.50) maps the two end-effector twists onto the three terminal link twists, which can be subsequently mapped onto the complete set of joint velocities as in Eq. (5.4).

5.5. EXAMPLE JACOBIAN ANALYSIS OF A THREE-LEGGED PM2E

IN this section the inverse Jacobian analysis is performed for the three-legged 2-DoF PM2E shown in Fig. 5.4, where n_1 and n_3 are considered as the end-effectors. The architecture of this PM2E was introduced as part of the kinematic design exercise in Appendix C and is also represented in Fig. 5.3c. The first DoF is a motion along the Z-axis, shared by both end-effectors, and the second DoF is a relative motion between the end-effectors along the X-axis, i.e., gripping. For the purpose of experimental validation, the end-effectors are connected to wrench sensors, which measure both force and moment. Additionally, the second joint of each leg is realized using a compliant joint, so that a pose-dependent wrench is applied on both end-effectors without the need of an actuation system. All other joints are realized using ball-bearings and are therefore considered as zero stiffness joints.

The inverse Jacobian matrix $\mathbf{J}^{-1}$, introduced in Eq. (5.5), for a three-legged PM2E with an internal closed-loop chain is obtained by combining the results from Sections 5.3 and 5.4. Then,

$$\begin{bmatrix} \dot{\mathbf{q}}_1 \\ \dot{\mathbf{q}}_2 \\ \dot{\mathbf{q}}_3 \\ \dot{\mathbf{q}}_{o_1^2} \\ \dot{\mathbf{q}}_{o_2^3} \\ \dot{\mathbf{q}}_{o_3^1} \end{bmatrix} = \mathbf{J}^{-1} \begin{bmatrix} \$_{t,e_1} \\ \$_{t,e_2} \end{bmatrix} \tag{5.51}$$

with

$$\mathbf{J}^{-1} = \mathbf{J}_n^{-1} \mathbf{M}_t \tag{5.52}$$

where the matrix $\mathbf{M}_t$ was introduced in Eq. (5.50) and for a three-legged PM2E with one internal closed-loop chain $\mathbf{J}_n^{-1}$ in Eq. (5.52) is developed as in Eq. (5.5), namely

$$\mathbf{J}_n^{-1} = \begin{bmatrix} \mathbf{J}_1^{-1} & \mathbf{0}_{6\times6} & \mathbf{0}_{6\times6} \\ \mathbf{0}_{6\times6} & \mathbf{J}_2^{-1} & \mathbf{0}_{6\times6} \\ \mathbf{0}_{6\times6} & \mathbf{0}_{6\times6} & \mathbf{J}_3^{-1} \\ -\mathbf{J}_{o_1^2}^{-1} & \mathbf{J}_{o_1^2}^{-1} & \mathbf{0}_{6\times6} \\ \mathbf{0}_{6\times6} & -\mathbf{J}_{o_2^3}^{-1} & \mathbf{J}_{o_2^3}^{-1} \\ \mathbf{J}_{o_3^1}^{-1} & \mathbf{0}_{6\times6} & -\mathbf{J}_{o_3^1}^{-1} \end{bmatrix} \tag{5.53}$$

The partial inverse Jacobian matrices in Eq. (5.53) are introduced in Appendix E, where they are expressed using the unit twists and unit wrenches for each serial chain. As explained in Section 5.4, the unit twists and unit wrenches that are identified for the two end-effector serial chains are also used in the analysis of the three internal serial chains, because they share the same kinematic structures.
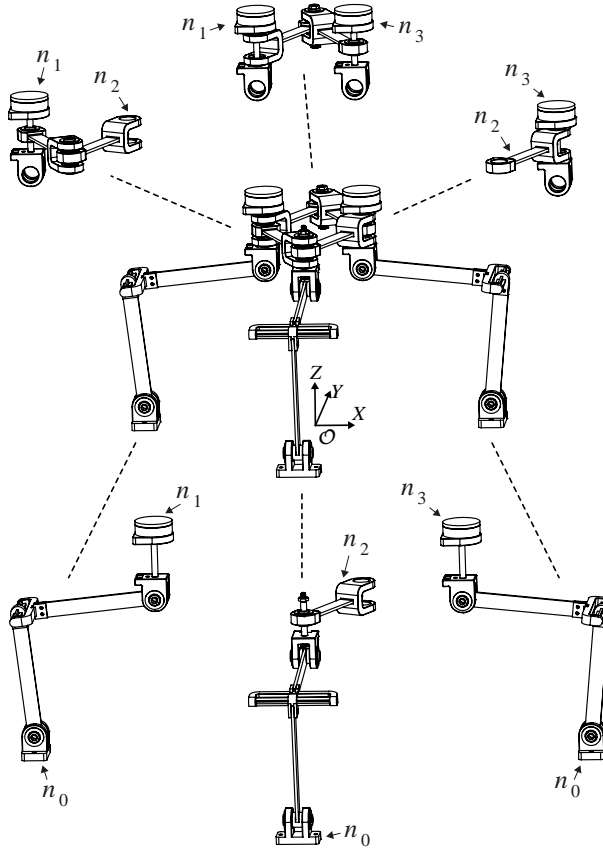
Figure 5.4: The example Jacobian analysis was performed for a 2-DoF PM2E, whose DoFs are a translation along Z-axis and a relative motion between terminal links n_1 and n_3 along the X-axis. Below the individual legs are shown, in which each second joint was designed as a compliant joint. The three internal serial chains are shown above.

To develop the matrix $\mathbf{M}_t$, which maps the end-effector twists on the full set of terminal link twists, $\mathbf{M}_{a,o_1^2}$ and $\mathbf{M}_{c,o_1^2}$ need to be developed. Because $C_{o_1^2} = 2$, the matrix $\mathbf{M}_{a,o_1^2}$ is obtained using Eq. (5.48), in which $\mathbf{J}_{a,o_1^2}$ is expressed by Eq. (5.42) as

$$\mathbf{J}_{a,o_1^2} = \begin{bmatrix} \hat{\$}_{ta_{o_{1,1}}} & \hat{\$}_{ta_{o_{1,2}}} \end{bmatrix} \tag{5.54}$$

and $\mathbf{J}_{a,o_1^2}^{-1}$ is expressed by Eq. (5.25) as

$$\mathbf{J}_{a,o_1^2}^{-1} = \begin{bmatrix} \hat{\$}_{wa_{o_{1,1}}}^{\top} / (\hat{\$}_{wa_{o_{1,1}}}^{\top} \hat{\$}_{ta_{o_{1,1}}}) \\ \hat{\$}_{wa_{o_{1,2}}}^{\top} / (\hat{\$}_{wa_{o_{1,2}}}^{\top} \hat{\$}_{ta_{o_{1,2}}}) \end{bmatrix} \tag{5.55}$$

The matrix $\mathbf{M}_{c,o_1^2}$ is constructed from three matrices: $\mathbf{J}_{c,o_1}$, $\mathbf{J}_{c,o_1}^{-1}$, and $\mathbf{M}_{q_{cm,o_1^2}}$, as expressed

in Eq. (5.49). Because $C_{o_1} = 3$, it follows from Eqs. (5.44) and (5.33) that

$$\mathbf{J}_{c,o_1} = \begin{bmatrix} \hat{\$}_{tc_{o_{1,1}}} & \hat{\$}_{tc_{o_{1,2}}} & \hat{\$}_{tc_{o_{1,3}}} \end{bmatrix} \tag{5.56}$$

$$\mathbf{J}_{c,o_1}^{-1} = \begin{bmatrix} \hat{\$}_{wc_{o_{1,1}}}^{\top} / (\hat{\$}_{wc_{o_{1,1}}}^{\top} \hat{\$}_{tc_{o_{1,1}}}) \\ \hat{\$}_{wc_{o_{1,2}}}^{\top} / (\hat{\$}_{wc_{o_{1,2}}}^{\top} \hat{\$}_{tc_{o_{1,2}}}) \\ \hat{\$}_{wc_{o_{1,3}}}^{\top} / (\hat{\$}_{wc_{o_{1,3}}}^{\top} \hat{\$}_{tc_{o_{1,3}}}) \end{bmatrix} \tag{5.57}$$

To express $\mathbf{M}_{q_{cm,o_1^2}}$ using Eq. (5.46), the compliance matrices $\mathbf{K}_{q_{cm,o_1^2}}^{-1}$ and $\mathbf{K}_{q_{cm,o_2^3}}$ are required, which are the compliance matrices of the internal serial chains expressed in the multiple constrained joint space, which is spanned by the twists associated to the virtual joints of the first end-effector serial chain. The compliance in these directions is assumed to originate solely in the links. Each internal serial chain contains one link, each of which was designed as a rectangular bar. The required compliance matrices are therefore developed by mapping the relevant link compliance matrix onto the constrained joint space of the first end-effector serial chain,

$$\mathbf{K}_{q_{cm,o_1^2}}^{-1} = \mathbf{J}_{c,o_1}^{-1} \mathbf{Ad}_{\mathbf{H}_{l_{o_{1,1}}}^{\mathcal{O}}} \mathbf{K}_{s,l_{o_{1,1}}}^{-1} \mathbf{Ad}_{\mathbf{H}_{l_{o_{1,1}}}^{\mathcal{O}}}^{\top} \mathbf{J}_{c,o_1}^{-\top} \tag{5.58}$$

$$\mathbf{K}_{q_{cm,o_2^3}}^{-1} = \mathbf{J}_{c,o_1}^{-1} \mathbf{Ad}_{\mathbf{H}_{l_{o_{1,2}}}^{\mathcal{O}}} \mathbf{K}_{s,l_{o_{1,2}}}^{-1} \mathbf{Ad}_{\mathbf{H}_{l_{o_{1,2}}}^{\mathcal{O}}}^{\top} \mathbf{J}_{c,o_1}^{-\top} \tag{5.59}$$

where $\mathbf{J}_{c,o_1}^{-1}$ was introduced in Eq. (5.57), and $\mathbf{Ad}_{\mathbf{H}_{l_{o_{1,i}}}^{\mathcal{O}}}$ is the Adjoint matrix which transforms a twist expressed in the reference frame connected to the end of the ith link of the first end-effector serial chain into its equivalent twist expressed in the inertial Cartesian reference frame, and $\mathbf{K}_{s,l_{o_{1,i}}}^{-1}$ is the compliance matrix of the ith link of the first end-effector serial chain. Both links were designed equal, such that

$$\mathbf{K}_{s,l_{o_{1,i}}}^{-1} = \begin{bmatrix} \frac{L_o}{GI_x} & 0 & 0 & 0 & 0 & 0 \\ 0 & \frac{L_o}{EI_y} & 0 & 0 & 0 & \frac{-L_o^2}{2EI_y} \\ 0 & 0 & \frac{L_o}{EI_z} & 0 & \frac{L_o^2}{2EI_z} & 0 \\ 0 & 0 & 0 & \frac{L_o}{AE} & 0 & 0 \\ 0 & 0 & \frac{L_o^2}{2EI_z} & 0 & \frac{L_o^3}{3EI_z} & 0 \\ 0 & -\frac{L_o^2}{2EI_y} & 0 & 0 & 0 & \frac{L_o^3}{3EI_y} \end{bmatrix} \tag{5.60}$$

For the developed mechanism, $L_o = 0.12$ m, $E = 1.95 \cdot 10^9$ N/m^2, and $G = 740 \cdot 10^6$ N/m^2 was subsequently calculated using

$$G = E/(2 + 2\nu) \tag{5.61}$$

with $\nu = 0.32$, where E and ν were determined as the average values of two tensile tests, which were performed on samples of the material used for the construction of the links, namely Stratasys ABS*plus* material in combination with a Stratasys Dimension BST 1200es

3D printer. Individual determined values for E had a 4% difference from this value. Furthermore, the area and the area moments of inertia, respectively, are

$$A = bh \qquad I_x = 1/12bh(h^2 + b^2), \qquad I_y = 1/12bh^3, \qquad I_z = 1/12b^3h$$

with $b = 3$ mm and $h = 16$ mm.

With the matrices introduced in Eqs. (5.54)-(5.60), the matrices $\mathbf{M}_{a,o_1^2}$ and $\mathbf{M}_{c,o_1^2}$ are developed according to Eqs. (5.48) and (5.49). Subsequently, $\mathbf{M}_t$ was developed using Eq. (5.50) and $\mathbf{J}_n^{-1}$ was constructed as in Eq. (5.53) using the partial inverse Jacobian matrices developed in Appendix E. Finally, the complete inverse Jacobian matrix of the PM2E presented in Fig. 5.4 was obtained using Eq. (5.52).

5.6. EXPERIMENTAL VALIDATION METHOD

To validate the developed Jacobian analysis, an experimental static force analysis was performed for the PM2E introduced in Section 5.5. The reason for using a static force analysis is because it is relatively easy to control the pose, which determines the torques applied by the compliant joints, and measure the resulting six-dimensional reaction wrenches at both end-effectors. On the other hand, it is considered much more difficult to simultaneously control the end-effector twists and measure the complete set of joint velocities. This is especially true for the constrained directions.

5.6.1. STATIC FORCE ANALYSIS

In a static force analysis, the transpose of an inverse Jacobian matrix can be used to map a known joint torque vector onto the equivalent wrenches applied by the end-effector on the environment. Therefore, if the compliant mechanism with two end-effectors as introduced in Fig. 5.4 is fixed in a specific pose through its end-effectors, the interaction wrenches can be predicted as a function of the pose, namely

$$\begin{bmatrix} \$_{w,e_1} \\ \$_{w,e_2} \end{bmatrix} = \mathbf{J}^{-\top} \boldsymbol{\tau} \tag{5.62}$$

where $\$_{w,e_1}$ and $\$_{w,e_2}$ are the net wrenches applied by the PM2E on the first and second end-effector respectively, $\mathbf{J}^{-\top}$ is the transpose of the full inverse Jacobian and $\boldsymbol{\tau}$ is the applied joint torque vector, which is expressed as

$$\boldsymbol{\tau} = \begin{bmatrix} \boldsymbol{\tau_1}^\top & \boldsymbol{\tau_2}^\top & \boldsymbol{\tau_3}^\top & \boldsymbol{\tau}_{o_1^2}^\top & \boldsymbol{\tau}_{o_2^3}^\top & \boldsymbol{\tau}_{o_3^1}^\top \end{bmatrix}^\top \tag{5.63}$$

where $\boldsymbol{\tau_i}$ is the six-dimensional joint torque vector for leg i, and $\boldsymbol{\tau}_{o_i^{i+1}}$ (or $\boldsymbol{\tau}_{o_i^1}$ if $i = N$) is the six-dimensional joint torque vector of the ith internal serial chain.

For the example that was introduced in Section 5.5, the various applied joint torque vectors can be expressed as

$$\boldsymbol{\tau}_i = \begin{bmatrix} 0 & \tau_{pf,i} & 0 & 0 & 0 & 0 \end{bmatrix}^\top, \qquad \text{for } i = 1,2,3 \tag{5.64}$$

$$\boldsymbol{\tau}_{o_1^2} = \boldsymbol{\tau}_{o_2^3} = \boldsymbol{\tau}_{o_3^1} = \mathbf{0}_{6 \times 1} \tag{5.65}$$
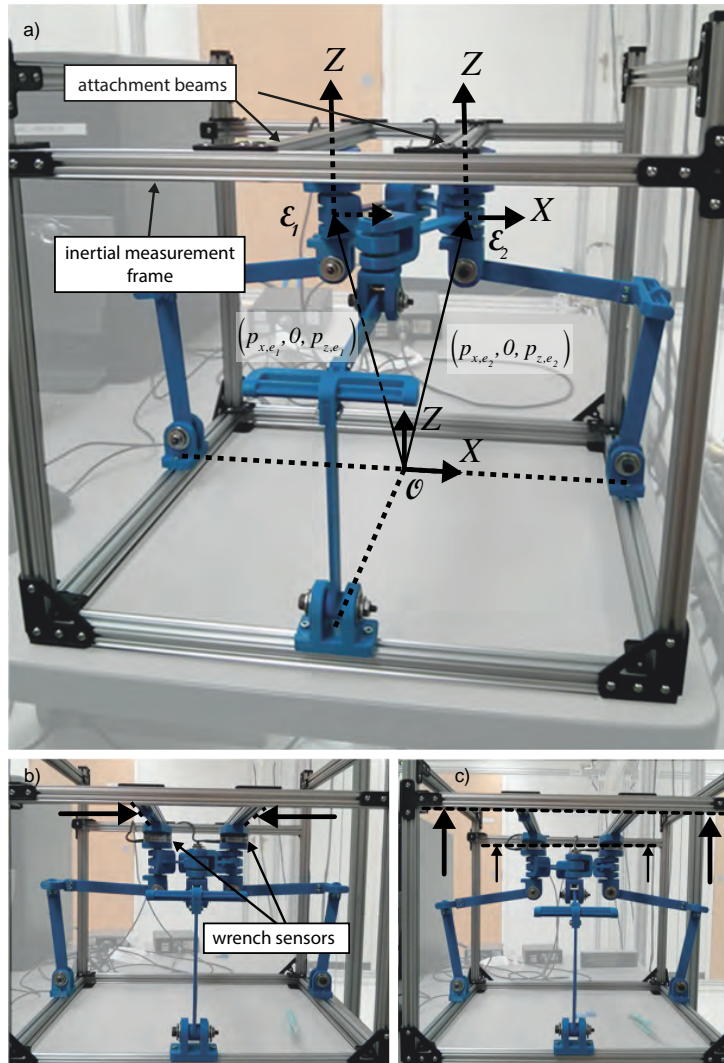
Figure 5.5: The set-up that was developed to validate the developed Jacobian analysis using a static force analysis, shown in three poses as presented in Table 5.1, namely a) in pose a0, in which the net wrench is approximately zero, b) in pose f0, where arrows indicate how the positions p_{x,e_1} and p_{x,e_2} are adjusted, and c) pose f1, where arrows indicate how p_{z,e_1} and p_{z,e_2} are changed by adjusting the measurement frame.

Table 5.1: The 18 poses at which the Jacobian analysis of the example PM2E has been validated using a static force analysis. The pose variables are also indicated in Fig. 5.5

Pose	p_{x,e_1} [m]	p_{z,e_1} [m]	p_{x,e_2} [m]	p_{z,e_2} [m]
a0	-0.0525	0.2165	0.0525	0.2165
a1	-0.0575	0.2165	0.0575	0.2165
a2	-0.0525	0.2215	0.0525	0.2215
b0	-0.070	0.2165	0.070	0.2165
b1	-0.075	0.2165	0.075	0.2165
b2	-0.070	0.2215	0.070	0.2215
c0	-0.065	0.200	0.065	0.200
c1	-0.070	0.200	0.070	0.200
c2	-0.065	0.205	0.065	0.205
d0	-0.055	0.205	0.055	0.205
d1	-0.060	0.205	0.060	0.205
d2	-0.055	0.210	0.055	0.210
e0	-0.055	0.190	0.055	0.190
e1	-0.060	0.190	0.060	0.190
e2	-0.055	0.195	0.055	0.195
f0	-0.060	0.220	0.060	0.220
f1	-0.065	0.220	0.065	0.220
f2	-0.060	0.225	0.060	0.225

where $\tau_{pf,i}$ is the joint torque resulting from the deflection of the compliant revolute joint that makes up the second joint of each leg, so that

$$\tau_{pf,i} = -k_i \left(q_{i,2} - q_{i,2_0} \right), \qquad \text{for } i = 1, 2, 3 \tag{5.66}$$

To express the stiffness k_i (Nm/rad) of the designed cross-type compliant revolute joint, the model presented by Trease et al. [25] was used, namely

$$k_i = \left(\frac{w}{t} - 0.373 \right) \frac{4Gt^4}{3L_j}, \qquad \text{for } i = 1, 2, 3 \tag{5.67}$$

where the designed cross-type compliant joint has width $w = 9$ mm, thickness $t = 2$ mm, length $L_j = 40$ mm, and is made of the same Stratasys ABS*plus* material as the links in the end-effector serial chains, so that $G = 740 \cdot 10^6$ N/m^2 and $E = 1.95 \cdot 10^9$ N/m^2. The angle of zero deflection, $q_{i,2_0}$ (rad), was designed as

$$q_{i,2_0} = \frac{3\pi}{2} \qquad \text{for } i = 1, 2, 3 \tag{5.68}$$

An expression for the angles $q_{i,2}$ can be found in Appendix E.
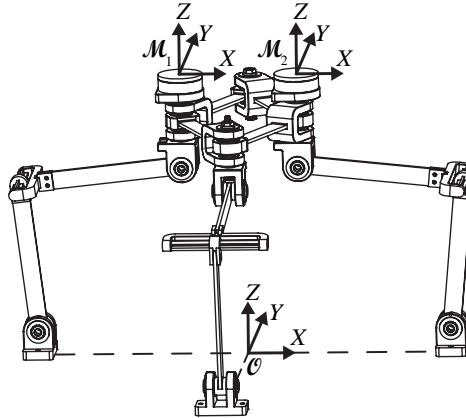
Figure 5.6: The inertial reference frame and the measurement reference frames as used in the example Jacobian analysis.

5.6.2. Measurement Procedure

The mapping of the applied joint torque vector onto the resulting interaction wrenches was performed in the 18 poses as introduced in Table 5.1. These reaction wrenches were measured using an ATI Mini40 wrench sensor with SI-40-2 calibration. The specified force measurement accuracy of this sensor along the X- and Y-axis is 1/100 N and 1/50 N along the Z-axis. The torque measurement accuracy is 1/4000 Nm for all three directions. Both wrench sensors were connected in series between one of the end-effectors and the inertial measurement frame, as can be seen in Fig. 5.5b. As such, the wrench sensors were displaced together with the end-effector bodies. Before the start of every measurement series, the wrench sensor was initialized at the pose where the net wrench on the end-effectors is approximately zero, which is pose a0 as introduced in Table 5.1. The position of the end-effector within the measurement frame was controlled manually using a caliper. This was done by moving the attachment beams of the two end-effectors in the X- and Z-directions, as shown in Figs. 5.5b and 5.5c.

There are various sources that may influence the measurement precision and accuracy. Firstly, next to the finite resolution of the wrench sensors, there are inevitable inaccuracies in the manual positioning of the end-effectors. Secondly, the model will not be perfect, because the change in gravity is not considered, nor is any friction in the ball bearings. Furthermore, the 3D-printed compliant joints will likely show some variation in their properties, and therefore not perfectly agree with the modeled joints.

5.6.3. Post-Processing

Post-processing of the data was necessary to express all wrenches in the measurement reference frame of either the first or the second end-effector, so that measured and predicted wrenches could be compared. The wrenches that are expressed using the Jacobian-based mapping of the compliant joint torques are all expressed in end-effector body-fixed reference frames collocated with the inertial reference frame. However, the measurements are made in measurement reference frames, as shown in Fig. 5.6. The map-

ping of the two predicted interaction wrenches onto the measurement reference frames was done using

$$
\begin{bmatrix} \$_{w,e_1,pred}^{\mathscr{M}} \\ \$_{w,e_2,pred}^{\mathscr{M}} \end{bmatrix} = \begin{bmatrix} \mathbf{Ad}_{\mathbf{H}_{\mathscr{M}_1}^{\mathscr{O}}}^{\top} & \mathbf{0}_6 \\ \mathbf{0}_6 & \mathbf{Ad}_{\mathbf{H}_{\mathscr{M}_2}^{\mathscr{O}}}^{\top} \end{bmatrix} \begin{bmatrix} \$_{w,e_1,pred}^{\mathscr{O}} \\ \$_{w,e_2,pred}^{\mathscr{O}} \end{bmatrix} \tag{5.69}
$$

where $\$_{w,e_1,pred}^{\mathscr{O}}$ and $\$_{w,e_2,pred}^{\mathscr{O}}$ are the predicted interaction wrenches expressed in the inertial reference frame and $\$_{w,e_1,pred}^{\mathscr{M}}$ and $\$_{w,e_2,pred}^{\mathscr{M}}$ are the equivalent wrenches expressed in their respective measurement frames. Matrices $\mathbf{Ad}_{\mathbf{H}_{\mathscr{M}_1}^{\mathscr{O}}}$ and $\mathbf{Ad}_{\mathbf{H}_{\mathscr{M}_2}^{\mathscr{O}}}$ are the adjoint matrices associated to the homogeneous matrices $\mathbf{H}_{\mathscr{M}_1}^{\mathscr{O}}$ and $\mathbf{H}_{\mathscr{M}_2}^{\mathscr{O}}$. These homogeneous matrices were expressed as

$$
\mathbf{H}_{\mathscr{M}_1}^{\mathscr{O}} = \begin{bmatrix} \mathbf{I}_3 & \mathbf{p}_{m_1} \\ \mathbf{0}_{1\times 3} & 1 \end{bmatrix}
$$

$$
\mathbf{H}_{\mathscr{M}_2}^{\mathscr{O}} = \begin{bmatrix} \mathbf{I}_3 & \mathbf{p}_{m_2} \\ \mathbf{0}_{1\times 3} & 1 \end{bmatrix}
$$

with

$$
\mathbf{p}_{m_1} = \begin{bmatrix} p_{x,e_1} & 0 & p_{z,e_1} + h_s \end{bmatrix}^{\top}
$$

$$
\mathbf{p}_{m_2} = \begin{bmatrix} p_{x,e_2} & 0 & p_{z,e_2} + h_s \end{bmatrix}^{\top}
$$

where $h_s = 42.6$ [mm] was the distance between the end-effector reference frame origins, as shown in Fig. 5.5, and the measurement reference frames, as shown in Fig. 5.6. After mapping as in Eq. (5.69), the wrenches predicted by Jacobian mapping can be compared with those measured.

5.7. RESULTS OF EXPERIMENTAL VALIDATION

THIS section presents the results of the experimental validation as described in section 5.6. The results are visualized in Figs. 5.7-5.9. Figure 5.7 plots the predicted interaction force values against those measured for the X- and Z-axis, which are the axes spanned by the DoFs of the analyzed PM2E. In Fig. 5.8 a similar plot is shown for the Y-axis, which represents a constraint of the PM2E for both end-effectors. Finally, the predicted and measured interaction moments are plotted against each other in Fig. 5.9, where the example PM2E is constrained in rotational motion along all three axes. The complete set of measurement data can be obtained from Ref. [26].

To express the percentage of variability in the measurements that has been accounted for by the Jacobian-based predictions, the coefficients of determination, R^2, are used. These coefficients are shown in Table 5.2 for the data shown in Figs. 5.7-5.9. The R^2 values express the variability around the linear trend lines which are included in Figs. 5.7-5.9. These linear trend lines do not perfectly follow the line $\Delta f_{pred} = \Delta f_{meas}$, but this inaccuracy is not considered in this paper.

Figure 5.7: The correlation between the measured force values and those predicted using $\mathbf{J}^{-\top}$ at the poses as listed in Table 5.1 along the axes spanned by the DoFs of the PM2E. Linear trend lines are added around which the coefficients of determination are calculated.
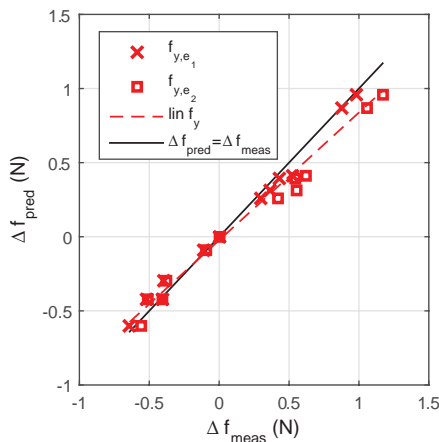
Figure 5.8: The correlation between the measured force values and those predicted using $\mathbf{J}^{-\top}$ at the poses listed in Table 5.1 along the axis in which the PM2E is constrained. A linear trend line is added around which the coefficient of determination are calculated.

5.8. DISCUSSION ON GENERALIZATION OF RESULTS

THE results from the experimental validation of the Jacobian analysis demonstrate that the presented Jacobian analysis is valid for the analyzed three-legged PM2E with
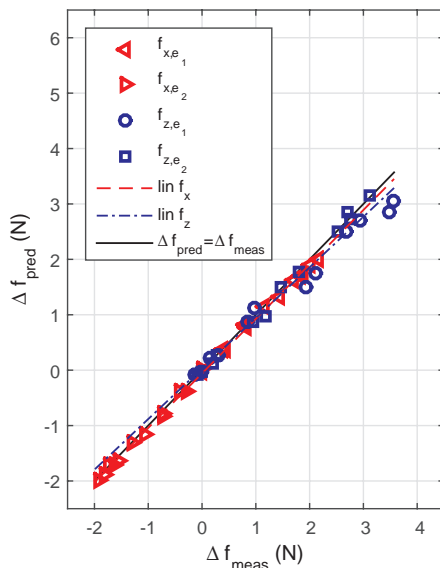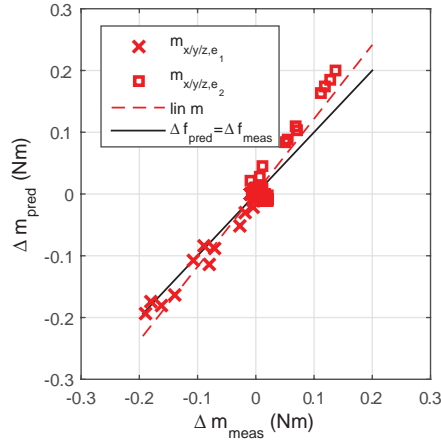
Figure 5.9: The correlation between the measured moment values and those predicted using $\mathbf{J}^{-\top}$ at the poses listed in Table 5.1 along all three axes, all of which are constrained directions for the analyzed PM2E. A linear trend line is added around which the coefficient of determination are calculated.

Table 5.2: The coefficients of determination of the different sets of measured and predicted values.

considered set	related figure	R^2 [-]
DoFs ($\mathbf{f}_{x/z}$)	Fig. 5.7	0.996
linear constraints ($\mathbf{f}_y$)	Fig. 5.8	0.962
angular constraints ($\mathbf{m}_{x/y/z}$)	Fig. 5.9	0.876

a single internal closed-loop chain. This is concluded from the high coefficients of determination for the three separately analyzed sets of predicted and measured force and moment values, as presented in Table 5.2. Although the coefficient of determination for the angular constraints is somewhat lower, this can be explained by the large number of values close to zero, which are more affected by measurement errors. Nonetheless, these values are considered sufficiently high to conclude that the Jacobian analysis that was used to predict the interaction wrenches is valid.

Although the presented Jacobian analysis was developed based on velocity relations, it was validated using a static force analysis for three reasons. Firstly, it was considered more practical to control the pose during static wrench measurements than during velocity measurements. Secondly, it was deemed much simpler to include the constraints in static force measurements than in velocity measurements. The third reason is that constraint relations are especially important in the static force analysis of PM2Es, since wrenches applied by the legs can be transferred via the constraints of internal serial chains. The inclusion of these constraint relations in the matrix $\mathbf{M}_t$, which represents the mapping from the two end-effector twists onto the full set of terminal link twists, has

been one of the main innovations of this chapter. Therefore, a static force analysis has allowed a direct validation of this innovation.

It is argued that the example PM2E is a representative example of more general PM2Es with an internal closed-loop chain. The main difficulty of the analysis was to find an expression for the mapping from the two end-effector twists onto the complete set of terminal link twists. A combination of velocity relations and static force relations was derived to deal with the internal constraints. As a result, the obtained expression is a function of the kinematic structure of the mechanism as well as the relative compliance of the internal serial chains. The proposed systematic approach can be extended to PM2Es with an internal closed-loop chain with more than three legs, knowing that more, comparable relations will need to be expressed to reflect its corresponding graph representation.

Furthermore, it is expected that the presented systematic approach can be easily adapted to other variations of PM2Es. Because the analysis relies on a Jacobian interpretation of a PM's graph theory representation, the same approach can also be applied to other, more complex parallel manipulators, e.g., with more than one internal closed-loop chain or with more than two end-effectors. Such manipulators will have different graph theory representations, which means that the structures of the corresponding matrices $\mathbf{J}_n^{-1}$ would be different than the one presented in Eq. (5.5). Nonetheless, the approach would be the same. As such, the systematic approach presented in this chapter could be used as a baseline for a wide range of more complex parallel manipulators.

5.9. CONCLUSIONS ON JACOBIAN ANALYSIS OF PM2ES

T HIS chapter introduced a systematic approach for the Jacobian analysis of PM2Es with an internal closed-loop chain, based on two novel insights. The first insight is that the structure that is revealed by graph theory can be translated into a Jacobian analysis. The resulting Jacobian analysis consists of a systematic combination of partial Jacobian matrices, which describes how the full set of terminal link twists is mapped onto the complete set of joint velocities.

However, the full set of terminal link twists is generally not available and cannot be derived based on velocity relations alone. This was demonstrated for a three-legged PM2E with an internal closed-loop chain. The second insight is that these relations can be complimented with static force relations so that the full set of terminal link twists can be expressed as a function of the known end-effector twists. The static force relations, which appear in the expression as compliance ratios, are required to deal with internal constraints. The possibility for internal constraints is typical for PM2Es and is particularly relevant if the resulting Jacobian is used in a static force analysis, because wrenches applied by the actuators can be transferred to the end-effectors via the internal constraints. The resulting dependency of a Jacobian analysis on mechanical properties is unprecedented in the field of parallel manipulator analysis.

The developed Jacobian analysis was validated using a static force analysis in an example PM2E with three legs and a single internal closed-loop chain. Compliant joints were implemented so that pose-dependent wrenches were applied to the end-effectors without the need of an actuation system. The end-effectors were fixed to an inertial frame via wrench sensors, so that the resulting interaction wrenches could be measured.

The interaction wrenches were measured along directions corresponding to the allowed DoFs as well as along constrained directions. These measurements were compared with predicted interaction wrenches based on the developed Jacobian analysis. It was shown that the variability in the measured values is predicted for 99.6% along directions corresponding to the allowed DoFs, and respectively 96.2% and 87.6% for the forces and moments along the constrained directions. Based on these values it is concluded that the example Jacobian analysis is valid.

This chapter presented and validated the first example of a Jacobian analysis of a PM2E that takes internal constraints into account. Although the Jacobian analysis presented in this chapter was developed for PM2Es with a single internal closed-loop chain and three legs, it was argued that the analysis can be adapted to other PM2Es with relative ease. This is thanks to the structure of the analysis, which can be directly derived from the graph theory representation of a mechanism. As such, the structured approach introduced in this chapter sets the stage for the Jacobian analysis of more complex PM2Es.

REFERENCES

[1] A. G. L. Hoevenaars, P. Lambert, and J. L. Herder, *Generalized Jacobian Analysis of Parallel Manipulators With Multiple End-Effectors,* in *Volume 5A: 38th Mechanisms and Robotics Conference* (ASME, 2014) p. V05AT08A081.

[2] K. Bengtsson, *Picking a winner and packing a punch: the second-generation Flex-Picker,* ABB Review **4**, 29 (2008).

[3] F. Pierrot, V. Nabat, O. Company, S. Krut, and P. Poignet, *Optimal Design of a 4-DOF Parallel Manipulator: From Academia to Industry,* IEEE Transactions on Robotics **25**, 213 (2009).

[4] J. Hesselbach, J. Wrege, A. Raatz, and O. Becker, *Aspects on design of high precision parallel robots,* Assembly Automation **24**, 49 (2004).

[5] L. Bruzzone and G. Bozzini, *A flexible joints microassembly robot with metamorphic gripper,* Assembly Automation **30**, 240 (2010).

[6] Q.-Z. Ang, B. Horan, H. Abdi, and S. Nahavandi, *Multipoint Haptic Guidance for Micrograsping Systems,* IEEE Systems Journal , 1 (2014).

[7] Force Dimension, *Sigma.7 Haptic Device,* Spec Sheet.

[8] F. Y. Chen, *Gripping mechanisms for industrial robots,* Mechanism and Machine Theory **17**, 299 (1982).

[9] P. O. Hugo, *Industrial Grippers: State-of-the-Art and Main Design Characteristics,* in *Grasping in Robotics,* edited by G. Carbone (2013) pp. 107–131.

[10] P. Lambert and J. Herder, *A novel parallel haptic device with 7 degrees of freedom,* in *2015 IEEE World Haptics Conference (WHC),* Vol. 31 (IEEE, 2015) pp. 183–188.

[11] M. G. Mohamed and C. M. Gosselin, *Design and analysis of kinematically redundant parallel manipulators with configurable platforms,* IEEE Transactions on Robotics **21**, 277 (2005).

[12] P. Lambert, H. Langen, and R. H. Munnig Schmidt, *A Novel 5 DOF Fully Parallel Robot Combining 3T1R Motion and Grasping,* in *Volume 2: 34th Annual Mechanisms and Robotics Conference, Parts A and B* (ASME, 2010) pp. 1123–1130.

[13] B.-J. Yi, Y. N. Heung, H. L. Jae, Y.-S. Hong, S.-R. Oh, I. H. Suh, and W. K. Kim, *Design of a Parallel-Type Gripper Mechanism,* The International Journal of Robotics Research **21**, 661 (2002).

[14] B.-J. Park, B.-J. Yi, and W.-K. Kim, *Design and analysis of a new parallel grasper having spherical motion,* in *2004 IEEE/RSJ International Conference on Intelligent Robots and Systems (IROS) (IEEE Cat. No.04CH37566),* Vol. 1 (IEEE, 2004) pp. 106–111.

[15] V. Nabat, M. de la O Rodriguez, O. Company, S. Krut, and F. Pierrot, *Par4: very high speed parallel robot for pick-and-place,* in *IEEE/RSJ International Conference on Intelligent Robots and Systems* (IEEE, 2005) pp. 553–558.

[16] P. Lambert and J. L. Herder, *Parallel robots with configurable platforms: Fundamental aspects of a new class of robotic architectures,* Proceedings of the Institution of Mechanical Engineers, Part C: Journal of Mechanical Engineering Science **0**, 1 (2015).

[17] S. Tadokoro, *Control of parallel mechanisms,* Advanced Robotics **8**, 559 (1993).

[18] D. Zlatanov, I. A. Bonev, and C. M. Gosselin, *Constraint singularities of parallel mechanisms,* in *IEEE International Conference on Robotics and Automation,* Vol. 1 (IEEE, 2002) pp. 496–502.

[19] J. P. Merlet, *Jacobian, Manipulability, Condition Number, and Accuracy of Parallel Robots,* Journal of Mechanical Design **128**, 199 (2006).

[20] F. Paccot, N. Andreff, and P. Martinet, *A Review on the Dynamic Control of Parallel Kinematic Machines: Theory and Experiments,* The International Journal of Robotics Research **28**, 395 (2009).

[21] H. Sung Kim and H. Lipkin, *Stiffness of Parallel Manipulators With Serially Connected Legs,* Journal of Mechanisms and Robotics **6**, 031001 (2014).

[22] A. G. L. Hoevenaars, P. Lambert, and J. L. Herder, *Jacobian-based stiffness analysis method for parallel manipulators with non-redundant legs,* Proceedings of the Institution of Mechanical Engineers, Part C: Journal of Mechanical Engineering Science (2015), 10.1177/0954406215602283.

[23] S. A. Joshi and L.-W. Tsai, *Jacobian Analysis of Limited-DOF Parallel Manipulators,* Journal of Mechanical Design **124**, 254 (2002).

[24] T. Huang, H. T. Liu, and D. G. Chetwynd, *Generalized Jacobian analysis of lower mobility manipulators,* Mechanism and Machine Theory **46**, 831 (2011).

[25] B. P. Trease, Y.-M. Moon, and S. Kota, *Design of Large-Displacement Compliant Joints,* Journal of Mechanical Design **127**, 788 (2005).

[26] A. G. L. Hoevenaars, *Wrench Measurements on a Spatial, Passive, 2-DoF Parallel Mechanism with Two End-Effectors,* (2015).

5

6

JACOBIAN-BASED STIFFNESS ANALYSIS OF PARALLEL MANIPULATORS WITH TWO END-EFFECTORS

I wish I could break
All the chains holding me

Billy Taylor and Richard Carroll Lamb
Nina Simone - I wish I knew how it would feel to be free

This chapter presents the Jacobian-based stiffness analysis of two examples of parallel manipulators with two end-effector (PM2Es). To perform these analyses, the Jacobian-based stiffness analysis method, derived in Chapter 2, is combined with the structured approach for the Jacobian analysis of PM2Es, which was presented in Chapter 5. The analyses are performed for two passive mechanisms: a planar underactuated 4-DoF mechanism and a spatial overconstrained 2-DoF mechanism. Subsequently, it is experimentally verified that the resulting stiffness analyses have an accuracy comparable to those of traditional parallel manipulators and that consideration of loading also increases accuracy of the stiffness analysis of PM2Es. Additionally, this chapter contains the first examples of stiffness matrices of PM2Es, namely 6×6 stiffness matrices for the analyzed planar mechanism and a 12×12 stiffness matrix for the analyzed spatial mechanism.

6.1. Introduction to Stiffness Analysis of PM2Es

In applications that require controlled gripping as well a high stiffness-over-inertia ratio [1–3], parallel manipulators with two end-effectors (PM2Es) are an interesting solution. In PM2Es, relative degrees of freedom (DoFs) between the end-effectors are allowed by internal mobilities, which can be controlled using actuators that are located at the base [4, 5]. Such architectures therefore enable controlled mechanical gripping while minimizing the effective contribution of the actuators to the inertia.

Because a high stiffness-over-inertia ratio enables faster motions [6, 7], it is not surprising that the concept behind PM2Es was originally developed with the pick-and-place industry in mind [4]. In the earliest examples, an internal closed-loop chain acted as the gripper [4, 8]. These manipulators have also been referred to as parallel manipulators with configurable platforms (PMCPs) [5], variations of which have also been explored in Refs. [9–11]. The term PM2E was introduced in this thesis for those manipulators where interaction occurs via two dedicated end-effectors. PM2Es have so far only been explored in the design of haptic devices [12, 13].

Existing research on the analysis of PM2Es is largely focused around kinematic relations. Mohamed and Gosselin [5] used kinematic relations to express the passive joint velocities as a function of the active joint velocities. Lambert and Herder [14] used kinematic relations to develop a mobility analysis based on screw theory and also discussed some of the aspects of PMCPs that makes their kinematics fundamentally different from traditional parallel manipulators [15].

In Chapter 5 it was realized that kinematic relations alone are often insufficient to develop a Jacobian analysis of a PM2E that is also valid for a static force analysis. This is because wrenches applied by the legs can be transferred to multiple end-effectors via the constraints that are imposed by the internal serial chains. This effect is not captured by kinematic relations alone and required the introduction of compliance ratios in the Jacobian analysis.

However, no research has yet been done on the dynamic analysis of PM2Es, while this will be required for the optimal design of PM2Es. Most notably, expressions for the stiffness and inertia matrices will be required in order to optimize the stiffness-over-inertia ratio. Moreover, stiffness is also key in the accuracy analysis of any parallel manipulator, including PM2Es.

The aim of this chapter is to perform the first stiffness analyses of PM2Es. This will be achieved using the combination of the Jacobian-based stiffness analysis method of Chapter 2 and the structured approach for the Jacobian analysis of PM2Es of Chapter 5. The same experimental setup is used as presented in Chapter 3.

The structure of this chapter is as follow. First, the integration of the stiffness analysis method and the structured approach for the Jacobian analysis of PM2Es is discussed. The stiffness analyses are performed for a planar 4-DoF PM2E and a spatial 2-DoF PM2E. Next, the experimental setup is described. In the Results section the first examples of stiffness matrices of PM2Es are presented, together with the processed measurement data. The measurement data shows that the accuracy of the stiffness analyses performed in this chapter is similar to the accuracies found in Chapter 3. The results are interpreted in the Discussion section.

6.2. STIFFNESS ANALYSES OF PM2ES

T HE main idea of this chapter is to integrate the Jacobian-based stiffness analysis method for PMs with non-redundant legs as presented in Chapter 2 and the structured approach for the Jacobian analysis of PM2Es as presented in Chapter 5. This integration is first introduced in this section. Next, the design and analysis of a passive planar 4-DoF PM2E is presented. For a second mechanism, the passive spatial 2-DoF PM2E that was previously introduced in Chapter 5, only those aspects are presented which have not been presented before.

6.2.1. INTEGRATION OF STIFFNESS ANALYSIS METHOD FOR PMS AND JACOBIAN ANALYSIS OF PM2ES

For a PM2E, a Cartesian stiffness matrix $\mathbf{K}$ is a 12×12 matrix that maps a combination of two displacement twists onto two differential wrenches,

$$\begin{bmatrix} d\$_{w,e_1,pred} \\ d\$_{w,e_2,pred} \end{bmatrix} = -\mathbf{K} \begin{bmatrix} \$_{d,e_1} \\ \$_{d,e_2} \end{bmatrix} \tag{6.1}$$

where $\$_{d,e_1}$ and $\$_{d,e_2}$ are the displacement twists of the first and second end-effector respectively, and $d\$_{w,e_1,pred}$ and $d\$_{w,e_2,pred}$ are the corresponding differential reaction wrenches. In this chapter each displacement twist and differential wrench is defined as

$$\$_d = \begin{bmatrix} d\boldsymbol{\phi} \\ d\mathbf{p} \end{bmatrix}, \quad d\$_w = \begin{bmatrix} d\mathbf{m} \\ d\mathbf{f} \end{bmatrix}$$

in which $d\boldsymbol{\phi}$ and $d\mathbf{p}$ are the differential angular and differential linear displacements of the respective end-effector, and $d\mathbf{m}$ and $d\mathbf{f}$ the resulting change in moment- and force vector applied by the PM2E to the end-effectors.

The general formulation of the stiffness analysis that is applied in this chapter was presented in Eq. (2.43), and is repeated here for convenience,

$$\mathbf{K} = \left(-\frac{\partial \mathbf{J}_e^{-\top}}{\partial \mathbf{q}} \boldsymbol{\tau}_e \right) \mathbf{J}^{-1} + \mathbf{J}_e^{-\top} \mathbf{K}_{q,e} \mathbf{J}_e^{-1} \tag{6.2}$$

where $\mathbf{q}$ is the vector that contains all real and virtual joint coordinates (the latter representing the constrained directions in joint space), $\boldsymbol{\tau}_e$ is the joint torque vector where all zero entries associated to zero stiffness joints were removed, $\mathbf{J}^{-1}$ is the full inverse Jacobian. The matrix $\mathbf{J}_e^{-1}$ is the inverse Jacobian of elasticity, which corresponds to the matrix $\mathbf{J}^{-1}$ with all rows associated to zero stiffness joints removed. Finally, matrix $\mathbf{K}_{q,e}$ is the stiffness matrix of the parallel manipulator expressed in the space spanned by the elastic joint coordinates, which includes the effect of actuated joints, compliant joints, as well as structural compliance.

In this chapter the stiffness analysis represented by Eq. (6.2) is combined with the structured approach for the Jacobian analysis of PM2Es, introduced in Chapter 5. This analysis is summarized as

$$\mathbf{J}^{-1} = \mathbf{J}_n^{-1} \mathbf{M}_t \tag{6.3}$$

where for a PM2E with N legs and a single internal closed loop chain $\mathbf{M}_t$ was described as the $6N \times 12$ matrix that maps the two end-effector twists on the set of N terminal link twists, and $\mathbf{J}_n^{-1}$ was expressed as

$$\mathbf{J}_n^{-1} = \begin{bmatrix} \mathbf{J}_1^{-1} & \mathbf{0}_{6\times6} & \ldots & \mathbf{0}_{6\times6} \\ \mathbf{0}_{6\times6} & \mathbf{J}_2^{-1} & \ldots & \mathbf{0}_{6\times6} \\ \vdots & \vdots & \ddots & \vdots \\ \mathbf{0}_{6\times6} & \mathbf{0}_{6\times6} & \ldots & \mathbf{J}_N^{-1} \\ -\mathbf{J}_{o_1^2}^{-1} & \mathbf{J}_{o_1^2}^{-1} & \ldots & \mathbf{0}_{6\times6} \\ \mathbf{0}_{6\times6} & -\mathbf{J}_{o_2^3}^{-1} & \ldots & \mathbf{0}_{6\times6} \\ \vdots & \vdots & \ddots & \vdots \\ \mathbf{J}_{o_N^1}^{-1} & \mathbf{0}_{6\times6} & \ldots & -\mathbf{J}_{o_N^1}^{-1} \end{bmatrix} \tag{6.4}$$

where each matrix $\mathbf{J}_i^{-1}$ is the inverse Jacobian of the ith leg, and each matrix $\mathbf{J}_{o_i^{i+1}}^{-1}$ is the inverse Jacobian for the internal serial chain connecting the terminal link of the ith leg with the terminal link of the $(i+1)$th leg, and where the $(N+1)$th leg is the first leg.

With $\mathbf{J}^{-1}$ expressed by Eqs. (6.3) and (6.4), $\mathbf{J}^{-1}$ is a $12N \times 12$ matrix, and $\mathbf{q}$ in Eq. (6.2) is a $12N \times 1$ vector. Matrix $\mathbf{J}_e^{-1}$ in Eq. (6.2) is obtained by removing those rows associated to zero stiffness joints in matrix $\mathbf{J}_n^{-1}$ that is part of $\mathbf{J}^{-1}$. Similar to a traditional PM, the stiffness matrix $\mathbf{K}_{q,e}$ is a block diagonal matrix, but where in this case the number of matrices is $2N$: N matrices for the legs and N matrices for the internal serial chains.

6.2.2. Mechanism III: Passive Planar 4-DoF PM2E.
The first PM2E that is analyzed is a planar underactuated mechanism. This mechanism is kept as simple as possible to minimize design uncertainties.

Mechanical Design of mechanism III
The designed planar mechanism is a PM2E consisting of four RPR legs with zero stiffness revolute joints and passive compliant prismatic joints constructed from linear springs. The internal closed loop chain is considered as two RRR end-effector serial chains. A schematic representation of mechanism III is shown in Fig. 6.1. Out-of-plane stiffness was not considered. The inverse kinematics of the mechanism are given in Appendix D. The stiffness k_i (N/m) and the zero length $q_{i,2_0}$ (m) of the linear spring in each leg were identified as

$$k_i = 221, \qquad q_{i,2_0} = 0.0715 \qquad \text{for } i = 1,2,3,4 \tag{6.5}$$

Due to the architecture of the mechanism, no moments can be transferred from the linear springs to the two end-effectors. Rotation of the two end-effectors is thus free and mechanism III can be thought of as a passively underactuated mechanism. Throughout the analysis the end-effectors are kept parallel to each other and to the inertial reference frame.

Although mechanism III is analyzed as a planar mechanism, it is constructed in three-dimensional space. Therefore, special care has been taken in the design to guarantee that all forces are acting in a plane in order to minimize deformations out of the plane. This is visualized in Fig. 6.2.
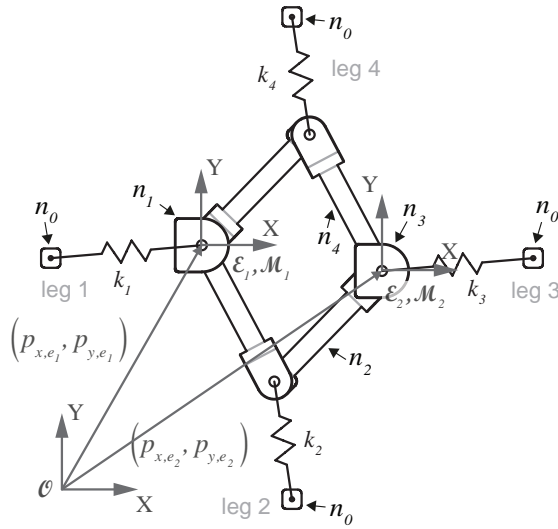
Figure 6.1: Mechanism III is a passive planar mechanism, where the interaction wrenches are the result of elongation/contraction of the linear springs, depending on the pose of the end-effector. The mechanism is here shown in pose III-b as introduced in Table 6.1, where the pose is determined by a position of reference frames $\mathscr{E}_1$ and $\mathscr{E}_2$ with respect to $\mathcal{O}$. The terminal link of leg i is indicated by n_i.

6
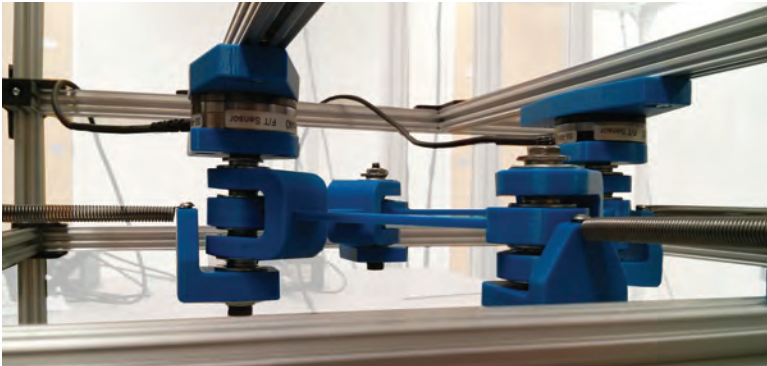
Figure 6.2: Mechanism III was designed such that the linear springs applied forces in the plane that also contains the links of the internal serial chains

JACOBIAN ANALYSIS OF MECHANISM III

The planar PM2E introduced in Fig. 6.1 has four legs and four internal serial chains. Therefore, following the approach described in Chapter 5, the matrix $\mathbf{J}_{III,n}^{-1}$ is

$$
\mathbf{J}_{III,n}^{-1} =
\begin{bmatrix}
\mathbf{J}_{III,1}^{-1} & \mathbf{0}_{6\times6} & \mathbf{0}_{6\times6} & \mathbf{0}_{6\times6} \\
\mathbf{0}_{6\times6} & \mathbf{J}_{III,2}^{-1} & \mathbf{0}_{6\times6} & \mathbf{0}_{6\times6} \\
\mathbf{0}_{6\times6} & \mathbf{0}_{6\times6} & \mathbf{J}_{III,3}^{-1} & \mathbf{0}_{6\times6} \\
\mathbf{0}_{6\times6} & \mathbf{0}_{6\times6} & \mathbf{0}_{6\times6} & \mathbf{J}_{III,4}^{-1} \\
-\mathbf{J}_{III,o_1^2}^{-1} & \mathbf{J}_{III,o_1^2}^{-1} & \mathbf{0}_{6\times6} & \mathbf{0}_{6\times6} \\
\mathbf{0}_{6\times6} & -\mathbf{J}_{III,o_2^3}^{-1} & \mathbf{J}_{III,o_2^3}^{-1} & \mathbf{0}_{6\times6} \\
\mathbf{0}_{6\times6} & \mathbf{0}_{6\times6} & -\mathbf{J}_{III,o_3^4}^{-1} & \mathbf{J}_{III,o_3^4}^{-1} \\
\mathbf{J}_{III,o_4^1}^{-1} & \mathbf{0}_{6\times6} & \mathbf{0}_{6\times6} & -\mathbf{J}_{III,o_4^1}^{-1}
\end{bmatrix}
\tag{6.6}
$$

where the individual matrices in Eq. (6.6) are developed in Appendix D.

The matrix $\mathbf{M}_t$ for mechanism III can also be developed using the approach described in Chapter 5. Because the end-effector serial chains span all DoFs of planar motion, matrix $\mathbf{M}_{III,t}$ is in this case defined by kinematic relations alone, i.e. no compliance ratios are required in its expression. The result is

$$
\mathbf{M}_{III,t} =
\begin{bmatrix}
\mathbf{I} & \mathbf{0} \\
\mathbf{I} - \mathbf{M}_{III,a,o_1^2} & \mathbf{M}_{III,a,o_1^2} \\
\mathbf{0} & \mathbf{I} \\
\mathbf{I} - \mathbf{M}_{III,a,o_1^4} & \mathbf{M}_{III,a,o_1^4}
\end{bmatrix}
\tag{6.7}
$$

where

$$
\begin{aligned}
\mathbf{M}_{III,a,o_1^2} =& \hat{\$}_{ta_{o_{1,1}}} \hat{\$}_{wa_{o_{1,1}}}^\top / (\hat{\$}_{wa_{o_{1,1}}}^\top \hat{\$}_{ta_{o_{1,1}}}) + \\
& \hat{\$}_{ta_{o_{1,2}}} \hat{\$}_{wa_{o_{1,2}}}^\top / (\hat{\$}_{wa_{o_{1,2}}}^\top \hat{\$}_{ta_{o_{1,2}}})
\end{aligned}
\tag{6.8}
$$

$$
\begin{aligned}
\mathbf{M}_{III,a,o_1^4} =& \hat{\$}_{ta_{o_{2,1}}} \hat{\$}_{wa_{o_{2,1}}}^\top / (\hat{\$}_{wa_{o_{2,1}}}^\top \hat{\$}_{ta_{o_{2,1}}}) + \\
& \hat{\$}_{ta_{o_{2,2}}} \hat{\$}_{wa_{o_{2,2}}}^\top / (\hat{\$}_{wa_{o_{2,2}}}^\top \hat{\$}_{ta_{o_{2,2}}})
\end{aligned}
\tag{6.9}
$$

in which $\hat{\$}_{ta_{o_{i,j}}}$ is the jth unit twist of permission of the ith end-effector serial chain and $\hat{\$}_{wa_{o_{i,j}}}$ its associated unit wrench of actuation, as defined in Appendix D. The first end-effector serial chain is that going from the first end-effector to the second end-effector via n_2.

Because the end-effector serial chains allow full planar motion, and the only compliance is in the linear springs, the Jacobian of elasticity for mechanism III can be obtained as

$$
\mathbf{J}_{III,e}^{-1} = \mathbf{J}_{III,n,e}^{-1} \mathbf{M}_{III,t}
\tag{6.10}
$$

where $\mathbf{M}_{III,t}$ was expressed by Eqs. (6.7)-(6.9) and

$$\mathbf{J}_{III,n,e}^{-1} = \begin{bmatrix} \mathbf{J}_{III,e,1}^{-1} & \mathbf{0}_{6\times6} & \mathbf{0}_{6\times6} & \mathbf{0}_{6\times6} \\ \mathbf{0}_{6\times6} & \mathbf{J}_{III,e,2}^{-1} & \mathbf{0}_{6\times6} & \mathbf{0}_{6\times6} \\ \mathbf{0}_{6\times6} & \mathbf{0}_{6\times6} & \mathbf{J}_{III,e,3}^{-1} & \mathbf{0}_{6\times6} \\ \mathbf{0}_{6\times6} & \mathbf{0}_{6\times6} & \mathbf{0}_{6\times6} & \mathbf{J}_{III,e,4}^{-1} \end{bmatrix} \tag{6.11}$$

in which

$$\mathbf{J}_{III,e,i}^{-1} = \hat{\$}_{wa_{i,2}}^{\top} / (\hat{\$}_{wa_{i,2}}^{\top} \hat{\$}_{ta_{i,2}}). \tag{6.12}$$

The required unit twists and unit wrenches are described in Appendix D.

STIFFNESS ANALYSIS FOR MECHANISM III

The only compliance of mechanism III is in the linear springs, which behave as described by Eq. (6.5). Then, the stiffness matrix in joint space is

$$\mathbf{K}_{III,q,e} = \mathrm{diag}\left([k_1 \quad k_2 \quad k_3 \quad k_4]\right) \tag{6.13}$$

In Eq. (6.2), the Jacobian $\mathbf{J}^{-1}$ can be replaced by Eq. (6.3), which is defined by Eqs. (6.6)-(6.7), $\mathbf{J}_e^{-1}$ by Eq. (6.10) and $\mathbf{K}_{q,e}$ by Eq. (6.13), so that Eq. (6.2) becomes

$$\mathbf{K}_{III}^{\mathcal{O}} = \left(-\frac{\partial \mathbf{J}_{III,e}^{-\top}}{\partial \mathbf{q}_{III}} \boldsymbol{\tau}_{III,e} \right) \mathbf{J}_{III}^{-1} + \mathbf{J}_{III,e}^{-\top} \mathbf{K}_{III,q,e} \mathbf{J}_{III,e}^{-1} \tag{6.14}$$

where $\mathbf{K}_{III}^{\mathcal{O}}$ is the stiffness matrix for mechanism III in which loading is considered, expressed in the inertial reference frame. Because the linear springs are the only joints that exert a force or torque, the vector $\boldsymbol{\tau}_{III,e}$ is obtained as

$$\boldsymbol{\tau}_{III,e} = \begin{bmatrix} -k_1\left(q_{1,2} - q_{1,2_0}\right) \\ -k_2\left(q_{2,2} - q_{2,2_0}\right) \\ -k_3\left(q_{3,2} - q_{3,2_0}\right) \\ -k_4\left(q_{4,2} - q_{4,2_0}\right) \end{bmatrix} \tag{6.15}$$

where k_i and $q_{i,2_0}$ were defined in Eq. (6.5). If the effect of loading is assumed negligible, the Jacobian-derivative term in Eq. (6.14) can be removed.

6.2.3. MECHANISM IV: PASSIVE SPATIAL 2-DOF PM2E.

To verify that the stiffness analysis of a more complex spatial mechanisms has an accuracy comparable to that found in Section 3.3, the stiffness of the 2-DoF PM2E introduced in Chapter 5 is analyzed. The mechanism is also shown schematically in Fig. 6.3.

MECHANICAL DESIGN OF MECHANISM IV

The elements of the mechanical design of Mechanism IV are the compliant joints, the links of the legs, and the links of the internal serial chains. The legs are the same as those introduced for mechanism II in Section 3.2.3, where their mechanical design was presented, as well as that of the compliant joints. The internal serial chains are all constructed from the same links, whose mechanical design was described in Section 5.5.
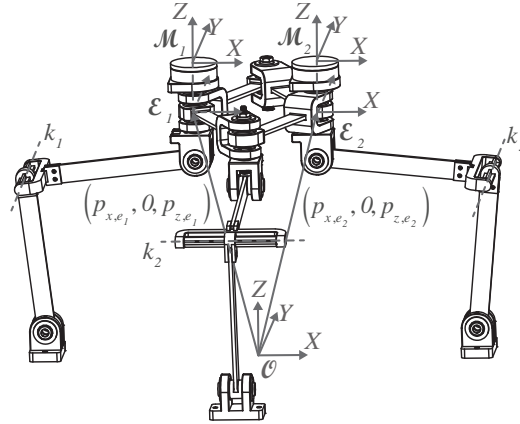
Figure 6.3: Mechanism IV is a passive spatial mechanism, where the interaction wrenches are the result of deformation of the compliant joints that make up the second joint of each leg. The mechanism is here shown in pose IV-a as introduced in Table 6.2, where the pose is determined by a position of reference frames $\mathcal{E}_1$ and $\mathcal{E}_2$ with respect to $\mathcal{O}$.

JACOBIAN ANALYSIS OF MECHANISM IV

The full inverse Jacobian matrix for mechanism IV was developed in Chapter 5 and is here complimented with the Jacobian of Elasticity. As described in Chapter 5, the first and the third leg are RRR serial chains, while the second leg is an RRRR serial chain. In all three legs only the second kinematic joints is not a zero stiffness joint. What separates the three legs is that the RRR legs have three constraints, while the RRRR leg has two constraints, so that the inverse Jacobian of Elasticity for each leg is

$$
\mathbf{J}_{IV,e,i}^{-1} = \begin{cases}
\begin{bmatrix}
\hat{\$}_{wa_{i,2}}^\top / (\hat{\$}_{wa_{i,2}}^\top \hat{\$}_{ta_{i,2}}) \\
\hat{\$}_{wc_{i,1}}^\top / (\hat{\$}_{wc_{i,1}}^\top \hat{\$}_{tc_{i,1}}) \\
\hat{\$}_{wc_{i,2}}^\top / (\hat{\$}_{wc_{i,2}}^\top \hat{\$}_{tc_{i,2}}) \\
\hat{\$}_{wc_{i,3}}^\top / (\hat{\$}_{wc_{i,3}}^\top \hat{\$}_{tc_{i,3}})
\end{bmatrix} & \text{for } i = 1,3 \\[4em]
\begin{bmatrix}
\hat{\$}_{wa_{i,2}}^\top / (\hat{\$}_{wa_{i,2}}^\top \hat{\$}_{ta_{i,2}}) \\
\hat{\$}_{wc_{i,1}}^\top / (\hat{\$}_{wc_{i,1}}^\top \hat{\$}_{tc_{i,1}}) \\
\hat{\$}_{wc_{i,2}}^\top / (\hat{\$}_{wc_{i,2}}^\top \hat{\$}_{tc_{i,2}})
\end{bmatrix} & \text{for } i = 2
\end{cases}
\tag{6.16}
$$

where the unit twists and unit wrenches are introduced in Appendix E.

The internal serial chains do not contain any actuated or compliant joints, so the Jacobian of elasticity only concerns the mapping of wrenches onto virtual joint displacements. More specifically, it concerns the mapping onto the multiple constrained joint displacements, because the simply constrained displacements are always zero as was

concluded in Section 5.4.1. Therefore,

$$\mathbf{J}_{IV,e,o_i^{i+1}}^{-1} = \begin{bmatrix} \hat{\$}_{wc_{o_{1,1}}}^{\top} / (\hat{\$}_{wc_{o_{1,1}}}^{\top} \hat{\$}_{tc_{o_{1,1}}}) \\ \hat{\$}_{wc_{o_{1,2}}}^{\top} / (\hat{\$}_{wc_{o_{1,2}}}^{\top} \hat{\$}_{tc_{o_{1,2}}}) \\ \hat{\$}_{wc_{o_{1,3}}}^{\top} / (\hat{\$}_{wc_{o_{1,3}}}^{\top} \hat{\$}_{tc_{o_{1,3}}}) \end{bmatrix} \text{ for } i = 1, 2 \tag{6.17}$$

while

$$\mathbf{J}_{IV,e,o_3^1}^{-1} = \begin{bmatrix} \hat{\$}_{wc_{o_{2,1}}}^{\top} / (\hat{\$}_{wc_{o_{2,1}}}^{\top} \hat{\$}_{tc_{o_{2,1}}}) \\ \hat{\$}_{wc_{o_{2,2}}}^{\top} / (\hat{\$}_{wc_{o_{2,2}}}^{\top} \hat{\$}_{tc_{o_{2,2}}}) \\ \hat{\$}_{wc_{o_{2,3}}}^{\top} / (\hat{\$}_{wc_{o_{2,3}}}^{\top} \hat{\$}_{tc_{o_{2,3}}}) \end{bmatrix} . \tag{6.18}$$

Then, the overall inverse Jacobian of elasticity is expressed as

$$\mathbf{J}_{IV,e}^{-1} = \mathbf{J}_{IV,n,e}^{-1} \mathbf{M}_{IV,t} \tag{6.19}$$

where $\mathbf{M}_{IV,t}$ was expressed in Eq. (5.50) and $\mathbf{J}_{IV,n,e}^{-1}$ is constructed from the partial inverse Jacobians of elasticity defined by Eqs. (6.16)-(6.18) as

$$\mathbf{J}_{IV,n,e}^{-1} = \begin{bmatrix} \mathbf{J}_{IV,e,1}^{-1} & \mathbf{0}_{4\times6} & \mathbf{0}_{4\times6} \\ \mathbf{0}_{3\times6} & \mathbf{J}_{IV,e,2}^{-1} & \mathbf{0}_{3\times6} \\ \mathbf{0}_{4\times6} & \mathbf{0}_{4\times6} & \mathbf{J}_{IV,e,3}^{-1} \\ -\mathbf{J}_{IV,e,o_1^2}^{-1} & \mathbf{J}_{IV,e,o_1^2}^{-1} & \mathbf{0}_{3\times6} \\ \mathbf{0}_{3\times6} & -\mathbf{J}_{IV,e,o_2^3}^{-1} & \mathbf{J}_{IV,e,o_2^3}^{-1} \\ \mathbf{J}_{IV,e,o_3^1}^{-1} & \mathbf{0}_{3\times6} & -\mathbf{J}_{IV,e,o_3^1}^{-1} \end{bmatrix} \tag{6.20}$$

STIFFNESS ANALYSIS OF MECHANISM IV

The stiffness analysis of mechanism IV expressed in the inertial reference frame is

$$\mathbf{K}_{IV}^{\mathscr{O}} = \left(-\frac{\partial \mathbf{J}_{IV,e}^{-\top}}{\partial \mathbf{q}_{IV}} \boldsymbol{\tau}_{IV,e} \right) \mathbf{J}_{IV}^{-1} + \mathbf{J}_{IV,e}^{-\top} \mathbf{K}_{IV,q,e} \mathbf{J}_{IV,e}^{-1} \tag{6.21}$$

where $\mathbf{J}_{IV}^{-1}$ was developed in Section 5.5, $\mathbf{J}_{IV,e}^{-1}$ is expressed by Eqs. (6.19)-(6.20) and where the expression for $\boldsymbol{\tau}_{IV,e}$ is equivalent to Eq. (6.15), but with k_i and $q_{i,2_0}$ now expressed as in Eqs. (5.67) and (5.68). The matrix $\mathbf{K}_{IV,q,e}$ in (6.21) is

$$\mathbf{K}_{IV,q,e} = \text{diag}\left(\mathbf{K}_{IV,q,e,1} \quad \mathbf{K}_{IV,q,e,2} \quad \mathbf{K}_{IV,q,e,3} \quad \mathbf{K}_{IV,q,e,o_1^2} \quad \mathbf{K}_{IV,q,e,o_2^3} \quad \mathbf{K}_{IV,q,e,o_3^1} \right) \tag{6.22}$$

where each matrix $\mathbf{K}_{IV,q,e,i}$ corresponds to the matrix $\mathbf{K}_{IV,q,e,ld+sc,i}$ in Section 3.2.3, while $\mathbf{K}_{IV,q,e,o_1^2}$ and $\mathbf{K}_{IV,q,e,o_2^3}$ are the inverse of respectively $\mathbf{K}_{q_{cm,o_1^2}}^{-1}$ and $\mathbf{K}_{q_{cm,o_2^3}}^{-1}$ introduced in Section 5.5. Equivalent to the latter matrices, $\mathbf{K}_{IV,q,e,o_3^1}^{-1}$ can be developed as

$$\mathbf{K}_{IV,q,e,o_3^1}^{-1} = \mathbf{J}_{IV,e,o_3^1}^{-1} \left(\sum_{i=1}^{2} \mathbf{Ad}_{\mathbf{H}_{l_{o_{2,i}}}^{\mathscr{O}}} \mathbf{K}_{s,l_{o_{2,i}}}^{-1} \mathbf{Ad}_{\mathbf{H}_{l_{o_{2,i}}}^{\mathscr{O}}}^{\top} \right) \mathbf{J}_{IV,e,o_3^1}^{-\top} \tag{6.23}$$

where the matrix $\mathbf{K}^{-1}_{s,l_{o_{2,i}}}$ is the compliance matrix of the ith link in the second end-effector serial chain, which is the same as $\mathbf{K}^{-1}_{s,l_{o_{1,i}}}$ introduced in Eq. (5.60), and $\mathbf{Ad}_{\mathbf{H}^{\mathscr{O}}_{l_{o_{1,2}}}}$ is the Adjoint matrix which transforms a vector expressed in the reference frame connected to the end of the ith link of the second end-effector serial chain into its equivalent vector expressed in the inertial Cartesian reference frame.

6.3. METHOD TO VERIFY STIFFNESS ANALYSES

T O verify that the resulting stiffness analyses of the PM2Es analyzed in Section 6.2 have similar accuracy as those presented in Chapter 3, the same measurement system is used as in that chapter. This measurement system is described briefly, not to repeat the work done in Chapter 3. Also, to further assess the measurement accuracy, differential wrench calculations are introduced in this chapter.

6.3.1. MEASUREMENT SYSTEM.

Changes in reaction wrenches $d\$_w$ predicted by the stiffness analyses will be compared to differential wrench measurements $\Delta\$_w$ for a set of displacements at different poses. Imposed displacements are assumed sufficiently small so that $\Delta\$_w \approx d\$_w$ for each wrench. To obtain the measurements, an inertial reference frame was used in which both the position of the leg base points as well as the end-effector poses can be controlled. The difference with Chapter 3 is that in this research two end-effectors are involved. As such, two end-effector poses are controlled, while also two reaction wrenches are recorded, as was also done in Chapter 5 for a different purpose. For mechanism III, the measurement setup is shown in Fig. 6.2, while pictures of mechanism IV in the inertial reference frame can be found in Fig. 5.5.

Because the same measurement system is used, the same positioning accuracy is achieved as in Chapter 3, namely

$$\epsilon_{\Delta\theta} = 1/80 \text{ rad}, \quad \epsilon_{\Delta p} = 1/2000 \text{ m} \tag{6.24}$$

Also, because in this research two versions of the same wrench sensor are used as in Chapter 3, also the same moment and force resolutions are achieved, which are

$$\epsilon_m = 1/4000 \text{ Nm}, \quad \epsilon_f = 1/100 \text{ N} \tag{6.25}$$

MEASUREMENT PLAN FOR MECHANISM III.
Mechanism III was analyzed at the five poses presented in Table 6.1, for four linear displacements. Rotational displacements were not considered, because the end-effectors of mechanism III are free to rotate. Indicating the first end-effector with EE1, and the second end-effector with EE2, the four linear displacements were:

1. a 5 mm displacement of EE1 along the X-axis,

2. a 5 mm displacement of EE2 along the X-axis,

3. a 5 mm displacement of EE1 along the Y-axis, and

4. a 5 mm displacement of EE2 along the Y-axis.

Table 6.1: Poses at which displacements were imposed on mechanism III to measure the resulting change in reaction wrench

Pose	p_{x,e_1} (m)	p_{y,e_1} (m)	p_{x,e_2} (m)	p_{y,e_2} (m)
III-a	0.1000	0.1800	0.2600	0.1800
III-b	0.1100	0.1900	0.2500	0.1700
III-c	0.1100	0.1700	0.2700	0.1600
III-d	0.0900	0.2000	0.2500	0.1800
III-e	0.0900	0.1700	0.2700	0.1900

Table 6.2: Poses at which displacements were imposed on mechanism IV to measure the resulting change in reaction wrench

Pose	p_{x,e_1} (m)	p_{z,e_1} (m)	p_{x,e_2} (m)	p_{z,e_2} (m)
IV-a	-0.0525	0.2165	0.0525	0.2165
IV-b	-0.0700	0.2165	0.0700	0.2165
IV-c	-0.0650	0.2000	0.0650	0.2000
IV-d	-0.0550	0.2050	0.0550	0.2050
IV-e	-0.0550	0.1900	0.0550	0.1900
IV-f	-0.0600	0.2200	0.0600	0.2200

MEASUREMENT PLAN FOR MECHANISM IV.

Mechanism IV was analyzed in six different poses, namely those listed in Table 6.2. In those poses the following nine displacements were imposed:

1. a 5 mm displacement of EE1 along the negative X-axis together with a 5 mm displacement of EE2 along the positive X-axis,

2. a 5 mm displacement of EE1 and EE2 along the Z-axis,

3. a 5 mm displacement of EE2 along the X-axis,

4. a 5 mm displacement of EE1 and EE2 along the X-axis,

5. a 5 mm displacement of EE2 along the Y-axis,

6. a 5 mm displacement of EE1 and EE2 along the Y-axis,

7. a 5 mm displacement of EE2 along the Z-axis,

8. a 1/8 rad rotation of EE2 around its Z-axis, and

9. a 1/8 rad rotation of EE1 and EE2 around the Z-axis that is positioned exactly in the middle of the two end-effectors, see Fig. 6.4.
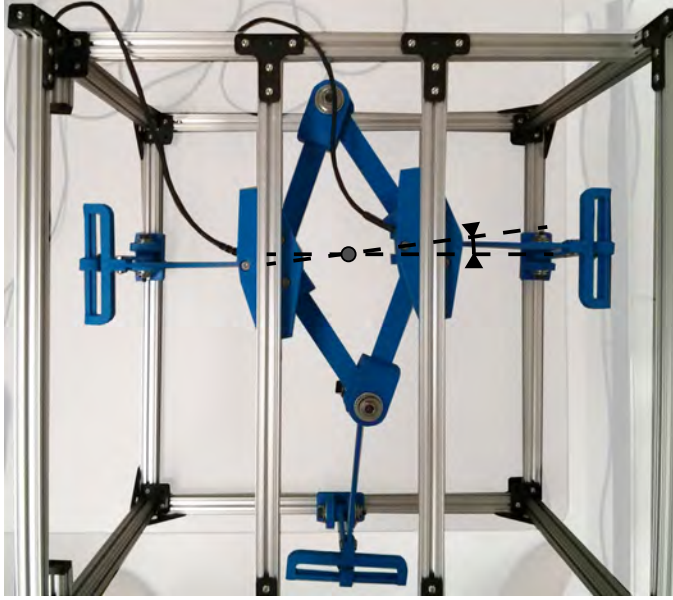
Figure 6.4: The ninth imposed displacement was a rotation of both end-effectors around an axis positioned exactly in between the two end-effectors and aligned with the Z-axis.

6.3.2. TRANSFORMATION OF STIFFNESS MATRICES.

The predicted change in differential wrenches were expressed by Eqs. (6.14) and (6.21). In order to compare the measured differential wrenches with the differential wrenches predicted by the stiffness analyses, they should all be expressed in the same reference frames. In this chapter all wrenches will be expressed in the respective measurement reference frames, which are the reference frames connected to the wrench sensors at the poses before displacements. The measurement reference frames for the two mechanisms are indicated by $\mathcal{M}_1$ and $\mathcal{M}_2$ in Figs. 6.1 and 6.3. Note that for mechanism III the measurement reference frames coincide with the end-effector reference frames.

To transform the stiffness matrices into the measurement reference frames, the following transformation is implemented,

$$\mathbf{K} = \begin{bmatrix} \mathbf{Ad}_{\mathbf{H}^{\mathcal{O}}_{\mathcal{M}_1}}^{\top} & \mathbf{0} \\ \mathbf{0} & \mathbf{Ad}_{\mathbf{H}^{\mathcal{O}}_{\mathcal{M}_2}}^{\top} \end{bmatrix} \mathbf{K}^{\mathcal{O}} \begin{bmatrix} \mathbf{Ad}_{\mathbf{H}^{\mathcal{O}}_{\mathcal{M}_1}} & \mathbf{0} \\ \mathbf{0} & \mathbf{Ad}_{\mathbf{H}^{\mathcal{O}}_{\mathcal{M}_2}} \end{bmatrix} \tag{6.26}$$

where $\mathbf{K}$ is a stiffness matrix expressed in the measurement reference frames, and where $\mathbf{Ad}_{\mathbf{H}^{\mathcal{O}}_{\mathcal{M}_1}}$ and $\mathbf{Ad}_{\mathbf{H}^{\mathcal{O}}_{\mathcal{M}_2}}$ are the adjoint matrices related to the following homogeneous matrices:

$$\mathbf{H}^{\mathcal{O}}_{\mathcal{M}_1} = \begin{bmatrix} \mathbf{I}_3 & \mathbf{p}_{e_1} \\ \mathbf{0}_{1 \times 3} & 1 \end{bmatrix} \tag{6.27}$$

$$\mathbf{H}^{\mathcal{O}}_{\mathcal{M}_2} = \begin{bmatrix} \mathbf{I}_3 & \mathbf{p}_{e_2} \\ \mathbf{0}_{1 \times 3} & 1 \end{bmatrix} \tag{6.28}$$

with

$$\mathbf{p}_{e_1} = \begin{bmatrix} p_{x,e_1} & p_{y,e_1} & p_{z,e_1} + h_s \end{bmatrix}^\top$$
$$\mathbf{p}_{e_2} = \begin{bmatrix} p_{x,e_2} & p_{y,e_2} & p_{z,e_2} + h_s \end{bmatrix}^\top$$

where p_{x,e_1}, p_{y,e_1}, p_{z,e_1}, p_{x,e_2}, p_{y,e_2}, and p_{z,e_2} express the positions of the two end-effectors as described by either Table 6.1 or Table 6.2, while h_s is the distance between the end-effector reference frame origins and the measurement reference frame origins, as shown in Fig. 6.3. For mechanism III $h_s = 0$ while for mechanism IV $h_s = 42.6$ mm.

6.3.3. Comparison with Differential Wrench Calculations.

To provide additional insight in the accuracy of displacements along the DoFs, differential wrench calculations are performed for those displacements. This is achieved using

$$\begin{bmatrix} \Delta\$_{w,e_1,calc} \\ \Delta\$_{w,e_2,calc} \end{bmatrix} = \begin{bmatrix} \mathbf{Ad}^\top_{H^{\mathcal{O}}_{\mathcal{M}_1}} & \mathbf{0} \\ \mathbf{0} & \mathbf{Ad}^\top_{M^{\mathcal{O}}_{\mathcal{M}_2}} \end{bmatrix} \left(\mathbf{J}^{-\top}_e \tau_e \big|_+ - \mathbf{J}^{-\top}_e \tau_e \big|_- \right) \tag{6.29}$$

where $\mathbf{J}^{-\top}_e \tau_e \big|_-$ is the set of wrenches applied to the end-effectors at the considered reference pose, $\mathbf{J}^{-\top}_e \tau_e \big|_+$ is the set of wrenches at the pose after displacement, both expressed in the inertial reference frame, while $\Delta\$_{w,e_1,calc}$ and $\Delta\$_{w,e_2,calc}$ are the equivalent wrenches expressed in the measurement reference frames. The homogeneous matrices related to the adjoint matrices in (6.29) were introduced in Eqs. (6.27) and (6.28).

6.3.4. Postprocessing of Measurement Data.

To draw conclusions on the accuracy of the predicted and calculated differential wrenches, some postprocessing of the measured wrenches was required. First, all wrenches were expressed in the same reference frames, followed by filtering and normalization.

Transformation of Measured Wrenches.

In order to be able to calculate the difference between the wrenches measured before and after displacement, they need to be expressed in the same reference frames. In this chapter all wrenches are expressed in the measurement reference frames at the poses before displacements, namely $\mathcal{M}_1$ and $\mathcal{M}_2$ as shown in Figs. 6.1 and 6.3. Then,

$$\begin{bmatrix} \Delta\$_{w,e_1,meas} \\ \Delta\$_{w,e_2,meas} \end{bmatrix} = \begin{bmatrix} \mathbf{Ad}^\top_{\mathbf{H}^{\mathcal{N}_1}_{\mathcal{M}_1}} & \mathbf{0} \\ \mathbf{0} & \mathbf{Ad}^\top_{\mathbf{H}^{\mathcal{N}_2}_{\mathcal{M}_2}} \end{bmatrix} \begin{bmatrix} \$^{\mathcal{N}_1}_{w,e_1,meas} \\ \$^{\mathcal{N}_2}_{w,e_2,meas} \end{bmatrix} - \begin{bmatrix} \$^{\mathcal{M}_1}_{w,e_1,meas} \\ \$^{\mathcal{M}_2}_{w,e_2,meas} \end{bmatrix} \tag{6.30}$$

which is similar to transformations performed in Section 3.2.5, but where here

$$\mathbf{H}_{\mathcal{M}_1}^{\mathcal{N}_1} = \begin{bmatrix} \cos\Delta\theta_{e_1} & \sin\Delta\theta_{e_1} & 0 & -\cos(\Delta\theta_{e_1})\Delta p_{x,e_1} - \sin(\Delta\theta_{e_1})\Delta p_{y,e_1} \\ -\sin\Delta\theta_{e_1} & \cos\Delta\theta_{e_1} & 0 & \sin\Delta\theta_{e_1}\Delta p_{x,e_1} - \cos(\Delta\theta_{e_1})\Delta p_{y,e_1} \\ 0 & 0 & 1 & -\Delta p_{z,e_1} \\ 0 & 0 & 0 & 1 \end{bmatrix}$$

$$\mathbf{H}_{\mathcal{M}_2}^{\mathcal{N}_2} = \begin{bmatrix} \cos\Delta\theta_{e_2} & \sin\Delta\theta_{e_2} & 0 & -\cos(\Delta\theta_{e_2})\Delta p_{x,e_2} - \sin(\Delta\theta_{e_2})\Delta p_{y,e_2} \\ -\sin\Delta\theta_{e_2} & \cos\Delta\theta_{e_2} & 0 & \sin(\Delta\theta_{e_2})\Delta p_{x,e_2} - \cos(\Delta\theta_{e_2})\Delta p_{y,e_2} \\ 0 & 0 & 1 & -\Delta p_{z,e_2} \\ 0 & 0 & 0 & 1 \end{bmatrix}$$

express the homogeneous matrices that transform measured wrenches in the measurement reference frames after displacement, $\mathcal{N}_1$ and $\mathcal{N}_2$, into to the measurement reference frames before displacements, $\mathcal{M}_1$ and $\mathcal{M}_2$. In those homogeneous matrices $\Delta\theta_{e_1}$, $\Delta p_{x,e_1}$, $\Delta p_{y,e_1}$, $\Delta p_{z,e_1}$, $\Delta\theta_{e_2}$, $\Delta p_{x,e_2}$, $\Delta p_{y,e_2}$, and $\Delta p_{z,e_2}$ depend on the imposed displacements as described in Section 6.3.1.

FILTERING AND NORMALIZATION OF WRENCH ELEMENTS.
Similar to Section 3.2.5, all elements below the measurement threshold in each vector $\Delta\$_{w,e_1,meas}$ and $\Delta\$_{w,e_2,meas}$ are removed. The moment- and force thresholds were described as

$$\Delta m_{thres} = k_{\phi,min}\epsilon_{\Delta\phi} + 2\epsilon_m \tag{6.31}$$

$$\Delta f_{thres} = k_{p,min}\epsilon_{\Delta p} + 2\epsilon_f \tag{6.32}$$

where $k_{\phi,min}$ and $k_{p,min}$ are the minimum angular and linear values found on the diagonals of the stiffness matrices evaluated at all poses introduced in Tables 6.1 and 6.2 respectively. The values for the angular and linear positioning resolution, $\epsilon_{\Delta\phi}$ and $\epsilon_{\Delta p}$, were introduced in Eq. (6.24). The moment and force measurement resolution values, ϵ_m and ϵ_f, were introduced in Eq. (6.25) and are multiplied by two because $\Delta\$_{w,e_1,meas}$ and $\Delta\$_{w,e_2,meas}$ each reflect the difference between two wrench measurements. The vectors $\Delta\$_{w,e_1,meas}$ and $\Delta\$_{w,e_2,meas}$ in which all elements below the respective thresholds have been removed are labeled $\Delta\$^*_{w,e_1,meas}$ and $\Delta\$^*_{w,e_2,meas}$. The same elements can also be removed from the various predicted and differentially calculated wrenches. Additionally, because in the planar mechanism III no moments can be transferred to the end-effectors, they are ignored in the results.

The difference between each $\Delta\$^*_{w,e_1,meas}$ and the related $\Delta\$^*_{w,e_1,pred}$ or $\Delta\$^*_{w,e_1,calc}$ gives the filtered differential wrench error for the first end-effector for either the stiffness analysis or the differential calculation. Similar to Section 3.2.5, normalization was performed with respect to $\Delta\$^*_{w,e_1,meas}$, namely

$$\boldsymbol{\epsilon}_{\Delta\$^*_{w,e_1,pred}} = \left(\Delta\$^*_{w,e_1,pred} - \Delta\$^*_{w,e_1,meas}\right)^\top \left[\mathrm{diag}\left(\Delta\$^*_{w,e_1,meas}\right)\right]^{-1} \tag{6.33}$$

where $\boldsymbol{\epsilon}_{\Delta\$^*_{w,e_1,pred}}$ is a non-dimensional vector. The same filtering and normalization can also be performed for the second end-effector as well as for each differentially calculated wrench.

Table 6.3: The coefficients of determination for the various linear regression lines through the values obtained using the stiffness analyses without or with consideration of the effect of loading ($\mathbf{K}_{ul}$ and $\mathbf{K}_{ld}$ respectively) as well as for the linear regression lines through the differential wrench calculations, $\Delta\mathbf{\$}_{w,calc}$

mechanism (f or m values)	$\mathbf{K}_{ul}$	$\mathbf{K}_{ld}$	$\Delta\mathbf{\$}_{w,calc}$
I (f)	0.77	0.97	0.98
II (m, DoFs)	-	0.77	0.80
II (m, cons)	-	0.86	-
II (f, DoFs)	-	0.94	0.94
II (f, cons)	-	0.79	-

6.4. VERIFICATION RESULTS

IN this section example stiffness matrices will be presented, as well as the processed measurement data. Ideally, the measured delta wrenches are exactly equal to the predicted delta wrench values. To visualize the coupling between the measured delta wrench values and the predicted delta wrench values, they are set out against each other in Figs. 6.5 and 6.7. The same is done for the differential wrench calculations. To quantify this coupling, the coefficient of determination is determined for each set of predicted or differentially calculated values in relation to the measured values. The coefficient of determination R^2 expresses the percentage of variability around a linear regression line that has been accounted for by the predictions based on either the stiffness analysis or the differential wrench calculations.

In order to assess the accuracy of stiffness analyses, box plots of the normalized errors are presented. A box plot summarizes a data set using a median (the central mark) and its confidence interval (the notch), while the outer edges of each box indicate the 25th and 75th percentiles. To test whether the medians of different sets of normalized errors are significantly different, Wilcoxon rank-sum tests are performed. A Wilcoxon rank-sum test determines the probability that two sets are sampled from two continuous distributions with equal medians. The medians of two sets are considered significantly different if the probability that they are equal is $< 5\%$.

6.4.1. RESULTS FOR MECHANISM III
Evaluation of the stiffness matrix of mechanism III in pose III-a gives

$$\mathbf{K}_{III,ld}\big|_a = \begin{bmatrix} 1\,\text{Nm} & 0\,\text{N} & 5\,\text{N} & 0\,\text{Nm} & 0\,\text{N} & -5\,\text{N} \\ 0\,\text{N} & 366\,\text{N/m} & 0\,\text{N/m} & 0\,\text{N} & -85\,\text{N/m} & 0\,\text{N/m} \\ 5\,\text{N} & 0\,\text{N/m} & 255\,\text{N/m} & 0\,\text{N} & 0\,\text{N/m} & 40\,\text{N/m} \\ 0\,\text{Nm} & 0\,\text{N} & 0\,\text{N} & 0\,\text{Nm} & 0\,\text{N} & 0\,\text{N} \\ 0\,\text{N} & -85\,\text{N/m} & 0\,\text{N/m} & 0\,\text{N} & 366\,\text{N/m} & 0\,\text{N/m} \\ -5\,\text{N} & 0\,\text{N/m} & 40\,\text{N/m} & 0\,\text{N} & 0\,\text{N/m} & 255\,\text{N/m} \end{bmatrix} \tag{6.34}$$

Evaluation of the stiffness matrix at the same pose but without considering the effect of
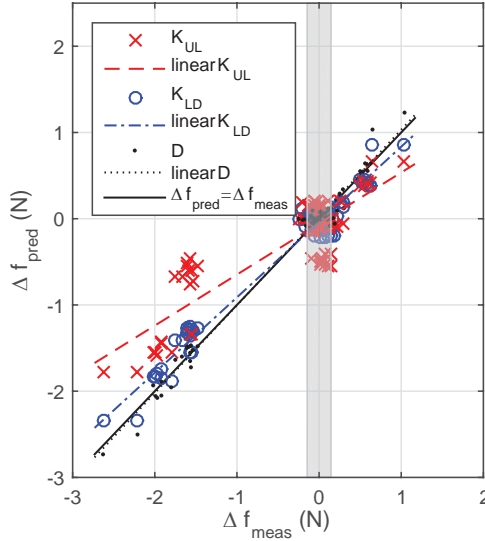
Figure 6.5: The correlation between the forces measured on mechanism III and the forces that were predicted using a stiffness analysis with the assumption of an unloaded mechanism (UL), a stiffness anlaysis where loading is taken into account (LD), or with differential wrench calculations (D). The grey patch indicates the range of measurements below the measurement threshold.

loading gives

$$
\mathbf{K}_{III,ul}\big|_a =
\begin{bmatrix}
0\,\text{Nm} & 0\,\text{N} & 0\,\text{N} & 0\,\text{Nm} & 0\,\text{N} & 0\,\text{N} \\
0\,\text{N} & 309\,\text{N/m} & 0\,\text{N/m} & 0\,\text{N} & -88\,\text{N/m} & 0\,\text{N/m} \\
0\,\text{N} & 0\,\text{N/m} & 111\,\text{N/m} & 0\,\text{N} & 0\,\text{N/m} & 111\,\text{N/m} \\
0\,\text{Nm} & 0\,\text{N} & 0\,\text{N} & 0\,\text{Nm} & 0\,\text{N} & 0\,\text{N} \\
0\,\text{N} & -88\,\text{N/m} & 0\,\text{N/m} & 0\,\text{N} & 309\,\text{N/m} & 0\,\text{N/m} \\
0\,\text{N} & 0\,\text{N/m} & 111\,\text{N/m} & 0\,\text{N} & 0\,\text{N/m} & 111\,\text{N/m}
\end{bmatrix}
\tag{6.35}
$$

In Fig. 6.5 the changes in force that are predicted by a stiffness analysis with and without considering the effect of loading are set out against the measured changes in force. Also, the differential wrench calculations are included. A linear regression line is fitted through each data set, while the spread around the linear regression line is expressed by the R^2 values in Table 6.3. The values show that the stiffness analysis which takes loading into account explains an almost equal amount of variance as the differential wrench calculations. A close fit between the data and a linear regression is a sign that the measured values and the predicted values are tightly coupled. However, as can also be observed from Fig. 6.5, the linear regression lines related to the delta force values predicted by the stiffness analyses do have lower slopes than the line $\Delta f_{pred} = \Delta f_{meas}$, which hints at an underestimation of the interaction forces.

To determine whether the underestimation of interaction forces is significant, the residual normalized errors are calculated for both stiffness analyses as well as for the
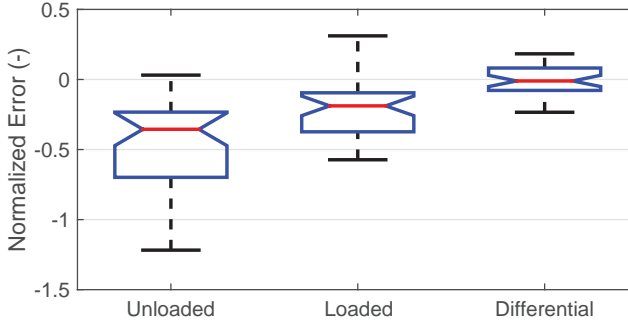
Figure 6.6: Box plots of the normalized errors for the stiffness analyses of mechanism III with and without considering the effect of loading, as well as the differential wrench calculations

differential wrench calculations. For that, the measurements below the measurement threshold are filtered out. For mechanism III in the poses presented in Table 6.1 it was found that $k_{p,min} = 2.5 \cdot 10^2$. Then, Eq. (6.25) results in

$$\Delta f_{thres} = 0.145$$

As a result of filtering with the above thresholds, 41 of initial 80 measurement sets were removed from further analysis. The raw data can be obtained from Ref. [16]. For the filtered data sets, the residual errors are visualized in Fig. 6.6. It can be seen from the notches that the median of the normalized errors obtained from differential calculations is not significantly different from zero. The median of the normalized errors for the loaded stiffness analysis is −19%, while that of the unloaded stiffness analysis is −36%. A Wilcoxon rank-sum test demonstrates the null hypothesis in which the two sets have equal medians can be rejected at the 5% significance level. Fifty percent of the normalized error values for the loaded stiffness analysis lie between −10% and −37%.

6.4.2. RESULTS FOR MECHANISM IV

Mechanism IV represents a more general PM2E, on which constraints and overconstraints are imposed by both the legs and the internal serial chains. For this mechanism it is therefore interesting to separate the analysis of the DoFs and the constrained directions. In Fig. 6.7 the changes in moments and forces as predicted by the stiffness analysis are plotted against the measured changes. The values obtained from differential wrench calculations are included too. A linear regression line is fitted through each data set, while the spread around these linear regression lines is expressed by the R^2 values in Table 6.3. The values show that for those displacements aligned with the DoFs of the mechanism, the amount of variance from the linear regression lines explained by the stiffness analysis is 77% and 94% for the moments and forces respectively, which is almost equal to the variance explained by the differential wrench calculations.

It can be seen from Fig. 6.7a that, on average, the stiffness analysis overestimates the moment changes for the displacements along constrained directions, while Fig. 6.7b
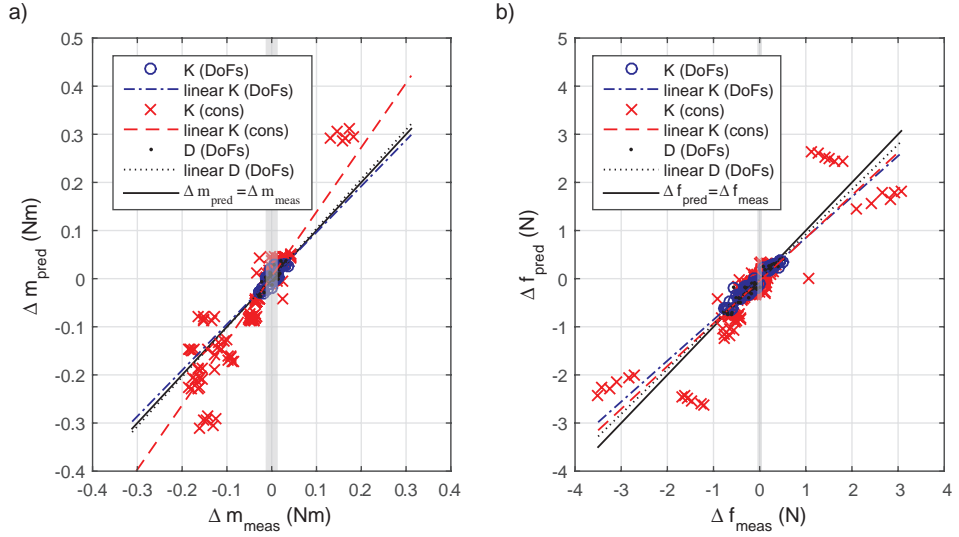
a)

b)

Figure 6.7: The correlation between a) the moments and b) forces measured on mechanism IV and the moments and forces that were predicted using either the stiffness model (K) or differential wrench calculations (D). The data points obtained using D only cover displacements 1 and 2. The grey patch indicates the range of measurements below the measurement threshold.

shows that the force changes for the displacements along the DoFs are slightly underestimated. The normalized errors are calculated to further assess the impact of these over- and underestimations. For that, first the measurements below the measurement threshold are filtered out. For mechanism IV in the poses presented in Table 6.2 it was found that $k_{\phi,min} = 1.04$ and $k_{p,min} = 60$. Then, Eqs. (6.31) and (6.32) result in

$$\Delta m_{thres} = 0.0135$$
$$\Delta f_{thres} = 0.050$$

As a result of filtering with the above thresholds, 204 of initial 648 vector elements were excluded from further analysis. The raw data can be obtained from Ref. [16].

For the filtered data sets, the residual errors are visualized in Fig. 6.8. It can be observed that the median of the normalized errors for the stiffness analysis is close to zero, namely −7%, while 50% of the values lie between −18% and +10% error. This spread is comparable to the differential wrench calculations. The median of the normalized errors calculated for the displacements along the constrained directions is significantly worse, namely 17%, while 50% of the values lie between −48% and +66% error.

The stiffness matrix of a PM2E maps the displacement twists of the two end-effectors on the two elastic reaction wrenches. As such, it is a 12 × 12 matrix. As an example, the stiffness matrix of mechanism IV is evaluated at pose IV-a, resulting in the matrix introduced in Eq. (6.36). The two displacement twists on which this matrix acts and the resulting interaction wrenches are defined in the two measurement reference frames, as expressed in Eq. (6.26).

$$
\mathbf{K}_{IV}\big|_a =
\begin{bmatrix}
5\ \text{Nm} & -1\ \text{Nm} & -1\ \text{Nm} & 0\ \text{N} & 18\ \text{N} & -2\ \text{N} & -2\ \text{Nm} & 1\ \text{Nm} & 0\ \text{Nm} & -1\ \text{N} & -1\ \text{N} & 1\ \text{N} \\
-1\ \text{Nm} & 5\ \text{Nm} & 0\ \text{Nm} & -7\ \text{N} & 4\ \text{N} & -21\ \text{N} & 1\ \text{Nm} & -3\ \text{Nm} & 0\ \text{Nm} & -2\ \text{N} & -3\ \text{N} & 16\ \text{N} \\
-1\ \text{Nm} & 0\ \text{Nm} & 1\ \text{Nm} & 0\ \text{N} & -8\ \text{N} & 0\ \text{N} & 0\ \text{Nm} & 0\ \text{Nm} & 0\ \text{Nm} & 0\ \text{N} & 0\ \text{N} & 0\ \text{N} \\
0\ \text{N} & -7\ \text{N} & 0\ \text{N} & 83\ \text{N/m} & -32\ \text{N/m} & 63\ \text{N/m} & 1\ \text{N} & -2\ \text{N} & 0\ \text{N} & 8\ \text{N/m} & 16\ \text{N/m} & -6\ \text{N/m} \\
18\ \text{N} & 4\ \text{N} & -8\ \text{N} & -32\ \text{N/m} & 179\ \text{N/m} & 25\ \text{N/m} & -1\ \text{N} & 3\ \text{N} & 0\ \text{N} & -16\ \text{N/m} & -32\ \text{N/m} & 13\ \text{N/m} \\
-2\ \text{N} & -21\ \text{N} & 0\ \text{N} & 63\ \text{N/m} & 25\ \text{N/m} & 487\ \text{N/m} & 1\ \text{N} & -24\ \text{N} & 0\ \text{N} & 6\ \text{N/m} & 13\ \text{N/m} & -362\ \text{N/m} \\
-2\ \text{Nm} & 1\ \text{Nm} & 0\ \text{Nm} & 1\ \text{N} & -1\ \text{N} & 1\ \text{N} & 5\ \text{Nm} & -1\ \text{Nm} & 1\ \text{Nm} & 18\ \text{N} & -4\ \text{N} & -2\ \text{N} \\
1\ \text{Nm} & -3\ \text{Nm} & 0\ \text{Nm} & -2\ \text{N} & 3\ \text{N} & -24\ \text{N} & -1\ \text{Nm} & 6\ \text{Nm} & 0\ \text{Nm} & -7\ \text{N} & -4\ \text{N} & 29\ \text{N} \\
0\ \text{Nm} & 0\ \text{Nm} & 0\ \text{Nm} & 0\ \text{N} & 0\ \text{N} & 0\ \text{N} & 1\ \text{Nm} & 0\ \text{Nm} & 1\ \text{Nm} & 0\ \text{N} & 8\ \text{N} & 0\ \text{N} \\
-1\ \text{N} & -2\ \text{N} & 0\ \text{N} & 8\ \text{N/m} & -16\ \text{N/m} & 6\ \text{N/m} & 0\ \text{N} & -7\ \text{N} & 0\ \text{N} & 83\ \text{N/m} & 32\ \text{N/m} & -63\ \text{N/m} \\
-1\ \text{N} & -3\ \text{N} & 0\ \text{N} & 16\ \text{N/m} & -32\ \text{N/m} & 13\ \text{N/m} & 18\ \text{N} & -4\ \text{N} & 8\ \text{N} & 32\ \text{N/m} & 179\ \text{N/m} & 25\ \text{N/m} \\
1\ \text{N} & 16\ \text{N} & 0\ \text{N} & -6\ \text{N/m} & 13\ \text{N/m} & -362\ \text{N/m} & -2\ \text{N} & 29\ \text{N} & 0\ \text{N} & -63\ \text{N/m} & 25\ \text{N/m} & 487\ \text{N/m}
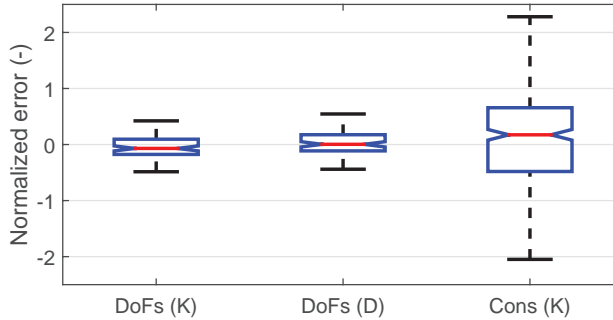\end{bmatrix}
\tag{6.36}
$$

6

Figure 6.8: Box plots of the normalized errors for the values predicted by the stiffness analysis (K) and the differential wrench calculations (D) for mechanism IV.

6.5. DISCUSSION OF VERIFICATION RESULTS

IT was shown that for the preloaded stiffness analysis of mechanism III, 50% of the values have an error between −10% and −37%. This spread is smaller than what was found in the analysis of a traditional planar parallel mechanism in Section 3.3.1. Similarly, the spread of the normalized error values obtained for mechanism IV in the directions of the DoFs as well as the constraints is similar to that found in the analysis of a comparable traditional parallel mechanism in Section 3.3.2. Thus, it is verified that the spread of error values, i.e. the precision of the stiffness analyses, is comparable to those found in the stiffness analysis of traditional parallel mechanisms.

On the other hand, the median of the normalized error values are different from zero for the analyzed PM2Es, which hints at an accuracy of the stiffness analysis of PM2Es that is worse than that of traditional PMs. To further analyze this accuracy, a comparison was made with the differential wrench calculations, which represent static modeling errors. This comparison showed that for both PM2Es the median of the errors of the stiffness analyses is indeed significantly different from these static modeling errors. This is in contrast to validation activities performed on traditional PMs in Chapter 3. For both analyzed PM2Es, in the direction of the DoFs the median of the normalized errors is negative, which represents an underestimation of the stiffness.

The lower accuracy in the stiffness analysis of PM2Es is thought to be a result of a higher degree of non-linearity in the Jacobian matrices of such mechanisms. Mechanism III forms the best illustration of this, because its stiffness analysis is only a function of Jacobian matrices and the stiffness values of the linear springs. The same matrices are also used for the differential wrench calculations. Because the median of the normalized error of the differential wrench calculations is not significantly different from zero, it can be concluded that the residual error cannot be attributed to inaccurate stiffness values or Jacobian matrices. Therefore, the lower accuracy is expected to be the effect of a higher degree of non-linearity in the Jacobian matrix. If the Jacobian matrix is highly non-linear, then the stiffness changes significantly over the imposed 5 mm displacements, so that $\Delta\$_w \neq d\$_w$, which was assumed in the measurement method. This implies that the

remaining inaccuracy is an effect of the measurement method and the magnitude of the imposed displacements, and not of the stiffness analysis.

While stiffness in the directions of the DoFs was underestimated for both PM2Es, it was overestimated in the direction of the constraints for mechanism IV, as can be seen in Fig. 6.8. From Fig. 6.7 it is concluded that this overestimation is in the reaction moments. During the measurements it was observed that there was play in the ball bearings, which allowed rotation of the joint axes. Because this effect was not captured in the model, this could explain the overestimation of the reaction moments.

Despite a lower accuracy compared to that observed in Section 3.3.1, it was possible to conclude that the median of the error is significantly closer to zero if loading is considered in the analysis of mechanism III. This is again in line with the findings in Chapter 3. From the values in Table 6.3 it can be further concluded that more variability in the measurements is explained if loading is considered, which is another indication that the stiffness analysis for mechanism III is valid. However, unexpected are the non-zero values for rotational stiffness in Eq. (6.34), because the mechanism cannot transfer any moments to the end-effectors. This is an effect of the Jacobian-derivative term as can be seen from comparison with Eq. (6.35). Thus, consideration of loading makes a stiffness analysis more accurate, but accuracy is sacrificed in some directions for better overall accuracy.

Finally, the example stiffness matrix introduced in Eq. 6.36 can be thought of as four 6×6 matrices, where the two off-diagonal matrices represent the coupling between the two end-effectors. The fact that this matrix is fairly dense shows the complexity of this coupling. Also, the example matrix illustrates that it becomes more difficult to interpret individual values in the stiffness matrix, especially because DoFs can be a combination of end-effector motions, such as the gripping motion in the considered spatial mechanism. The second DoF of this mechanisms is a shared motion along the Z-axis, but a relative motion along the Z-axis between the end-effectors is constrained, which explains the strong negative coupling for displacements along the Z-axis.

6.6. Conclusions on Stiffness Analysis of PM2Es

T HIS chapter has presented the integration of a Jacobian-based stiffness analysis and the Jacobian analysis of PM2Es, resulting in the first stiffness analyses of PM2Es. For two mechanisms it was verified that the accuracy of the resulting stiffness analyses is comparable to that of traditional parallel manipulators. Also, example stiffness matrices of PM2Es were presented, which are 6×6 matrices for planar PM2Es and 12×12 matrices for spatial PM2Es.

The stiffness analyses were performed for a 4DoF planar underactuated mechanism and a 2DoF spatial overconstrained mechanism. An example stiffness matrix for the planar PM2E showed that consideration of loading in the mechanism resulted in a reduction of the accuracy in some directions in order to achieve better overall accuracy. In the example analysis this manifested itself as non-zero values for the rotational stiffness, while no moments can be transferred to the end-effectors in the considered mechanism.

To analyze the accuracy of the stiffness analyses, changes in interaction wrenches were compared to measured changes in interaction wrenches as a function of various displacements. This comparison showed that for the planar mechanism the median of

the errors of the predicted changes was different from zero. Comparison of the measured changes with differential wrench calculations showed that this residual error could not be attributed to the Jacobian analysis or modeling of the linear springs. It was therefore argued that PM2Es demonstrate a significantly larger degree of non-linearity than traditional PMs.

REFERENCES

[1] F. Pierrot, V. Nabat, O. Company, S. Krut, and P. Poignet, *Optimal Design of a 4-DOF Parallel Manipulator: From Academia to Industry,* IEEE Transactions on Robotics **25**, 213 (2009).

[2] L. Bruzzone and G. Bozzini, *A flexible joints microassembly robot with metamorphic gripper,* Assembly Automation **30**, 240 (2010).

[3] Q.-Z. Ang, B. Horan, H. Abdi, and S. Nahavandi, *Multipoint Haptic Guidance for Micrograsping Systems,* IEEE Systems Journal , 1 (2014).

[4] B.-J. Yi, Y. N. Heung, H. L. Jae, Y.-S. Hong, S.-R. Oh, I. H. Suh, and W. K. Kim, *Design of a Parallel-Type Gripper Mechanism,* The International Journal of Robotics Research **21**, 661 (2002).

[5] M. G. Mohamed and C. M. Gosselin, *Design and analysis of kinematically redundant parallel manipulators with configurable platforms,* IEEE Transactions on Robotics **21**, 277 (2005).

[6] C. Germain, S. Briot, S. Caro, and P. Wenger, *Natural Frequency Computation of Parallel Robots,* Journal of Computational and Nonlinear Dynamics **10**, 021004 (2015).

[7] A. Taghvaeipour, J. Angeles, and L. Lessard, *Elastodynamics of a two-limb Schonflies motion generator,* Proceedings of the Institution of Mechanical Engineers, Part C: Journal of Mechanical Engineering Science **229**, 751 (2015).

[8] B.-J. Park, B.-J. Yi, and W.-K. Kim, *Design and analysis of a new parallel grasper having spherical motion,* in *2004 IEEE/RSJ International Conference on Intelligent Robots and Systems (IROS) (IEEE Cat. No.04CH37566),* Vol. 1 (IEEE, 2004) pp. 106–111.

[9] V. Nabat, M. de la O Rodriguez, O. Company, S. Krut, and F. Pierrot, *Par4: very high speed parallel robot for pick-and-place,* in *IEEE/RSJ International Conference on Intelligent Robots and Systems* (IEEE, 2005) pp. 553–558.

[10] A. G. L. Hoevenaars, P. Lambert, and J. L. Herder, *Kinematic Design of Two Elementary 3DOF Parallel Manipulators with Configurable Platforms,* in *Proceedings of the 6th International Workshop on Computational Kinematics (CK2013),* Mechanisms and Machine Science, Vol. 15, edited by F. Thomas and A. Perez Gracia (Springer Netherlands, Dordrecht, 2014) pp. 315–322.

[11] M. Pfurner, *Analysis of a Delta Like Parallel Mechanism with an Overconstrained Serial Chain as Platform,* in *Proceedings of the 14th IFToMM World Congress* (2015) pp. 365 – 372.

[12] P. Lambert, H. Langen, and R. H. Munnig Schmidt, *A Novel 5 DOF Fully Parallel Robot Combining 3T1R Motion and Grasping,* in *Volume 2: 34th Annual Mechanisms and Robotics Conference, Parts A and B* (ASME, 2010) pp. 1123–1130.

[13] P. Lambert and J. Herder, *A novel parallel haptic device with 7 degrees of freedom,* in *2015 IEEE World Haptics Conference (WHC)*, Vol. 31 (IEEE, 2015) pp. 183–188.

[14] P. Lambert and J. L. Herder, *Mobility Analysis of Non Series-Parallel Mechanisms,* in *New Trends in Mechanism and Machine Science*, Mechanisms and Machine Science, Vol. 7, edited by F. Viadero and M. Ceccarelli (Springer Netherlands, Dordrecht, 2013) pp. 63–71.

[15] P. Lambert and J. L. Herder, *Parallel robots with configurable platforms: Fundamental aspects of a new class of robotic architectures,* Proceedings of the Institution of Mechanical Engineers, Part C: Journal of Mechanical Engineering Science **0**, 1 (2015).

[16] A. G. L. Hoevenaars, *Wrench Measurements on a Planar, Passive, 4-DoF Parallel Mechanism with Two End-Effectors and a Spatial, Passive, 2-DoF Parallel Mechanism with Two End-Effectors,* (2015).

6

7

CONCLUSIONS

We may be in the cage
But the cage is not in us

Benjamin Duterde

Ben l'Oncle Soul - Walk the line

This thesis has developed a Jacobian-based stiffness analysis method that is also valid for compliant PM2Es, which enables the design of a new generation of gripper robots. In this chapter, first the five main original contributions of this thesis are summarized and interpreted in the context of existing literature. Next, the broader scientific implications of this thesis are discussed. This includes links to other fields of mechanism and robotics research, which have not been explored in this thesis, but which can benefit from the findings in this thesis.

7.1. ORIGINAL CONTRIBUTIONS

T HIS thesis has developed a Jacobian-based stiffness analysis method that is also valid for compliant parallel manipulators with two end-effectors (PM2Es). The five chapters of this thesis have made five main original contributions. With the essence of the originality in bold, these contributions are:

1. A novel Jacobian-based stiffness **analysis method** that takes both mechanical compliance and loading into account and thereby generalizes much of existing stiffness analysis methods (Chapter 2).

2. **Empirical evidence** that the stiffness analysis of a parallel manipulator can become significantly more accurate both if loading is considered and also if structural compliance is included (Chapter 3).

3. A novel **explanation** for the long-standing problem of asymmetry in stiffness matrices obtained in previous research where loading was considered (Chapter 4).

4. A structured approach for the Jacobian **analysis** of PM2Es with a single internal closed-loop chain, which was supported by the first empirically validated Jacobian analysis of a PM2E (Chapter 5).

5. An **integration** of the introduced stiffness analysis method and the introduced Jacobian analysis, resulting in the first two stiffness analyses of PM2Es (Chapter 6).

7.1.1. STIFFNESS ANALYSIS METHOD

The novel Jacobian-based stiffness analysis method that was developed in Chapter 2 is based on screw theory and generalizes much of the existing Jacobian-based stiffness analysis methods. This generalization was achieved by reducing the number of assumptions in the derivations. Firstly, the proposed method does not make any assumptions about the types of joints. Secondly, it does not assume that the stiffness of structural elements is negligible. Finally, the method also considers the effect of loading. In general, stiffness is load dependent because the transfer of an applied force or moment to the end-effector is generally pose-dependent. Consideration of this effect was enabled by a newly derived symbolic expression of its effect on the stiffness of a parallel manipulator.

Inclusion of structural stiffness was achieved through a novel use of Jacobian relations that express the constraints of each individual serial chain. These Jacobian relations are obtained using the reciprocal properties between twists and wrenches, i.e. six-dimensional motion vectors and six-dimensional force/moment vectors, as described by screw theory. The resulting stiffness analysis is more compact and more directly formulated than existing stiffness analyses that consider the effect of structural stiffness.

The use of screw theory has also led to an important novel insight, namely that all wrenches must be defined at the point where they are acting on the end-effector. It was shown in Chapter 4 that an inconsistent definition of the vectors that define the wrenches of actuation results in asymmetric stiffness matrices. This asymmetry arises when the derivative is taken of the Jacobian with respect to the joint coordinates, because the Jacobian is a function of the wrenches of actuation. The asymmetry is a result of the fact that a Jacobian which is constructed from inconsistently defined vectors does

not fully capture the dependency on the various joint coordinates. With this insight, the asymmetry in the stiffness matrices obtained by Griffis and Duffy in 1993 could finally be explained and corrected.

By considering the effect of loading and the influence of structural stiffness, this thesis has enabled the Jacobian-based stiffness analysis of parallel manipulators where the end-effector is partially constrained by its kinematic structure and which is operated under loading. This includes, but is not limited to, more complex PMs such as compliant PM2Es.

7.1.2. JACOBIAN ANALYSIS OF PM2ES

To apply the developed stiffness analysis method to PM2Es, a Jacobian analysis of PM2Es is required. Because no method existed for the Jacobian analysis of PM2Es, this thesis has developed a novel structured approach for the Jacobian analysis of PM2Es. In Chapter 5 this was done for PM2Es with a single internal closed-loop chain, although the approach can be extended to other types of parallel manipulators with internal serial chains. The main idea behind this method is that any manipulator is assembled from a set of serial chains, which is reflected in its graph theory notation.

In the derivation of this method the constraint relations have played a crucial role, because wrenches applied by the legs of a PM2E can be transferred to the two end-effectors by the constraints in the internal serial chains. Since Jacobian relations alone were insufficient to represent the dependency on internal constraints, the resulting Jacobian analysis is also a function of compliance ratios. This is unprecedented in the Jacobian analysis of parallel manipulators and is a precedent for the Jacobian analysis of other complex mechanisms and manipulators.

7.1.3. COMPATIBILITY OF ANALYSES

Both the introduced stiffness analysis method and the structured approach for the Jacobian analysis of PM2Es are based on screw theory. Both analyses rely on a set of six twists and six wrenches for each serial chain. As such, there is a significant overlap in the required effort to perform either the stiffness analysis or the Jacobian analysis. This overlap makes the two analyses directly compatible and reduces the overall analysis effort, because the effort to express the twists and wrenches only has to be done once. Their compatibility also enabled the straightforward integration of both analyses in Chapter 6.

7.1.4. EXPERIMENTAL VALIDATION AND VERIFICATION

All analysis methods presented in this thesis were validated and verified using experiments, which gives great confidence in the results obtained in this thesis. Firslty, this thesis has experimentally demonstrated that the effect of loading can have a significant effect on the accuracy of the stiffness analysis of a PM. Experiments also confirmed that consideration of structural stiffness improves analysis accuracy, while it was also verified that the stiffness analyses for two example PM2Es have a similar accuracy. The latter analysis did hint at more non-linear behavior of these mechanisms. Future efforts to analyze this non-linearity in more detail could reveal some fascinating new insights about the stiffness properties of PM2Es. To facilitate such future studies, the measurement data collected throughout this research are publicly available.

7.2. BROADER IMPLICATIONS

S EVERAL contributions of this thesis have implications that go beyond the stiffness analysis of PM2Es.

7.2.1. MECHANISMS AND MANIPULATORS OPERATED UNDER LOADING

Firstly, this thesis has provided new proof that the effect of loading is an inherent aspect of the stiffness analysis of parallel mechanisms. This effect is a consequence of the non-linear kinematics of a mechanism, and is caused by the change in the internal wrench as a function of a change in configuration. This effect is not limited to parallel manipulators, but is relevant for any kind of kinematic linkage which is under loading. One example are compliant mechanisms, because internal loading is an inherent aspect of such mechanisms. A second example are cable-driven parallel robots, which are always operated under internal loading to maintain cable tension. More detailed studies regarding the effect of loading in these more specific mechanisms and manipulators are made possible by the analysis and validation methods that were developed in this thesis, but this is left for future work.

7.2.2. INTEGRATION OF KINEMATIC AND STRUCTURAL ANALYSIS

A second contribution with wider implications regards the role of constraint relations in the analysis of parallel manipulators. It was shown in Chapter 2 how constraint relations are essential for the inclusion of structural compliance in a Jacobian-based stiffness analysis of lower mobility parallel manipulators. As such, the inclusion of constraint relations has brought mechanical analysis and kinematic analysis together for a wide range of parallel manipulators. This enables more integral design optimization where mechanical and kinematic properties are optimized simultaneously. The development of such integral optimization methods is expected to produce exciting future research.

It was also illustrated how the Jacobian analysis of a PM2E can be a function of mechanical properties, which is unprecedented in the field of parallel manipulator analysis. Until now, it was sufficient to only consider the kinematic relations in a Jacobian analysis, but this thesis has shown that this is not necessarily true. This thesis has thereby challenged the implicit assumption in existing Jacobian analyses that kinematic relations are all that is required. Undoubtedly, future research will lead to other manipulators and mechanisms where internal constraints play a role in the static force analysis. This thesis may serve as a reference for their analysis.

7.2.3. MANIPULATORS WITH INTERNAL CLOSED LOOPS

Finally, the developed stiffness analysis method and the structured approach for the Jacobian analysis of PM2Es open up the possibility to design compliant PM2Es. In doing so, this thesis has brought the static analysis of PM2Es on par with traditional parallel manipulator analysis. The next frontier in the analysis of PM2Es is the dynamic analysis, for which this thesis may serve as a starting point.

Thanks to the level of generalization in the presented stiffness analysis, it is foreseen that the derivations in this thesis can be exploited in a similar fashion for the stiffness analysis of other, more complex mechanisms. For this, a Jacobian analysis of the mech-

anism in question will be required. The presented structured approach for the Jacobian analysis of PM2Es with a single internal closed-loop chain may act as an inspiration for such Jacobian analysis. As more complex mechanisms will undoubtedly be developed in the future, it will be exciting to learn where the boundaries of the presented analysis lie.

7

ACKNOWLEDGEMENTS

Over the course of four years, ideas have turned into equations, expectations have turned into reflections, and dreams have turned into memories. Hereby I would like to thank everyone who has helped me shape these metamorphoses. These metamorphoses transcend my academic life and therefore, before I continue, I wish to thank my parents, family and friends for providing a world away from research, the value of which cannot be overstated. Turning back to this thesis, there are several people who have had a specific impact and who therefore deserve a special mention.

Firstly, I would like to thank Just for recognizing the researcher in me, feeding the enthusiasm in me, and supporting the explorer in me. You have created and maintained an academic environment that enabled me to thrive, both in Delft and abroad. I am deeply grateful for introducing me to your international network, which has greatly enriched my academic experience as well as my passport.

Secondly, I would like to thank Patrice for all our discussions on Jacobians, kinematics, Canadian cuisine, the Dutch immigration process, and much more. As my daily supervisor, you have helped me in my struggle with (and against) twists and wrenches, and I want to thank you for the patience with which you did so. Also, I thank you for helping me to 'condense' the number of equations in this thesis to a 'mere' 304.

Next, I wish to thank the M.Sc. students who have accompanied me along the way. Matthijs, Alfons, Erik, Kashmira, Sa, and Vinayak, you have been a great source of inspiration and reflection. The same appreciation goes to all my colleagues from the PME department with whom I have exchanged ideas.

My gratitude also goes to the Laval Robotics Laboratory for the fantastically fun and productive time I had in, and around, Québec City. Special thanks to Clément for his profound and continued involvement in my research, and to Thierry and Simon without whom I would not have been able to collect all the data that support this thesis. Also, I want to thank Sébastien from the LIRMM, who willingly offered me to torment his Heli4 robot in the name of science. Although the results of that exercise are not included in this thesis, it has excited the confidence in my modeling method in its natural frequency.

Finally, there are several colleagues-turned-friends that deserve special mentioning. During my Ph.D. research I have had the great pleasure of being part of the Delft Haptics Lab, which introduced me to its inhabitants: David, Patrice, Jeroen, Roel, Henri, Bram, Jack, Tricia, and Jeroen. Their questions, critical reflections, and jokes on my work have been invaluable to its realization. More specifically, without Roel's real-time support on real-time systems a significant source of delay would have undoubtedly been introduced. More generally, without this biomechanically oriented bunch I would not have been introduced to the brilliantly fun minds behind the H-Haptics programme as well as those of the BME department. As two of their representatives, I am honored to have Bram and Jeroen by my side as paranymphs during my last act as Ph.D. candidate. Thank you all.

A

INVERSE KINEMATICS AND UNIT TWISTS AND UNIT WRENCHES OF MECHANISM I

To perform the experimental validation of the stiffness analysis method of Chapter 2 two mechanisms were developed in Chapter 3. The first mechanism is a passive planar 3-DoF mechanism. This appendix presents the inverse kinematics of this mechanism, as well as the unit twists and unit wrenches of each leg.
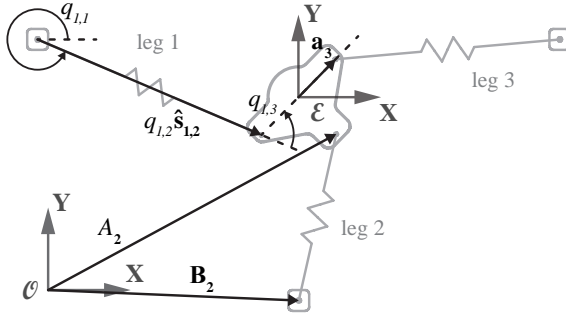
Figure A.1: The definition of vectors and scalars for mechanism I

Table A.1: Vector elements of $\mathbf{A_i}$, which was designed with $|\mathbf{a}_i| = 38$ mm

	leg 1	leg 2	leg 3
A_x	$p_x - |\mathbf{a}_1|\cos\theta$	$p_x + |\mathbf{a}_2|\sin\theta$	$p_x + |\mathbf{a}_3|\cos\theta$
A_y	$p_y - |\mathbf{a}_1|\sin\theta$	$p_y - |\mathbf{a}_2|\cos\theta$	$p_y + |\mathbf{a}_3|\sin\theta$
B_x	-0.0075	0.1800	0.3675
B_y	0.1800	-0.0075	0.1800

The inverse kinematics and unit twists and unit wrenches of the planar mechanism that was introduced in Fig. 3.1, and which is also presented in Fig. A.1, are presented in this appendix.

A.1. Inverse kinematics of Mechanism I

THE inverse of mechanism I can be expressed as

$$q_{i,1} = \tan^{-1}\left(\frac{A_{y,i} - B_{y,i}}{A_{x,i} - B_{x,i}}\right)$$

$$q_{i,2} = \sqrt{(A_{x,i} - B_{x,i})^2 + (A_{y,i} - B_{y,i})^2}$$

$$q_{i,3} = 2\pi + \theta - q_{i,1}$$

where Table A.1 presents $A_{x,i}$, $A_{y,i}$, $B_{x,i}$, and $B_{y,i}$ for each leg i.

A.2. UNIT TWISTS AND UNIT WRENCHES OF MECHANISM I

THE planar parallel mechanism consists of three identical legs, for which first three unit twists of permission can be identified as

$$\hat{\$}_{ta_{i,1}} = \begin{bmatrix} \hat{\mathbf{e}}_3 \\ -(q_{i,2}\hat{\mathbf{s}}_{i,2} - \mathbf{a}_i) \times \hat{\mathbf{e}}_3 \end{bmatrix} \tag{A.1}$$

$$\hat{\$}_{ta_{i,2}} = \begin{bmatrix} \mathbf{0}_{3\times 1} \\ \hat{\mathbf{s}}_{i,2} \end{bmatrix} \tag{A.2}$$

$$\hat{\$}_{ta_{i,3}} = \begin{bmatrix} \hat{\mathbf{e}}_3 \\ \mathbf{a}_i \times \hat{\mathbf{e}}_3 \end{bmatrix} \tag{A.3}$$

where $\hat{\$}_{ta_{i,1}}$, $\hat{\$}_{ta_{i,2}}$, and $\hat{\$}_{ta_{i,3}}$ are the unit twists of permission associated to the lower zero stiffness revolute joint, the passive compliant prismatic joint, and the upper zero stiffness revolute joint respectively. The vector $\hat{\mathbf{e}}_3$ is the unit vector aligned with the Z-axis (pointing out of the page), while the other vectors are illustrated in Fig. A.1. Together these unit twists span the 2D space of the mechanism, namely the XY-plane.

Above set of unit twists then allow three unit wrenches of actuation to be identified in the XY-plane, namely

$$\hat{\$}_{wa_{i,1}} = \begin{bmatrix} \mathbf{a}_i \times (\hat{\mathbf{e}}_3 \times \hat{\mathbf{s}}_{i,2}) \\ (\hat{\mathbf{e}}_3 \times \hat{\mathbf{s}}_{i,2}) \end{bmatrix} \tag{A.4}$$

$$\hat{\$}_{wa_{i,2}} = \begin{bmatrix} \mathbf{a}_i \times \hat{\mathbf{s}}_{i,2} \\ \hat{\mathbf{s}}_{i,2} \end{bmatrix} \tag{A.5}$$

$$\hat{\$}_{wa_{i,3}} = \begin{bmatrix} -(q_{i,2}\hat{\mathbf{s}}_{i,2} - \mathbf{a}_i) \times (\hat{\mathbf{e}}_3 \times \hat{\mathbf{s}}_{i,2}) \\ (\hat{\mathbf{e}}_3 \times \hat{\mathbf{s}}_{i,2}) \end{bmatrix} \tag{A.6}$$

Because the mechanism is not constrained in the plane, no wrenches of constraint and twists of restrictions exist. To do a planar analysis, the first, second, and sixth entry of the six-dimensional vectors presented in Eqs. (A.1) - (A.6) was removed.

B

INVERSE KINEMATICS OF MECHANISM II

To perform the experimental validation of the stiffness analysis method of Chapter 2 two mechanisms were developed in Chapter 3. The second mechanism is a passive spatial 1-DoF mechanism. This appendix presents the inverse kinematics of this mechanism. The unit twists and unit wrenches of each leg were already introduced in Section 2.3.
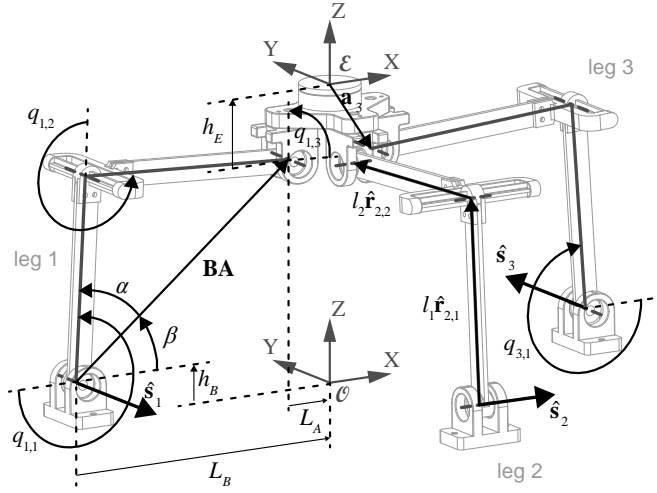
Figure B.1: The definition of vectors and scalars for mechanism II

inverse kinematics of the spatial mechanism presented in Fig. B.1 can be expressed as

$$q_{i,1} = \pi + \alpha + \beta$$

$$q_{i,2} = \begin{cases} \pi + \sin^{-1}\left(\frac{|\mathbf{BA}|}{l_2}\sin\alpha\right) & \text{if} \quad |\mathbf{BA}|^2 \le l_1^2 + l_2^2 \\ 2\pi - \sin^{-1}\left(\frac{|\mathbf{BA}|}{l_2}\sin\alpha\right) & \text{if} \quad |\mathbf{BA}|^2 > l_1^2 + l_2^2 \end{cases}$$

$$q_{i,3} = \frac{7\pi}{2} - q_{i,1} - q_{i,2}$$

where $l_1 = 135$ mm, $l_2 = 150$ mm, and

$$\mathbf{BA} = [L_B - L_A \quad 0 \quad p_z - h_E - h_B]^\top$$

$$\alpha = \cos^{-1}\left(\frac{l_1^2 - l_2^2 + |\mathbf{BA}|^2}{2l_1|\mathbf{BA}|}\right)$$

$$\beta = \tan^{-1}\left(\frac{BA_z}{BA_x}\right)$$

where $L_B = 187.5$ mm, $L_A = 30$ mm, $h_E = 47$ mm, and $h_B = 24$ mm.

C

KINEMATIC DESIGN OF TWO ELEMENTARY 3-DoF PARALLEL MANIPULATORS WITH CONFIGURABLE PLATFORMS

Parallel manipulators with two end-effectors (PM2Es) are an interpretation of parallel manipulators with configurable platforms (PMCPs). PMCPs have internal degrees of freedom and form a class of manipulators that is not covered by existing type synthesis methods. Because the minimum number of legs for a PMCP is three, fully parallel 3DOF PMCPs may be considered an elementary subset of PMCPs. To support the extension of type synthesis methods to PMCPs, this appendix presents the first kinematic designs of manipulators from this subset. A structured design method has led to the kinematic design of two spatial manipulators that are both capable of independently performing one translation, one rotation and one internal platform motion.

C.1. Introduction to Synthesis of PMCPs

R OBOTIC manipulation sometimes requires additional degrees of freedom (DoF) such as grasping on top of the rigid end-effector motion. Multiple solutions have been proposed to achieve this additional motion. One example is to combine two separate mechanisms [2] and another is to attach a gripper mechanism in series to the end-effector, as is the case in the commercial omega.7 by Force Dimension. The first solution increases the complexity of the system while the latter adds the inertia of an additional motor to the end-effector. Because low inertia at the end-effector is one of the distinguishing features of parallel manipulators, additional inertia especially affects the performance of parallel manipulators.

In the past decade it has been recognised that additional DoF can also be added to the end-effector of a parallel manipulator without compromising its parallel structure. This is achieved by replacing the rigid end-effector with an additional closed loop. Following the 4-DoF planar manipulator with grasping motion by Yi et al. [3], Mohamed and Gosselin generalised the analysis of this new class of manipulators called Parallel Manipulators with Configurable Platforms (PMCP) [4]. Other examples of such PMCPs are the Par4 by Nabat et al. [5] and a 5-DoF design by Lambert et al. [6].

An illustrative method to discuss kinematic structures is graph theory [7], which represents every mechanism as a series of joints (lines) and rigid bodies (nodes). Fig. C.1 illustrates how in graph theory a PMCP with two legs is kinematically equivalent to a *series-parallel architecture*, while a PMCP with three legs is not; in fact it belongs to a different category labelled *non-series-parallel architectures* [8]. PMCPs with three legs (serial chains) may therefore be regarderd as the most basic subset of PMCP designs. In this appendix only *fully parallel manipulators* are considered, for which the number of legs is strictly equal to the number of DoF of the end-effector [9]. Thus, if only the joints located at the base are actuated, three legs allow 3-DoF. Consequently, it is argued in this appendix that fully parallel 3-DoF PMCPs represent an elementary subset of PMCP designs.

Interestingly, PMCPs discussed in the literature all have a minimum of 4-DoF. They have not been developed using a type synthesis method such as the one introduced by Kong and Gosselin [10] or Gogu [11], since existing methods do not cover PMCPs. Because fully parallel 3-DoF PMCPs are argued to form an elementary subset of PMCP designs, examples from this subset may provide interesting input for the future development of a type synthesis method that does cover PMCPs.

The goal of this appendix is to verify the existence of fully parallel 3DOF PMCPs and present the first architectures from this elementary subset. The structure of the appendix is as follows. First the design method is discussed that leads to the two kinematic architectures presented in this appendix. Next, the inverse Jacobian is derived for one of the two kinematic designs and four singular configurations are identified.

C.2. Structured Method to Design Novel PMCPs

B ECAUSE no type synthesis method exists for PMCPs, the method in this appendix relies on the structured combination of a four-bar mechanism (the platform) with a set of pre-defined legs. Furthermore, two restricting conditions are posed on the designs.
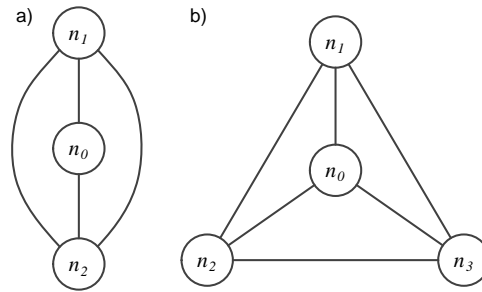
Figure C.1: a) Using graph theory a PMCP mechanism with two legs can be represented as a series-parallel mechanism with a base n_0 and two link nodes n_1 and n_2, b) A PMCP with three legs cannot be represented as a series-parallel mechanism, but yields a so-called wheel graph

The first condition is that the resulting 3-DoF PMCPs shall be fully parallel. The number of legs is therefore strictly limited to three. Secondly, the axis associated with each DoF shall coincide with an axis of either the inertial reference frame XYZ or the platform reference frame $X^*Y^*Z^*$. This condition facilitates a straightforward description of the resulting mobilities.

The design method applied in this appendix consists of four steps. First, the building blocks are defined: a planar four-bar mechanism and three identical legs. A four-bar mechanism with links of equal length is used, which is known to have three overconstraints and one internal DoF. Thus, the total number of platform DoF is seven. The internal DoF is expressed as the distance P_g between one of the joints and the platform reference frame origin. On the premise that a fully parallel 3-DoF PMCP requires each of the three legs to have a minimum of three DoF, a minimal leg consists of two links and three joints and describes planar motion. One of the end joints is connected to an actuator at the base. In this appendix the choice was made to use rotating actuators but this choice does not impact the DoF of the individual legs. The described building blocks are shown in Fig. C.2a.

The second step is to constrain the motion of the platform reference frame origin to a plane, which is achieved through the connection of two legs to opposite joints of the four-bar mechanism. These legs are connected such that the resulting plane of motion of the platform reference frame origin is perpendicular to either X^* or Y^*. This is to ensure that the remaining DoF are all alligned with an axis of either the inertial reference frame or the platform reference frame. The plane of motion of the platform reference frame origin is here defined as the XZ-plane, as shown in Fig. C.2b. The mechanism now has four DoF.

In the third step an additional DoF is constrained using the third leg. To constrain the platform in another DoF, the third leg is oriented in either of the planes perpendicular to the first two legs. Connecting the third leg in this orientation to one of the two remaining platform joints adds two additional constraints (and one overconstraint) to the platform. The state of the two kinematic designs after this step is shown in Figs. C.2c and C.2d.

By constraining five of the original seven DoF, both mechanisms shown in Figs. C.2c and C.2d have two DoF remaining. The final step is therefore to relieve one of the con-
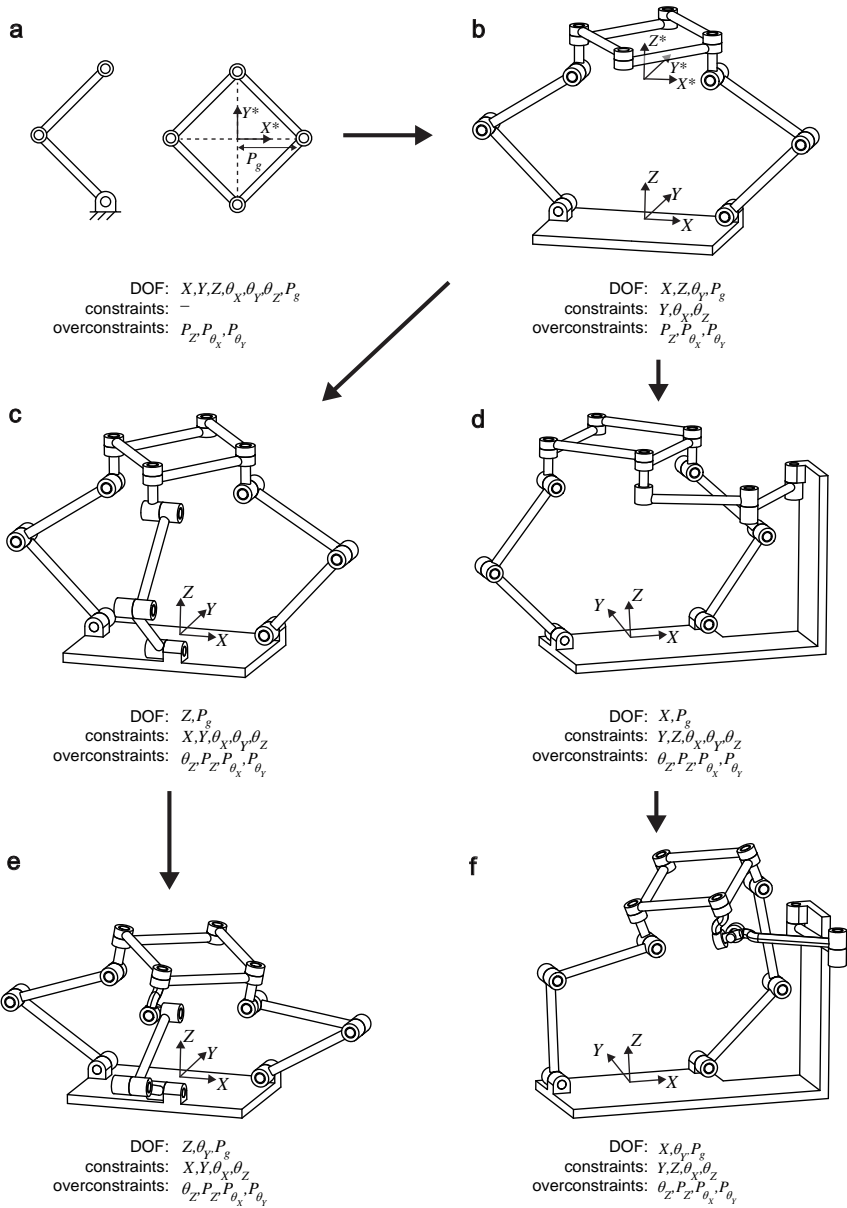
C

Figure C.2: a) the minimum building blocks for a fully parallel 3-DoF PMCP, b) the mechanism after connection of the first two legs, c) one of two possibilities for connecting the third leg, d) the second possibility for connecting the third leg, e) one of the resulting fully parallel 3-DoF PMCPs, and f) the second resulting fully parallel 3-DoF PMCP.
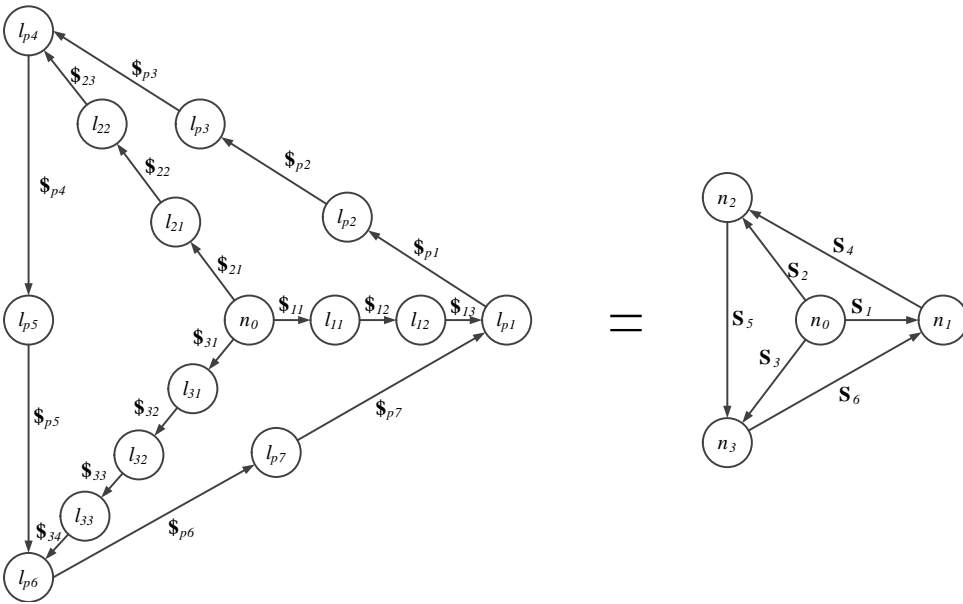
Figure C.3: Representation of the mechanisms shown in Figs. C.2e and C.2f using graph theory where l_{il} stands for the lth link of the leg i and $\$_{ij}$ for the screw associated with joint j of leg i, while in the reduced graph after serial reduction n_i and $\mathbf{S}_i$ are respectively the ith link node and screw system

strained DoF by introducing an additional joint. For the mechanism shown in Fig. C.2d this also requires a change in the orientation of the joint connecting the third leg to the platform. The two resulting kinematic designs are shown in Figs. C.2e and C.2f.

This section has described the kinematic design of two fully parallel 3-DoF PMCPs, both of which have four overconstraints. In graph theory notation, both architectures are represented by the graph in Fig. C.3 which is equivalent to the one shown in Fig. C.1b after serial reductions [8].

C.3. CONCLUSION

THIS appendix has presented the first kinematic designs of fully parallel 3DOF PMCPs, which were identified as an elementary subset of PMCP designs. The resulting mechanisms are spatial manipulators that can be independently controlled in one rotation, one translation and one internal platform motion. Since existing type synthesis methods do not cover PMCPs, this appendix has applied a structured, but not yet formalised, design method. Because the presented manipulators are considered to be part of an elementary subset of PMCP designs, they may prove to be useful input for the development of a type synthesis method that does cover PMCPs. Also, they are relatively simple PMCPs, which makes them suitable examples for novel analyses, such as the structured approach for the Jacobian analysis introduced in Chapter 5.

REFERENCES

[1] A. G. L. Hoevenaars, P. Lambert, and J. L. Herder, *Kinematic Design of Two Elementary 3DOF Parallel Manipulators with Configurable Platforms,* in *Proceedings of the 6th International Workshop on Computational Kinematics (CK2013)*, Mechanisms and Machine Science, Vol. 15, edited by F. Thomas and A. Perez Gracia (Springer Netherlands, Dordrecht, 2014) pp. 315–322.

[2] V. Kumar, *Instantaneous Kinematics of Parallel-Chain Robotic Mechanisms,* Journal of Mechanical Design **114**, 349 (1992).

[3] B.-J. Yi, Y. N. Heung, H. L. Jae, Y.-S. Hong, S.-R. Oh, I. H. Suh, and W. K. Kim, *Design of a Parallel-Type Gripper Mechanism,* The International Journal of Robotics Research **21**, 661 (2002).

[4] M. G. Mohamed and C. M. Gosselin, *Design and analysis of kinematically redundant parallel manipulators with configurable platforms,* IEEE Transactions on Robotics **21**, 277 (2005).

[5] V. Nabat, M. de la O Rodriguez, O. Company, S. Krut, and F. Pierrot, *Par4: very high speed parallel robot for pick-and-place,* in *IEEE/RSJ International Conference on Intelligent Robots and Systems* (IEEE, 2005) pp. 553–558.

[6] P. Lambert, H. Langen, and R. H. Munnig Schmidt, *A Novel 5 DOF Fully Parallel Robot Combining 3T1R Motion and Grasping,* in *Volume 2: 34th Annual Mechanisms and Robotics Conference, Parts A and B* (ASME, 2010) pp. 1123–1130.

[7] C. F. Earl and J. Rooney, *Some Kinematic Structures for Robot Manipulator Designs,* Journal of Mechanisms Transmissions and Automation in Design **105**, 15 (1983).

[8] P. Lambert and J. L. Herder, *Mobility Analysis of Non Series-Parallel Mechanisms,* in *New Trends in Mechanism and Machine Science*, Mechanisms and Machine Science, Vol. 7, edited by F. Viadero and M. Ceccarelli (Springer Netherlands, Dordrecht, 2013) pp. 63–71.

[9] J.-P. Merlet, *Parallel Robots*, 2nd ed., edited by G. Gladwell, Solid Mechanics and its Application, Vol. 128 (Springer, Dordrecht, 2006).

[10] X. Kong and C. Gosselin, *Type Synthesis of Parallel Mechanisms*, edited by B. Siciliano;, O. Khatib;, and F. Groen (Springer Berlin Heidelberg, 2007).

[11] G. Gogu, *Structural Synthesis of Parallel Robots, Part 1: Methodology*, edited by G. Gladwell (Springer, 2008).

D

INVERSE KINEMATICS AND PARTIAL JACOBIANS FOR MECHANISM III

To perform the experimental verification of the synthesized stiffness analyses of PM2Es, as presented in Chapter 6, two mechanisms were developed in that chapter. The first mechanism is a passive planar 4-DoF mechanism. This appendix presents the inverse kinematics of this mechanism, the unit twists and unit wrenches of each serial chain, as well as the partial inverse Jacobian matrices.
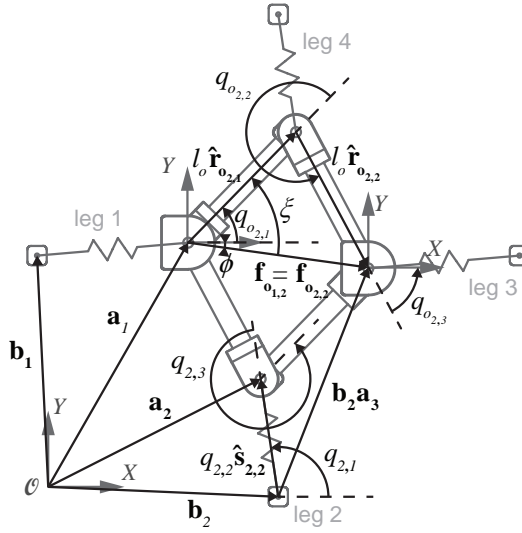
Figure D.1: An example of the various vectors that are used in the inverse kinematics and expressions of Jacobian matrices for mechanism III.

For the planar 4-DoF PM2E that was introduced in Chapter 6 as mechanism III, this appendix develops the inverse kinematics as well as the unit twists and unit wrenches. These unit twists and unit wrenches are also used to develop the partial Jacobian matrices for each individual chain of the mechanism.

D.1. Inverse Kinematics of Mechanism III

THE inverse kinematics of the example 4-DoF planar PM2E are developed for each individual serial chain. The inverse kinematics of the legs are presented first, where expression for the angles as shown in Fig. D.1 can be obtained as

$$q_{i,1} = \tan^{-1}\left(\frac{\mathbf{a}_{y,i} - \mathbf{b}_{y,i}}{\mathbf{a}_{i,x} - \mathbf{b}_{i,x}}\right)$$

$$q_{i,2} = \sqrt{\left(\mathbf{a}_{x,i} - \mathbf{b}_{x,i}\right)^2 + \left(\mathbf{a}_{y,i} - \mathbf{b}_{y,i}\right)^2}$$

$$q_{i,3} = \begin{cases} 2\pi - q_{i,1} & \text{if} \quad i = 1,3 \\ \pi + \cos^{-1}\left(\frac{q_{i,2}^2 + l_o^2 - |\mathbf{b_i a_3}|^2}{2q_{i,2}l_o}\right) & \text{if} \quad i = 2,4 \text{ and } \beta_i < q_{i,1} \\ \pi - \cos^{-1}\left(\frac{q_{i,2}^2 + l_o^2 - |\mathbf{b_i a_3}|^2}{2q_{i,2}l_o}\right) & \text{if} \quad i = 2,4 \text{ and } \beta_i \geq q_{i,1} \end{cases}$$

where $l_o = 120$ mm,

$$\mathbf{a}_1 = \begin{bmatrix} p_{x,e_1} \\ p_{y,e_1} \\ 0 \end{bmatrix}, \quad \mathbf{a}_2 = \begin{bmatrix} p_{x,e_1} + l_o \cos(\xi - \phi) \\ p_{y,e_1} - l_o \sin(\xi - \phi) \\ 0 \end{bmatrix}, \quad \mathbf{a}_3 = \begin{bmatrix} p_{x,e_2} \\ p_{y,e_2} \\ 0 \end{bmatrix},$$

$$\mathbf{a}_4 = \begin{bmatrix} p_{x,e_2} - l_o \cos(\xi - \phi) \\ p_{y,e_2} + l_o \sin(\xi - \phi) \\ 0 \end{bmatrix}, \quad \mathbf{b}_1 = \begin{bmatrix} -0.0075 \\ 0.1800 \\ 0 \end{bmatrix} \text{ m},$$

$$\mathbf{b}_2 = \begin{bmatrix} 0.1800 \\ -0.0075 \\ 0 \end{bmatrix} \text{ m}, \quad \mathbf{b}_3 = \begin{bmatrix} 0.3675 \\ 0.1800 \\ 0 \end{bmatrix} \text{ m}, \quad \mathbf{b}_4 = \begin{bmatrix} 0.1800 \\ 0.3675 \\ 0 \end{bmatrix} \text{ m},$$

D

and

$$\mathbf{b_i a_3} = \mathbf{a_3} - \mathbf{b_i}, \quad \phi = \tan^{-1}\left(\frac{p_{y,e_2} - p_{y,e_1}}{p_{x,e_2} - p_{x,e_1}} \right)$$

$$\xi = \cos^{-1}\left(\frac{\sqrt{(p_{x,e_2} - p_{x,e_1})^2 + (p_{y,e_2} - p_{y,e_1})^2}}{2l_o} \right)$$

Next, the inverse kinematics of the end-effector serial chains are developed, where expression for the angles as shown in Fig. D.1 can be obtained as

$$q_{o_{1,1}} = \phi - \xi, \quad q_{o_{1,2}} = 2\xi, \quad q_{o_{1,3}} = 4\pi - \phi - \xi$$
$$q_{o_{2,1}} = \phi + \xi, \quad q_{o_{2,2}} = 2\pi - 2\xi, \quad q_{o_{2,3}} = -\phi + \xi$$

D.2. UNIT TWISTS, UNIT WRENCHES, AND PARTIAL JACOBIANS FOR MECHANISM III

THIS section presents the unit twists and unit wrenches for mechanism III and presents the partial inverse Jacobian matrices for each leg and for the two end-effector serial chain.

D.2.1. FULL INVERSE JACOBIAN FOR LEGS

The four legs of the planar PM2E are identical, with the following unit twists of permission,

$$\hat{\$}_{ta_{i,1}} = \begin{bmatrix} \hat{\mathbf{e}}_3 \\ -(q_{i,2}\hat{\mathbf{s}}_{i,2} - \mathbf{a}_i) \times \hat{\mathbf{e}}_3 \end{bmatrix} \tag{D.1}$$

$$\hat{\$}_{ta_{i,2}} = \begin{bmatrix} \mathbf{0}_{3 \times 1} \\ \hat{\mathbf{s}}_{i,2} \end{bmatrix} \tag{D.2}$$

$$\hat{\$}_{ta_{i,3}} = \begin{bmatrix} \hat{\mathbf{e}}_3 \\ \mathbf{a}_i \times \hat{\mathbf{e}}_3 \end{bmatrix} \tag{D.3}$$

where for the ith leg, $\hat{\$}_{ta_{i,1}}$, $\hat{\$}_{ta_{i,2}}$, and $\hat{\$}_{ta_{i,3}}$ are the unit twists of permission associated to the lower zero stiffness revolute joint, the passive compliant prismatic joint, and the upper zero stiffness revolute joint respectively. The vector $\hat{\mathbf{e}}_3$ is the unit vector aligned with the Z-axis (pointing out of the page), while the other vectors are illustrated in Fig. D.1. Together these unit twists span the 2D space of the mechanism, namely the XY-plane.

Above set of unit twists then allow three unit wrenches of actuation to be identified in the XY-plane, namely

$$\hat{\$}_{wa_{i,1}} = \begin{bmatrix} \mathbf{a}_i \times (\hat{\mathbf{e}}_3 \times \hat{\mathbf{s}}_{i,2}) \\ (\hat{\mathbf{e}}_3 \times \hat{\mathbf{s}}_{i,2}) \end{bmatrix} \tag{D.4}$$

$$\hat{\$}_{wa_{i,2}} = \begin{bmatrix} \mathbf{a}_i \times \hat{\mathbf{s}}_{i,2} \\ \hat{\mathbf{s}}_{i,2} \end{bmatrix} \tag{D.5}$$

$$\hat{\$}_{wa_{i,3}} = \begin{bmatrix} -(q_{i,2}\hat{\mathbf{s}}_{i,2} - \mathbf{a}_i) \times (\hat{\mathbf{e}}_3 \times \hat{\mathbf{s}}_{i,2}) \\ (\hat{\mathbf{e}}_3 \times \hat{\mathbf{s}}_{i,2}) \end{bmatrix} \tag{D.6}$$

Because the mechanism is not constrained in the plane, no wrenches of constraint and twists of restrictions exist. For the planar analysis the first, second, and sixth entry of each six-dimensional twist or wrench presented in Eqs. (D.1) - (D.6) are removed.

Equations (D.1)-(D.6) can be used to develop the full inverse Jacobian matrix for each individual leg as

$$\mathbf{J}_i^{-1} = \begin{bmatrix} \hat{\$}_{wa_{i,1}}^\top / (\hat{\$}_{wa_{i,1}}^\top \hat{\$}_{ta_{i,1}}) \\ \hat{\$}_{wa_{i,2}}^\top / (\hat{\$}_{wa_{i,2}}^\top \hat{\$}_{ta_{i,2}}) \\ \hat{\$}_{wa_{i,3}}^\top / (\hat{\$}_{wa_{i,3}}^\top \hat{\$}_{ta_{i,3}}) \end{bmatrix} \tag{D.7}$$

D.2.2. Full Inverse Jacobian for Internal Serial Chains

In order to develop the inverse Jacobian matrices for the internal serial chains, first a set of basis twists and basis wrenches is developed for the two end-effector serial chains. Both these serial chains are RRR chains and their linearly independent basis twists of permission are

$$\hat{\$}_{ta_{o_{i,1}}} = \begin{bmatrix} \hat{\mathbf{e}}_3 \\ -(l_o\hat{\mathbf{r}}_{o_{i,1}} + l_o\hat{\mathbf{r}}_{o_{i,2}} - \mathbf{a}_3) \times \hat{\mathbf{e}}_3 \end{bmatrix} \tag{D.8}$$

$$\hat{\$}_{ta_{o_{i,2}}} = \begin{bmatrix} \hat{\mathbf{e}}_3 \\ -(l_o\hat{\mathbf{r}}_{o_{i,2}} - \mathbf{a}_3) \times \hat{\mathbf{e}}_3 \end{bmatrix} \tag{D.9}$$

$$\hat{\$}_{ta_{o_{i,3}}} = \begin{bmatrix} \hat{\mathbf{e}}_3 \\ \mathbf{a}_3 \times \hat{\mathbf{e}}_3 \end{bmatrix} \tag{D.10}$$

where $\hat{\$}_{ta_{o_{i,1}}}$, $\hat{\$}_{ta_{o_{i,1}}}$, and $\hat{\$}_{ta_{o_{i,1}}}$ are the unit twists of permission associated to the first, second, and third joints encountered in each end-effector serial chain, going from the first to the second end-effector. The vector $\hat{\mathbf{e}}_3$ is the unit vector along the Z-axis. Examples of scalars and other vectors in Eqs. (D.8)-(D.10), are illustrated in Fig. D.1, where l_o is the length of each link in the end-effector serial chains. As such, $\hat{\mathbf{r}}_{o_{i,l}}$ is the unit vector pointing along the lth link of the ith end-effector serial chain. Together, the three twists of permission span the plane in which the mechanism is operating, so that no wrenches of constraint exist.

Following the methodology described by Huang et al. [1], the set of unit twists of permission in Eqs. (D.8)-(D.10) led to the identification of a set of unit wrenches of actuation as

$$\hat{\$}_{wa_{o_{i,1}}} = \begin{bmatrix} \mathbf{a}_3 \times \hat{\mathbf{r}}_{o_{i,2}} \\ \hat{\mathbf{r}}_{o_{i,2}} \end{bmatrix} \tag{D.11}$$

$$\hat{\$}_{wa_{o_{i,2}}} = \begin{bmatrix} \mathbf{a}_3 \times \hat{\mathbf{f}}_{o_{i,2}} \\ \hat{\mathbf{f}}_{o_{i,2}} \end{bmatrix} \tag{D.12}$$

$$\hat{\$}_{wa_{o_{i,3}}} = \begin{bmatrix} -(l_o \hat{\mathbf{r}}_{o_{i,2}} - \mathbf{a}_3) \times \hat{\mathbf{r}}_{o_{i,1}} \\ \hat{\mathbf{r}}_{o_{i,1}} \end{bmatrix} \tag{D.13}$$

with

$$\hat{\mathbf{f}}_{o_{i,2}} = \frac{l_o \hat{\mathbf{r}}_{o_{i,1}} + l_o \hat{\mathbf{r}}_{o_{i,2}}}{|l_o \hat{\mathbf{r}}_{o_{i,1}} + l_o \hat{\mathbf{r}}_{o_{i,2}}|}. \tag{D.14}$$

The unit twists and wrenches presented in Eqs. (D.8)-(D.13) were then used to develop the inverse Jacobian matrices for the four internal serial chains, $\mathbf{J}_{o_1^2}^{-1}$, $\mathbf{J}_{o_2^3}^{-1}$, $\mathbf{J}_{o_3^4}^{-1}$, and $\mathbf{J}_{o_4^1}^{-1}$. Considering that the internal serial chain connecting n_1 and n_2 contains the first two kinematic joints of the first end-effector serial chain, then

$$\mathbf{J}_{o_1^2}^{-1} = \begin{bmatrix} \hat{\$}_{wa_{o_{1,1}}}^{\top} / (\hat{\$}_{wa_{o_{1,1}}}^{\top} \hat{\$}_{ta_{o_{1,1}}}) \\ \hat{\$}_{wa_{o_{1,2}}}^{\top} / (\hat{\$}_{wa_{o_{1,2}}}^{\top} \hat{\$}_{ta_{o_{1,2}}}) \\ \hat{\$}_{wa_{o_{1,3}}}^{\top} / (\hat{\$}_{wa_{o_{1,3}}}^{\top} \hat{\$}_{ta_{o_{1,3}}}) \end{bmatrix} \tag{D.15}$$

where the first and second row of Eq. (D.15) map the relative twist between the two end-effectors onto $\dot{q}_{a_{o_1^2,1}}$ and $\dot{q}_{a,o_1^2,2}$, the third row maps that relative twist onto the simple constrained joint velocity, $\dot{q}_{c_s,o_1^2,1}$. See Section 5.4.1 for more details on simple constrained velocities.

The internal serial chain that connects n_2 and n_3 contains the third kinematic joint of the first end-effector serial chain, so that

$$\mathbf{J}_{o_2^3}^{-1} = \begin{bmatrix} \hat{\$}_{wa_{o_{1,3}}}^{\top} / (\hat{\$}_{wa_{o_{1,3}}}^{\top} \hat{\$}_{ta_{o_{1,3}}}) \\ \hat{\$}_{wa_{o_{1,1}}}^{\top} / (\hat{\$}_{wa_{o_{1,1}}}^{\top} \hat{\$}_{ta_{o_{1,1}}}) \\ \hat{\$}_{wa_{o_{1,2}}}^{\top} / (\hat{\$}_{wa_{o_{1,2}}}^{\top} \hat{\$}_{ta_{o_{1,2}}}) \end{bmatrix} \tag{D.16}$$

where the first row maps the relative end-effector twist onto $\dot{q}_{a,o_2^3,1}$, and the second and third rows map the relative end-effector twist onto the two simple constrained joint velocities, $\dot{q}_{c_s,o_2^3,1}$ and $\dot{q}_{c_s,o_2^3,2}$.

The internal serial chain that connects n_3 to n_4 contains the third kinematic joint of the second end-effector serial chain, but considered in the opposite direction as the twists in (D.8)-(D.10),

$$\mathbf{J}_{o_3^4}^{-1} = \begin{bmatrix} -\hat{\$}_{wa_{o_{2,3}}}^{\top} / (\hat{\$}_{wa_{o_{2,3}}}^{\top} \hat{\$}_{ta_{o_{2,3}}}) \\ -\hat{\$}_{wa_{o_{2,1}}}^{\top} / (\hat{\$}_{wa_{o_{2,1}}}^{\top} \hat{\$}_{ta_{o_{2,1}}}) \\ -\hat{\$}_{wa_{o_{2,2}}}^{\top} / (\hat{\$}_{wa_{o_{2,2}}}^{\top} \hat{\$}_{ta_{o_{2,2}}}) \end{bmatrix} \tag{D.17}$$

where the first row maps the relative end-effector twist onto $\dot{q}_{a,o_3^4,1}$, and the second and third rows map the relative end-effector twist onto the two simple constrained joint velocities, $\dot{q}_{c_s,o_3^4,1}$ and $\dot{q}_{c_s,o_3^4,2}$.

Finally, the internal serial chain that connects n_4 to n_1 contains the first and second kinematic joint of the second end-effector serial chain, but again considered in the opposite direction as the twists in Eqs. (D.8)-(D.10),

$$
\mathbf{J}_{o_3^4}^{-1} = \begin{bmatrix} -\hat{\mathbf{\$}}_{wa_{o_{2,2}}}^{\top} / (\hat{\mathbf{\$}}_{wa_{o_{2,2}}}^{\top} \hat{\mathbf{\$}}_{ta_{o_{2,2}}}) \\ -\hat{\mathbf{\$}}_{wa_{o_{2,1}}}^{\top} / (\hat{\mathbf{\$}}_{wa_{o_{2,1}}}^{\top} \hat{\mathbf{\$}}_{ta_{o_{2,1}}}) \\ -\hat{\mathbf{\$}}_{wa_{o_{2,3}}}^{\top} / (\hat{\mathbf{\$}}_{wa_{o_{2,3}}}^{\top} \hat{\mathbf{\$}}_{ta_{o_{2,3}}}) \end{bmatrix}
\tag{D.18}
$$

where the first and second row map the relative end-effector twist onto $\dot{q}_{a,o_4^1,1}$ and $\dot{q}_{a,o_4^1,2}$, and the second and third rows map the relative end-effector twist onto the simple constrained joint velocity $\dot{q}_{c_s,o_4^1,1}$.

REFERENCES

[1] T. Huang, H. T. Liu, and D. G. Chetwynd, *Generalized Jacobian analysis of lower mobility manipulators,* Mechanism and Machine Theory **46**, 831 (2011).

E

INVERSE KINEMATICS AND PARTIAL JACOBIANS FOR MECHANISM IV

To perform the experimental verification of the synthesized stiffness analyses of PM2Es, as presented in Chapter 6, two mechanisms were developed in that chapter. The second mechanism is a passive spatial 2-DoF mechanism. This appendix presents the inverse kinematics of this mechanism, the unit twists and unit wrenches of each serial chain, as well as the partial inverse Jacobian matrices.

For the spatial 2-DoF PM2E that was introduced in Chapter 5, this appendix develops the inverse kinematics as well as the unit twists and unit wrenches. These unit twists and unit wrenches are also used to develop the partial Jacobian matrices for each individual chain of the mechanism. The mechanism will be referred to as mechanism IV in agreement with Chapter 6.

E.1. INVERSE KINEMATICS OF MECHANISM IV

I N this section the inverse kinematics are developed for mechanism IV. First the inverse kinematics of the legs are developed, where expression for the angles as shown in Figs. E.1 and E.2 can be obtained as

$$q_{i,1} = \pi + \alpha + \beta$$

$$q_{i,2} = \begin{cases} \pi + \sin^{-1}\left(\frac{|\mathbf{BA_i}|}{l_2}\sin\alpha\right) & \text{if} \quad |\mathbf{BA_i}|^2 \leq l_1^2 + l_2^2 \\ 2\pi - \sin^{-1}\left(\frac{|\mathbf{BA_i}|}{l_2}\sin\alpha\right) & \text{if} \quad |\mathbf{BA_i}|^2 > l_1^2 + l_2^2 \end{cases}$$

$$q_{i,3} = \frac{7\pi}{2} - q_{i,1} - q_{i,2}$$

where $l_1 = 135$ mm, $l_2 = 150$ mm, and

$$\mathbf{BA_1} = \begin{bmatrix} L_{B,1} + p_{x,e_1} \\ 0 \\ p_{z,e_1} - l_3 - h_B \end{bmatrix} \quad \mathbf{BA_3} = \begin{bmatrix} L_{B,3} - p_{x,e_2} \\ 0 \\ p_{z,e_2} - l_3 - h_B \end{bmatrix}$$

$$\mathbf{BA_2} = \begin{bmatrix} L_{B,2} - 0.5\sqrt{(2l_o)^2 - \left(p_{x,e_2} - p_{x,e_1}\right)^2} \\ 0 \\ p_{z,e_1} - l_3 - h_B \end{bmatrix}$$

$$\alpha = \cos^{-1}\left(\frac{l_1^2 - l_2^2 + |\mathbf{BA}|^2}{2l_1|\mathbf{BA}|}\right)$$

$$\beta = \tan^{-1}\left(\frac{BA_z}{BA_x}\right)$$

where $L_{B,1} = L_{B,3} = 187.5$ mm, $L_{B,2} = 242.5$ mm, $l_o = 120$ mm, $h_B = 24$ mm, and where it is assumed that $p_{z,e_1} = p_{z,e_2}$. Next the inverse kinematics of the end-effector serial chains are developed, where expression for the angles as shown in Fig. E.3 can be obtained as

$$q_{o_{1,1}} = 2\pi - \xi, \quad q_{o_{1,2}} = 2\xi, \quad q_{o_{1,3}} = 2\pi - \xi \tag{E.1}$$

$$q_{o_{2,1}} = \xi, \quad q_{o_{2,2}} = 2\pi - 2\xi, \quad q_{o_{2,3}} = \xi \tag{E.2}$$

where

$$\xi = \cos^{-1}\left(\frac{p_{x,e_2} - p_{x,e_1}}{2l_o}\right) \tag{E.3}$$

E.2. UNIT TWISTS, UNIT WRENCHES, AND PARTIAL JACOBIANS FOR MECHANISM IV

A LL twists and wrenches introduced in this appendix are expressed in a right-handed Cartesian reference frame connected to the moving body of the serial chain in ques-

tion, whose origin coincides with the point $\mathcal{O}$. This reference frame is an arbitrary choice, but considered most convenient and logical. Whatever reference frame is chosen, it is important that all vectors are expressed in this same reference frame.

E.2.1. Full Inverse Jacobian for First and Third Leg

The first and third leg are identical RRR serial chains, and are shown in Fig. E.1. Their linearly independent basis twists of permission were obtained as

$$\hat{\$}_{ta_{i,1}} = \begin{bmatrix} \hat{\mathbf{s}}_i \\ -(l_1\hat{\mathbf{r}}_{i,1} + l_2\hat{\mathbf{r}}_{i,2} + l_3\hat{\mathbf{r}}_{i,3} - \mathbf{a}_i) \times \hat{\mathbf{s}}_i \end{bmatrix} \tag{E.4}$$

$$\hat{\$}_{ta_{i,2}} = \begin{bmatrix} \hat{\mathbf{s}}_i \\ -(l_2\hat{\mathbf{r}}_{i,2} + l_3\hat{\mathbf{r}}_{i,3} - \mathbf{a}_i) \times \hat{\mathbf{s}}_i \end{bmatrix} \tag{E.5}$$

$$\hat{\$}_{ta_{i,3}} = \begin{bmatrix} \hat{\mathbf{s}}_i \\ -(l_3\hat{\mathbf{r}}_{i,3} - \mathbf{a}_i \times)\hat{\mathbf{s}}_i \end{bmatrix} \tag{E.6}$$

where $\hat{\$}_{ta_{i,1}}$, $\hat{\$}_{ta_{i,2}}$, and $\hat{\$}_{ta_{i,3}}$ are the basis twists of permission associated to the first, second, and third joints respectively. Furthermore, $\hat{\mathbf{s}}_1 = -\hat{\mathbf{e}}_2$ and $\hat{\mathbf{s}}_3 = \hat{\mathbf{e}}_2$, where $\hat{\mathbf{e}}_2$ is the unit vector aligned with the Y-axis. The other vectors are illustrated in Fig. E.1, where $\hat{\mathbf{r}}_{i,l}$ is the unit vector pointing along the lth link of leg i and $\hat{\mathbf{a}}_i$ is the vector pointing from $\mathcal{O}$ to the center of the third joint.

Next, taking the conditions posed by Ref. [1] into account, a set of basis wrenches of constraint were identified,

$$\hat{\$}_{wc_{i,1}} = \begin{bmatrix} \mathbf{0}_{3\times 1} \\ \hat{\mathbf{s}}_i \end{bmatrix} \tag{E.7}$$

$$\hat{\$}_{wc_{i,2}} = \begin{bmatrix} \hat{\mathbf{e}}_3 \\ \mathbf{0}_{3\times 1} \end{bmatrix} \tag{E.8}$$

$$\hat{\$}_{wc_{i,3}} = \begin{bmatrix} \hat{\mathbf{e}}_3 \times \hat{\mathbf{s}}_i \\ \mathbf{0}_{3\times 1} \end{bmatrix} \tag{E.9}$$

Following the methodology described by Huang et al. [2], the set of basis twists of permission described in Eqs. (E.4)-(E.6) and the set of basis wrenches of constraint presented in Eqs. (E.7)-(E.9) can be used to identify a set of basis wrenches of actuation. Namely,

$$\hat{\$}_{wa_{i,1}} = \begin{bmatrix} -(l_3\hat{\mathbf{r}}_{i,3} - \mathbf{a}_i) \times \hat{\mathbf{r}}_{i,2} \\ \hat{\mathbf{r}}_{i,2} \end{bmatrix} \tag{E.10}$$

$$\hat{\$}_{wa_{i,2}} = \begin{bmatrix} -(l_3\hat{\mathbf{r}}_{i,3} - \mathbf{a}_i) \times \hat{\mathbf{f}}_{i,2} \\ \hat{\mathbf{f}}_{i,2} \end{bmatrix} \tag{E.11}$$

$$\hat{\$}_{wa_{i,3}} = \begin{bmatrix} -(l_2\hat{\mathbf{r}}_{i,2} + l_3\hat{\mathbf{r}}_{i,3} - \mathbf{a}_i) \times \hat{\mathbf{r}}_{i,1} \\ \hat{\mathbf{r}}_{i,1} \end{bmatrix} \tag{E.12}$$

with

$$\hat{\mathbf{f}}_{i,2} = \frac{l_1\hat{\mathbf{r}}_{i,1} + l_2\hat{\mathbf{r}}_{i,2}}{\left| l_1\hat{\mathbf{r}}_{i,1} + l_2\hat{\mathbf{r}}_{i,2} \right|} \tag{E.13}$$
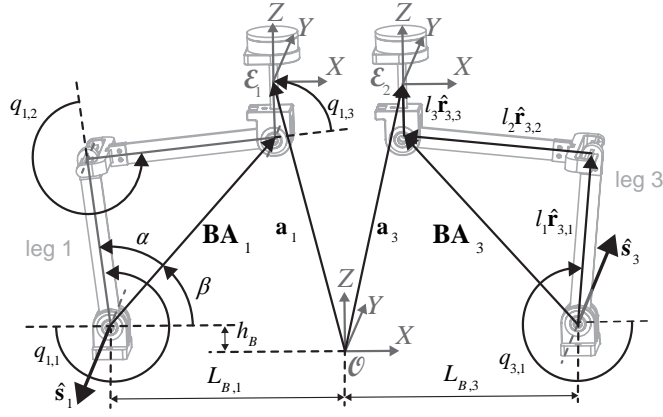
Figure E.1: Legs one and three and examples of all vectors and scalars that are used in the expression of the basis twists, the basis wrenches, and the inverse kinematics.

E

and finally also a set of twists of constraint was identified,

$$\hat{\$}_{tc_{i,1}} = \begin{bmatrix} \mathbf{0}_{3\times 1} \\ \hat{\mathbf{s}}_i \end{bmatrix} \tag{E.14}$$

$$\hat{\$}_{tc_{i,2}} = \begin{bmatrix} \hat{\mathbf{e}}_3 \\ \mathbf{0}_{3\times 1} \end{bmatrix} \tag{E.15}$$

$$\hat{\$}_{tc_{i,3}} = \begin{bmatrix} \hat{\mathbf{e}}_3 \times \hat{\mathbf{s}}_i \\ \mathbf{0}_{3\times 1} \end{bmatrix} \tag{E.16}$$

Equations (E.4)-(E.16) were then used to obtain the full inverse Jacobian for the first ($i = 1$) or third leg ($i = 3$),

$$\mathbf{J}_i^{-1} = \begin{bmatrix} \hat{\$}_{wa_{i,1}}^\top / (\hat{\$}_{wa_{i,1}}^\top \hat{\$}_{ta_{i,1}}) \\ \hat{\$}_{wa_{i,2}}^\top / (\hat{\$}_{wa_{i,2}}^\top \hat{\$}_{ta_{i,2}}) \\ \hat{\$}_{wa_{i,3}}^\top / (\hat{\$}_{wa_{i,3}}^\top \hat{\$}_{ta_{i,3}}) \\ \hat{\$}_{wc_{i,1}}^\top / (\hat{\$}_{wc_{i,1}}^\top \hat{\$}_{tc_{i,1}}) \\ \hat{\$}_{wc_{i,2}}^\top / (\hat{\$}_{wc_{i,2}}^\top \hat{\$}_{tc_{i,2}}) \\ \hat{\$}_{wc_{i,3}}^\top / (\hat{\$}_{wc_{i,3}}^\top \hat{\$}_{tc_{i,3}}) \end{bmatrix} \tag{E.17}$$
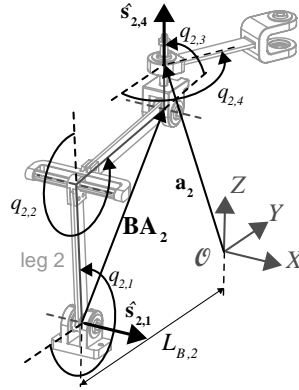
Figure E.2: Leg two and examples of vectors and scalars that are used in the expression of the basis twists, the basis wrenches, and the inverse kinematics.

E.2.2. Full Inverse Jacobian for 2nd Leg, $\mathbf{J}_2^{-1}$

The second leg is an RRRR serial chains, and a set of linearly independent basis twists of permission was obtained as

$$\hat{\$}_{ta_{2,1}} = \begin{bmatrix} \hat{\mathbf{s}}_{2,1} \\ -(l_1\hat{\mathbf{r}}_{2,1} + l_2\hat{\mathbf{r}}_{2,2} + l_3\hat{\mathbf{r}}_{2,3} - \mathbf{a}_2) \times \hat{\mathbf{e}}_1 \end{bmatrix} \tag{E.18}$$

$$\hat{\$}_{ta_{2,2}} = \begin{bmatrix} \hat{\mathbf{s}}_{2,2} \\ -(l_2\hat{\mathbf{r}}_{2,2} + l_3\hat{\mathbf{r}}_{2,3} - \mathbf{a}_2) \times \hat{\mathbf{e}}_1 \end{bmatrix} \tag{E.19}$$

$$\hat{\$}_{ta_{2,3}} = \begin{bmatrix} \hat{\mathbf{s}}_{2,3} \\ (-l_3\hat{\mathbf{r}}_{2,3} - \mathbf{a}_2) \times \hat{\mathbf{e}}_1 \end{bmatrix} \tag{E.20}$$

$$\hat{\$}_{ta_{2,4}} = \begin{bmatrix} \hat{\mathbf{s}}_{2,4} \\ -(l_3\hat{\mathbf{r}}_{2,3} - \mathbf{a}_2) \times \hat{\mathbf{e}}_3 \end{bmatrix} \tag{E.21}$$

where $\hat{\mathbf{s}}_{2,1} = \hat{\mathbf{s}}_{2,2} = \hat{\mathbf{s}}_{2,3} = \hat{\mathbf{e}}_1$ is the unit vector aligned with the X-axis, and $\hat{\mathbf{s}}_{2,4} = \hat{\mathbf{e}}_3$ is the unit vector aligned with the Z-axis.

Subsequently, a set of basis wrenches of constraint was identified as

$$\hat{\$}_{wc_{2,1}} = \begin{bmatrix} \mathbf{a}_2 \times \hat{\mathbf{e}}_1 \\ \hat{\mathbf{e}}_1 \end{bmatrix} \tag{E.22}$$

$$\hat{\$}_{wc_{2,2}} = \begin{bmatrix} \hat{\mathbf{e}}_2 \\ \mathbf{0}_{3\times1} \end{bmatrix} \tag{E.23}$$

$$\tag{E.24}$$

The set of basis twists of permission described in Eqs. (E.18)-(E.21) and the set of basis wrenches of constraint presented in Eqs. (E.22)-(E.23) enabled the identification of a set

of basis wrenches of actuation as

$$\hat{\$}_{wa_{2,1}} = \begin{bmatrix} -(l_3\hat{\mathbf{r}}_{2,3} - \mathbf{a}_2) \times \hat{\mathbf{r}}_{2,2} \\ \hat{\mathbf{r}}_{2,2} \end{bmatrix} \tag{E.25}$$

$$\hat{\$}_{wa_{2,2}} = \begin{bmatrix} -(l_3\hat{\mathbf{r}}_{2,3} - \mathbf{a}_2) \times \hat{\mathbf{f}}_{2,2} \\ \hat{\mathbf{f}}_{2,2} \end{bmatrix} \tag{E.26}$$

$$\hat{\$}_{wa_{2,3}} = \begin{bmatrix} -(l_2\hat{\mathbf{r}}_{2,2} + l_3\hat{\mathbf{r}}_{2,3} - \mathbf{a}_2) \times \hat{\mathbf{r}}_{2,1} \\ \hat{\mathbf{r}}_{2,1} \end{bmatrix} \tag{E.27}$$

$$\hat{\$}_{wa_{2,4}} = \begin{bmatrix} \mathbf{0}_{3\times1} \\ \hat{\mathbf{e}}_2 \end{bmatrix} \tag{E.28}$$

where $\hat{\mathbf{f}}_{2,2}$ was already described by Eq. (E.13). A set of twists of constraint was then identified as

$$\hat{\$}_{tc_{2,1}} = \begin{bmatrix} \hat{\mathbf{e}}_3 \\ \mathbf{0}_{3\times1} \end{bmatrix} \tag{E.29}$$

$$\hat{\$}_{tc_{2,2}} = \begin{bmatrix} \hat{\mathbf{s}}_{c,2,2} \\ \mathbf{0}_{3\times1} \end{bmatrix} \tag{E.30}$$

where

$$\hat{\mathbf{s}}_{c,2,2} = \frac{1}{\sqrt{(a_{2,y}/a_{2,z})^2 + 1}} \begin{bmatrix} 0 & a_{2,y}/a_{2,z} & 1 \end{bmatrix}^\top$$

in which $a_{2,y}$ and $a_{2,z}$ are the elements in the vector $\mathbf{a}_2$ aligned with respectively the Y- and Z-axis.

Equations (E.18)-(E.30) are then used to obtain the full inverse Jacobian for the second leg,

$$\mathbf{J}_2^{-1} = \begin{bmatrix} \hat{\$}_{wa_{2,1}}^\top / (\hat{\$}_{wa_{2,1}}^\top \hat{\$}_{ta_{2,1}}) \\ \hat{\$}_{wa_{2,2}}^\top / (\hat{\$}_{wa_{2,2}}^\top \hat{\$}_{ta_{2,2}}) \\ \hat{\$}_{wa_{2,3}}^\top / (\hat{\$}_{wa_{2,3}}^\top \hat{\$}_{ta_{2,3}}) \\ \hat{\$}_{wa_{2,4}}^\top / (\hat{\$}_{wa_{2,4}}^\top \hat{\$}_{ta_{2,4}}) \\ \hat{\$}_{wc_{2,1}}^\top / (\hat{\$}_{wc_{2,1}}^\top \hat{\$}_{tc_{2,1}}) \\ \hat{\$}_{wc_{2,2}}^\top / (\hat{\$}_{wc_{2,2}}^\top \hat{\$}_{tc_{2,2}}) \end{bmatrix} \tag{E.31}$$

E.2.3. FULL INVERSE JACOBIAN FOR INTERNAL SERIAL CHAINS, $\mathbf{J}_{o_1^2}^{-1}$, $\mathbf{J}_{o_2^3}^{-1}$, AND $\mathbf{J}_{o_3^1}^{-1}$

In order to develop matrices $\mathbf{J}_{o_1^2}^{-1}$, $\mathbf{J}_{o_2^3}^{-1}$, and $\mathbf{J}_{o_3^1}^{-1}$, first a set of basis twists and basis wrenches is developed for the end-effector serial chains. Both these serial chains are RRR chains
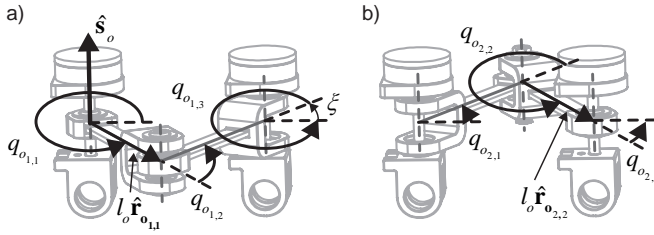
Figure E.3: a) the first end-effector serial chains and b) the second end-effector serial chain, which is also the third internal serial chain, both with examples of vectors and scalars that are used in the expression of the basis twists, the basis wrenches, and the inverse kinematics.

and their linearly independent basis twists of permission are

$$\hat{\$}_{ta_{o_{i,1}}} = \begin{bmatrix} \hat{\mathbf{e}}_3 \\ -(l_o\hat{\mathbf{r}}_{o_{i,1}} + l_o\hat{\mathbf{r}}_{o_{i,2}} - \mathbf{a}_3) \times \hat{\mathbf{e}}_3 \end{bmatrix} \tag{E.32}$$

$$\hat{\$}_{ta_{o_{i,2}}} = \begin{bmatrix} \hat{\mathbf{e}}_3 \\ -(l_o\hat{\mathbf{r}}_{o_{i,2}} - \mathbf{a}_3) \times \hat{\mathbf{e}}_3 \end{bmatrix} \tag{E.33}$$

$$\hat{\$}_{ta_{o_{i,3}}} = \begin{bmatrix} \hat{\mathbf{e}}_3 \\ \mathbf{a}_3 \times \hat{\mathbf{e}}_3 \end{bmatrix} \tag{E.34}$$

where $\hat{\$}_{ta_{o_{i,1}}}$, $\hat{\$}_{ta_{o_{i,1}}}$, and $\hat{\$}_{ta_{o_{i,1}}}$ are the basis twists of permission associated to the first, second, and third joints encountered in each end-effector serial chain, going from the first to the second end-effector. The vector $\hat{\mathbf{e}}_3$ is the unit vector along the Z-axis. This vector, as well as examples of scalars and other vectors in Eqs. (E.32)-(E.34), are illustrated in Fig. E.3, where l_o is the length of all links in the end-effector serial chains. As such, $\hat{\mathbf{r}}_{o_{i,l}}$ is the unit vector pointing along the lth link of the ith end-effector serial chain.

Next, taking the conditions posed by Ref. [1] into account, a set of wrenches of constraint was identified. Namely,

$$\hat{\$}_{wc_{o_{i,1}}} = \begin{bmatrix} \mathbf{0}_{3\times1} \\ \hat{\mathbf{e}}_3 \end{bmatrix} \tag{E.35}$$

$$\hat{\$}_{wc_{o_{i,2}}} = \begin{bmatrix} \hat{\mathbf{e}}_1 \\ \mathbf{0}_{3\times1} \end{bmatrix} \tag{E.36}$$

$$\hat{\$}_{wc_{o_{i,3}}} = \begin{bmatrix} \hat{\mathbf{e}}_2 \\ \mathbf{0}_{3\times1} \end{bmatrix}. \tag{E.37}$$

Following the methodology described by Huang et al. [2], the set of basis twists of permission in Eqs. (E.32)-(E.34) and the set of basis wrenches of constraint in Eqs. (E.35)-

(E.37) enabled the identification of a set of basis wrenches of actuation as

$$\hat{\$}_{wa_{o_{i,1}}} = \begin{bmatrix} \mathbf{a}_3 \times \hat{\mathbf{r}}_{o_{i,2}} \\ \hat{\mathbf{r}}_{o_{i,2}} \end{bmatrix} \tag{E.38}$$

$$\hat{\$}_{wa_{o_{i,2}}} = \begin{bmatrix} \mathbf{a}_3 \times \hat{\mathbf{f}}_{o_{i,2}} \\ \hat{\mathbf{f}}_{o_{i,2}} \end{bmatrix} \tag{E.39}$$

$$\hat{\$}_{wa_{o_{i,3}}} = \begin{bmatrix} -(l_o \hat{\mathbf{r}}_{o_{i,2}} - \mathbf{a}_3) \times \hat{\mathbf{r}}_{o_{i,1}} \\ \hat{\mathbf{r}}_{o_{i,1}} \end{bmatrix} \tag{E.40}$$

with

$$\hat{\mathbf{f}}_{o_{i,2}} = \frac{l_o \hat{\mathbf{r}}_{o_{i,1}} + l_o \hat{\mathbf{r}}_{o_{i,2}}}{\left| l_o \hat{\mathbf{r}}_{o_{i,1}} + l_o \hat{\mathbf{r}}_{o_{i,2}} \right|} \tag{E.41}$$

and finally also a set of twists of constraint was identified,

$$\hat{\$}_{tc_{o_{i,1}}} = \begin{bmatrix} \mathbf{0}_{3 \times 1} \\ \hat{\mathbf{e}}_3 \end{bmatrix} \tag{E.42}$$

$$\hat{\$}_{tc_{o_{i,2}}} = \begin{bmatrix} \hat{\mathbf{e}}_1 \\ \mathbf{0}_{3 \times 1} \end{bmatrix} \tag{E.43}$$

$$\hat{\$}_{tc_{o_{i,3}}} = \begin{bmatrix} \hat{\mathbf{e}}_2 \\ \mathbf{0}_{3 \times 1} \end{bmatrix} \tag{E.44}$$

The basis twists and wrenches presented in Eqs. (E.32)-(E.44) were then used to develop $\mathbf{J}_{o_1^2}^{-1}$, $\mathbf{J}_{o_2^3}^{-1}$, as well as $\mathbf{J}_{o_3^1}^{-1}$. With joint velocity vectors defined as in Eq. (5.13), and considering that the internal serial chain connecting n_1 and n_2 contains the first two kinematic joints of the first end-effector serial chain, then

$$\mathbf{J}_{o_1^2}^{-1} = \begin{bmatrix} \hat{\$}_{wa_{o_{1,1}}}^{\top} / (\hat{\$}_{wa_{o_{1,1}}}^{\top} \hat{\$}_{ta_{o_{1,1}}}) \\ \hat{\$}_{wa_{o_{1,2}}}^{\top} / (\hat{\$}_{wa_{o_{1,2}}}^{\top} \hat{\$}_{ta_{o_{1,2}}}) \\ \hat{\$}_{wa_{o_{1,3}}}^{\top} / (\hat{\$}_{wa_{o_{1,3}}}^{\top} \hat{\$}_{ta_{o_{1,3}}}) \\ \hat{\$}_{wc_{o_{1,1}}}^{\top} / (\hat{\$}_{wc_{o_{1,1}}}^{\top} \hat{\$}_{tc_{o_{1,1}}}) \\ \hat{\$}_{wc_{o_{1,2}}}^{\top} / (\hat{\$}_{wc_{o_{1,2}}}^{\top} \hat{\$}_{tc_{o_{1,2}}}) \\ \hat{\$}_{wc_{o_{1,3}}}^{\top} / (\hat{\$}_{wc_{o_{1,3}}}^{\top} \hat{\$}_{tc_{1,3}}) \end{bmatrix} \tag{E.45}$$

where the first and second row of Eq. (E.45) map the relative twist between the two end-effectors onto $\dot{q}_{a_{o_1^2,1}}$ and $\dot{q}_{a,o_1^2,2}$, the third row maps that relative twist onto $\dot{q}_{c_s,o_1^2,1}$, and rows four to six map it onto $\dot{\mathbf{q}}_{c_m,o_2^1}$.

The internal serial chain that connects n_2 and n_3 contains the third kinematic joint

of the first end-effector serial chain, so that

$$
\mathbf{J}_{o_2^3}^{-1} = \begin{bmatrix}
\hat{\$}_{wa_{o_{1,3}}}^{\top} / (\hat{\$}_{wa_{o_{1,3}}}^{\top} \hat{\$}_{ta_{o_{1,3}}}) \\
\hat{\$}_{wa_{o_{1,1}}}^{\top} / (\hat{\$}_{wa_{o_{1,1}}}^{\top} \hat{\$}_{ta_{o_{1,1}}}) \\
\hat{\$}_{wa_{o_{1,2}}}^{\top} / (\hat{\$}_{wa_{o_{1,2}}}^{\top} \hat{\$}_{ta_{o_{1,2}}}) \\
\hat{\$}_{wc_{o_{1,1}}}^{\top} / (\hat{\$}_{wc_{o_{1,1}}}^{\top} \hat{\$}_{tc_{o_{1,1}}}) \\
\hat{\$}_{wc_{o_{1,2}}}^{\top} / (\hat{\$}_{wc_{o_{1,2}}}^{\top} \hat{\$}_{tc_{o_{1,2}}}) \\
\hat{\$}_{wc_{o_{1,3}}}^{\top} / (\hat{\$}_{wc_{o_{1,3}}}^{\top} \hat{\$}_{tc_{1,3}})
\end{bmatrix}
\tag{E.46}
$$

where the first row maps the relative end-effector twist onto $\dot{q}_{a,o_2^3,1}$, and the second and third rows map the relative end-effector twist onto $\dot{q}_{c_s,o_2^3,1}$ and $\dot{q}_{c_s,o_2^3,2}$, while again rows four to six map this twist onto $\dot{\mathbf{q}}_{c_m,o_2^1}$.

Finally, because in Eq. (5.53) the internal chain connecting n_1 and n_3 is defined in the opposite direction as the twists in Eqs. (E.32)-(E.34),

$$
\mathbf{J}_{o_3^1}^{-1} = \begin{bmatrix}
-\hat{\$}_{wa_{o_{2,1}}}^{\top} / (\hat{\$}_{wa_{o_{2,1}}}^{\top} \hat{\$}_{ta_{o_{2,1}}}) \\
-\hat{\$}_{wa_{o_{2,2}}}^{\top} / (\hat{\$}_{wa_{o_{2,2}}}^{\top} \hat{\$}_{ta_{o_{2,2}}}) \\
-\hat{\$}_{wa_{o_{2,3}}}^{\top} / (\hat{\$}_{wa_{o_{2,3}}}^{\top} \hat{\$}_{ta_{o_{2,3}}}) \\
\hat{\$}_{wc_{o_{2,1}}}^{\top} / (\hat{\$}_{wc_{o_{2,1}}}^{\top} \hat{\$}_{tc_{o_{2,1}}}) \\
\hat{\$}_{wc_{o_{2,2}}}^{\top} / (\hat{\$}_{wc_{o_{2,2}}}^{\top} \hat{\$}_{tc_{o_{2,2}}}) \\
\hat{\$}_{wc_{o_{2,3}}}^{\top} / (\hat{\$}_{wc_{o_{2,3}}}^{\top} \hat{\$}_{tc_{2,3}})
\end{bmatrix}
\tag{E.47}
$$

E

REFERENCES

[1] T. Huang, S. Yang, M. Wang, T. Sun, and D. G. Chetwynd, *An Approach to Determining the Unknown Twist/Wrench Subspaces of Lower Mobility Serial Kinematic Chains,* Journal of Mechanisms and Robotics **7**, 031003 (2014).

[2] T. Huang, H. T. Liu, and D. G. Chetwynd, *Generalized Jacobian analysis of lower mobility manipulators,* Mechanism and Machine Theory **46**, 831 (2011).

Curriculum Vitæ

Antonius Gerardus Leonardus (Teun) Hoevenaars

31-01-1985	Born in 's-Hertogenbosch, the Netherlands.

Education

1997–2003	Pre-University Education (Grammar School / High School) Maurick College, Vught
2004–2008	B.Sc. in Aerospace Engineering Delft University of Technology, Faculty of Aerospace Engineering, Delft, The Netherlands
2009–2012	M.Sc. in Space Systems Engineering Delft University of Technology, Faculty of Aerospace Engineering, Delft, The Netherlands
2012–2016	Ph.D. in Mechanical Engineering Delft University of Technology, Faculty of Mechanical, Maritime and Materials Engineering, Delft, The Netherlands

Thesis: Parallel Manipulators with Two End-Effectors
Promotor: Prof. dr. ir. J.L. Herder

Awards

2003	Cum laude pre-university degree
2010	Regional winner South Holland in the European Satellite Navigation Competition
2012	Cum laude M.Sc. degree
2014	2nd place in Voice of Innovation
2015	1st place in ASME Student Mechanism and Robot Design Competition (Graduate Division)

LIST OF PUBLICATIONS

PUBLICATIONS AS PART OF PH.D.

8. **A. G. L. Hoevenaars**, S. Krut, and J. L. Herder, *Jacobian-Based Natural Frequency Analysis of Parallel Manipulators*, International Journal of Robotics Research (submitted 2016).

7. **A. G. L. Hoevenaars**, C. Gosselin, P. Lambert, and J. L. Herder, *A Systematic Approach for the Jacobian Analysis of Parallel Manipulators with Two End-Effectors*, Mechanism and Machine Theory (submitted 2016).

6. **A. G. L. Hoevenaars**, C. Gosselin, P. Lambert, and J. L. Herder, *Consistent Modeling Resolves Asymmetry in Stiffness Matrices*, Mechanism and Machine Theory (accepted 2016).

5. **A. G. L. Hoevenaars**, C. Gosselin, P. Lambert, and J. L. Herder, *Experimental Validation of Jacobian-Based Stiffness Analysis Method for Parallel Manipulators with Non-Redundant Legs*, Journal of Mechanisms and Robotics (2015).

4. **A. G. L. Hoevenaars**, P. Lambert, and J. L. Herder, *Jacobian-Based Stiffness Analysis Method for Parallel Manipulators with Non-Redundant Legs*, Proceedings of the Institution of Mechanical Engineers, Part C: Journal of Mechanical Engineering Science (2015).

3. **A. G. L. Hoevenaars**, P. Lambert, and J. L. Herder, *Generalized Jacobian Analysis of Parallel Manipulators With Multiple End-Effectors*, Volume 5A: 38th Mechanisms and Robotics Conference, V05AT08A081 (2014).

2. **A. G. L. Hoevenaars**, P. Lambert, and J. L. Herder, *Kinematic Design of Two Elementary 3DOF Parallel Manipulators with Configurable Platforms*, Proceedings of the 6th International Workshop on Computational Kinematics (CK2013), 315 (2014).

1. **A. G. L. Hoevenaars** and J. L. Herder, *Application-specific modelling of assisted telemanipulation systems in the early design phase using the i* framework*, IEEE/ASME International Conference on Advanced Intelligent Mechatronics: Mechatronics for Human Wellbeing, AIM 2013, 692 (2013).

EARLIER PUBLICATIONS

2. **T. Hoevenaars**, S. Engelen, and J. Bouwmeester, *Model-based discrete PID Controller for Cubesat reaction wheels based on COTS brushless DC Motors*, Proceedings of the 1st IAA Conference on Dynamics and Control of Space Systems, (2012).

1. J. Bouwmeester, J. P. J. Reijneveld, **T. Hoevenaars**, and D. Choukroun, *Design and verification of a very compact and versatile attitude determination and control system for the Delfi-n3Xt Nano satellite*, Proceedings of the 4S Symposium, (2012).